EVALUATING VOLCANIC HOSTED MASSIVE SULPHIDE FAVOURABILITY USING GIS-BASED SPATIAL DATA INTEGRATION MODELS, SNOW LAKE AREA, MANITOBA

by

Daniel Frederick Wright

A thesis submitted to the School of Graduate Studies in partial fulfilment of the requirements for the degree of Ph.D. in Earth Sciences

OTTAWA-CARLETON GEOSCIENCE CENTRE

UNIVERSITY OF OTTAWA

OTTAWA, CANADA, 1996

ISBN 0-612-16477-2

UNIVERSITÉ D'OTTAWA
UNIVERSITY OF OTTAWA

ABSTRACT

Maps showing spatial variation of volcanic-hosted massive sulphide (VHMS) potential in the Snow Lake area have been generated by combining digital data from a variety of sources. An exploration model, based on a VHMS deposit model, but expanded to include regional exploration datasets, provides a conceptual framework for the extraction of predictive evidence from the raw data sources. The evidence is divided into five factors: stratigraphic evidence, evidence related to available heat, alteration evidence, geophysical evidence and geochemical evidence. Stratigraphic evidence is derived from the presence of favourable volcanic lithologies, and the proximity to contacts between volcanic flows and volcanic breccia. Heat evidence is derived from proximity to subvolcanic tonalite sills (the inferred primary heat source) and proximity to synvolcanic dykes. The alteration evidence is deduced from the presence and proximity to mapped alteration, mainly silicification, Fe-Mg metasomatism and pyritization. The geochemical evidence is a combination of a lake sediment signature (derived by principal components analysis), and individual maps of Pb, Zn and Cu in till. The geophysical factor is a combination of magnetic, gravity and VLF components.

Four approaches have been applied for combining spatial evidence to predict mineral potential. (1) The weights of evidence method (data-driven) is used to characterize the spatial associations between the known deposits, and to calculate weights

for each predictive map layer. The output is a favourability map expressed as the posterior probability of a VHMS deposit occurring per unit area. The magnitude of the weights allow the evidence to be ranked according to predictive capability. (2) A second data-driven method, area weighted logistic regression, was applied using the same binary evidence maps as used in the weights of evidence method. The binary maps, representing the independent variable in the model, were combined to form irregularly shaped polygons with unique combinations of evidence. The observations for each polygon were weighted according to the area of the unique-polygon. The dependent variable was the presence of a deposit. This model was not constrained by the assumption of conditional independence. (3) In the fuzzy logic method, evidence is expressed in terms of fuzzy membership functions, subjectively assigned by an expert, for each predictor map. An inference network is constructed to mimic the decisions made by an exploration geologist, using a variety of fuzzy combination rules that reflect varying degrees of logical AND and OR. (4) Dempster-Shafer belief theory is more flexible than fuzzy logic for representing uncertainty in the data, but is somewhat restricted in the expressiveness of the combination rules. The Dempster-Shafer output consists of favourability maps for "support" (conservative), "plausibility" (optimistic), and "ignorance" (uncertainty).

Comparing the results from the four different methods shows that they all have a similar spatial distribution of areas of high favourability. The known deposits are in highly favourable zones, as expected, and a number of prospective areas have the right combination of factors, but no known deposits. The new VHMS discovery at Photo Lake made during summer 1994 is in a favourable zone as predicted by these models.

TABLE OF CONTENTS

LIST OF TABLES

LIST OF FIGURES

ACKNOWLEDGEMENTS

Though a single name, mine, appears as the author of this thesis, I am under no illusion that this was a solo effort. I would like to sincerely acknowledge some of the people without whose help this thesis would never have been completed.

I am particularly fortunate to have had a supervisor, Dr. Graeme Bonham-Carter, who was genuinely interested in my work, took time to discuss problems and work through solutions, encouraged me to participate in presentations at conferences, and provided an excellent role model for carrying out scientific research. Most of the problems encountered in implementing the methods used in this study were resolved through his help. Many thanks are due to my colleagues in the Geomathematics section at the Geological Survey of Canada. Dr. Frits Agterberg reviewed most of this manuscript and provided useful suggestions and much encouragement. I have the deepest respect for these two men for proving by example that achieving excellence in scientific research does not preclude taking a personal interest and caring for the people around them. I thank them for their interest in me and my family. Dr. Chang-Jo Chung spent time explaining some of the more difficult (at least to me) mathematical problems associated with the modelling used in this study. Dr. Alex Desbarats helped coach me through my comprehensive exams especially in the area of geostatistics.

I am indebted to the Geological Survey of Canada for allowing me time to attend classes at the University of Ottawa and work on this thesis and for providing funding through the Exploration Science and Technology Initiative. Dr. Bill Coker gave encouragement and facilitated all the necessary administration. Mr. Phil O'Regan digitally drafted many of the black and white diagrams.

None of the data used in this study was collected by myself. A special thanks to all those who spent months and years in the field doing "real" geology, especially Dr. Al Bailes and Dr. Al Galley who carried out the geological mapping and also spent hours enthusiastically discussing and explaining the VHMS model to me.

Thanks to my friends, Paul Racine and Ron Starra, for holding me accountable to the truth and, not in any way least, I thank my wife, Colette, and my children, Laurelle, Allison and James, who are the definition of love.

To my father and mother, my first and favourite teachers, who taught me the important things in life.

Happy is the man who finds wisdom,
and the man who gets understanding,
for the gain from it is better than from silver
and its profit better than gold.
She is more precious than jewels,
and nothing you desire can compare with her.

Proverbs 3:13-15

1. Introduction

1.1 General

Mineral exploration is the starting point for many processes that have a significant influence on the well being of our society as well as having a vital impact on our economy. Minerals are needed to feed the manufacturing industry that produces commodities that are an integral part of all our lives, both necessities and comforts. The agricultural industry is becoming more dependent on minerals to be used as fertilizers to keep up to the ever increasing demands for food. In Canada, the mineral and mineral product exports, including fuels, totalled 36.1 billion dollars for 1993. This represents 25 percent of Canada's total annual domestic exports (Dunn and Pilsworth, 1994).

It has been recognized over the last few decades that locating new mineral resources is becoming more difficult as fewer and fewer deposits that outcrop at the surface, and are hence easier to find, remain undiscovered. In order to find concealed orebodies the exploration geologist has had to rely increasingly on integrated studies using detailed geological mapping, geophysical techniques and geochemical techniques (Rose et al., 1981).

The components of a mineral exploration program will differ depending on the commodity being looked for, the resources available, and the environment it is being carried out in, however, it generally involves the collection, analysis and integration of data from a variety of sources. Typically data will include geological map data, structural information, geochemical data, mineral deposit data, and geophysical data or remote sensed data. The overall objective is to progress from large areas at a small scale to relatively small areas at a large scale and identify targets for mineral deposits.

Integration of exploration datasets to investigate overlap relationships between anomalies has traditionally been done manually by overlaying analog maps on a light table. This method made it difficult to deal with data of different scales or projections, making changes was time consuming and labour intensive, and the process was highly subjective making it hard to duplicate results.

Dramatic advances in technology since the mid 1980s have resulted in two tools that have the potential to make a strong impact on the efficiency with which an exploration geologist can carry out the collection, analysis and integration of large and diverse geoscience datasets; 1) the availability of relatively inexpensive, high-powered computing workstations and 2) Geographic Information Systems (GIS), software for managing spatial data.

Computer-based methods related to data integration problems in mineral exploration have been in use since the 1970s. The early computer methods were predominantly regression techniques (Agterberg et al., 1972; Chung and Agterberg, 1980; Harris, 1984). Interactive computer graphics precipitated improved versions of regression based software including SIMSAG (Chung, 1983), GIAPP (Fabbri, 1985), NCHARAN (Botbol, 1971; McCammon et al., 1983) and FINDER (Singer and Kouda, 1988). Expert-based systems used in mineral exploration became available in the mid 1970s, most notably with the development of PROSPECTOR (Duda et al., 1977; McCammon, 1989).

Many of the earlier efforts at using quantitative computer methods for aiding in mineral exploration were not widely adopted by the exploration industry. Some important reasons for this include, the high costs of computers and associated support before the microcomputer, the difficulty of importing diverse data types in geographically co-registered databases, the lack of good graphics and slow user interaction. GIS in a microcomputer environment has resolved many of these issues.

Recently, new research has been published that has incorporated a variety of methods for combining spatial data in a GIS suitable for mineral exploration applications (Bonham-Carter, 1994a, Chung and Moon, 1991). These methods can be broadly subdivided according to whether they are data-driven or knowledge driven (Reddy and Bonham-Carter, 1991). In data-driven methods, evidence maps are weighted based on a measured association between patterns on the map and areas with known mineralization. In knowledge-driven approaches the evidence maps are weighted according to an expert's opinion.

Multivariate regression analysis and two probabilistic procedures, Bayesian and Dempster-Shafer methods, are reviewed and discussed by Chung and Moon (1991). The techniques are illustrated using an artificial dataset. Some new approaches for expert-system models, notably the fuzzy logic and Dempster-Shafer methods have been applied by An, (1992), An et al., (1992), An et al., (1991), An et al., (1994a) and An et al., (1994b) using airborne geophysical data and bedrock geology for base metal exploration. The Bayesian model, in a log-linear form, known as weights of evidence, has been applied using known deposits to statistically evaluate the importance of different evidence to evaluate gold potential in parts of Nova Scotia and New Brunswick. (Agterberg et al., 1990; Bonham-Carter et al., 1988; Watson et al., 1989). Decision-tree analysis has been interfaced with a GIS and applied to base metal exploration by Reddy and Bonham-Carter (1991). The Prospector model has also been applied in a GIS context (Campbell et al., 1982; Katz, 1991; Reddy et al., 1992).

1.2 Objectives

It is recognized that in many of these studies, there is an emphasis on methodology development, the datasets are restricted to a small number of layers, the data are hypothetical, or they focus on a particular factor or factors that do not represent the complete exploration model. To effectively evaluate mineral potential for an area and to investigate the feasibility of doing this as an automated process in a GIS environment, it is necessary to establish a comprehensive exploration model, have a dataset that can represent that model and have a GIS that can accommodate the data and execute an appropriate spatial combination method.

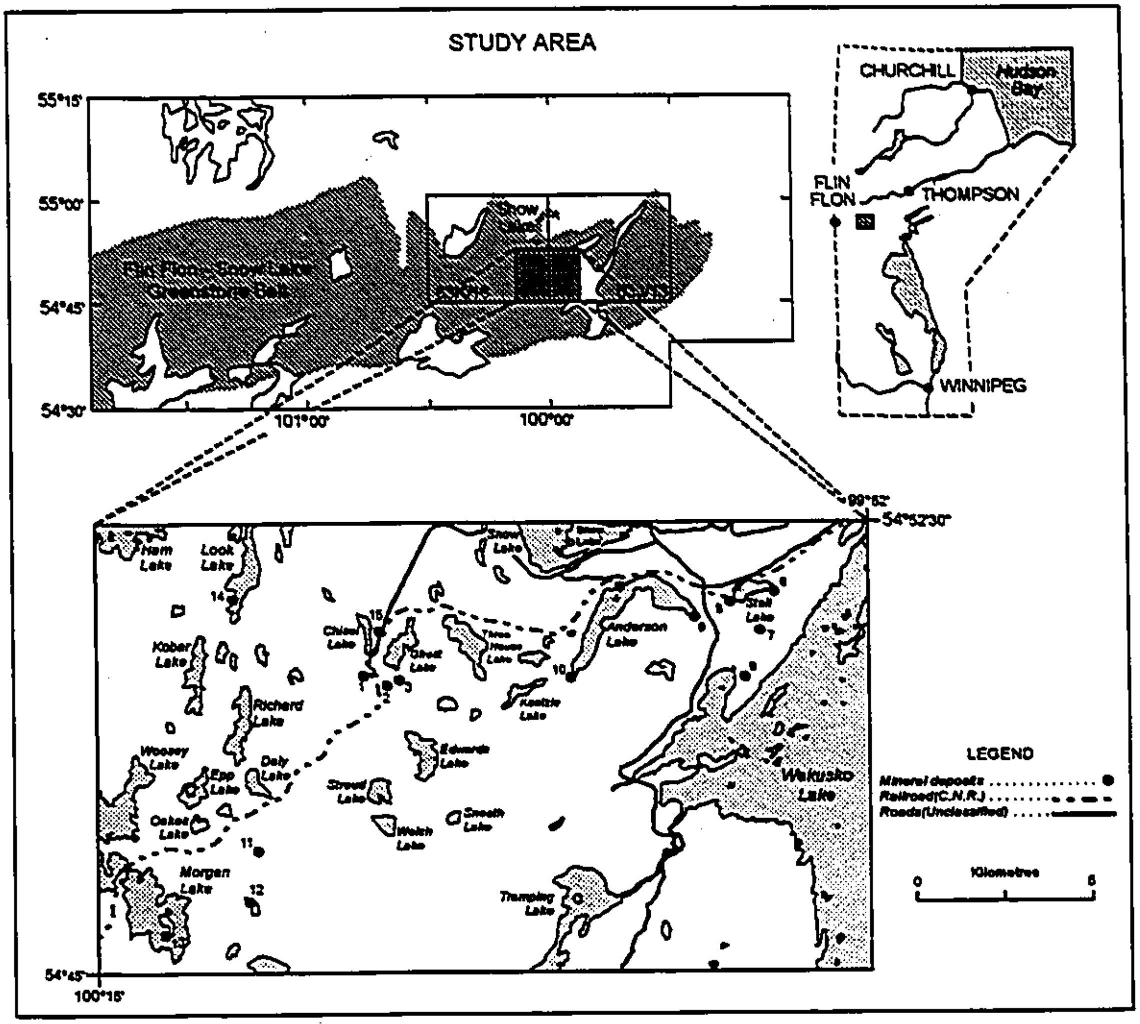

Figure 1.1. The study area straddles the boundary between the NTS map sheets 63K/16 and 63J/13 east of Flin Flon in central Manitoba. It has dimensions of approximately 20 x 15 km with a total area of 335 km^2. The key to the VHMS mineral deposits, labelled 1 to 15, is found in Table 2.2.

It is the objective of this thesis to evaluate the favourability for Volcanic Hosted Massive Sulphide (VHMS) deposits for the Chisel-Anderson Lake area in Manitoba by integrating diverse geoscience data sets, representing evidence based on a comprehensive exploration model, using data-driven and knowledge-driven spatial data combination models implemented in a GIS on micro computer platform.

1.3 Exploration Science and Technology Initiative (EXTECH)

A critical component to any data integration project is the data. This study required a diverse and up-to-date comprehensive geoscience dataset that could be used to reflect geological controls on the VHMS deposits as defined by the exploration model. The data used in this study came largely from EXTECH, which was a cooperative effort between the Geological Survey of Canada, the Manitoba Department of Mines and Energy and the mining industry (Bonham-Carter and Hall, in prep.). Besides data collection, one of the principal goals of EXTECH was to improve the concepts and technologies applicable to exploration for volcanic hosted massive sulphide deposits through the development of integrated regional and deposit-scale models. This provided an invaluable pool of expertise to consult while establishing the deposit and exploration model and assigning importance to the various evidence maps.

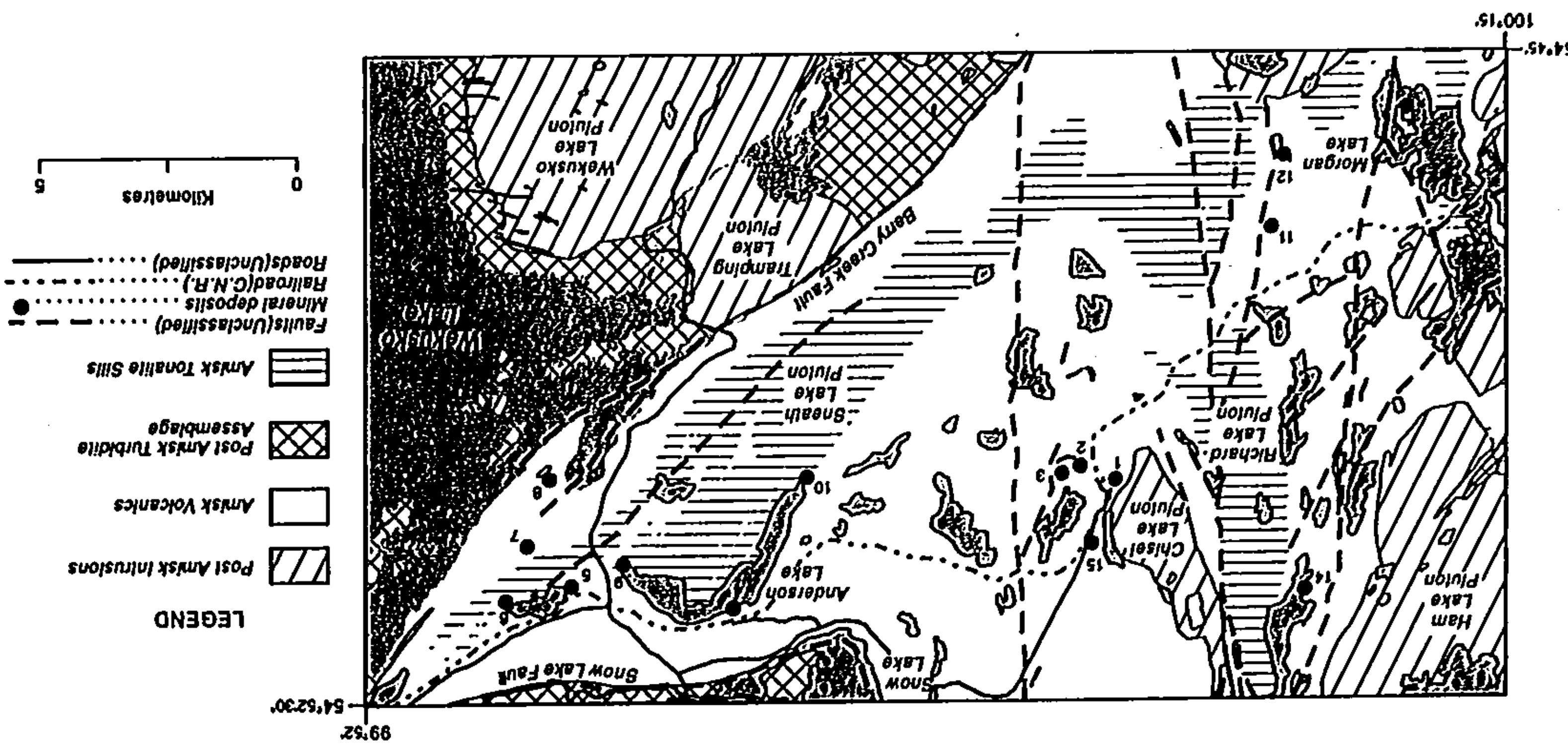

Figure 1.2. Study area showing VHMS deposits and key geological and geographical features of the region. Deposit names: 1. Chisel, 2. Lost, 3. Ghost, 4. Anderson, 5. Stall, 6. Rod, 7. Linda 1, 8. Linda 2, 9. Ram Zone, 10. Joannie, 11. Raindrop, 12. Pot, 13. Morgan, 14. Bomber Zone, 15. North Chisel (See Table 2.2)

1.4 Location

The study area straddles the boundary between the two 1:50000 scale NTS map sheets, 63J/13 and 63K/16, bounded by the intervals 54.75 - 55.00 N and 90.50 - 100.5 W, see Figure 1.1. The area is approximately 20 km by 15 km, extending from Wekusko Lake in the east to Ham Lake in the west, and from Snow Lake in the north to Morgan Lake in the south. This area is referred to as the Chisel-Anderson map area, see Figure 1.2.

1.5 Framework for Methodology

Details as to how each spatial data combination method is implemented are quite different for each approach, however, in general terms the process for producing mineral favourability maps using GIS can be considered in four main steps: (1) establish a conceptual model, (2) build a spatial data base, (3) process the data, and (4) apply integration modelling to generate favourability maps.

Beginning the process by establishing a conceptual model is critical as it guides many of the decisions throughout the study from what data is actually collected to how it is weighted in the actual integration step. The spatial database in a GIS is an organized collection of individual data sets, incorporating a variety of data structures (raster, vector, relational, for example). The data processing step involves many operations to extract and enhance critical predictive information from each of the raw data layers. Integration modelling, as used here, refers to the methods for combining predictive data layers into favourability maps, by statistical or expert-system methods. This process is illustrated in Figure 1.3.

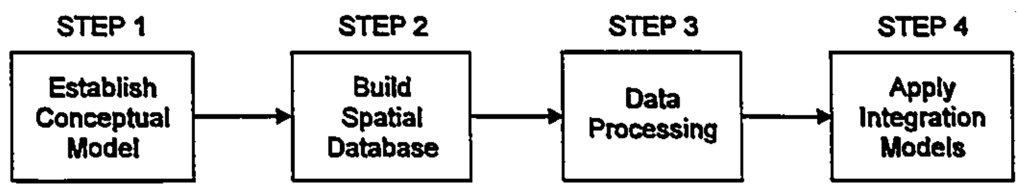

Figure 1.3. The four step process for evaluating mineral favourability in a GIS environment (modified from Bonham-Carter, 1994).

1.6 Previous GIS Work Related to the EXTECH Project

Pilot GIS studies were carried out within a western portion the study area described in this thesis that were associated with the EXTECH project, before much of the detailed data collected during the EXTECH project was available and with emphasis on methodology development. These initial studies used data from 1:50000 scale mapping and broad-scale regional geophysical and geochemical coverage acquired from the Provincial and Federal Geological Surveys. VHMS potential was evaluated using statistical methods, including Bayesian weights of evidence (Reddy et al., 1990), decision tree (classification and regression tree) analysis (Reddy and Bonham-Carter, 1991), and area-weighted logistic regression analysis (Reddy et al., 1991). Potential was also estimated using an expert-system approach, with a Prospector-type model modified for regional datasets (Reddy, Bonham-Carter and Galley, 1992; Bonham-Carter, Reddy and Galley, 1994). The work described in this thesis benefited from these earlier pilot studies, taking advantage of the new datasets collected during EXTECH and the improved understanding of the mineral deposit model developed during EXTECH.

1.7 Thesis Outline

This thesis is organized to follow the process described in the general framework for methodology, outlined above, for producing mineral favourability maps.

Chapter 2 focuses on the conceptual model for VHMS deposits in the Snow Lake area. The chapter begins by describing the regional geological setting followed by detailed descriptions of the known VHMS deposits in the area. This is used as a basis for understanding the geologic controls on the deposits. The conceptual model is then developed distinguishing between the "deposit model" and the "exploration model".

Chapter 3 introduces some fundamental concepts and terminology related to GIS especially as it is related to mineral potential mapping. It is recognized that GIS technology, though generally accepted by the earth sciences as a potentially powerful tool, is still relatively new and not well understood by many geologists.

Chapter 4 deals with establishing the database. The choice of datasets used in this study was based primarily on the exploration model developed in Chapter 2. Much of the data could not be used directly as predictor maps and had to be processed. How the raw data was processed to make it suitable to be used in the integration models is also described in Chapter 4. The concerns related to errors in data are considered here.

Chapters 5 to 8 describe the four different integration models used in this study. The two data driven methods, weights of evidence and area weighted logistic regression, are discussed in Chapters 5 and 6 respectively. The two knowledge-driven methods, fuzzy logic and Dempster-Shafer, are discussed in the following two chapters.

The integration methods applied in Chapters 5 to 8 result in four different "favourability maps". A cursory examination indicates that spatial patterns are broadly similar. Chapter 9 quantitatively compares the results from the four methods to measure the overall similarity and to identify specific areas of difference.

Chapter 10 contains summary remarks and discussion.

Three appendices are included. The first contains tables of the fuzzy logic membership functions and Dempster-Shafer belief functions used for each evidence map and other lengthy data summaries. The second appendix can be thought of as a manual describing the detailed steps for carrying out the methods applied in this study using the SPANS GIS. Finally the third appendix contains the digital data files necessary to follow the manual in the second appendix.

2. Geological Model

2.1 Regional Geological Setting

The Snow Lake area base metal deposits are found within the Flin Flon metavolcanic belt which is in turn part of the Trans-Hudson orogen.

The Trans-Hudson orogen is the Early Proterozoic (1.9 - 1.8 Ga) collision zone between the Superior Province and the Archaean domains of the north western Churchill Province (Hearn Province) of the Canadian Shield. To the south, the orogen has been outlined in the subsurface between the Wyoming and the Superior provinces (Figure 2.1). It is one of a network of fifteen Early Proterozoic orogenic belts that have welded together Archaean provinces to form the Laurentia or North American craton (Hoffman, 1988; Lucas, 1993). The orogen, outcropping in parts of Saskatchewan and Manitoba, has been mapped as having widths of up to 500 km, and forms a dogleg convex to the northwest (Figure 2.1) where it crosses beneath the Palaeozoic Hudson Bay basin and so assuming its name, (Hoffman, 1990). Essentially, the orogen is comprised of an internal zone of intraoceanic rocks flanked by ensialic external belts (Hoffman, 1990).

The Flin Flon metavolcanic belt has a length of 250 km, extending across the Manitoba and Saskatchewan border, and an exposed width of between 32 and 48 km (Figure 2.1). It is composed of deformed juvenile Early Proterozoic subaqueous and subordinate subaerial volcanic rocks and associated sediments, known as the Amisk Group, an unconformably overlying fluvial-alluvial sequence of sandstones and

Figure 2.1. Spatial relationship of study area with respect to the Flin Flon greenstone belt. The inset map shows the location of the study area with respect to the Trans-Hudson and other orogens (dark grey) and Archaean provinces (named). From Syme and Bailes, 1993.

conglomerate, known as the Missi Group and intruded by calc-alkaline plutons (Syme, 1990; Syme and Bailes, 1993; Bailes and Galley, in prep). The belt is bounded on the north by the Kisseynew metatsedimentary gneiss belt and to the south it is overlain by the Ordovician dolomitic limestones. The Amisk Group is dominated by volcanic rocks characteristic of oceanic island arc and back arc environments. Minor amounts of epiclastic shoshonites, typical of mature arc environments, have also been identified (Syme and Bailes, 1993). The Amisk Group rocks are economically important as they host all of the known volcanogenic massive sulphide deposits. The Missi Group rocks are primarily continental alluvial quarzofeldspathic sediments and intercalated volcanics. The portion of the belt in Manitoba has two distinct arc segments, one centred near the town of Flin Flon and one at Snow Lake (Bailes and Galley, in prep).

A 335 km^2 economically important area, containing 6 past producing deposits and at least 9 other VHMS type occurrences (Figure 1.1; Figure 2.2; Table 2.2), south of Snow Lake has recently been remapped in detail (Bailes, 1993; Bailes, 1992; Bailes and Galley, 1992; Bailes and Galley, 1991; Bailes, 1990ab; Bailes and Galley, 1989). A detailed description summarizing this work is currently in preparation (Bailes and Galley, in prep). This is also the study area used in this thesis. A summary of some of the main geological features is given below.

Table 2.1. Metal grades for VHMS deposits, Flin Flon greenstone belt.*

Deposit	District	Status CL= Closed OP= Operating	Cu (%)	Zn (%)	Production + Reserves (t)
Flin Flon	Flin Flon	CL	2.19	4.2	62,446,734
Trout Lake	Flin Flon	OP	2.11	4.79	10,180,608
Chisel Lake	Snow Lake	CL	0.60	10.94	7,299,816
Stall Lake	Snow Lake	CL	4.29	0.57	6,263,779
Osborne Lake	Snow Lake	CL	3.14	1.52	3,380,061
Anderson Lake	Snow Lake	CL	3.41	0.10	3,189,601
Callinan	Flin Flon	OP	1.43	3.7	2,800,000
Spruce Point	Snow Lake	OP	2.36	2.80	1,931,000
Schist Lake	Flin Flon	CL	4.21	7.00	1,877,813
Centennial	Flin Flon	CL	1.41	2.48	1,624,550
Westarm	Flin Flon	CL	3.34	1.25	1,579,403
Coronation	Saskatchewan	CL	4.24	0.30	1,282,088
Dickstone	Snow Lake	CL	2.47	3.13	1,083,590
Chisel Open Pit	Snow Lake	CL	0.25	8.5	1,000,000
White Lake	Flin Flon	CL	1.97	4.63	849,598
Rod 2	Snow Lake	CL	6.39	2.2	645,027
Ghost/Lost Lake	Snow Lake	CL	1.34	8.87	605,690
Cuprus	Flin Flon	CL	3.24	6.42	462,002
Flexar	Saskatchewan	CL	3.75	0.47	305,940
Birch	Saskatchewan	CL	6.15		278,825
North Star	Flin Flon	CL	6.11		241,643
Mandy	Flin Flon	CL	5.63	13.95	123,116
Don Jon	Flin Flon	CL	3.07		79,313
Rod 1	Snow Lake	CL	5.00	4.5	22,267
Avg. production grade			3.25	4.40	
Total production plus reserves					109,552,872

* From Syme and Bailes, 1993.

2.1.1 Supracrustal Rocks

In the Snow Lake area, the Amisk group volcanic rocks are exposed mainly between the Berry Creek fault and the McLeod Road fault. They are generally north facing and exhibit structural features indicating broad folding around the northeast trending Threehouse syncline (Figure 2.2). Bailes and Galley (in prep) have divided this 6 km thick assemblage into five distinct depositional phases based on geochemical signatures and geological attributes. Cu-rich massive sulphide deposition has occurred in the arc volcanic rocks of the first phase near Anderson Lake and is clearly associated with a rhyolite complex. Zn-rich deposits affiliated with dacite volcaniclastic rocks and rhyolite flows occur in the third phase near Chisel Lake.

The stratigraphy has been described by Bailes (1990) and Bailes and Galley (1993). The first phase consists of over 3 km of pillowed aphyric sparsely porphyritic basalt, basaltic andesite and andesite flows (see Welch Lake Aphyric mafic flows Figure 2.2) overlain by thick bedded felsic breccia (see Stroud Lake Felsic Breccia). Minor amounts of aphyric to sparsely quartz-phyric rhyolites (see Daly Lake rhyolite) can be found within the basalts. The second phase is a variable assemblage of volcanic rocks including porphyritic basalt flows (see Snell Lake basalt) and thick bedded mafic breccias (see Edwards Lake mafic breccia). The third phase is composed of mafic to felsic flows up to 1 km thick (see Moore-Powderhouse-Ghost sequence). These rocks

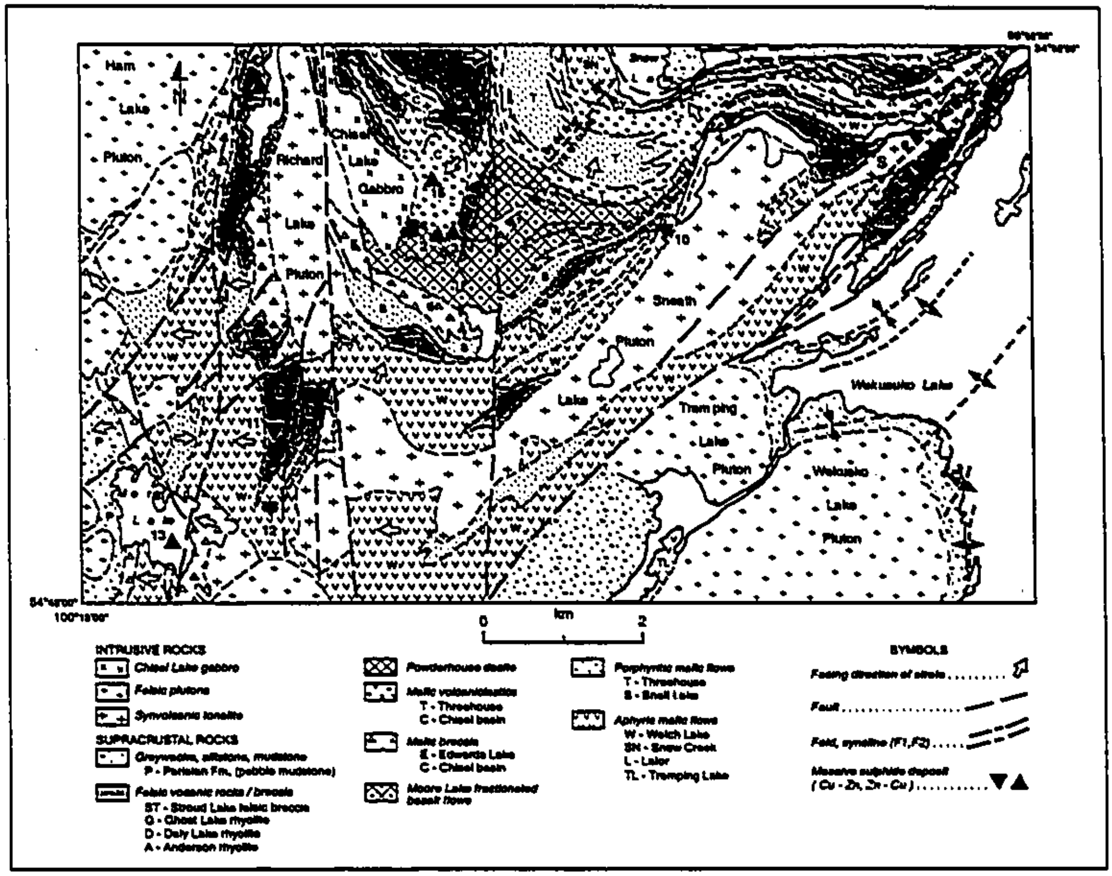

Figure 2.2. Geology of the Snow Lake mining camp. Deposits are keyed to Table 2.2. (From Galley et al., 1993)

form the footwall to the Chisel Lake, Lost Lake, Ghost Lake and Chisel North Zn-Cu massive sulphide deposits. These units are absent in the Anderson Lake area where the known Cu-Zn deposits occur. The fourth phase is comprised of mafic tuff, lappilli tuff, tuff breccia and related porphyritic basalt flows (see Chisel and Threehouse units). This sequence of rocks is important as they generally form the stratigraphic hanging wall to the known base metal deposits in the Snow Lake area. The final phase consists of heterolithologic mafic breccias , aphyric basalt flows and felsic breccias. The formation names used herein are useful for grouping lithologies that, in general, can be related based on their common geochemical and geological attributes. However, they are informal names (Bailes and Galley, 1989) and are restrictive in the modelling process when specific lithologies are of interest. For these reasons the formation names are not generally used in this thesis.

2.1.2 Felsic and Late tectonic Plutons

The Amisk Group volcanic rocks in this area are intruded by the Sneath Lake and Richard Lake tonalite plutons. Dates determined by U-Pb zircon methods indicate that these plutons are both synvolcanic (Bailes, 1992), however, geochemical signatures demonstrate they are likely not related (Bailes, 1988). A number of mafic to felsic sills, dykes and plugs are found, primarily in the western portion of the study area, intruding the units below the Chisel Lake, Lost Lake and Ghost Lake Zn-Cu massive sulphide deposits. These intrusions are cross cut by a significant dacite dyke complex interpreted to be a subvolcanic feeder system for the Powderhouse dacites (Bailes and Galley, 1989). U-Pb zircon ages date the Sneath Lake Pluton at 1886 Ma and the Richard Lake Pluton at 1889 Ma which is a similar age to the Amisk Group volcanics (1886 Ma). Also the Sneath Lake pluton and deposit hosting felsic volcanic strata in the Anderson Lake area both display low flat REE profiles and low contents of HFS elements. This can be used as evidence for the proposal that the Sneath Lake pluton was a heat engine to elevate the overall geothermal gradient to drive the hydrothermal activity. (Bailes and Galley, 1991).

Post Amisk rocks are found to the south of the Berry Creek fault in the so-called Wekusko Domain (Bailes, 1992). The Wekusko Lake domain is underlain by a thick greywacke, siltstone and mudstone turbidite assemblage intruded by the Wekusko Lake and Tramping Lake granitic plutons. A similar Post Amisk turbidite assemblage is found to the north of the McLeod Road fault. The Wekusko Lake domain has no known volcanic hosted massive sulphide deposits, though a recently discovered sediment hosted massive sulphide occurrence, (Bur Zone) indicates that other exploration models should be considered for this area (Bailes, 1992). Other late tectonic (Post Amisk) plutons include the Ham Lake intrusion in the northwest part of the study area, Bujarski Lake pluton and plutons west of Epp and Morgan Lakes.

2.1.3 Alteration

The Snow Lake area is characterized by megascopically altered rocks (Figure

2.4) occurring in semi-conformable zones of up to 1000 m wide, in evidence in up to 25% of the area. These large zones suggest that the area was significantly affected by circulatory hydrothermal fluid flow (Bailes and Galley, in prep). Field work resulted in the identification of six mappable alteration types: 1) alteration pipes and completely altered rocks, 2) Quartz and plagioclase-rich rocks (silicification), 3) Chlorite and biotite-rich rocks (Fe-Mg alteration), 4) Amphibole-rich rocks, 5) Disseminated sulphide and 6) epidote and hematite-rich rocks (Bailes and Galley, 1993). Both the Cu-Zn deposits in the Anderson Lake area and the Zn-Cu of the Chisel Lake area have distinct extensive zones of semi-conformable alteration underlying the mineralization.

In the Chisel Lake area, a regionally extensive semi-conformable zone of silicification, having a width of up to 1000 m and a length of over 5 km, occurs in the footwall volcanics of the Welch, Edwards and Moore formations. A second disconformable alteration zone is also found in the Chisel Lake area characterized by three broad zones of biotite-garnet alteration, chlorite-staurolite and sericite-kyanite alteration forming an apron under the deposits (Bailes, 1990; Bailes and Galley, in prep).

Alteration in the Anderson Lake deposits footwall rocks has three main domains; weak, pervasive quartz-biotite-staurolite-garnet alteration in the rhyolites; a large semi-conformable zone of chlorite rich rocks occur mainly in the Anderson rhyolites but also in the Welch Lake basalts and the upper 300 m of the Sneath Lake pluton; and discordant zones of completely altered rocks in the immediate footwall rocks of the Stall and

Anderson deposits. These discordant alteration zones may have been fracture- or fault-controlled channel ways for discharging hydrothermal fluids involved in the formation of the sulphide deposits (Bailes and Galley, in prep).

2.1.4 Structure

The Snow Lake area rocks exhibit at least two major deformational episodes identified as F_1 and F_2 (Froese and Moore, 1980; Bailes, 1987). In the west part of the study area the F_1 folds trend west and northwest and the F_2 folds are north-northeast-trending. These two structures combine to form flat lying surfaces in the structural basin northwest of Chisel Lake. In the eastern portion of the study area F_1 is reflected in well developed isoclinal folds in the greywacke turbidite suite south of the Berry Creek fault but not so well developed in the volcanic rocks to the north. The F_2 fold event is also observed as a series of major north-northeast trending broad warps that deform the geological formations (Bailes, 1992). The peak metamorphic episode (F_2) post-dated the volcanism and hydrothermal activity by a span of time in the order of 80 million years (Bailes and Galley, in prep). In the Wekusko Lake area, F_2 folds are locally crosscut by a north-northeast-trending crenulation cleavage and small scale F_3 folds. No major structures have been noted in association with F_3 events (Bailes, 1992).

Several major north-south trending faults, some juxtaposing strata with opposing facing directions, occur in the west portion of the map. These faults post date the F_1 and

F_2 folds and the late tectonic felsic plutons (Bailes, 1987). In the eastern portion of the study area three major faults, the McLeod Road, the Snow Lake and the Berry Creek, and numerous parallel subsidiary faults have been identified. The McLeod Road fault and the Snow Lake Fault are suggested as being thrust faults synchronous with the F_1 fold event. (Froese and Moore, 1980; Bailes, 1992). The Berry Creek fault, with a strike length of over 150 km, provides a natural division between the Amisk volcanic rocks suite and their associated volcanic hosted massive sulphide deposits to the north and the post Amisk turbidite assemblage and granitic intrusions to the south. Synvolcanic faults, an important component for focusing deposit related hydrothermal fluids, are difficult to map directly, but may often be inferred from mapping alteration.

2.2 VHMS Deposits in Snow Lake area

The Flin Flon belt, which includes the 62 million tonne Flin Flon base metal deposit, is one of the most productive base metal mineral regions in Canada, with production plus reserves totalling 109.5 million metric tonnes (Syme and Bailes, 1993; Table 2.1). The study area for this thesis, immediately south of Snow Lake, contains 6 past producing deposits and accounts for production of over 19 million metric tonnes (Figure 1.1; Table 2.2). Some deposit specific studies of base metal mineralization in the Snow Lake area have been carried out by Coats et al. (1970), Martin (1966), Walford and

Map No.	Name	*Tonnage (t) (reserves and production)	Grades Cu (%), Zn (%), Au (g/t), Ag(g/t)	Past or Present Producer
1	Chisel Chisel Open Pit	7,299,816 1,000,000	0.60 Cu, 10.94 Zn 0.25 Cu, 8.5 Zn, 2.74 Au, 54.86 Ag	Past
2 3	Lost Ghost	590,233	8.5 Zn, 1.3 Cu, 32.6 Au, 3.8 Ag	Past
4	Anderson	3,189,601	3.41 Cu, 0.10 Zn	Past
5	Stall	6,263,779	4.29 Cu, 0.57 Zn	Past
6	Rod1 Rod2	22,675 810,440	4.5 Cu, 0.74 Zn 6.6 Cu, 2.9 Zn	Past
7	Linda 1	N/A	N/A	Occurrence
8	Linda 2	13,000,000	0.30 Cu, 0.79 Zn	Non-producer
9	Ram Zone	N/A	N/A	Occurrence
10	Joannie	N/A	N/A	Occurrence
11	Rain Drop			
12	Pot Lake	123,000	1.43 Cu, 4.5 Zn, 0.4 Au, 18 Ag	Non-producer
13	Morgan Lake	N/A	N/A	Occurrence
14	Bomber Zone	N/S	0.4 Cu, 1.0 Zn, 0.1 Au, 8.6 Ag	Occurrence
15	North Chisel	2,580,000	0.22 Cu, 8.9 Zn, 2.54 Au, 23.3 Ag	Non-producer
16	Photo Lake (approx. location)	1,000,000(aprox.)	discovered summer, 1994	

Table 2.2. VHMS deposit names and characteristics for the Chisel-Anderson study area (See Figure 1.1 and Figure 2.2).
* Sources: Fedikow (1988), Fedikow (1993), Syme and Bailes (1993).

Franklin (1982), Zaleski (1989) and Galley et al. (1993). Descriptions of all mineral deposits and occurrences in the study area can be found in Fedikow et al. (1989, 1993) and descriptions of the base metal deposits found in the study area can be found in Bailes and Galley (in prep). A brief description of the 6 past producing volcanic hosted massive sulphide deposits found in the study, taken from the above sources is given below. The Chisel, Lost and Ghost deposits are representative of the Zn-Cu-rich deposits found in the third phase of volcanic rocks and the Anderson, Stall and Rod are representative of the Cu-Zn-rich deposits found in the first phase of volcanic rocks.

2.2.1 Chisel Lake Zn-Cu-rich Deposits

Chisel Lake Deposit

The Chisel deposit was discovered in 1956 by the diamond drilling of an electromagnetic anomaly and production began in 1960 at 1000 tonnes per day (Martin, 1966). It is the largest Zn-rich ore body in the Snow Lake area at 7.5 million tonnes, grading 10.9% Zn and 0.5% Cu (Bailes and Symes, 1993; Table 2.2). Detailed studies of the Chisel mine have been published by Martin (1966) and Galley et al. (1993). Sphalerite is the main ore mineral plus minor amounts of chalcopyrite, pyrrhotite, galena and arsenopyrite and traces of lead-arsenic sulphides, tellurides and native Au, Ag, Bi and As. The sulphides occur in stacked massive lenses, averaging 12 m thick, that strike NW, dip northeast at 65° .

The units which underlie the Chisel deposit, the Moore Lake Basalt, the Powderhouse dacite and the Ghost Lake rhyolite, are a mafic to felsic sequence from a fractionated magma. The Powderhouse dacite and the Ghost Lake rhyolite form the immediate footwall to the Chisel deposit (Bailes and Galley, in prep.). Alteration is observed in the footwall rocks for up to 2 km below the deposits and is comprised mainly of two semi-conformable zones of alteration displaying Fe-Mg metasomatism and Si-Ca addition (Bailes and Galley, 1989).

Lost Lake and Ghost Lake Deposits

The Lost Lake and Ghost Lake Zn-Cu massive sulphide deposits occur at or near the same stratigraphic position as the Chisel Lake deposit and all are within a 1.3 km strike length of each other. The Ghost Lake deposit was discovered in 1956 at the same time as the Chisel Deposit but production did not begin till 1972. The Lost Lake deposit was discovered in 1974 and production began in 1979 (Fedikow et al. 1989). The deposits were mined out by 1988 having produced approximately 600,000 tonnes grading 8.7% Zn, 1.3% Cu, 32.61g/t Ag and 3.83 g/t Au (Bailes and Galley, in prep). Primary mineralization is sphalerite with lesser chalcopyrite, pyrrhotite, pyrite and galena (Fedikow, 1989). The footwall rocks for both deposits are dacites and directly associated with rhyolite flow complexes. The hanging wall rocks for the Chisel deposit are primarily turbidite deposited mafic wackes while the Ghost deposit is overlain by a basalt flow (Bailes and Galley, in prep).

North Chisel Deposit

Though this deposit has not been mined, it is a significant deposit of 2.58 million tonnes of 8.9% Zn, 0.22% Cu, 0.4% Pb, 23.3% g/t Ag and 2.54 g/t Au (Bailes and Galley, in prep). It is 1.6 km north of the Chisel deposit along the same stratigraphic position (Bailes and Galley, 1989). The ores in this deposit are silicate-dolomite rich semi-massive sulphides rather than the massive sulphide ore as at Chisel (Bailes and Galley, in prep.).

General Stratigraphic Associations for Chisel Lake area Zn-Cu rich deposits

Bailes and Galley (1989) have summarized a number of stratigraphic associations typical of the Zn-Cu rich deposits: 1) they occur in a volcanic sequence that displays arc tholeiite affinities, 2) they are spatially associated with fractionated volcanic rocks (eg. the Moore-Powderhouse-Ghost formations), 3) they are at the same stratigraphic position as a major rhyolite complex, 4) they are spatially associated with major synvolcanic plutons (Sneath Lake tonalite and Richard Lake tonalite), 5) large semi-conformable alteration zones occur stratigraphically below the deposits, and 6) they are spatially associated with a volumetrically significant underlying synvolcanic dyke complex. These stratigraphic associations are important for developing an exploration model.

2.2.2 Anderson Lake Cu-Zn-rich Deposits

Anderson Lake Deposit

The Anderson deposit was discovered in 1963 and mined out in 1988 after producing 3.2 million tonnes of grading 3.41% Cu and 0.10 % Zn (Bailes and Galley, in prep.). A detailed study of the Anderson deposit has been carried out by Walford and Franklin (1982). The deposit was a single elongated lens conformable with the volcanic host rocks, striking north 65°, dipping 60° to the northwest and plunging 55° to the northeast. The ore zone had a maximum thickness of 10 m, strike length of 120 m and can be traced 1220 m down plunge. The primary mineralization consists of pyrite, chalcopyrite and pyrrhotite with minor sphalerite (Walford and Franklin, 1982). The footwall rocks are a 350 meter thick assemblage of mainly quartz-phyric and aphyric rhyolites. Alteration at the Anderson Mine consists of 150 m of discordant alteration composed of chlorite-kyanite-staurolite schist at the core surrounded by zones of muscovite-kyanite schist and sericite-garnet-magnetite bearing rhyolites. This discordant zone merges into a semi-conformable zone of Fe-Mg and Fe-Mg-Ca alteration (Bailes, 1992). It is noted that the semi-conformable zone of silicification found in the footwall rocks at the Chisel deposits are not present in the Anderson area (Baile, 1992).

Stall Lake Deposit

The Stall Lake deposit was also discovered in 1963. Total production plus reserves is 6.3 million tonnes grading 4.29% Cu and 0.57% Zn (Table 2.1). A study of the deposit was carried out by Studer (1982). The ore is found in four main lenses and a number of smaller hanging wall lenses semi-conformable to the stratigraphy striking approximately east-west and dipping 45° to the north. Of the four main lenses, the largest is the No. 4 orebody. It consists of a series of connected anticlines and synclines with their axes parallel to the D_2 lineation (Threehouse synform) having a strike length of approximately 90 m and widths of up to 40 m. The west end of this lens is consistently higher in copper grade that the east end by a factor of two. Both the No.1 and No. 4 lenses commonly contain Cu grades in excess of 10%. The massive sulphides are composed mainly of pyrrhotite with lesser pyrite and chalcopyrite (Struder, 1975). The lenses occur at the contact between the lower aphyric and middle quartz phyric members of the Anderson rhyolite (Bailes and Galley, 1991).

Rod Deposit

A small massive sulphide lens having a strike length of approximately 30 meters and containing 22,675 tonnes with grades of 5.0% Cu and 4.5% Zn (Rod No. 1), was first discovered in 1957. This deposit was mined from 1962 to 1964. A second larger massive sulphide lens, approximately 200 m down plunge of the first lens, was discovered in 1969 (Rod No. 2). Over 6.5 million tons of ore were mined from Rod 2 during the years 1984 to 1991 grading 6.39% Cu and 2.2% Zn (Coats et al., 1970, Table

2.1). The Rod deposit has been described in detail by Coats et al. (1970).

The deposits occur in fine-grained felsic rock with 5 mm quartz phenocrysts. This has been described by Coats et al. (1970) as a felsic volcanic pyroclastic rock. Bailes and Galley (in prep.) argue that the host rock is more likely a quartz porphyry phase of the subvolcanic Sneath Lake pluton.

Linda 2 Deposit

The Linda 2 deposit, located approximately 2 km south of the Stall deposit in the quartz phyric phase of the Anderson rhyolites, is the largest known deposit in the Snow Lake area at 13 million tonnes grading 0.30% Cu and 0.79% Zn (Bailes and Galley, in prep.), however, it is subeconomic. It has been described in terms of its metamorphic petrology by Zaleski et al. (1991).

Comparison of Anderson and Chisel areas

As a result of 1:20000 scale mapping in the Chisel-Anderson Lake area (Bailes, 1990b), some differences between the Anderson Cu-Zn and Chisel Lake Zn-Cu stratigraphic settings have been identified (Bailes, 1990). Some of these are; 1) The Anderson Lake area deposits are stratigraphically below the Moore-Powderhouse-Ghost volcanic sequence, 2) there is not an equivalent thick sequence of the rhyolites hosting the Stall and Anderson deposits in the Chisel area, 3) the Chisel Lake area deposits area underlain by dyke complexes not found in the Anderson Lake area, and 4) alteration patterns suggest that the hydrothermal systems associated with the Chisel Lake deposits are unrelated to the Anderson Lake deposits.

2.3 VHMS Deposit and Exploration Model

An ore deposit model can be broken down into two components; 1) a descriptive model and 2) a genetic model (Lydon, 1984). The descriptive model documents features considered being characteristic of the deposit such as the geological setting, morphology, chemistry, mineralogy and zoning. It can be considered to be an idealized example of the deposit type simplified to a great extent based on data from many examples (Lydon, 1984). The genetic model for a mineral deposit type is an attempt to give a rational and consistent explanation of the characteristics of the deposit type in terms of physical and chemical processes (Lydon, 1988). For example, the descriptive model would document the zones of alteration associated with alteration pipes underlying the mineralization commonly consisting of inner chloritized cores surrounded by sericitized peripheries. The genetic model would document the properties, such as temperature, pressure, and pH, of the hydrothermal fluids that would be necessary for this type of zonation to occur.

The ore deposit model, includes many features on a mine scale. When an exploration program is being initiated and several hundreds of square kilometres or more are being covered many of the features in the ore deposit model would be difficult, if not impossible, to identify. At this point the term "exploration model" is introduced.

The exploration model includes features from the deposit model and other characteristics that can be recognized at a regional scale that are associated with the deposit type of interest. For example, the shape and mineralogy of the massive sulphide lenses that form the deposit are important elements of the deposit model and at the mine scale are critical to developing the mine. Commonly the ore is buried or the surface expression is extremely small, making this information relatively less important in terms of a regional exploration program. However, regional expressions of geochemical anomalies in tills or lake sediments that could reflect the buried deposit, potentially become very useful in determining the location of a deposit.

A summary of the descriptive deposit model, focusing primarily on the features that can be recognized on a regional scale, specifically for the Snow Lake area is given below followed by an exploration model for the Snow Lake area.

2.3.1 Deposit Model

Detailed geological mapping (Bailes, 1990b) and deposit studies (Galley, 1993) in the Snow lake area have resulted in the identification of six controls, pertinent to an exploration model, that influence the location of VHMS deposits. These geologic controls have been summarized by Bailes and Galley (in prep.).

1) Deposits occur within thick sequences of fractionated mafic to felsic subaqueous volcanic rocks having an arc tholeiite geochemical signature. Geochemically, arc tholeiite flows can be distinguished from ocean floor-back arc types by higher concentrations of large ion lithophile elements, moderate to strong depletion of high field strength elements and strong depletion of Ni and Cr. These assemblages are characterized by the presence of felsic flows and abundant volcaniclastic units. VHMS deposits are commonly associated with the felsic extrusive rocks within or at the top of these sequences. This represents a period of cessation of volcanism, which would allow for the dposition of sulphides in sufficient quanitities to develop a deposit. Identifying these thick fractioned volcanic sequences with felsic flows and volcaniclastics at the top could be and important indicator for the presence of VHMS deposits.

2) Deposits occur within or adjacent to rhyolite flow complexes. The Cu-rich deposits in the Anderson Lake area are contained in rhyolite complexes and all the Zn-rich deposits in the Chisel Lake area are contained in, or along the same stratigraphic horizon as rhyolite bodies.

3) Most of the known deposits occur within 3 km stratigraphically above the contact between tonalitic intrusions (Sneath Lake and Richard Lake plutons) and the subaqueous volcanics. Similar ages of these plutons and the Amisk volcanics combined with similar

chemical signatures suggest that these plutons could be the source of heat that drove hydrothermal convection cells. Sea water was pumped through the volcanic rocks from which metals were dissolved and redeposited at or near vents on the sea floor.

4) A prominent dacite dyke complex occurs in the footwall rocks to the Chisel Lake area deposits. It is likely that vent areas were fed from vertical fractures that cut through the volcanic rocks, localizing the upward flow of hydrothermal fluids, and that dykes were intruded along fractures. Heat from the dykes also helped to drive the hydrothermal circulation.

5) Deposits are associated with volumetrically significant zones of silicification and Fe-Mg metasomatized rocks. These zones were produced by rock-water interaction, the hydrothermal fluids reacting with volcanic rocks to produce alteration minerals.

6. The deposits at Snow Lake occur above synvolcanic faults. These features are difficult to identify and are generally recognized by the presence of strong alteration resulting from interaction of the adjacent rocks and hydrothermal fluids.

The stratigraphic controls influencing the location of massive sulphide deposit are shown in an idealized section in Figure 2.3 and the idealized relationship between regional alteration patterns and massive sulphide deposits are shown in Figure 2.4.

2.3.1 Exploration Model

The six characteristics outlined above can all be recognized from regional datasets and represented as evidence useful for mapping regional favourability. The two critical datasets for this study area from which this evidence can be derived are the 1:20000 geological and alteration mapping.

The first two components are related to what might be termed *stratigraphic evidence* for VHMS deposits.

To represent the important lithologic units of felsic flows and felsic volcaniclastic rocks as a layer of evidence, the geological map may be classified as shown in Figure 2.3. Each map unit varies in importance: felsic flows are the most important, felsic volcaniclastic units are moderately important; mafic and other volcanic rocks would follow and nonvolcanic lithologies are least important.

The association of deposits to felsic flows (being close but not necessarily hosted by) can be represented by a layer showing proximity to the surface trace of the contact of felsic flows, with proximal being most important and distal being least important. Proximity to other contacts between volcanic lithologies may also be predictive.

The next two components are also stratigraphic, but are related to the source of

A

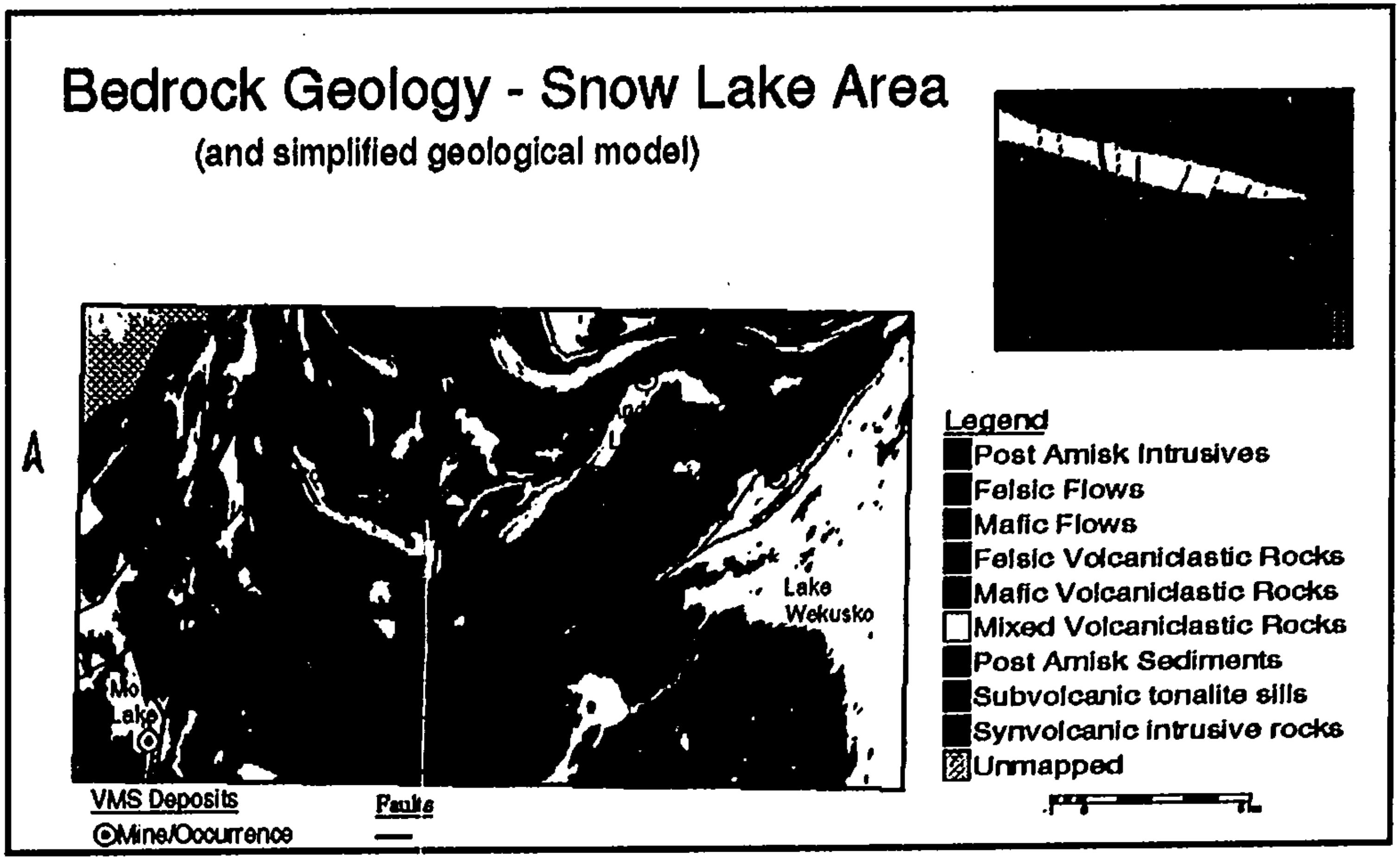

Figure 2.3. Geolgocial setting for the Chisel Anderson study area, with simplified model for VHMS deposits.

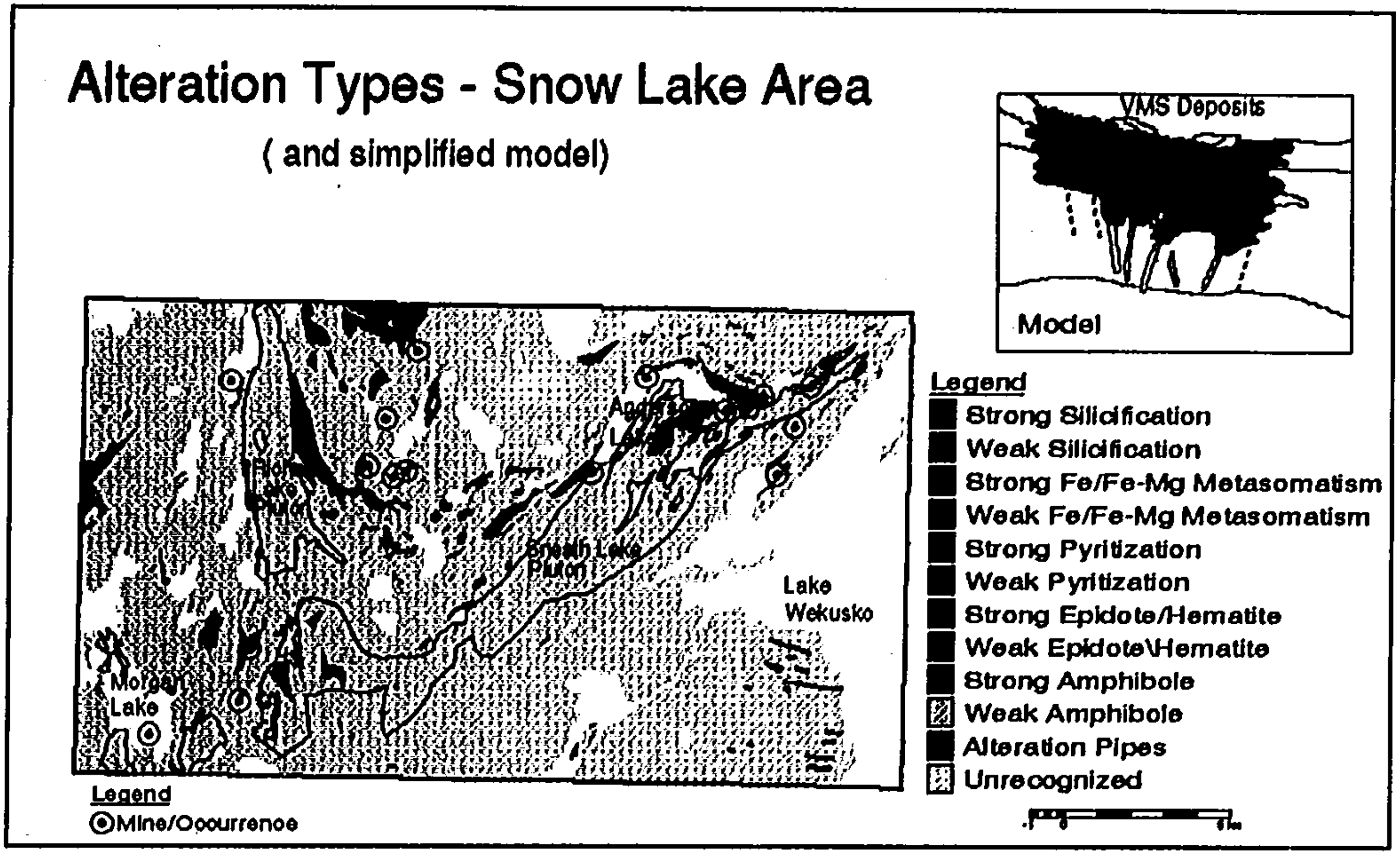

Figure 2.4. Mapped alteration based on mineral assemblages. Typical regioal alteration associated with VHMS deposits is shown in cartoon at upper right..

heat for driving the hydrothermal circulation and can be called *heat evidence*.

Maps representing the proximity to the surface trace of the contact between the tonalitic intrusions and the subaqueous volcanics and one showing proximity to synvolcanic dykes can be used as layers of evidence indicating the importance of being close to a subvolcanic tonalite and/or synvolcanic dykes. Close proximity indicates a greater probability of an active hydrothermal circulation, and therefore greater favourability of a VHMS deposit, whereas far proximity suggests a lower favourability.

The next components are related to evidence of hydrothermal alteration, that in turn may indicate the activity of mineralization processes. This evidence can be obtained from mapping of alteration patterns of various types and may be called *alteration evidence*.

This evidence would consist of layers showing presence and proximity to zones of silica and Fe-Mg alteration, with higher favourability assigned to presence or close proximity than zones with no evidence of alteration.

Synvolcanic dykes were not mapped directly but inferred from zones of intense alteration characteristic of alteration pipes. A layer showing the presence or proximity to one of these zones could represent evidence of synvolcanic dykes.

The other evidence that can be used in the exploration model comes from regional geochemical surveys, and from geophysical surveys. The *geochemical evidence* is based on a combination of indicators from till and from lake sediments. In general, one would expect that sulphide deposits occurring at the surface would be detectable in lake sediment samples, and in till samples. Hydromorphic dispersion in groundwater may also occur around buried deposits, with re-precipitation in lakes under varying conditions of pH, particularly for elements such as Zn. Evidence from geochemical data could include lake sediment and till geochemical layers for Zn, Pb, Cu, and possibly other metallic trace elements.

Geophysical evidence, the evidence used widely by exploration companies for finding VHMS targets, has not been strongly emphasised in the present study. EM surveys have been particularly useful for detecting buried sulphide bodies in the Snow Lake area, however, no consistent regional public EM survey was available for this study area. The radiometric, magnetic, gravity and VLF surveys proved of marginal value as direct evidence of VHMS mineralization, due mainly to the relatively wide line-spacing compared with the size of VHMS targets. For this study and at this scale, the regional geophysical data were valuable for geological mapping, interpretation of plutonic composition and differentiation trends, for recognizing gradients due to geophysical contrasts across contacts, and possibly for recognizing alteration effects. Nevertheless, buried sulphide bodies are associated with the following *geophysical evidence*; a layer of EM data, a layer of magnetic data, a layer of gravity data and a layer of VLF data.

A number of factors for VHMS exploration are not considered here, for a variety of reasons. Lithogeochemical evidence was not used, because the available data were too sparse, and unsuitable for interpolation to continuous geochemical surfaces. Information on the details of the volcanic cycles was not included, because even at the detailed scale of the mapping, there was too much uncertainty in tracing individual units over the whole map area. Satellite imagery was not used, because the spectral information was dominated by the states of vegetation, and the effects of forest-fires, and the structural information visible on satellite images failed to reveal lineaments that could be related to synvolcanic faults. A number of faults are clearly visible on the images, confirmed by ground mapping, but they postdate the mineralization. Uranium, thorium and potassium distributions show interesting patterns, but the VHMS deposits do not appear to be correlated with radiometric signatures. The radiometric data yield information about the composition of rock units, but at the scale of the present study are not directly usable for predicting VHMS deposits.

2.4 Discussion

From the above descriptions of the regional geology and the more detailed deposit geology it is recognized that even in this relatively small area that the VHMS deposits can be characterised into two different groups. There are the Cu rich deposits in the Anderson Lake area and the Zn rich deposits in the Chisel Lake area. These distinct groups have different mineralogy, different alteration associations and different stratigraphy. It is noted that the exploration model, described above, does not focus on the details that identify the differences between these two groups.

It could be argued that for an exploration model to be most effective it would have to focus on very specific characteristics, and indeed, to find target areas that have very specific characteristics this would be true. However, it is argued here, that in general, an exploration model must be more general in nature. This is in view of the fact that the exploration model, as defined here, is designed to identify areas that have potential for VHMS type deposits in general that will warrant further detailed investigation, not to immediately identify a drill target for a VHMS deposit with specific qualities. It is also exceptional to have the type of detail that is available in this study area and must be assumed that in a typical exploration program a more general model would be suitable.

The following chapter introduces some of the fundamental concepts and terms related to geographic information systems (GIS) to help provide a base for discussions addressing the next steps in the modelling process where GIS plays a critical role.

3. Geographic Information Systems

3.1 Introduction

Geologists and geoscientists have become skilled in observing, recording, and analyzing complex spatial relationships. The exploration geologist is routinely required to combine spatial geoscience information including bedrock geology, till cover, structure, geochemistry and geophysics in order to identify high potential targets for mineral deposits.

Geographic information systems (GIS), a relatively new technology emerging in the early 1960's (Coppock and Rhind, 1991, Aronoff, 1989), is a computer system designed specifically for managing spatial data. Though not specifically created for use in the earth sciences, it has been recognized by the geological community as a potentially powerful tool for geological applications. Indeed, one of the objectives of this thesis is to demonstrate the effectiveness of GIS as tool for managing spatial data to aid in the mineral exploration process

Computer-based techniques for problem solving in a mineral exploration context have been in use since the early 1970's (Agterberg, 1989c, 1992a), however, in general they have been slow to be adopted by and has involved the minority of geologists. The use of GIS in geology is no exception. It is the purpose of this chapter to introduce some fundamental GIS concepts and terminology that are used in this thesis which may not be familiar to geologists without a GIS background. A more complete introduction to GIS has been compiled by Aronoff (1989), Burroughs (1987), Maguire et al. (1991) and ESRI (1994). An excellent discussion of GIS in a geological context can be found in Bonham-Carter (1994).

3.1.1 Definition of GIS

GIS is the acronym for the singular or plural term, Geographic Information System(s). Definitions of GIS abound in the literature. Maguire (1991), lists eleven selected definitions, however, points out that they all have the single common feature of managing spatial data. Though, a case could be made that GIS include both manual (light tables) and computer-based information systems (Aronoff, 1989; Burrough, 1987), in practice all contemporary GIS are computer based (Maguire, 1991). A formal definition is given below:

> "An organized collection of computer hardware, software, geographic data, and personnel designed to efficiently capture, store, update, manipulate, analyze, and display all forms of geographically referenced data". (ESRI, 1994)

Within this definition can be found the four basic elements of a GIS: computer hardware, computer software, data and liveware. Most fully functional GIS, those that have a well-designed and implemented database, strong analytical capability and cartographic aspects, are designed around high performance workstations using the UNIX operating system, though personal computers are capable of running fully functional GIS software and mainframes are still acceptable for enormous national or global scale GIS applications.

The second element in a GIS is the software. GIS software design has evolved in three basic directions: file processing design, hybrid design and extended designs. The file processing design organizes each data set in separate files that are linked during analytical operations by the GIS software. In the hybrid design, DBMS are used to store and manage attribute data while custom software is used to store and manage spatial data. The extended design uses a DBMS to store both the attribute and geographical data. The DBMS is "extended" to provide analytical functions (Aronoff, 1989; Maguire, 1991).

Data is the third component of a GIS. The collection, transformation of data into a suitable structure and import into the GIS in use is usually the most expensive and time consuming part of any GIS project.

The final and most critical of the elements defining a GIS is the liveware or people. Without competent properly trained personnel a GIS is of little use.

3.1.2 History and evolution of GIS

It could be argued that GIS , systems that collect, store and analyze spatial information have been in existence ever since maps have been made (Burrough, 1987). However, if the definition given above, requiring a computer component, is adhered to, the first true GIS have their origins in the early 1960's. It is generally recognized that many of the early significant developments in GIS originated in North America with possibly the first true GIS, the Canada Geographic Information System, being credited to the work of Roger Tomlinson in conjunction with the Canadian Government (Coppock and Rhind, 1991). This system evolved out of a need to develop a national land classification capability of all productive land in Canada. This involved integrating information related to agricultural, forestry, recreation and wildlife. The technology was based on an IBM 360/65 mainframe computer (Coppock and Rhind, 1991; Aronoff, 1989; Tomlinson, 1967). Other organizations that played a key role in the early development of GIS include the US Bureau of the Census, the US Geological Survey, the Harvard Laboratory for Computer Graphics and the work of Howard Fisher and in Briton the Experimental Cartography Unit and the work of David Bickmore. The Census Bureau was responsible for the development of Dual Independent Map Encoding (DIME) scheme, and eventually the creation of the Topologically Integrated Geographic Encoding and Referencing (TIGER) system. These products were driven by a need to integrate census data based on locational data supplied by postal codes. The Harvard Laboratory for Computer Graphics, influenced strongly by the field of landscape architecture, focused on developing a computer mapping system and produced products including SYMAP, GRID and ODYSSEY. The successful commercial GIS ARC/INFO has its roots in the people (Jack Dangermond) and products of this effort.

This early development stage in the growth of GIS, extending from the early 1960's to the mid 1970's was hampered by computer technology, primarily the lack of high quality interactive graphics but also the high costs of operating mainframe computers and limitations imposed due to the paucity of digitally available data. During this time advances were made in the areas of cartographic accuracy and visual quality and also on spatial analysis. Development continued slowly through the 1970's to the early 1980's generally through government-funded research. At this time rapid and significant improvements in computer technology especially in the area of graphics combined with decreased computer costs led to large growth in GIS with many commercial packages becoming available. Two major designs of GIS emerged at this time, one with emphasis on raster methodology and the other on vector methodology.

GIS is now an indispensable tool, with most major GIS combining raster and vector methodology, in a wide range of applications in areas including agriculture, forestry, wildlife management, archaeology, geology, urban planning, marketing and environmental issues.

3.2 Fundamentals of GIS

GIS software can be considered to have five basic functions that deal with: 1) data input and verification, 2) data storage and database management 3) data output and presentation 4) data transformation and modelling and 5) interaction with the user (Burrough, 1987).

Perhaps the function that sets GIS apart from Computer Aided Design (CAD) systems and automated mapping systems (AM) and Data Base Management Systems (DBMS), which on there own perform many of the operations of a GIS, is the data transformation function. Data transformations covers a broad range of operations that can be considered in terms of data maintenance, such as changing scales or projections, and utilization and analysis, including area analysis, reclassification, buffering and surface analysis. To understand some of the concepts of transformations it is also important to understand the data storage and management component which is concerned with the data is organized (data modelling) and structured (data structure and file format). Some of the salient points related to data storage and transformations are discussed below.

3.2.1 Data models and structures

When constructing a digital map database two basic types of map information must be considered: 1) spatial information, which describes the location, shape and topological characteristics of a map feature and 2) descriptive information. On a two dimensional map, features can be represented as discrete spatial objects such as points, lines and areas. The process of defining and organizing data from the real world and into a consistent digital dataset that is useful and reveals information is called data modelling and the logical organization of data according to a scheme is known as a data model (Bonham-Carter, 1994). Two of the most common models for organizing spatial data are the vector and raster model and discussed very briefly below. For an in-depth discussion on digital data models and structures in a GIS context see Burrough (1987), Aronoff (1989), Bonham-Carter (1994) and Davis and Simonett (1991).

3.2.2 Raster Model and Structures

In the raster model the space represented on the map is divided into a regular grid of square or rectangular cells. These cells are commonly called pixels (for picture element) and have an area usually dictated by the size of the feature that needs to be represented. Each pixel is assigned a value to represent the feature it represents which can be used as a link to an attribute table often containing non-spatial data related to the feature.

A number of raster structures exist for the raster model including the full raster, run-length encoding and quadtree. The most common structure is the full raster or expanded raster where the map is defined as an array of pixel values, in which the row and column coordinates define a particular location.

When features being represented in a digital file are homogeneous over large areas, the full raster structure will have a large number of adjacent cells with similar values. Run-length encoding is a simple raster data structure that provides a method for reducing the space requirements for rasters that have many repeated values (see Figure 3.1(b)). The strategy is to have all the adjacent cells in a row with the same value treated as a group or run. Instead of storing the value for each pixel, the pixel value is stored

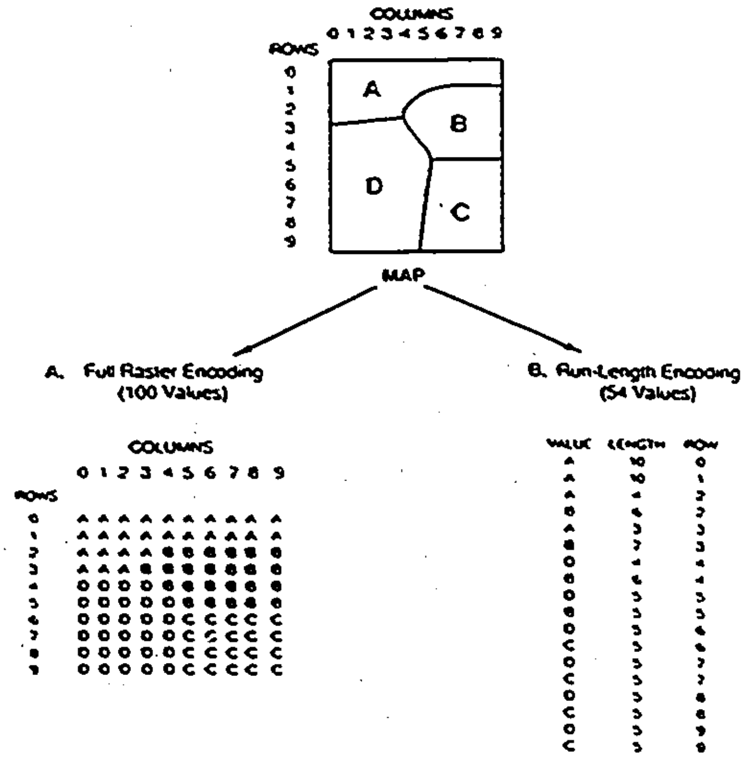

Figure 3.1. The thematic map in the diagram represented as a full raster data structure (a) and as a run-length encoded raster structure (b). Note that the run-length encoded structure requires approximately half the values of a full raster data structure. (modified from Burrough, 1987)

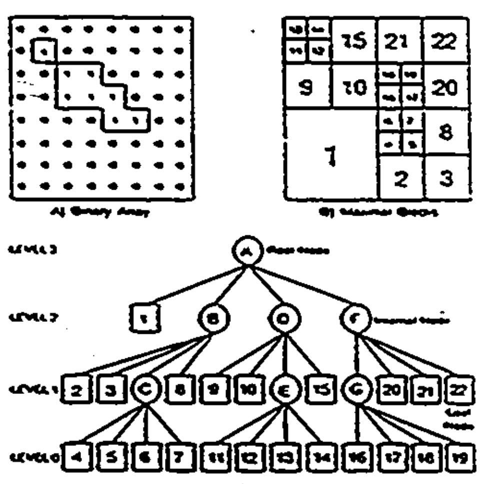

Figure 3.2. The full raster structure in A shown as a quadtree structure in B. Note that blocks are only subdivided if they are not homogeneous. The image can also be shown as a tree as in C. (modified from Bonham-Carter, 1994)

together with the number of times that the value occurs in a run and in which row it occurs.

Quadtrees are another raster model that allows full raster files to be stored in a much more space efficient way and is shown in Figure 3.2. This structure uses variable pixel sizes to represent the mapped features so that smaller pixels are used in areas of finer detail. Quadtrees are hierarchial data structures in which a map represented digitally by successively dividing blocks on the map into quadrants. Pixels in a quadtree structure are commonly indexed using the Morton system of spatial coordinates. The Morton coordinates are a single number along a trajectory that connects all the pixels in an image. This indexing system results in a file where the coordinates are close together for cells that are physically close together on the map. This allows carrying out operations such as identifying the nearest neighbour to a point and for identifying a polygon in which a point is located very efficiently. The organization of data using the quadtree model is discussed in Aronoff (1989), Bonham-Carter (1994) and Sammet (1990).

3.2.3 Vector Model and Structures

The vector model assumes that the map area is a continuous coordinate space where point, line and area features on the map can be defined by lists of coordinates. The limit on the precision of the representation of these features is the size of the word (number of bits) defined in the computer system. In general vector systems allow a finer

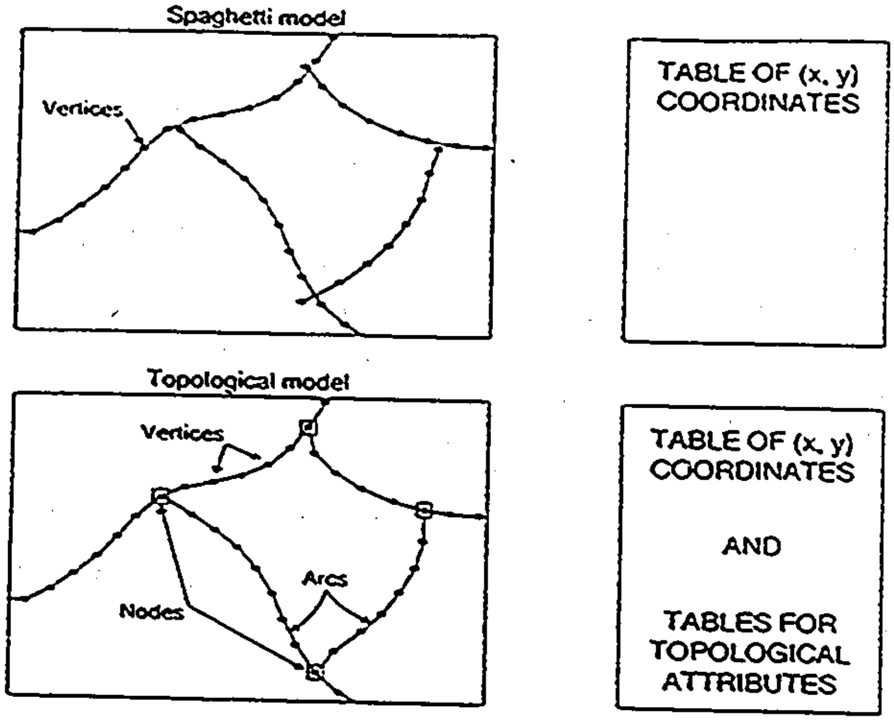

Figure 3.3. The spaghetti and topological vector models. (a) In the spaghetti model, lines are defined by vertices whose spatial locations are recorded in tables of geometric coordinates. (b) The topological model has additional information about the adjacency, containment and connectivity of arcs and nodes (from Bonham-Carter, 1994).

resolution compared to raster models, though with very high capacity storage devices and fast processing speeds, the precision of raster models can approach that of vector models.

A common vector model structure is the spaghetti structure (Figure 3.3(A)). In this structure map objects are represented by an associated table of locational coordinate, usually a separate table for points, lines and polygons, with no topological data. Topology can be defined as a mathematical procedure for explicitly defining spatial relationships between spatial objects. Some of the basic topological concepts are; 1) connectivity, defining where and if arcs connect to each other, 2) closure, defining if arcs connect to define a polygon and 3) contiguity, defining an arc direction and right and left sides. Knowing the topological relationships allows typical modelling procedures such as area analysis, combining adjacent polygons, reclassification and overlaying map features. Though the spaghetti structure has some redundancy in the data because shared arcs between polygons must be repeated, the simple sequential organization of the locational information makes plotting very efficient. Also because there is no topological information spatial analysis is computationally intensive.

One of the most widely used vector structures used to overcome the problems encountered in the spaghetti structure is the topological structure (Figure 3.3(B)). As indicated by the name this model includes topology as well as locational information of map features. In this structure arcs or lines are the basic spatial element. The arc starts and ends on a node while the intermediate points defining the shape of the arc are called vertices. A polygon is an area defined by a closed chain of arcs. Typically, in the topological model, tables are created to record the topological information for each of these four spatial elements.

3.2.4 Attribute Data

The tables containing the topological information for the objects on a map, described above, can be called spatial attribute tables. Often it is necessary to know other information about objects on a map that is nonspatial. For example knowing whether an arc on a map is a road, geological contact or fault trace is important nonspatial information. Polygons identifying parcels of land having various landuse classifications may have a number of attributes indicating soil type, population, access to major roads and so on. This information is stored in nonspatial attribute tables structured such that the rows are keyed to the objects or entities on the map and the columns are the attributes. Both vector and raster models can have nonspatial attribute tables.

3.3 Spatial Data Transformations

Many different data transformations, the process used to change the manner by which a spatial entity is represented in a GIS, can be carried out in a GIS. These transformations can be grouped into two types: geographic space transformations and spatial data transformations. The former type include geometric correction operations, projection transformation, mosaic or edge matching and clipping while the latter involve the manipulation of the principal types of spatial data objects, namely points, lines and areas. Spatial data transformations allow the creation of new entities and attribute data from the original source data. These are some of the most powerful tools associated with a GIS and are used extensively in this study. Two of the most common transformations, point-to-area and line-to-area as used in this study are discussed below. It is noted that there are also many spatial transformations between different data models and structures though they are not discussed here.

3.3.1 Point-to-Area Conversions

Much of the source data used in this study were collected at points. The airborne magnetic and VLF surveys took measurements at points along flight lines, the gravity survey was taken at ground stations spaced at 8 km and many observations used to generate the geological map could be considered to point locations at a 1:20000 scale. Geochemical information from till surveys and lake sediment surveys were also collected at point locations and converted from point information to a surface in this study. Bonham-Carter (1994) identifies several methods for carrying out point-to-area conversions based on the level of measurement of the point attribute being considered and whether the points are natural spatial objects (such as sink holes) or imposed objects for sampling. The primary method for natural spatial objects is density mapping. For imposed sample points either interpolative methods or non-interpolative methods can be used.

Non-interpolative methods are generally most appropriate for, though not limited to, point attribute data measured on a categorical measurement scale. These methods include converting points to a cellular grid, converting points to circles, converting points to Thiessen polygons, converting points to Thiessen polygons and then imposing a confining circle, and converting points to catchment basins. The lake sediment data for this study was converted to areas using this last method. This was the most appropriate for lake sediment data because the lake sediments are representative of the area draining into the lake and the catchment basin is the most likely zone of influence for the sample. The catchment basins in this study were constructed manually using a topographic map such that there was only one sample per catchment basin. Automated methods for determining catchment basins from digital elevation models can be used (Jensen and Domingue, 1988). If more than one sample is located in a catchment basin, an averaging rule for aggregation must be applied.

Interpolative methods are most appropriate for attribute data that is spatially continuous. In general the interpolation methods involve estimating the value of the modelled variable at points between the known sample points, usually on a square lattice, a process which is called griding. These points on the lattice can be treated as the centre of a grid cell or pixel to create a raster image or isolines can be threaded through the points to create a contour map. Some of the many methods of surface modelling used to convert points-to-areas include triangulation, distance weighting and kriging. The till data used in this study was converted to a surface using the kriging method. Further information on interpolative methods can be found in Watson (1992) and Lam (1983).

Kriging and Variograms

Kriging is a weighted-moving-average interpolation method where the set of weights assigned to samples minimizes the estimation variance. The variance is computed as a function of the variogram model and locations of the samples relative to each other, and to the point or block being estimated. Variograms, an integral part of the kriging process, are used to measure quantitatively how well one sample represents another at a different location of a given distance. The variogram or semi-variogram is a plot of the variance (one half the mean squared difference) of paired sample measurements as a function of the distance and direction between samples. For a comprehensive explanation of kriging see Isaaks and Srivastava (1989). Variograms and kriging were carried out using a software package called GEOEAS (Englund et al., 1988), a collection of interactive programs for performing geostatistical analyses of spatially distributed data, running in a PC DOS environment.

3.3.2 Line-to-area Conversions

In mineral exploration applications, as well as many others, it is important to know the proximity or distance from a feature. Examples for mineral exploration applications would include knowing the distance from a geologic contact or fault (line object), a fault intersection or deposit (point object) and lithologic units (area object). One approach to measuring proximity is to dilate the spatial objects resulting in their expansion. This process is also known as buffering or spreading and can be applied to point, line or area objects in either vector or raster data models. In this study knowing the proximity to different geologic contacts was critical to applying the deposit model.

An example of determining proximity to the contact of subvolcanic tonalitic intrusions, an important heat source, is shown in Figure 3-4(a)-(b). Generating a "proximity map" from a vector map generally requires 2 steps; 1) extracting the line feature of interest and 3) generating corridors or buffers of a known width around the vectors. For geological contacts and faults this process requires a two dimensional assumption that we have vertically dipping contacts so that the distance that we are from the contact at the surface is the same distance at depth. This assumption is obviously not completely true, however, in general the lithologic contacts are very steeply dipping for this area. Figure 3.4(a) shows the vector outline of the tonalite sills. For the tonalite sills, eight buffers with a width of 0.5 km were made (Figure 3.4(b)). The buffers are assigned a class value of 1 through 8 as they progress outwards from the contact. The distance from the tonalite subvolcanic sill contact can now be established for any point on the map, such as a mineral deposit, by sampling the map and determining the class of the corridor at that point (with an error of plus or minus the width of the buffer).

3.4 Tools for Spatial Analysis

GIS provide powerful tools to assist in the process of spatial analysis and map modelling. These operations can be carried out directly on map layers, indirectly on tables of attributes linked to spatial map objects, or some combination of map objects and table attributes. Results can be output as a map or as attribute tables and may involve nonspatial as well as spatial attributes. Analysis can involve a single map, two maps or

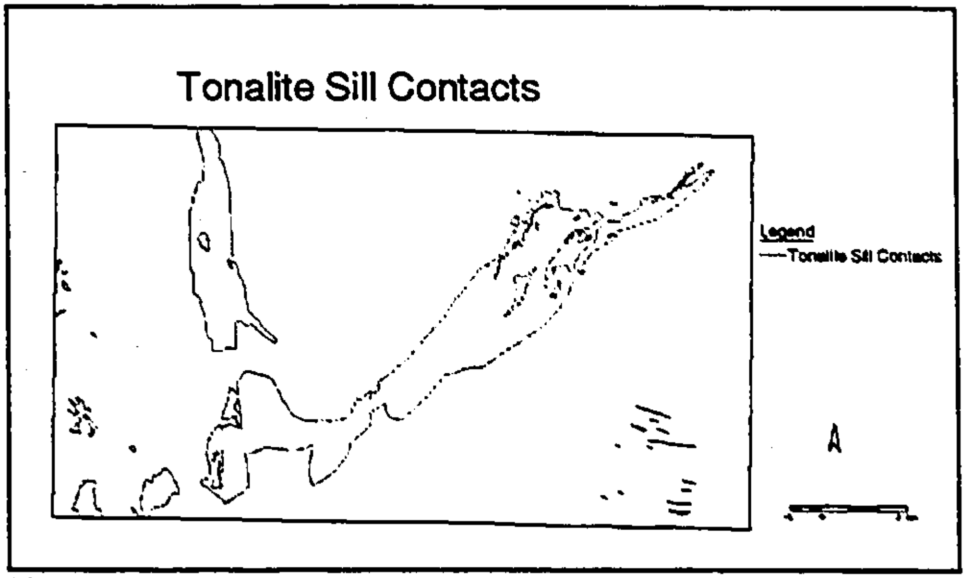

(a)

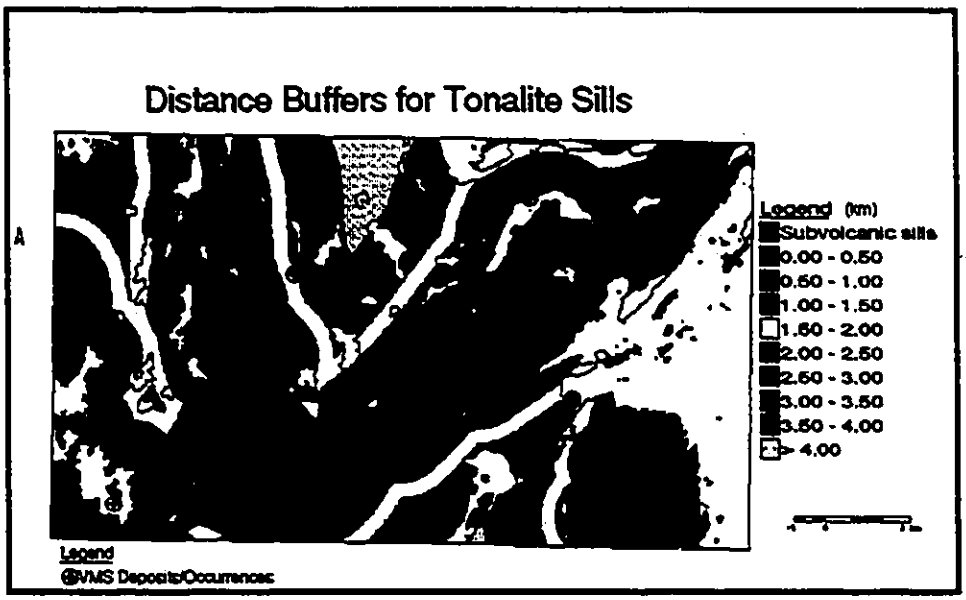

(b)

Figure 3.4 (a) - (b). An example of transforming lines to areas by creating distance buffers. a) vector outline of subvolcanic sills. b) eight distance buffers around the contact, each buffer having a width of 0.5 km. Note that the subvolcanic sills have been "stamped" back on the buffer map so that the buffers extend outwards from the subvolcanic sills only.

many. Potentially the most significant tools for analysis in the GIS are those that provide the ability to combine spatial data from different sources on two or more different map layers. Some of these tools are used frequently in this study and are mentioned here very briefly to provide a foundation for following discussion.

3.4.1 Reclassification

Classification is generally used to reduce the complex nature of many types of information and involves the ordering, scaling and grouping of data. It is one of various methods used in the more general concept of generalizing maps. Other means of generalizing maps may include simplification, symbolizaiton and induction (SPANS, 1993). It is an operation that is generally performed on a single map.

In this study, almost all of the original data went through a classification process in order to make the often complex and overwhelming amount of data more useable in the context of the exploration model. The geochemical and geophysical data, examples of ratio scale data, were classified using classification tables that contained breakpoints that grouped the data based on a percentile scale. Mineral deposit data actually went through a classification, where all deposits were classified as VHMS deposits or other, followed by a simplification process, where all non VHMS deposits were removed. The bedrock geology map, an example of categorical data, was grouped according to major lithological types. In this study a lookup table was constructed (see Table A1, Appendix

A) that relates the class of the original map to the class or the output map. The original 1:20000 mapping resulted in 94 different lithologic categories (see column 3 in Table A1). In the context of the exploration model all this information was not necessary and, in fact, complicated the modelling. Whether a felsic flow was quartz-phyric, fragmental or plagioclase-phyric did not modify the importance a felsic flow had with respect to its relationship to VHMS deposits. All the subunits of felsic flows were simply reclassified as felsic flows. In general, the critical information necessary to represent the exploration model could be gleaned from a geological map that showed the major lithologic types resulting in the output map classes shown in the last column in Table A1. The actual reclassified map is shown in Figure 2-3.

3.4.2 Tools for Map Combination

Ultimately, once a model has been established, data collected and transformed to represent the critical components of the model, there is a need to combine the spatial data to describe spatial associations and use models to make predictions related to the spatial information. A number of tools for combining maps are available in most GIS and some of the ones used this study are described below.

Join

Commonly in a GIS study, spatial information critical to the investigation is

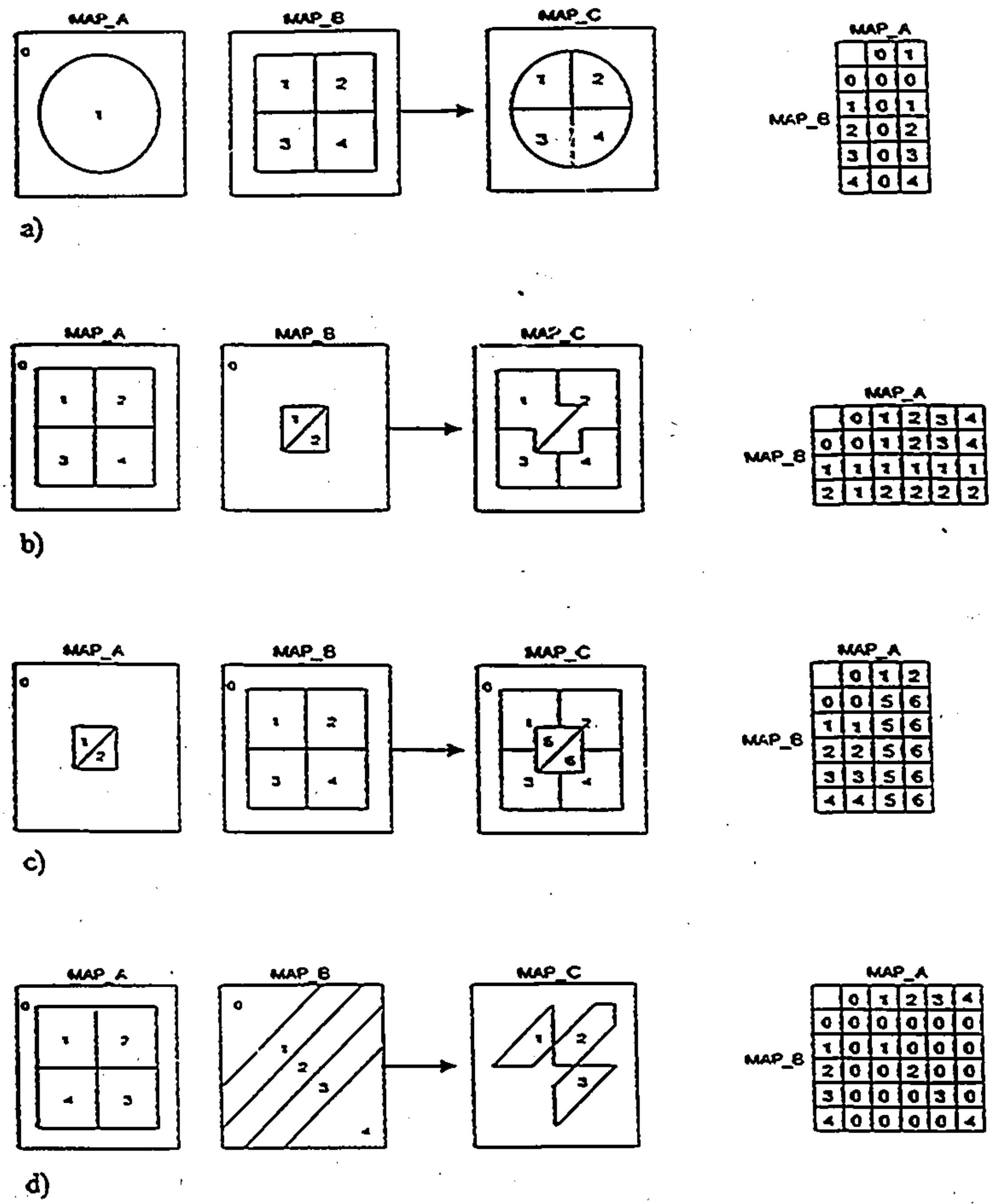

Figure 3.5 (a) -(d) a) Two map overlay in which MAP_A is imposed on MAP_B, b) Two-map overlay illustrating the join operation (MAP_B takes priority over MAP_A), c) Two-map overlay showing the stamp operation and d) example of matrix overlay or compare operation. (modified after Bonham-Carter, 1994)

found on two or more adjacent map sheets or the data is collected over the study area in blocks over an extended period of time requiring the map sheets to be joined together to form a continuous geographical coverage. The process of combining two maps so that map classes that are the same on each map will form a continuous coverage may be called a join operation. The geologic mapping for the Chisel-Anderson map sheet in this area was carried out over three summers moving from west to east resulting in three separate maps for the single study area. At the end of the second and third field seasons an adjacent map sheet was joined to the existing map. An artificial example is shown in Figure 3.5 (b) to demonstrate the join process.

Impose

It is often necessary to cut away portions of a map that lie outside of the area of interest. The process where one map is overlayed on a second map so that only the area underlying the first map is considered in any further modelling or map analysis may be called an impose operation.

The geophysical and geochemical surveys used in this study extended over a much larger area than where the detailed geological mapping was carried out. The decision was made to limit the modelling to the area covered by the detailed geologic mapping. This was carried out in the GIS by first reclassifying the geology map so that it contained only one class: land. The resulting single class map became the "basemap" and was used to impose the limits of the modelling on all the other input maps. An example of the impose or "cookie cutter" process is shown in Figure 3.5(a).

Stamp

A third map overlay operation that is useful for investigating spatial patterns involving two maps is known as the stamp operation. In this process information from one map, usually a single class map, is "stamped" on the second map so that the information on the second map is replaced by the information from the first map. In this study the areas underlying subvolcanic tonalite intrusions (important as a heat source but not for hosting VHMS deposits) were stamped on predictive maps to emphasize the potential outside the limits of the intrusions. The stamp operation is shown diagrammatically in Figure 3.5(c).

Matrix (Compare)

The impose, join and stamp overlay operations usually require one of the maps to be a single class map. The matrix overlay is a general way for combining two maps that have multiple classes. If the two maps have the same number of matched classes, it can be a simple but effective method for comparing the maps and identifiying the areas that are the same (or different) on both maps. This method was used in this study to compare the predictive maps generated by different models. The matrix overlay method is

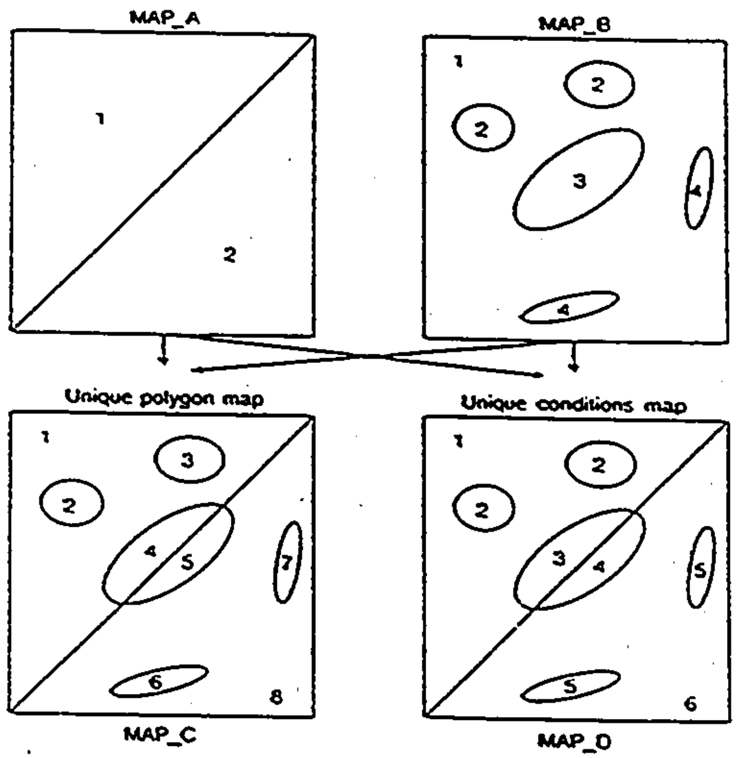

ATTRIBUTE TABLE OF MAP_C
"UNIQUE POLYGONS"

MAP_C	MAP_A	MAP_B
1	1	1
2	1	2
3	1	2
4	1	3
5	2	3
6	2	4
7	2	4
8	2	1

ATTRIBUTE TABLE OF MAP_D
"UNIQUE CONDITIONS"

MAP_D	MAP_A	MAP_B
1	1	1
2	1	2
3	1	3
4	2	3
5	2	4
6	2	1

Figure 3.6. Diagram illustrating the generation of unique polygon overlay and a unique conditions overlay. (from Bonham-Carter, 1994)

illustrated in Figure 3.5(d).

Unique Conditions

One of the most powerful map combination tools that results not only in an output map but also a table that contains information from the input maps that is directly linked to the resulting output map is known as the unique conditions overlay. One of the reasons that this method is so powerful is that modelling operation can be carried out on the table, not on the map itself. The overlay map is reclassified based on the new results appended to the overlay table. Because the overlay map is not directly involved in the modelling, it allows modelling operations to be carried out outside of a GIS, providing a great deal of flexibility. The results can be brought back into the GIS and linked to the overlay map. The unique conditions overlay can result in unique polygons, where each new polygon created in the overlay process is assigned a unique class, or a unique conditions map, where polygons that are created in the overlay process are assigned the same class value if their characteristics are the same, as defined by the input maps.

Unique conditions overlays can be carried out using two or more maps where the maps are not restricted by the number of classes in the map (though the GIS may have some restrictions on the number of unique conditions that can be handled by the software). In this study the unique conditions overlay was used in the weights of evidence, area weighted logistic regression and Dempster-Shafer models. A simple example of a unique conditions overlay for two maps is shown in Figure 3.6.

3.5 SPANS GIS

The GIS used in this study is called SPANS, a PC based system developed by an Ottawa company, TYDAC Technologies (SPANS, 1993b). It is a general purpose GIS but provides very strong analytical functionality, efficient data structures and flexibility in interfacing with other software outside the GIS that made it an excellent system for modelling mineral-potential. Some of the specifics are described below.

3.5.1 Software

The SPANS software is a hybrid GIS incorporating both vector and raster data models. The primary raster data structure was the quadtree data structure, especially effective for raster data compression, and carrying out operations such as identifying the nearest neighbour to a point and for identifying a polygon in which a point is located. Library information including, attribute tables, unique conditions (overlay) tables, raster headers, map legends and titles and classifications can all be exported as ASCII files allowing easy interface with third party or custom software. Illustrations and maps for output can be enhanced using the companion desktop-mapping package SPANSMAP. Data import and export modules allowed easy interface with a variety of other raster and data structures supported by other GIS (such as ARC/INFO).

The PC version of SPANS requires the OS/2 Extended Edition operating system.

3.5.2 Hardware

The hardware used in this study was a desk top Personal Computer running on an Intel 486-66 mhz processor. Memory included 16 MB of RAM and 1.2 GB of hard disk storage. The colour monitor was driven by a high resolution (1025 X 768) colour video card with 2 MB of video RAM. Hardcopy was generated on an HP 300XL paint jet plotter.

The following chapter discusses the second step in the modelling process - building the database. There are two important components at this step 1) capturing raw data as a digital database on the GIS and 2) processing the raw data to reflect information that can be considered as evidence for the exploration model.

4. Spatial Datasets

4.1 Introduction

A major component of this project, and any GIS project that involves the integration of a number of different data layers, is the assemblage of the various spatial data to be used in the study in digital form and properly registering it so that the spatial components overlap correctly. Because the data used in this study were assembled specifically for this project without the intention of long term maintenance or for multiple users, the words "spatial datasets" are used instead of "database" (Bonham-Carter, 1994). The term "database" or "custodial database" is more appropriate for large amounts of data that are gathered for the purpose of serving as data sources for a large group of users over and extended period of time. The custodial database should also employ data standards for data entry and data maintenance that can be applied by different groups of people over time (Bonham-Carter, 1994).

The choice of datasets used in this study was guided primarily by the exploration model as discussed in the previous chapter. Data that was captured from map information and input as attribute tables or other sources but not directly suitable for use as evidence, is considered as "raw data". Data that resulted from processing the raw data and could be used as a predictor layer is considered to be "derived" data. The processing and production of derived datasets are discussed in section 4.3. The raw datasets are summarized in Table 4.1 and discussed briefly below with respect to source, data structure, data format and error. All source data were transformed to the working map projection for this study which is the Universal Transverse Mercator (UTM).

4.2 Raw Data Descriptions

4.2.1 Bedrock Geology

Geological maps of the bedrock were available at two scales, 1:50000 and 1:20000. The 1:50000 scale maps were manually digitized as topological vector data from a geological compilation of the sheets for NTS 63/J/13 (Fedikow et al., 1993) and NTS 63/K/16 (Fedikow et al., 1889) using the TYDIG (a module of the SPANS GIS package) digitizing software. These data were imported into the GIS and converted to a quadtree raster format with a digital spatial resolution (size of smallest quad or pixel) of approximately 10 m. The 1:20000 scale map (Bailes, 1992a), generated as the result of mapping during the course of this study, was also digitized manually and imported into the GIS with a digital resolution of approximately 10 m. The digitizing was done so that all ninety-four lithologic units identified on the map were retained. A lookup table showing the relationship of the original units and units created by grouping similar units is found in Appendix A (Table A1).

Many sources of error are recognized throughout the history of these maps. The 1:50000 maps are the result of compiling information from a number of maps ranging in scale from 1:63,360 to 1:5000 (Fedikow, 1993; 1988). Spatial errors in the original maps would result from inaccuracies in pace-and-compass distance measurements and distortion in aerial photographs used to derive the base maps. These errors would then be

Table 4.1. Summary of datasets used for generating evidence maps to predict VHMS potential in the Snow Lake area.

DATA TYPE	DESCRIPTION
GEOLOGY	Geology from field mapping at scales of 1:50000, 1:20000, and 1:5000
ALTERATION	Alteration was mapped based on mineral assemblages 1)qtz-cp-plag, 2)chl-bio-amp, 3)cp-hem for 1:20000 only
GEOCHEMISTRY -till -lake sediments -drainage basins -whole rock	A total of 346 lake sediment samples were analyzed for 32 different elements using AAS and INAA. Regional tills were collected and analysis of 240 samples, 32 elements done for <2 and <80 mesh. Whole rock has not been input into GIS
VLF	Collected by GSC Skyvan using Hertz Totem VLF unit at 500 m EW line spacing resampled to 100 m GSC Open file 2300.
GRAVITY -Bouger -Free Air -Vertical Gradient	GSC Geophysical Data Centre, National Gravity Bank, 2 km resolution resampled to 200 m All calculated.
MAGNETICS - Total Field - Vertical Gradient - Horizontal Gradient	GSC Geophysical Data Centre, Regional Coverage, 800 m spacing resampled to 200m
MINERAL DEPOSITS	Compiled from 1:50000 maps (Fedikow et al. 1988, 1989)

carried over as this information was transferred to the compiled 1:50000 base. The minimum resolutions of 1:5000, 1:50000 and 1:63360 scale maps, based on a 0.5 mm line width, are 2.5 m, 25 m and 31.6 m respectively (Fisher, 1991). Since much of the original data has been taken from 1:63,360 scale maps, the true accuracy of the 1:50000 compilation maps is in the order of 32 m. Further positional error is introduced during the transfer of the source map to a digital format through digitizing. Though it is not dealt within this study, digitizing error models have been discussed by Maffini et al. (1989) and Keefer et al., (1990). Positional errors for the 1:20000 scale geology map are also present due to errors generated through pace-and-compass distance measurement and distortion of aerial photographs. The inherent accuracy of a 1:20000 scale map based on a 0.5 mm thick line is 10 m.

The 1:20,000 scale mapping was completed during this project so very little error should be expected because the data is out of date, however the 1:50,000 compilation maps were based on maps dating back to 1935 (Fedikow, 1993) so some inaccuracies may be present due to changes in the understanding of the geology over that time period. Other errors such as missing contacts (logical errors) have been checked manually and none were found.

4.2.2 Alteration Map

As part of the 1:20 000 bedrock mapping project, alteration data were also collected. Six main types of alteration were identified based on visible mineral assemblages. Bailes and Galley (1993) identified the following alteration types: (1) silicification, (2) Fe/ Fe-Mg metasomatism, (3) pyritization, (4) epidote/hematite, (5) amphibole and (6) alteration pipes, and mapped them as mutually exclusive zones. Accordingly, the polygons digitized on this map were identified as being predominantly one of these alteration types, see for example Figure 2.4.

The main error component associated with the alteration map would be contact positions. Mapping was carried out using pace-and-compass distance measurements and aerial photos scaled to 1:20000. Data recorded in the field was transferred to a mylar base map representing another source of potential positional error. Accuracy on a 1:20000 scale map is 10 m assuming a 0.5 mm line width and where the capture and transfer of field data to a base map is error free.

4.2.3 Lake Sediment Geochemistry

A lake sediment geochemical survey was conducted by GSC over the whole of NTS sheet 63/K/16, and over the western two-thirds of 63/J/13. A total of 346 samples were collected at a sample density of approximately 1 per 6 km^2 in the Snow Lake area with 79 falling within the study area. The sample distribution is shown in Figure 4.1. Samples were analyzed for 42 elements using atomic absorption spectrometry (AAS) and instrumental neutron activation (INAA). The atomic absorption method determined values for Zn, Cu, Pb, Ni, Co, Ag, Mn, As, Mo, Fe, Hg, LOI, U, F, V, Cd, and Sb. Acceptable values from INAA included Au, As, Ba, Br, Co, Cr, Cs, Fe, Hf, Na, Rb, Sb, Sc, Ta, Th, U, W, La, Ce, N, Sm, Eu, Tb, Yb, and Lu. The data were input into the GIS as point attribute tables, with a record for each sample containing geographic coordinates followed by element concentrations, see Friske et al., (1995; in prep).

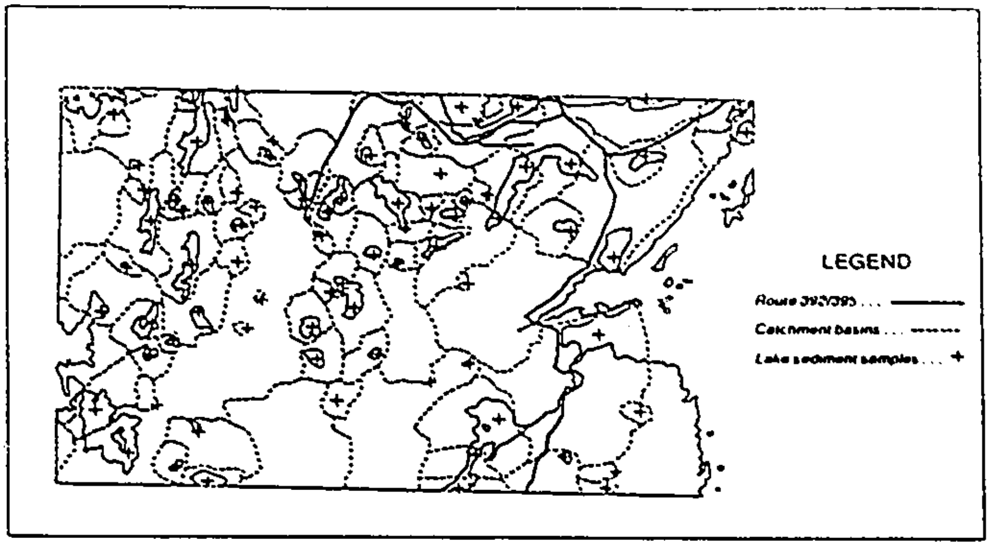

Figure 4.1. Lake sediment sample locations. A total of 79 samples were collected within the Chisel-Anderson map sheet.

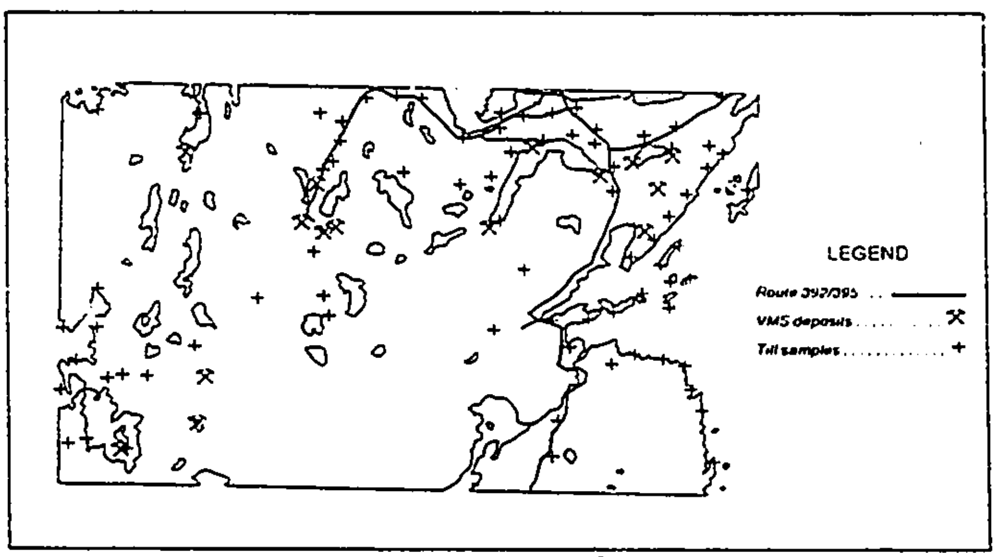

Figure 4.2. Till sample locations. A total of 84 samples were collected within the study area.

The primary source of error in this data set is associated with the analytical data. Quality control of the analytical data is maintained by monitoring control references and blind duplicate data. A control reference, a blind duplicate and a field duplicate are inserted into each block of 20 samples being analyzed. The field duplicates are used to measure sampling variability while the blind duplicates allow checks to be made on the analytical error. Knowing the magnitude of the analytical error relative to the sampling error is useful for interpreting the results. The control references are used to check bias (accuracy). The mean and standard deviation are calculated for all the elements for each reference sample. Results are only accepted if control reference and blind duplicate values are within predefined limits specified to the company doing the analysis, for example, control reference data must be within 2.5 standard deviations (Frisk, pers. com.). General discussions on geochemical survey methods and analysis can be found in Garrett (1974) and Frisk and Hornbrook (1991). Positional error is not a significant factor as sample locations can be determined well within the limits of the size of lakes being sampled.

4.2.4 Catchment Basin Map

A map of the lake catchment basins was prepared with the use of 1:50000 scale topographic sheets and digital plots of the sample locations. Basins were constructed by manually tracing the drainage divides defined by the contour lines on the topographic map so that there was one basin for each sample. The basin outlines were manually digitized (Figure 4.1), input into the GIS as vectors in arc-node format and then rasterised. The catchment basin map was then linked to the geochemical attribute table allowing map construction for any variable in the table.

Position of the drainage divides are subjective being based on a visual interpretation of contour lines on 1:50000 topographic maps. In general the terrain is very flat lying and horizontal distances between contours (7.6 m contour intervals) is commonly over 1 km and up to 4 km. This combined with errors related with digitizing would suggest that the minium error associated with the placement of the drainage divides to be in the order of 1 km.

4.2.5 Till Geochemistry

Both regional and detailed till sampling surveys were carried out in the study area (Kaszycki, 1989; Kaszycki et al., 1992). C-horizon till and humus were sampled at 254 sites for the regional survey and C-horizon, B-horizon and an organic rich fraction were sampled at 86 sites (around Chisel, Chisel North and Linda-2 deposits) for the detailed study. The <2μ size fraction of all till samples has been analyzed by AAS for Ag, As, Cd, Co, Cr, Cu, Fe, Hg, Mn, Ni, Pb, and Zn. The <60μm size fraction of all till samples has been analyzed by INAA using a standard "Au-plus 34 element" package. The heavy mineral fraction for C-Horizon till samples has been extracted and analyzed for visible gold. These multivariate point data were input as tables with records with geographic coordinates, followed by element concentrations as attributes.

Figure 4.2 shows the distribution of till sample locations and indicates irregular and incomplete coverage of the study area. Though this is not an error by itself Burroughs (1986) identifies this incomplete coverage as a possible source of error requiring well-defined methods for using this data with respect to the whole study area. Standard analytical quality control for till surveys is monitored by inserting 10% standards and blind duplicates within each sample batch allowing checks on precision and accuracy respectively (Kaszycki, 1989). Analytical results used in this study are preliminary and errors can be assumed to be present though no results from analysis of field duplicates or control samples were obtained with the data.

4.2.6 Very Low Frequency (VLF) Electromagnetics

Included as part of the airborne radiometric survey was a VLF electromagnetic survey using a Totem 1A VLF unit (Hetu, 1991). Georeferenced digital raster files of Total Field VLF and Quadrature (out-of- phase component) VLF, resampled to 100 m pixels were imported directly into the GIS.

4.2.7 Gravity

Gravity data for the Snow Lake area were obtained from the GSC Geophysical

Data Centre (GDC). These data comprise part of the regional national gravity mapping database, where samples were collected at average station spacings of approximately 8 km (Goodacre et al., 1987). Data were obtained as georeferenced digital raster files resampled to a 2 km grid and included Bouguer anomaly, free air anomaly, vertical and horizontal derivative maps.

Positional and analytical errors are not published, however, reports submitted with the data by the contractor collecting the data, indicate that the gravity data has an accuracy of plus or minus 0.9 milligals and a horizontal positional accuracy of plus or minus 100 m (Miles, 1995 pers. comm.)

4.2.8 Magnetics

Airborne magnetic data were also obtained from the Geophysical Data Centre These data were part of the national regional coverage, with flight lines spaced at 800 m. Digital raster files were georeferenced and resampled to 200 m pixels by GDC, who supplied total field and calculated vertical and horizontal gradient grid files.

4.2.9 Mineral Deposits

Information regarding mineral deposits for map sheets 63J13 and 63K16 was derived from mineral deposit and occurrence summary reports (Fedikow et al., 1993 and Fedikow et al., 1989) and entered manually as digital tables in the GIS. The tables included information on location, name, mineral occurrence classification, size and main commodities.

Deposit sites are given as UTM coordinates, suggesting that the location is a point known to an accuracy of within of one meter. In reality deposits are areas that can extend parallel to the surface for distances in the order of 100's of meters. This becomes significant when a deposit is near a contact between two lithologies. Sampling a geology map at deposit points may result in associating an incorrect lithology to a deposit.

4.2.10 Other Datasets

A number of other datasets were collected for the study area though were not used directly in the modelling process. These datasets are summarized in Table 4.2.

Table 4.2. Summary of data collected but not used in this study.

DATA TYPE	DESCRIPTION
RADIOMETRICS -U, Th, K -U/Th, U/K, K/Th	Collected by GSC Skyvan using 256 ch gamma ray spectrometer at 500m line spacing EW. GSC Open File 2300
RADAR	Collected by CCRS, Data Acquisition Division, C band (HH), 15 m ground resolution.
LANDSAT TM - Bands 1-7	Landsat TM acquired from CCRS at 30 m resolution
DIGITAL ELEVATION	Digital Terrain Elevation Data from Defense Mapping Agency, 1:250000 coverage

4.3 Data Processing

Having compiled the spatial datasets, the next step is to process the data to extract evidence critical to the prediction of VHMS deposits, bearing in mind the guidelines imposed by the exploration model. There are three different approaches used to process the data: 1) generating buffers with a known width around linear features, such as contacts, to help investigate proximity relationships, 2) generating surface maps from point attribute data, which involved statistical treatment of the data such as kriging or principal component analysis and 3) enhancement through mathematical manipulation such as taking the spatial derivatives of VLF data. These processes are discussed below in describing how evidence maps were created through processing the various initial data layers to represent the conceptual model. The evidence maps are considered under five types of evidence or "factors" to help facilitate the understanding of how the various evidence layers contribute to the final result. The five factors are 1) geochemical factor, 2) alteration factor, 3) stratigraphic factor, 4) heat factor and 5) geophysical factor.

4.3.1 Geochemical Factor

Glaciation in the Snow Lake area, as in much of Canada, has resulted in many lakes and abundant till cover. Sampling tills and lake sediments for geochemical analysis has proven an effective method for selecting target areas related to anomalous mineralization (Hornbrook et al., 1990). Both lake sediment and till surveys have been carried out in the Snow Lake area and are available as digital point files. To be used in an integrated study, especially using GIS, it is effective to process this point data to generate maps of geochemical surfaces that show the spatial behavior of the elements related to VHMS deposits.

Tailings ponds are present at the Chisel Lake deposit area and at the Anderson Deposit area. It is reasonable to expect that these may cause contamination of lake sediment samples or till samples that have been collected down stream and result in false anomalies in these areas. However, the sampling density included enough samples in these areas that were not in the immediate drainage of the tailings ponds that the overall pattern of the concentrations can be used. The smelter at Flin Flon, approximately 200 km to the west of the study area, may also be a source of contamination. Coring studies of the lake sediments are necessary to evaluate the actual effect.

Lake Sediment Geochemistry

Of the total of 346 samples that were collected in the lake sediment geochemical survey described above, 79 samples fell within the Chisel-Anderson study area.

A map of the lake catchment basins was prepared by plotting sample sites on 1:50000 topographic map sheets and manually digitizing the catchment basins so that there was one catchment basin per sample. Each basin was treated as a spatial entity containing a geochemical sample, and was linked to the corresponding record of the geochemical attribute table.

Typically a frequency distribution of the raw element concentration data shows a marked skewness. Performing a log-transformation on the concentration values often results in a nearly normal distribution allowing statistical tests based on normal distributions to be carried out on the data. Lognormal data is discussed more fully in Ahrens (1954) and Davis (1986).

Since each sample had been analyzed for 32 elements, Principal Component Analysis (PCA) was applied to the logarithmically-transformed data to search for multi-element associations in an effort to reduce the number of variables to be included in the model. Table 4.3 lists the varimax-rotated principal component loadings for the elements analyzed by INAA. The first four components explain over 80% of the total variance. Component scores were added to the attribute table, and component maps for PC-1 to PC-3 are shown in Figure 4.3(a)-(c).

The first component, PC-1, is a combination of Fe, V, F, Ni, Co, Pb, Sb, Mn and Cu and explains 52.1 % of the total variance. Interestingly, the Cu-rich deposits (Anderson, Stall and Rod) are associated with elevated PC-1 scores, indicated by the red-coloured basins in the northwest part of the study area. PC-2 is a combination of Zn and Cd and explains 14.7 % of the total variance. The Zn-rich deposits (Chisel, Lost and Ghost) in the centre of the study area, are generally associated with higher PC-2 scores, although the Stall deposit is also associated with high PC-2 scores. Molybdenum stands

Table 4.3. Principal component loading for first four axes on elements analyzed for by INAA methods.

Variables	PC - 1	PC - 2	PC - 3	PC - 4
Fe	0.945*	-0.064	0.109	-0.042
V	0.918*	-0.122	0.001	-0.043
F	0.907*	-0.160	0.182	-0.069
Ni	0.904*	-0.160	0.041	0.003
Co	0.888*	0.198	0.070	-0.028
Pb	0.860*	0.143	0.052	0.249
Sb	0.787*	0.155	-0.286	0.201
Mn	0.786*	-0.065	0.224	-0.064
Cu	0.693*	0.154	-0.380	0.266
Zn	0.204	0.917*	-0.015	0.200
Cd	-0.272	0.874*	-0.193	0.175
Mo	-0.139	0.118	-0.911*	0.041
Hg	0.020	0.331	-0.066	0.918*
Percent Total	52.110	14.694	9.244	8.469

* Multielement grouping for each principal component.

out on its own in PC-3 showing a strong negative loading implying a deficiency in Mo. It is noted that the average concentration of Mo for lake sediment samples associated with Amisk volcanic rocks is 1.54 ppm while the average concentration for intrusive rocks and sediments is 1.75 ppm. Elevated PC-3 scores have a spatial association with both the Zn rich and Cu rich VHMS deposits. The distinct behaviour of Cu and Zn is consistent with the notion of Cu and Zn-rich horizons in the subaqueous volcanics, but the sample density is inadequate to resolve the spatial variation that one might expect given the details of the volcanic cycles in the stratigraphy.

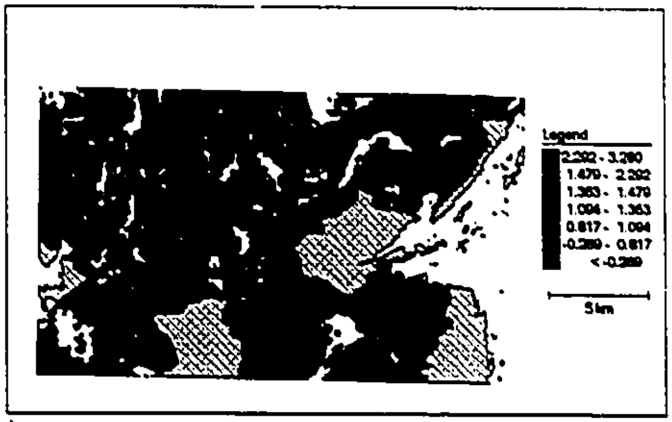

(a)

(b)

(c)

Figure 4-3(a)-(c). Principal component scores for lake sediment chemistry mapped onto catchment basin map. (a) PC1 shows an association of Cu, Pb, Fe, Ni, V, F, and Co and has larger scores in the area of the Cu rich Stall Rod and Anderson mines. (b) PC2 shows an association of Zn and Cd and has larger scores in the area of the Zn rich Chisel Lost and Ghost mines. (c) Mo is the main element for PC3.

Only the first three principal components were used as evidence as no clear spatial association of PC-4 with deposits was observed.

Till Geochemistry

A regional till geochemical survey was carried out over the Snow Lake area in which 254 samples were collected covering the two 1:50000 map sheets NTS 63K/16 and 63J/13. The Chisel-Anderson study area contained 84 samples. Where possible, C and B horizon till samples and organics were collected at each site. The <2 μm size fraction of all till samples has been analyzed by AAS (following an aqua regia leach) for Ag, As, Cd, Co, Cr, Cu, Fe, Hg, Mn, Ni, Pb, and Zn. The <60μm size fraction of all till samples has been analyzed by neutron activation using a standard Au plus 34 element package. All organic samples have been analyzed using a standard ICP-ES package. Preliminary results indicate that both B-horizon and C-horizion samples produce similar geochemical trends. For this study the C-horizion analyses for the <63μm where used to represent the till geochemical component.

Principal component analysis was applied to the till data, but produced no clearly interpretable results. We do not see the same associations in the till data as were observed in the lake-sediment data. Therefore, the spatial distributions of Cu, Pb and Zn data were studied as individual elements, because of their likely value as VHMS predictors. Because the samples were spaced irregularly, and were not uniformly distributed throughout the area, it was decided to use Kriging to generate a surface model for the three elements. The Kriged results for Cu, Pb and Zn are shown in Figures 4.4(a)-(c). A

Table 4.4. Model parameters for variogram plots of ln Cu, ln Pb and ln Zn

Element	Model Type	Nugget	Sill	Range (m)	Direction
ln Cu	Spherical	0.025	0.3	1500	0.0
ln Pb	Spherical	0.45	0.4	1000	0.0
ln Zn	Gaussian	0.01	0.11	1300	0.45

summary of the variogram model parameters used to generate the three maps are summarized in Table 4.4.

The variograms, see Figures 4.5(a)-(c), show that there is autocorrelation present out to a distance of 1 to 1.5 km. The Pb has the shortest range, and Cu the longest range, suggesting that Pb is less mobile than Cu and Zn. It is noted that none of the variograms show a very well defined structure. The variogram for Pb shows the weakest structure and it could be argued that the range is considerably less that 1000 m. The kriging variance was used to screen out areas where the estimated element value is relatively uncertain. The kriging variance is inversely related to sample density, and uncertain areas are predominantly those where the distance to the nearest sample is greater than the range of the variogram.

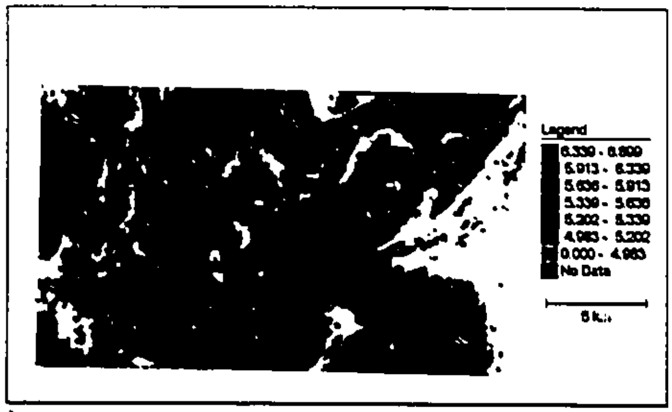

(a)

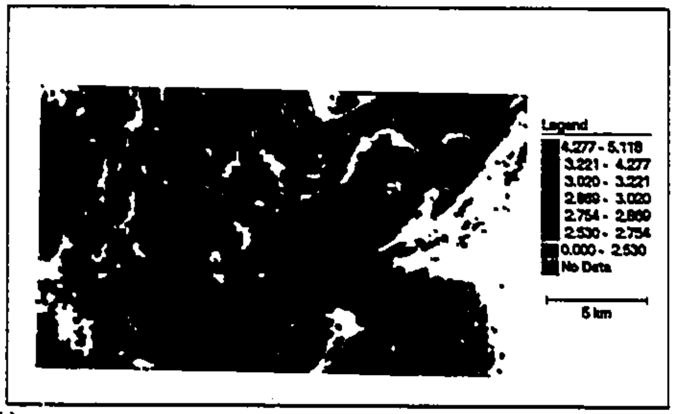

(b)

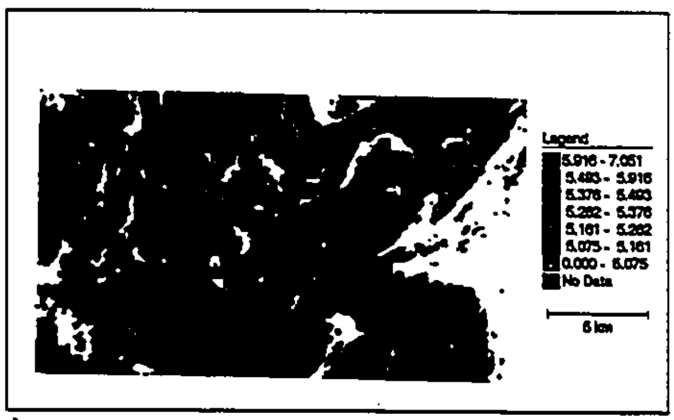

(c)

Figure 4-4(a)-(c). Kriged natural log concentrations of (a) Cu, (b) Pb, and (c) Zn. Small black dots are sample locations and large gold dots are VHMS deposits.

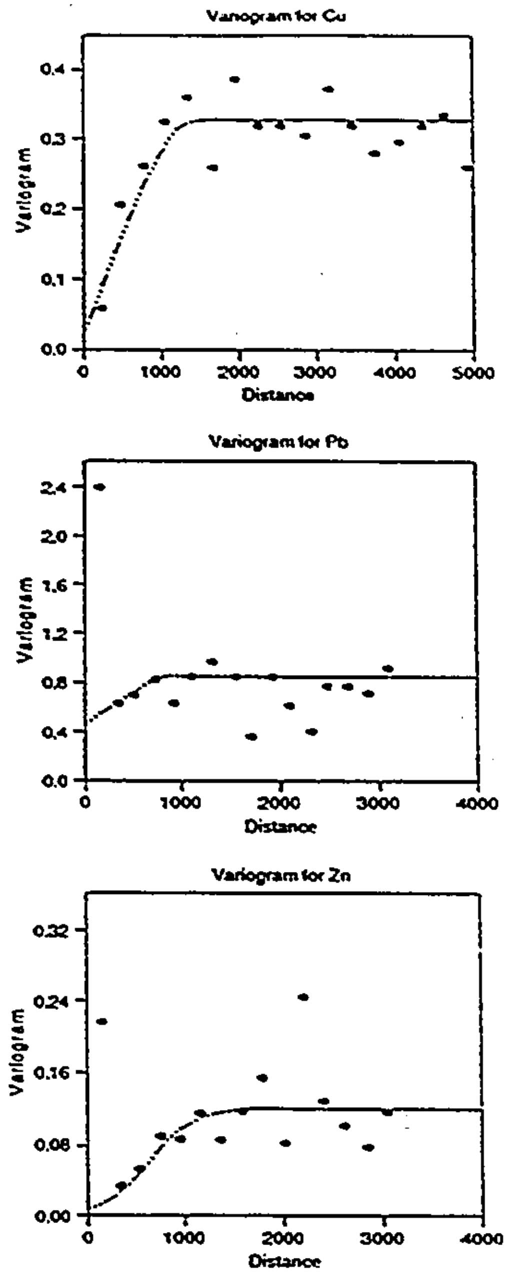

Figure 4.5. Variograms for till data showing the autocorrelation present for Cu, Pb and Zn. Pb has the shortest range, in the order of 1000 m while Cu shows the longest range, in the order of 1500 m.

Stall and Rod are associated with elevated levels of Cu and Zn. Pb and Cu appear to be enriched in a large zone in the central north part of the area, north of the Chisel-Lost-Ghost deposits. The till patterns are quite different from the lake sediment patterns, and again, the till samples are spaced too far apart to resolve the spatial variability that one would expect from the stratigraphy.

In summary six maps were derived from the geochemical data to be used as VHMS predictors: lake sediment PC1 to PC3 (dominated by Zn, Cu, and Mo, respectively) and till Zn, Cu and Pb. The combination of these six maps is used as the *geochemical factor*.

4.3.2 Heat Factor

Essential to the VHMS model is the requirement of a "heat engine" to drive the hydrothermal system which in turn causes alteration of the overlying rocks and eventually the deposition of the base metal massive sulphide deposits. In the Snow Lake area there are three significant subvolcanic intrusions, clearly related to alteration events, that could potentially play this role: these are the Sneath Lake tonalite pluton, the Richard Lake tonalite pluton and the Edwards Lake area dacite dyke complex. Some evidence to support this proposal is discussed below.

The Sneath Lake complex has dimensions at the surface of of approximately 22 km by 2 km and estimated to have a size of over 1.2 X 10^{12} metric tonnes. The Richard Lake tonalite is an order of magnitude smaller, measuring 7.3 km by 1.6 km and estimated to have been over 1.1 X 10^{11} metric tonnes in size. The ingneous mass thought to be the heat source for the Kuroko base metal deposits in the Hokuroko basin Japan, is in the order of 1.5 X 10^{11} metric tonnes (Cathles, 1983) suggesting that the Snow Lake area subvolcanic tonalites would be large enough to drive a prominent geothermal system.

The Amisk Group volcanics have been dated at 1886 Ma using U-Pb zircon ages. These rocks are intruded by the Sneath Lake and Richard Lake tonalite plutons that have U-Pb zircon ages of 1886 Ma nd 1889 Ma respectively supporting the interpretation that these plutons are synvolcanic (Bailes and Galley, 1991).

Geochemically the Sneath Lake Pluton and the base metal-hosting felsic volcanic strata in the Anderson Lake area have low flat REE profiles and low contents of HFS elements. Further, fragments of Sneath Lake tonalite were found in the metal-hosting felsic volcanics in proximity to the Rod and Linda Deposit (Bailes and Galley, 1991).

Large parts of the Sneath Lake pluton have been affected by intense Fe-Mg metasomatism of the same type as that associated with the massive sulphide deposits (Bailes and Galley 1991). A number of discordant alteration “pipes” have been identified in the volcanic stratigraphy underlying the Stall and Anderson deposits that can be traced back to an altered mesotonalite phase in the Sneath Lake pluton (Bailes and Galley, in press).

The dacite sill/dyke complex west of Edwards Lake, although not large enough to generate a prominent geothermal-hydrothermal system on its own most likely helped focus the hydrothermal activity. Extensive silicification and epidotization adjacent to the dykes indicate temperatures in the order of 380° C (Bailes and Galley, in press).

Although not all the factors that need to be considered to argue for a plausible heat source, such as rate of temperature change, porosity and permability of the overlaying strata are considered here, the above observations support the interpretation that these subvolcanic intrusions could be the heat source for the hdyrothermal activity in the Snow Lake area.

Two pieces of evidence can be used to predict favourable thermal conditions: (1) proximity to the large subvolcanic intrusions (tonalite sills) and/or (2) proximity to synvolcanic dyke swarms (predominantly dacites and diorites) that are often associated with the subvolcanic intrusions. This is one of many situations in geological problems were proximity to mapped features is important.

Following the process for generating proximity maps as discussed in Chapter 3, proximity maps were generated for the synvolcanic dykes (Figure 4.6) and the subvolcanic tonalite sills (Figure 4.7) These two evidence maps are used to represent the *heat factor* in the integration modelling.

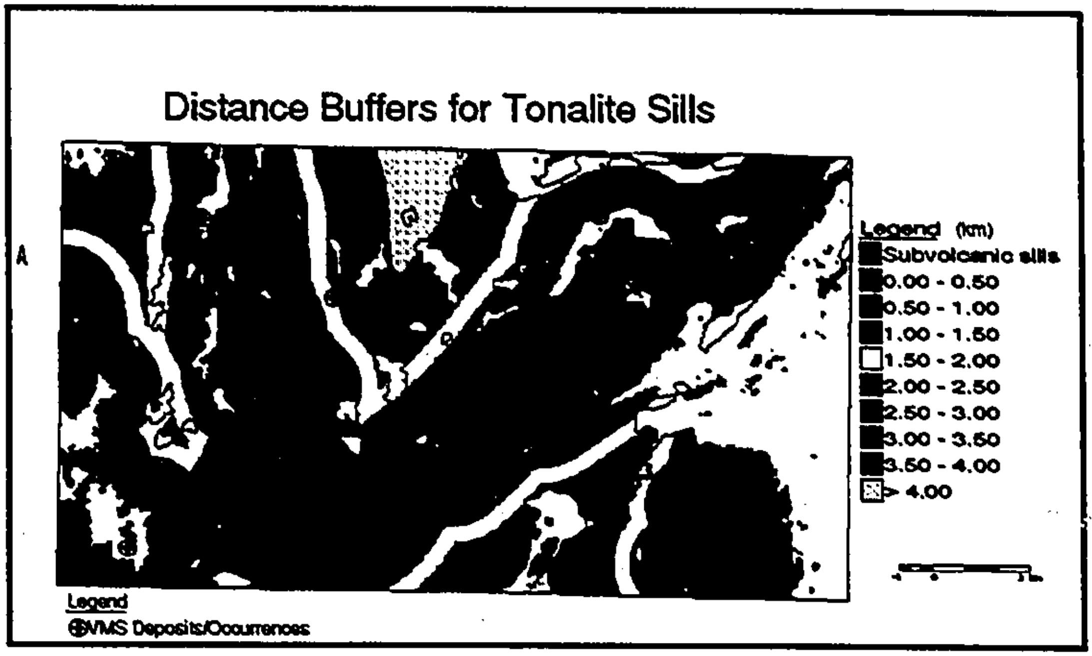

Figure 4-6. Distance buffers around subvolcanic sills. Subvolcanic intrusions can be used as evidence of heat source for driving hydrothermal fluids.

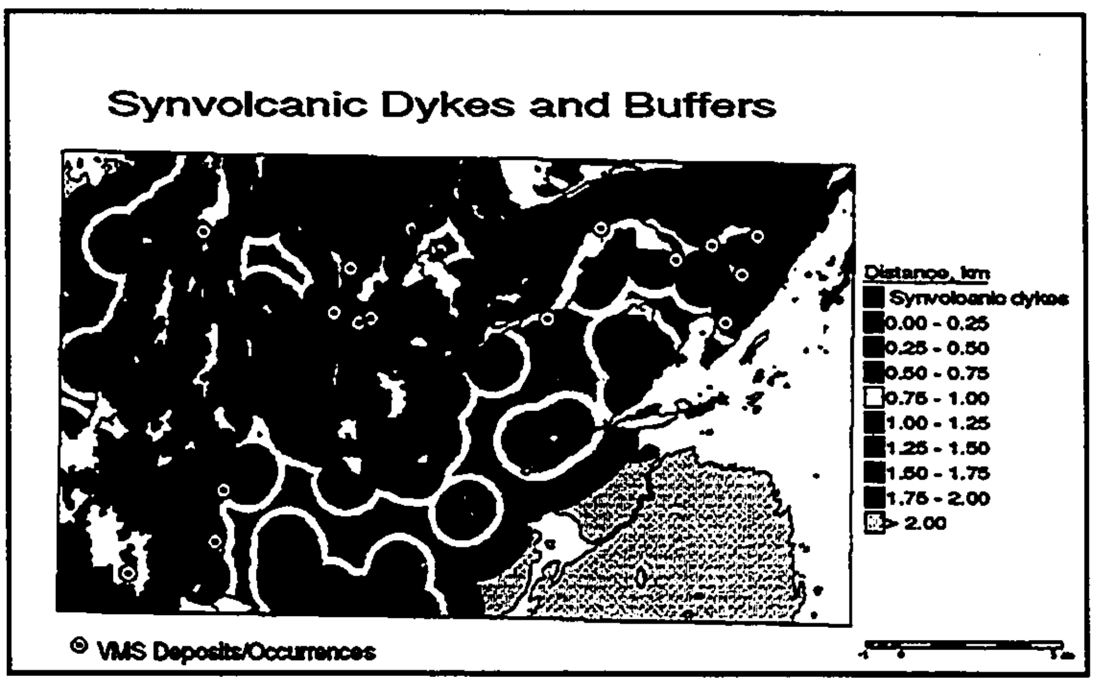

Figure 4.7. Distance buffers around synvolcanic dykes The presence of synvolcanic dykes can also be used as evidence for a heat source.

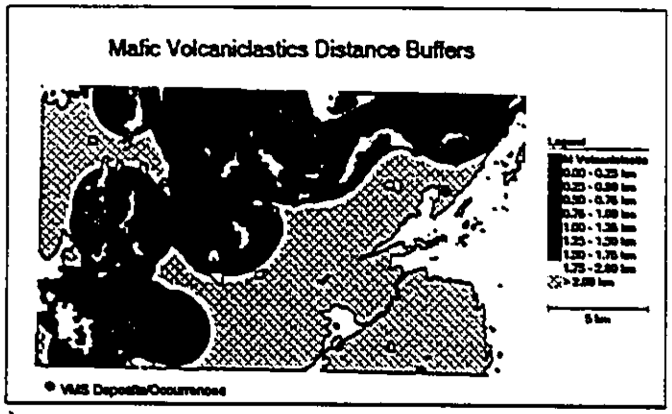

(a)

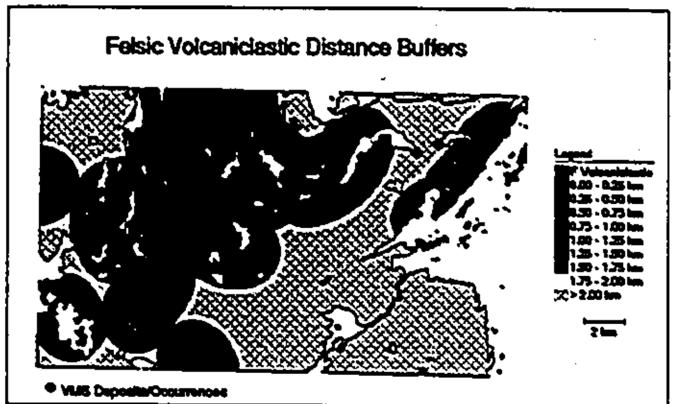

(b)

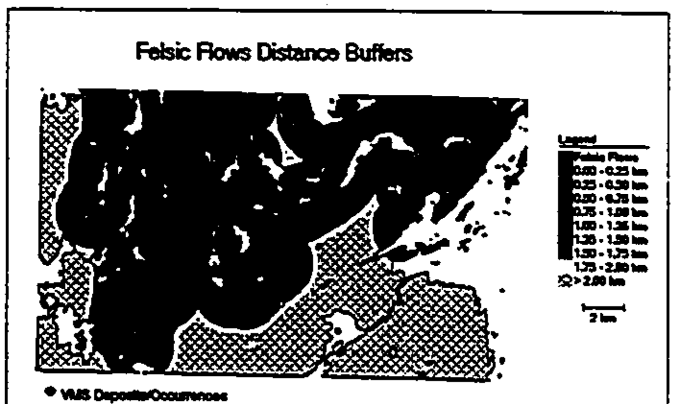

(c)

Figure 4-8(a)-(c). Evidence maps related to stratigraphy. (a) map showing proximity to mafic volcaniclastic rocks, (b) map showing proximity to felsic volcaniclastic rocks, and (c) map showing proximity to felsic flows.

4.3.3 Stratigraphic Factor

Detailed mapping at the 1:20000 scale has allowed the geologists to understand, to a large degree, the relationship between the stratigraphy and mineralization. In general the VHMS deposits are associated with thick sequences of subaqueously deposited volcanic rocks. They are commonly affiliated with felsic flows, particularly those that occur near the top of individual volcanic sequences. Deposits also occur selectively in those portions of the volcanic sequence in which coarse volcaniclastic units are abundant; they are most prominent in the stratigraphic hangingwall to such volcanic sequences. Proximity to units of coarse volcaniclastics is considered a favourable condition for the occurrence of VHMS deposits, though, felsic volcaniclastic units have a much lower potential for hosting VHMS deposits than felsic flows in the Snow Lake area.

Evidence maps that could be generated to reflect these stratigraphic relationships include a geology map that identifies felsic flows, felsic and mafic volcaniclastics and subaqueously deposited volcanic rocks. The geology map shown in Figure 2.3, has been generalized from a more detailed map into a smaller number of map units but preserving the information believed to be significant, and can be used as evidence to show the important lithologies. The reclassification lookup table of the 1:20000 scale map units is shown in Appendix A, Table A1.

Evidence maps that reflect information related to proximity to felsic volcaniclastics, felsic flows and mafic volcaniclastics can be generated by extracting the contacts of the units of interest as vectors and generating proximity maps as described in Chapter 3. Corridors for both evidence maps were constructed with a width of 0.25 km and are shown in Figure 4.8.

It is noted that detailed lithologic mapping has resulted in understanding important stratigraphic relationships. It has been clearly established that deposits are associated with felsic flows that occur close to the top of a volcanic sequence. Being able to identify which way is up in the volcanic stratigraphy is obviously critical for interpreting which stratigraphic contacts are significant or tracing metalogenic horizons. For example, the presence of a contact between a felsic flow and a mafic to intermediate volcaniclastic unit will have a much greater importance if the mafic to intermediate volcaniclastic is underlying the felsic flow than if it is overlying the felsic flow where it would more likely be interpreted as being the base of the next volcanic sequence. Unfortunately, much of the stratigraphy is overturned or discontinuous because the area is strongly deformed having complicated fold structures and faults. Because of this, the stratigraphic direction could only be determined for a few selected areas and could not be obtained systematically for the whole map area. (Bailes, pers. comm.)

In addition to the generalized geology map, the three proximity maps showing distance relationships to mafic volcaniclastics, mafic flows and felsic flows, can be used to reflect the information related to stratigraphy.

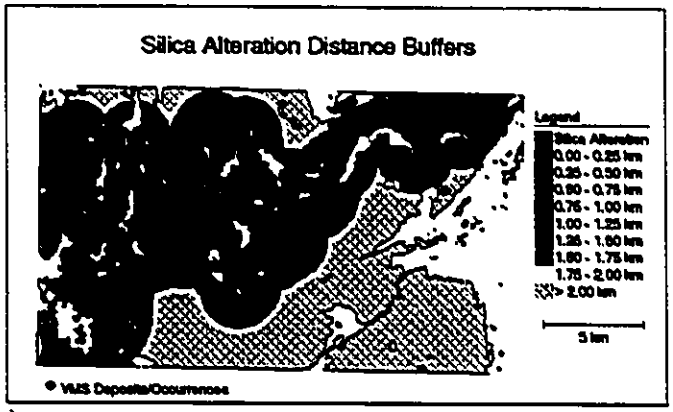

(a)

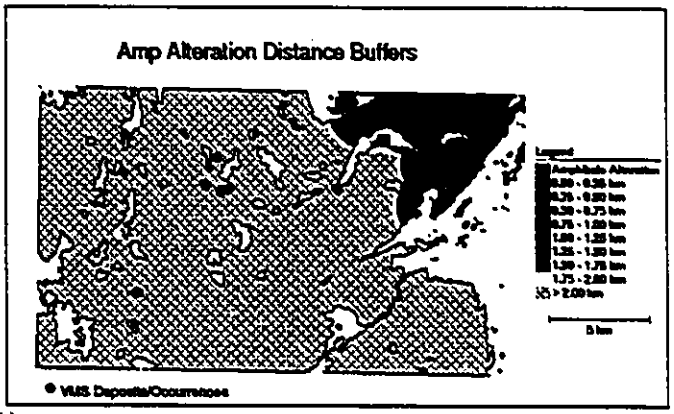

(b)

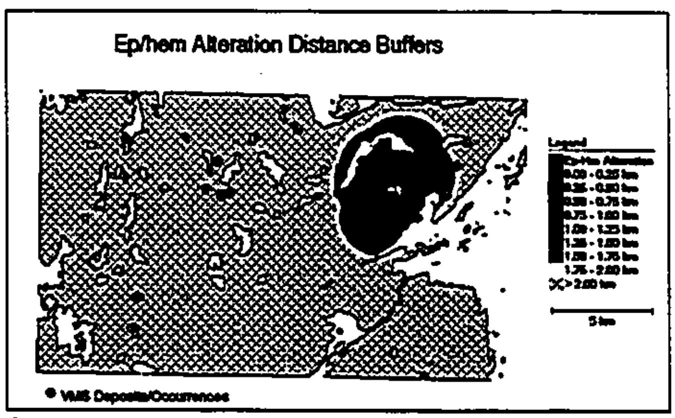

(c)

Figure 4-9(a)-(f). Maps showing proximity to the six different mapped alteration types. (a) proximity to silical alteration , (b) proximity to amphibole alteration , (c) proximity to epidote/hematitie alteration (see over).

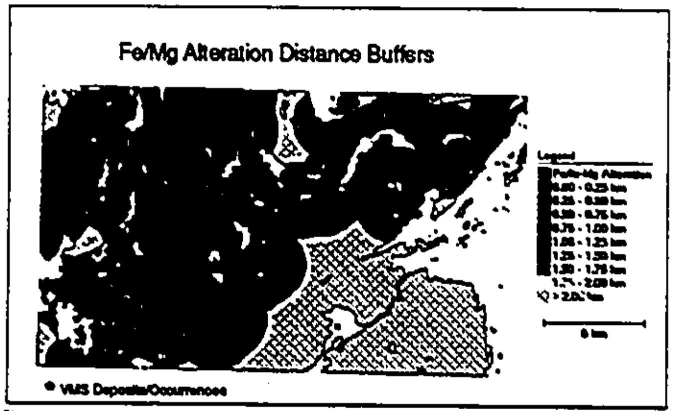

(d)

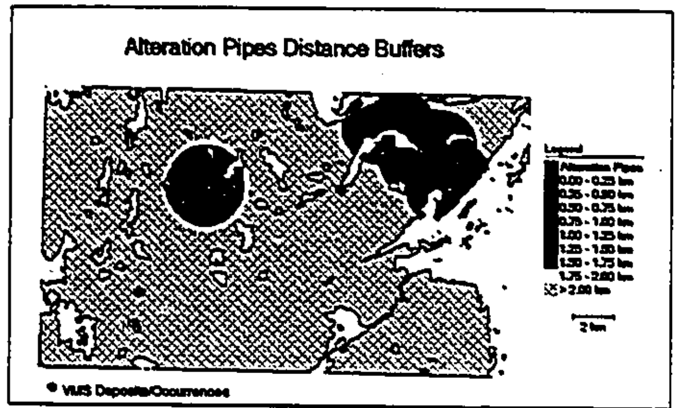

(e)

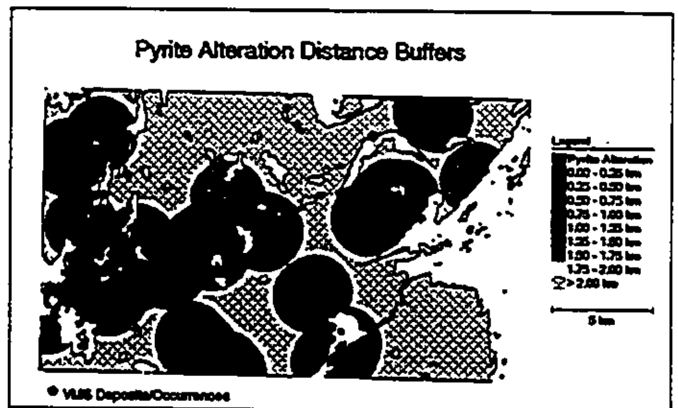

(f)

Figure 4.9 (cont'd) (d) proximity to Fe/Mg alteration, (e) proximity to alteration pipes and (f) proximity to pyrite alteration. These six maps were used as evidence to identify favourable locations for VHMS deposits with respect to alteration.

4.3.4 Alteration Factor

Recognizing alteration zones in the volcanic stratigraphy is critical to exploring for VHMS deposits. Alteration zones have been mapped by Bailes and Galley (1990b) and discussed in relation to other VHMS deposits in Galley (1993). The presence of a large-scale hydrothermal system in volcanics overlying large subvolcanic intrusive complexes results in the formation of semi-conformable alteration zones due to movement of seawater into the cooling volcanic pile. The presence of Si-rich semi-conformable alteration zones define a paleoseafloor on which there is a high potential for sulphide precipitation. Semiconformable zones of silicification and cross-cutting zones of Fe-Mg metasomatized rocks are typical of a deeper, more mature VHMS producing hydrothermal cells. Proximity to zones of silicification or Fe-Mg metasomatism is considered a favourable indicator for the occurrence of VHMS deposits.

Though not commonly identified at regional scale mapping, the identification of highly altered crosscutting alteration pipes, Fe-Mg rich and Na depleted discharge conduits, are also a very important type of alteration related to VHMS deposits.

The Chisel-Anderson study area is exceptional relative to many areas being accessed for mineral potential because of the amount and detail of data available. The alteration mapping is an example of data that is not typically available to a geologist at the beginning of a mineral exploration project. Because mapping alteration was part of the geologic mapping objectives each outcrop was examined for alteration resulting in a relatively complete map though it is recognized that there is a fairly high uncertainty in areas lacking outcrop exposure. Because the alteration map is relatively complete, buffering is an appropriate method for determining distance to the various types of alteration, which in turn can be used to evaluate an area's importance based on the alteration model, as discussed in Chapter 2. If poor exposure or limited mapping resulted in a less complete alteration map buffers could also be used but would have to be treated more as a probability surface to predict the presence or absence of alteration.

Proximity maps have been generated for zones of silicification, Fe-Mg metasomatism, and alteration pipes (Figure 4.9(a), (b) and (f)). Other types of alteration associated with VHMS deposits including pyrite, epidote-hematite and amphibole alteration have been identified and proximity maps generated as shown in Figure 4.9(c)-(e).

4.3.5 Geophysical Factor

The use of geophysical data is an important and useful component for exploring for VHMS deposits. A variety of geophysical data are available for the Snow Lake area including airborne VLF, magnetics, and gravity (see Table 4.1). Unfortunately, EM data, one of the most successful geophysical tools for prospecting for VHMS deposits in this area, was not available on an official basis, so the study was completed without it.

In general, VHMS deposits are characterized by relatively high conductivity, moderate magnetic response, and moderate to high gravity response. Radiometric data is useful for eliminating areas of younger post mineralization lithologies or for identifying low K intrusions which are commonly subvolcanic. Details of how the data was processed to generate geophysical evidence maps are described below.

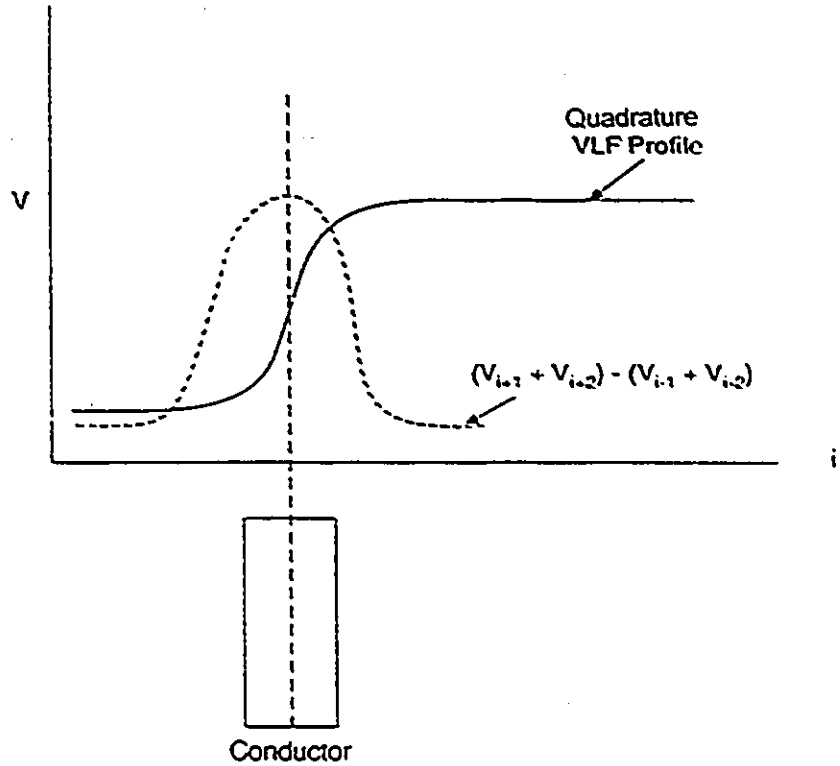

Figure 4.10. Method for processing quadrature VLF data to isolate crossover points.

Conductivity

Good conductivity is typically characteristic of Cu-Zn VHMS deposits (Chisel, Lost and Ghost). Total field VLF is a measure of conductivity but can respond to changes in elevation, permeability and other factors besides conductivity. When a primary electromagnetic field is passed over a conductor, a secondary field approximately 90 degrees out of phase with the primary field is generated. Quadrature VLF, a measure of the percent of the induced field to the primary field, tends to be less affected by other factors and gives a more reliable indication of conductivity. Significant VLF conductors can be identified where high Total Field VLF and high "processed" Quadrature VLF coincide. Both total VLF and Quadrature data are measured values recorded by a Hertz Totem 1A VLF unit. Because raw quadrature data tends to show conductors where a "cross-over" occurs (Figure 4.10) it is useful to process the raw quadrature data to enhance zones of conductivity.

The quadrature VLF data used as evidence for conductivity was processed using the expression

$$Vi = (V_{i+1} + V_{i+2}) - (V_{i-1} + V_{i-2})$$

to emphasize the points of inflection as shown in Figure 4.10. which are related to conductive zones. The processed Quadrature VLF and Total Field VLF are shown in Figure 4.11. The 25 classes shown in the legends are a result of taking the original data values and applying a linear transformation to a range of 1 to 25.

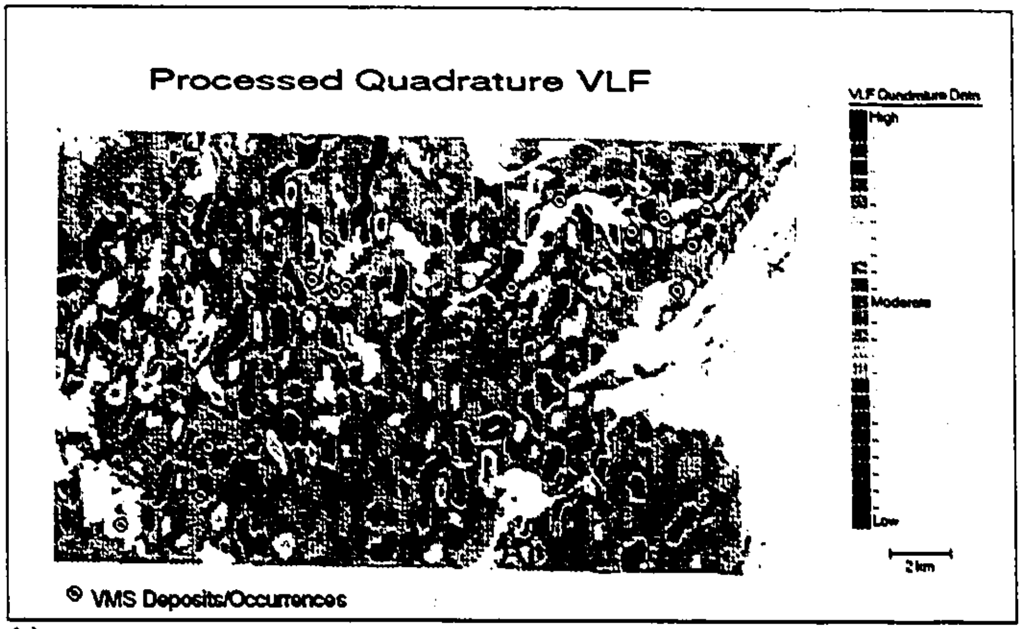

(a)

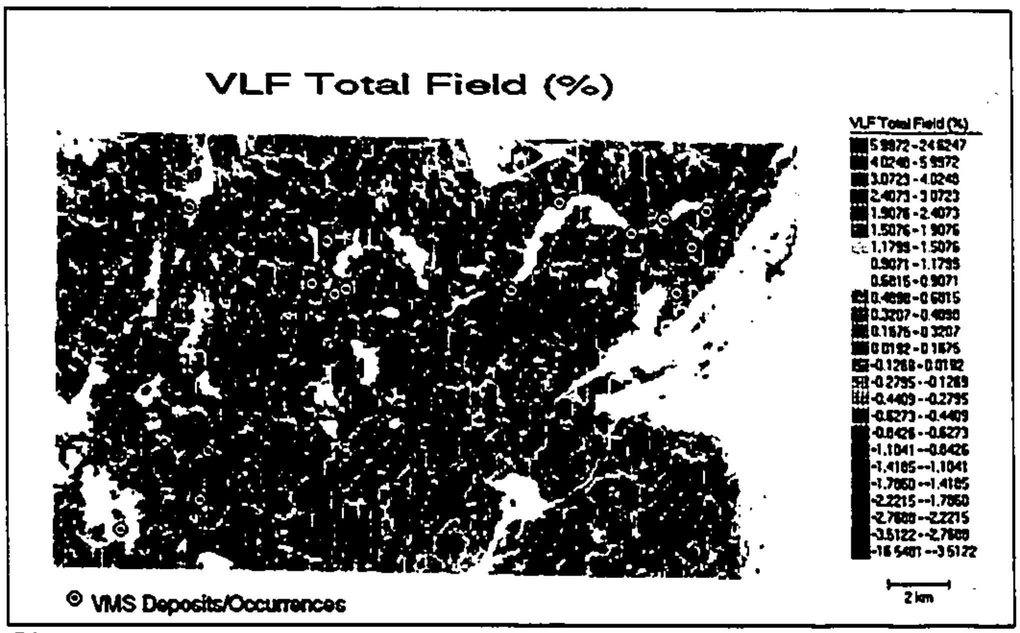

(b)

Figure 4.11 (a) - (b). Two of the five maps used for the geophysical evidence. (a) processed quadrature VLF data (b) VLF total field (%) data. The other geophyscial evidence maps are in Figures 4.12 and 4.13.

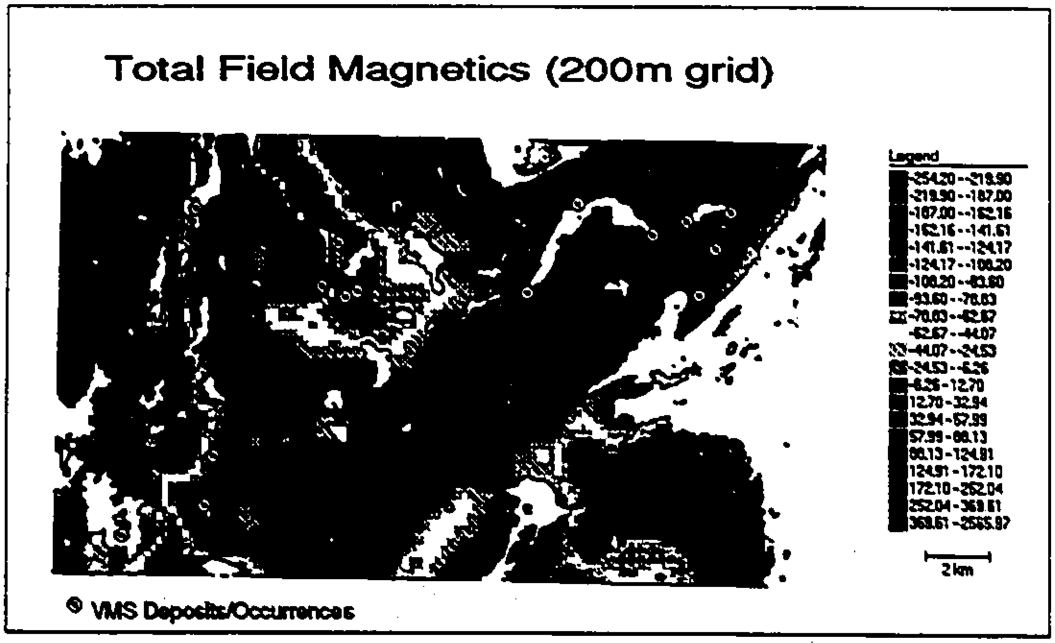

(a)

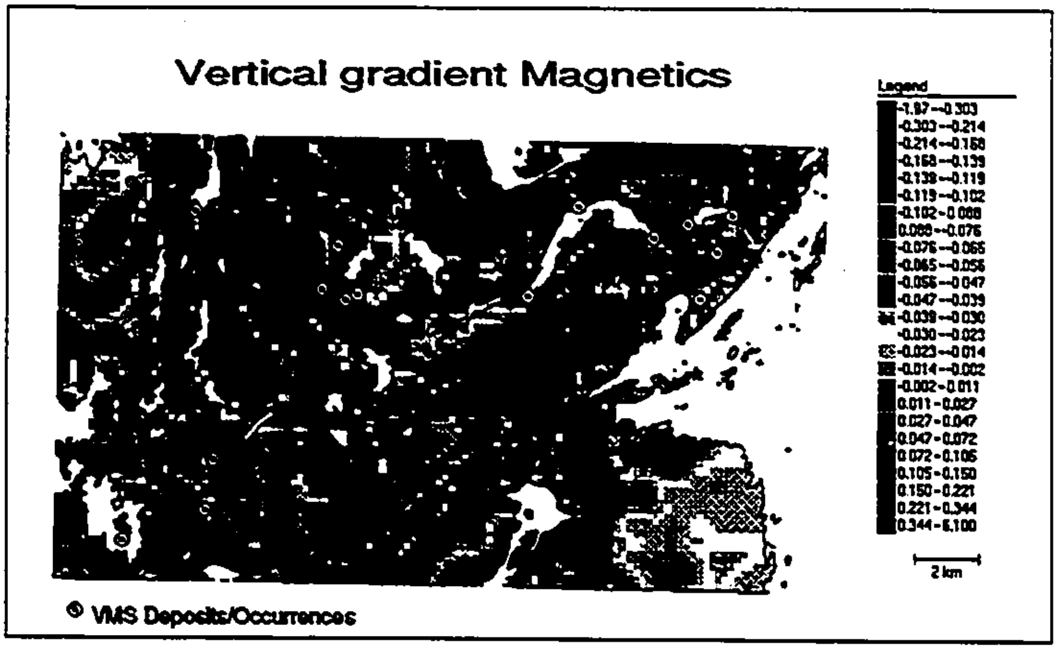

(b)..

Figure 4.12 (a) -(b). Airborne magnetic maps used as geophysical evidence. (a) total field magnetics (b) vertical gradient magnetics.

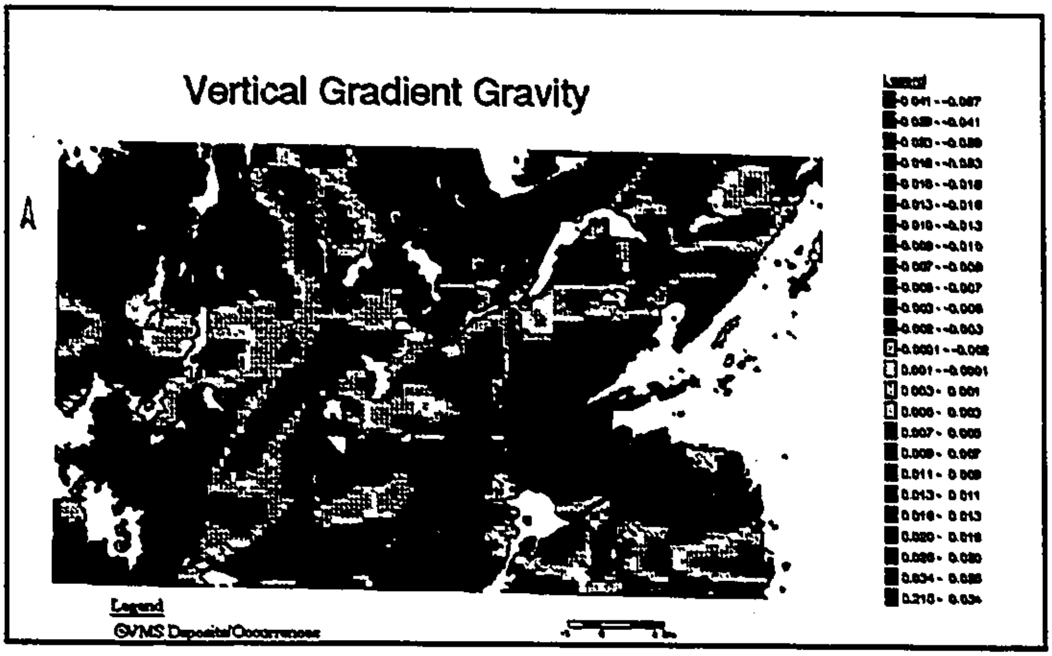

(a) **Figure 4.13.** Airborne vertical gradient gravity, 8 km grid data resampled to 2 km grid.

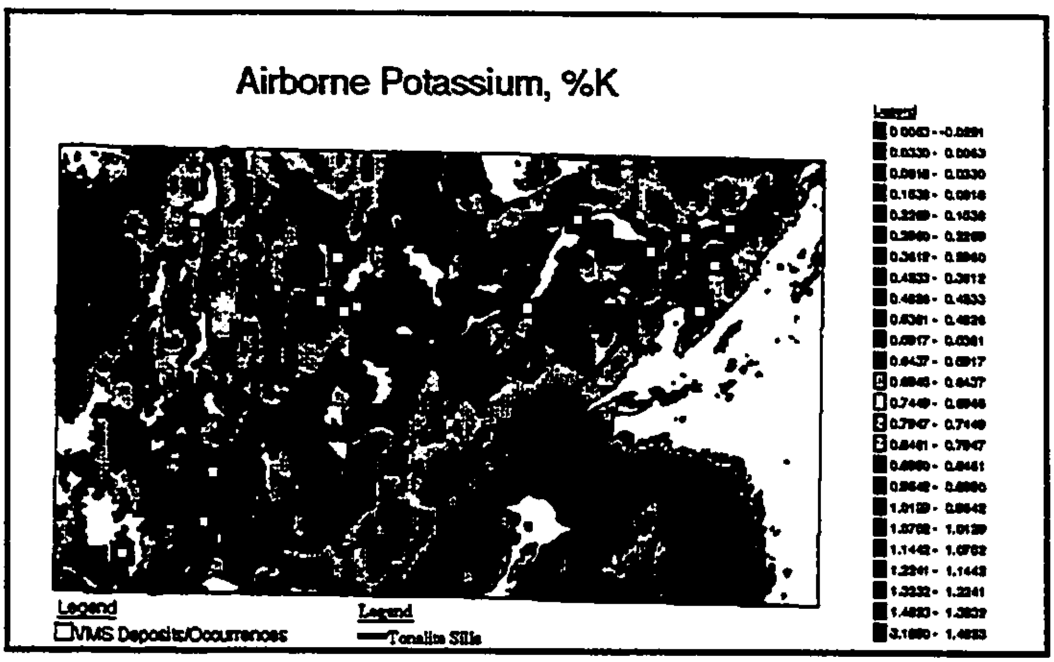

Figure 4.14. Airborne radiometrics are useful for identifying younger igneous intrusions characterized by their higher radiometric signatures. The older subvolcanic intrusives are outlined by the heavy black line.

Magnetic Signature

VHMS deposits are expected to have a relatively strong magnetic signature due to the presence of magnetite (Sinha and Palacky, in prep.). However, in the Snow Lake area, the VHMS deposits are generally associated with more moderate magnetic signatures due to the presence of several iron formations with very strong magnetic signatures.

Two data sets were used to identify potential magnetic anomalies associated with VHMS deposits; Total Field Magnetics (Figure 4.12(a)) and Vertical Gradient Magnetics (Figure 4.12(b)). The TF Magnetics show broad regional trends while the VG show more distinctive trends as it effectively removes the regional signature. The most reliable signatures are where TF and VG highs coincide. The total field Magnetic data was measured (G-803 Magnetometer) and the vertical gradient was calculated as described in Grant and West (1965).

Gravity

The gravity data available for the Snow Lake area was collected at a very low density of 8 km grid spacing and then resampled to a 2 km grid. Gravity signatures can be a very effective tool for identifying targets for potential VHMS deposits but because of the low density sampling for this survey and the relatively small size of the deposits this data is really only effective for eliminating regions of low density lithologies such as felsic intrusives which have low potential for hosting VHMS deposits. The vertical gradient gravity signature (Figure 4.13) was used as evidence. It was calculated as described in Grant and West (1965).

Radiometrics

VHMS deposits in the Snow Lake area tend to be associated with igneous and volcanic suites which tend to have relatively low radiometric signatures (Sneath Lake and Richard Lake tonalite plutons). A map of the airborne U survey is shown in Figure 4.14. It is noted that the high radiometric signatures are associated primarily with the Ham Lake pluton in the northwest, the Wekusko Pluton in the southeast and the Missi sediments in the northeast. These are all younger post Amisk lithologies and do not have any associations with VHMS deposits. The potassium and thorium maps show similar patterns.

Radiometric surveys can be effective for mapping lithologies on a regional scale. In the study region, bedrock mapping at the 1:20000 scale had identified the post Amisk lithologies (considered in the Stratigraphic Factor) and so the radiometrics were redundant. However, based on the correlation seen in Figure 4.14, radiometrics would be a potentially effective tool for identifying important lithologies where detailed mapping was unavailable.

Thus, five evidence maps were generated and combined to represent the geophysical factor: total field VLF, processed quadrature VLF, total field magnetics,

Table 4.5. Summary of evidence maps used in modelling.

Factor	Evidence Map
Stratigraphic	Bedrock geology Proximity to felsic volcaniclastics Proximity to mafic volcaniclastics Proximity felsic flows (rhyolites)
Heat	Proximity to subvolcanic intrusions (tonalite sills) Proximity to synvolcanic dykes
Geochemical	Lake sediment chemistry - Principal Component 1 Lake sediment chemistry - Principal Component 2 Lake sediment chemistry - Principal Component 3 Till chemistry - Kriged ln Cu (C horizon) Till chemistry - Kriged ln Pb (C horizon) Till chemistry - Kriged ln Zn (C horizon)
Alteration	Presence and proximity to silica alteration Presence and proximity to Fe-Mg metasomatism Presence and proximity to alteration pipes Presence and proximity to amphibole alteration Presence and proximity to epidote-hematite alteration Presence and proximity to pyritic alteration
Geophysical	Total field VLF (measured) Processed quadrature VLF (calculated) Total field magnetics (measured) Vertical gradient magnetics (calculated) Vertical gradient gravity (calculated)
Total	23 evidence maps

vertical gradient magnetics and vertical gradient gravity.

The 23 evidence maps described above and summarized in Table 4.5 are common to the integration methods described in the next four chapters.

4.4 Error Considerations

There are many different aspects of the problem of error and error propagation in spatial data analysis and includes the components of attribute accuracy, positional accuracy, lineage, logical consistency, completeness and temporal accuracy and resolution (Heuvelink, 1993; Aronoff, 1989). The term error includes not only "mistakes" but also the statistical concept of error meaning "variation" (Burroughs, 1986). Error is a component of quality of data which is defined by Chrisman (1991) as "fitness for use". It is argued by Chrisman (1991) that error is an integral part of spatial information processing and is inherent in all dimensions (space, attribute and time) of data used in spatial analysis. He also suggests that error must not be treated as a potentially embarrassing inconvenience but should be dealt with in order to evaluate the quality of data being used and the resulting products. In agreement with these statements, it is acknowledged that the error component in this study is undoubtably significant with potential problems associated with all levels of data handling from collection through input to processing. Errors associated with modelling spatial data in this study will be dealt with primarily by calculating variances associated with the results in the data-driven methods and including an uncertainty factor in the knowledge-driven methods.

5. Weights of Evidence Approach

5.1 Introduction

The weights of evidence method is data-driven in the sense that statistical calculations are used to estimate the weights, based on the measured associations between locations of known deposits and predictor map patterns. A preliminary study employing the weights of evidence method, but using a partial dataset for the western half of this study area, is found in Reddy et al., (1990).

5.2 Theory

A detailed discussion of weights of evidence modelling for integrating geoscience datasets to predict mineral potential may be found in Bonham-Carter et al. (1989), Bonham-Carter et al. (1988), Bonham-Carter and Agterberg (1990), Agterberg (1989) and Bonham-Carter (1994a,b). The following is a brief summary from these publications.

Each mineral deposit or occurrence within the study area is assigned to a small unit cell of area u km^2. The total number of unit cells containing a deposit is represented by N(D), where N is the count of unit cells and D refers to the presence of deposits. Cells either contain a deposit or not; there is no provision for modelling deposit size. The total area of the region being studied is t km^2, or $N(T)=t/u$ unit cells. The average density of known deposits in the area is then $N(D)/N(T)$. This ratio is taken as the prior probability of a cell containing a deposit, P(D). The goal is to estimate the posterior probability, given the presence or absence evidence, which may be larger or smaller than the prior, depending on the favourability of the evidence.

The predictor (evidence) maps are commonly reduced to binary form in order to obtain robust estimates of the weights. Each binary predictor map has an area that is more favourable for deposits (pattern present) and an area less favourable for deposits (pattern absent). For the j-th binary predictor map, B_j, the area with the pattern present is denoted as $N(B_j)$ unit cells, and $N(\overline{B}_j) = N(T) - N(B_j)$ is the area with the pattern absent (except in the case of missing data).

If the prior probability that a unit cell contains a deposit is assumed to be constant over the whole study region, then from Bayes' Rule the posterior probability that a cell contains a deposit, given the presence of the j-th binary pattern is:

$$P(D|B_j) = \frac{P(B_j|D)\ P(D)}{P(B_j|D)P(D) + P(B_j|\overline{D})P(\overline{D})} \tag{5.1}$$

where the bar over the D refers to absence of deposits. Similarly, the posterior probability that a cell contains a deposit given the absence of pattern B_j is

$$P(D|\overline{B}_j) = \frac{P(\overline{B}_j|D)\ P(D)}{P(\overline{B}_j|D)P(D)\ +\ P(\overline{B}_j|\overline{D})P(\overline{D})} \tag{5.2}$$

Recasting these equations in loglinear form results in the following expressions for the posterior logit (posterior log odds) of a cell containing a deposit, given the presence/absence of the j-th binary pattern:

$$posterior\ logit(D|B_j) = prior\ logit(D) + W_j^+ \tag{5.3}$$

and

$$posterior\ logit(D|\overline{B}_j) = prior\ logit(D) + W_j^- \tag{5.4}$$

where the positive weight of evidence is defined as

$$W_j^+ = \ln \frac{P(B_j|D)}{P(B_j|\overline{D})} \tag{5.5}$$

and the negative weight of evidence as

$$W_j^- = \ln \frac{P(\overline{B}_j|D)}{P(\overline{B}_j|\overline{D})} \tag{5.6}$$

The contrast, C, for the j-th map is an overall measure of spatial association between the deposits and the binary pattern:

$$C_j = |W_j^+ - W_j^-| \tag{5.7}$$

It is assumed that there are only two mutually exclusive hypotheses, either that a cell contains a deposit, or does not contain a deposit, so that

$$P(D|B_j) = 1 - P(\overline{D}|B_j) \tag{5.8}$$

If n binary predictor maps are used as evidence, a general expression for the posterior logit can be written as

$$posterior\ logit(D|B_1^{k(1)} \cap B_2^{k(2)} \ldots \cap B_N^{k(n)}) = prior\ logit(D) + \sum_{j=1}^{n} W_j^{k(j)} \tag{5.9}$$

where the superscript k(j) refers to the presence or absence of the j-th binary pattern. The logits are usually transformed to probability for mapping, but they can also be left in logit units because the transformation does not affect the rank order of values.

Conditional Independence - Pairwise test

Equation (5.9) assumes that the binary predictor maps are conditionally independent (CI) with respect to the deposits. If the assumption is violated, the posterior probability will be either over- or under-estimated. In practice this assumption is generally violated to some degree, particularly if a large number of maps are being combined. Pairwise tests of independence can be carried out, to reveal whether particular map pairs are in serious violation.

For pairwise tests, a normal (2X2) contingency table for testing the independence of two factors is used but is applied only where deposits are present. This test is explained in detail in Bonham-Carter (1994a). The contingency table layout is shown algebraically in Table 5.1.

Table 5.1 Contingency table for testing conditional independence, based on cells containing a deposit only.

	B_1 *Present*	B_1 *Absent*	*Totals*
B_2 *Present*	$N(B_1 \cap B_2 \cap D)$	$N(\overline{B_1} \cap B_2 \cap D)$	$N(D\overline{B_1}B_2)$
B_2 *Absent*	$N(B_1 \cap \overline{B_2} \cap D)$	$N(\overline{B_1} \cap \overline{B_2} \cap D)$	$N(\overline{D}\,\overline{B_1}B_2)$
	$N(B_1 \cap D)$	$N(\overline{B_1} \cap D)$	$N(D)$

The value $N(B_1 \cap B_2 \cap D)$ can be read as the number of cells that contain a deposit where binary pattern one and binary pattern two are both present. For each of the cells both the observed area and the expected area are required. The observed area (or frequency of unit cells) is measured directly from the map. The expected area is calculated by multiplying the marginal frequencies together and dividing by the total. Because the deposits are considered as points or small unit cells, the resulting values of χ^2 are unaffected by the units of area measurement. This is a distinct advantage over a similar test for conditional independence descibed in Bonham-Carter and Agterberg, (1990), in which eight overlap conditions between two binary maps are considered including overlap areas where there are no deposits present. This test is strongly dependent on the unit cell size.

When the observed and expected values are determined then the chi-square test is calculated using the expression

$$X^2 = \sum_{i=1}^{8} \frac{(Observed_i - Expected_i)^2}{Expected_i} \tag{5.10}$$

and compared to the tabled value of chi-square with two degrees of freedom (Bonham-Carter and Agterberg, 1990) or alternatively G^2 is calculated using

$$G^2 = -2\sum_{i=1}^{2} Observed_i \log_e \frac{Expected_i}{Observed_i} \qquad (5.11)$$

which has a similar distribution to chi-square with 1 degree of freedom.

Maps that are in serious violation can be rejected from the posterior probability calculations, or combined. In practice, it appears that even where CI is violated, the rank order of the polygons by posterior probability is not greatly affected, but each application should be evaluated for this independently.

Conditional Independence - Overall Goodness-of-fit

An overall comparison of goodness-of-fit between the observed distribution of occurences and expected distribution can be carried out to test whether the assumption of conditional independence is statisfied using a chi-square or the Kolmogorov-Smirnov test.

The chi-square test is described in Agtetberg et al.,(1988). For this test the posterior probabilities are classified into relatively few categories such that there are a reasonable number of known deposits in each class (in the order of 5 or more). Then, suppose that p_i is the posterior probability set equal to the midpoint of the probabilites for the $i\text{-}th$ class, A_i is the joint area of all polygons with posterior probability p_i, and n is the is the total number of deposits for the study area, the expecteded frequency is

$$f_{ei} = \frac{A_i\, p_i\, n}{\sum A_i\, p_i} \tag{5.12}$$

It is then possible to apply the chi-square test using equation (5.10) with the number of degrees of freedom set to the number of classes minus one (Agterberg et al., 1990).

A problem with the chi-square test is that the posterior probabilities must be binned and the results can be sensitive to selection cutoffs. An alternative is the Kolmogorov-Smirnov test which does not require grouping the posterior probabilities making it especially suitable for where there are only a small number of known deposits. Given a unique conditions map with N_2 unique condition polygons having an area A_j and an associated calculated posterior probability P_j for the $j = 1,2,..N_2$ unique conditions and that there are N_1 known deposits with a calculated probability P_i^* , $i = 1,2,..N_1$ at each deposit location, then the expected cumulative frequency distribution can be calculated using the expression

$$F_e(P \le P_i^*) = \frac{\sum_{j=1}^{N_2} A_j\, P_j}{S} \quad for\ P_j \le P_i^*,\ i=1,2,..N_1 \tag{5.13}$$

where

$$S = \sum_{j=1}^{N_2} A_j\, P_j \tag{5.14}$$

The observed cumulative distribution is

$$F_o(P \le P_i^*) = \frac{i}{N_1}, \quad for\ i = 1,2...N_1 \tag{5.15}$$

The Kolmogorov-Smirnov statistic is defined as

$$d = |F_e - F_o|_{max} \quad over\ i = 1,2,...N_1 \tag{5.16}$$

The two tailed null hypothesis states that the observed distribution is equal to the theoretical distribution. This hypothesis is accepted if the absolute value of the largest difference is less than $1.36/\sqrt{n}$ (Davis, 1986, p.102) for $\alpha = 0.05$, where n is the number of observations.

Uncertainty

The variance of the posterior probability values is given by the expression

$$s^2_{(P\,post)} = \frac{1}{N(D)} + \sum_{j=1}^{N} s^2(W_j^{k(j)})\ P^2_{post} \tag{5.17}$$

where $s^2(W_j^{k(j)})$ is the variance of the weight for the j-th map, and k(j) is assigned + for presence - for absence of the binary pattern, as before. The variances of the weights become large for cases with a small number of deposits. The variance formulas are

$$s^2(W_j^+) = \frac{1}{N(B_j \cap D)} + \frac{1}{N(B_j \cap \overline{D})} \tag{5.18}$$

$$s^2(W_j^-) = \frac{1}{N(\overline{B}_j \cap D)} + \frac{1}{N(\overline{B}_j \cap \overline{D})} \tag{5.19}$$

where $N(B_j \cap D)$ is the number of unit cells where both deposits and the j-th binary pattern are present, and the other terms are defined similarly.

If one or more of the binary maps being used as evidence is incomplete, Agterberg et al. (1990), show how a variance component can be calculated in areas of missing data. The variance component for missing data can be calculated as

$$\sigma_j^2(P_{post}) = \{P(D|B_j) - P(D)\}^2 P(B_j) + \{P(D|\overline{B}_j) - P(D)\}^2 P(\overline{B}_j) \tag{5.20}$$

5.3 Application

5.3.1 Generating Binary Predictor maps

The predictor maps used in the weights of evidence approach are the same as the ones summarized in Table 4.5, however, each multiclass map was reclassified to binary form. Multiclass weights of evidence can be carried out (see Goodacre at al., 1993; Bonham-Carter, 1994b, for example), but with only a small number of known deposits the weight estimates are unstable, and their variances are large. Transformation to binary maps, besides improving the robustness of the estimated weights, is also advantageous for facilitating interpretation. The weight calculations are invaluable for determining optimal thresholds objectively between 'anomaly' and 'background' that maximize the spatial association between the deposits and each predictor pattern.

For maps with an ordinal, interval or ratio level of measurement, weights are calculated at successive class cutoffs, using cumulative areas, with each cutoff as the threshold between pattern present and pattern absent. This process is illustrated using proximity to felsic flows as an example.

The evidence map showing the distances from felsic flows is shown in Figure 4.8(c). There are 10 buffers, or corridors, each 250 m wide, extending out from the felsic flow contacts. By superimposing the deposit locations on this buffer map, and appending the distance buffer class as an attribute to the deposit attribute table (a straightforward operation in GIS), the distance distribution of the deposits can be summarized by

Table 5.2. Variation of weights with cumulative distance from felsic flows, for unit cell of 1 km^2. Contrast, C, has a maximum at class 2 (< 0 .5 km).

Class	Distance	Area	Deposits	W+	s(W+)	W-	s(W-)	C
1	0.25 km	18	7	2.2995	0.4764	-0.5807	0.3593	2.8802
2	**0.50 km**	**56**	**12**	**1.5122**	**0.3251**	**-1.4154**	**0.5815**	**2.9277**
3	0.75 km	81	13	1.1602	0.3024	-1.6979	0.7109	2.8581
4	1.00 km	104	13	0.8727	0.2963	-1.5653	0.7115	2.4380
5	1.25 km	125	13	0.6683	0.2929	-1.4275	0.7121	2.0958
6	1.50 km	145	14	0.5852	0.2811	-1.9744	1.0041	2.5596
7	1.75 km	163	14	0.4578	0.2795	-1.8152	1.0048	2.2730
8	2.00 km	177	14	0.3693	0.2784	-1.6721	1.0055	2.0414
9	2.25 km	167	14	0.3116	0.2778	-1.5578	1.0062	1.8693

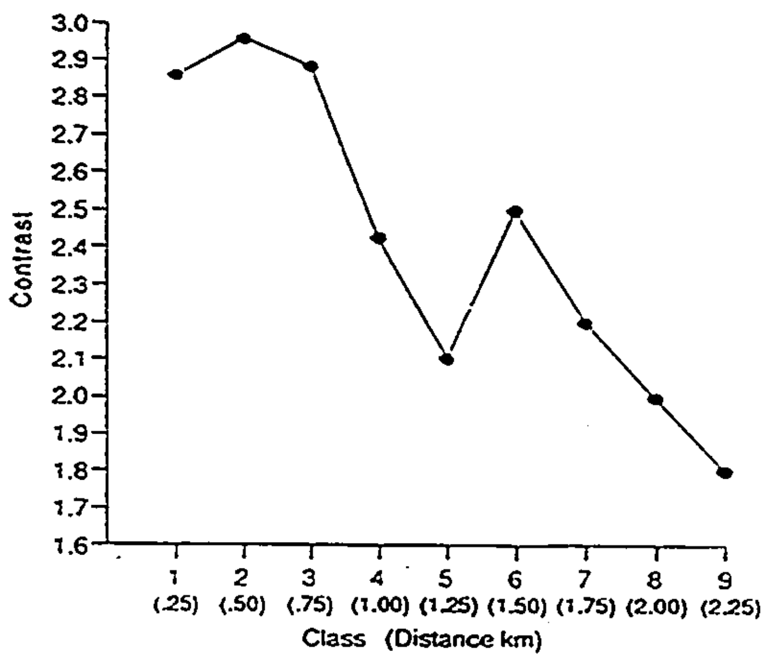

Figure 5.1. Graph of contrast versus distance from felsic flows. Cutoff between binary classes is set at 500 m, where contrast is maximum

counting the number of deposits in each class. Visual inspection clearly indicates that a major proportion of the deposits are situated close to the felsic flows. The question is whether there are more than would be expected due to chance. To quantify this relationship, weights are calculated using Equations 5.5 and 5.6 for cumulative distances, as shown in Table 5.1. Figure 5.1 is a plot of the contrast against distance, and reveals a maximum contrast at 0.5 km. At this distance 12 of the 15 deposits are present and the area of the region lying within 0.5 km is only 56 km^2 out of a total study area of 268 km^2. If the deposits are located at random and independent of the flows, the weights and contrast values are zero, or negligibly small. This result shows that there is a strong spatial association of deposits with proximity to felsic flows. For the first buffer zone, W^+ is positive (nearly 2.3) because 7 out of the 18 cells in this buffer zone contain a deposit, far more than would be expected due to chance. Similarly W^- is -0.58, because the buffer zones greater than 250 m from the flows contain fewer deposits than expected due to chance. The contrast, calculated as 2.2995 - (-0.5807) = 2.8802 for the first zone is a measure of this association. However, notice that the contrast is greater in buffer zone 2 (the cumulative area of buffer zones 1 and 2), and then decreases with increasing distance away from the flow contact. Of course this calculation could be refined by using a smaller interval than 250 m, but in general the result would be similar; and because this calculation makes a simplifying 2-D assumption about the flow contacts being vertical, the more accurate distance measurements are not justified.

It is noted that there is not always a simple maximum and that some subjective judgement must be used in interpreting these contrast relationships. The variances of the weights and contrasts are also helpful for determining the optimum cutoff level for binary conversion. The variance of C is the sum of the variances of the weights. When the ratio of C to its standard deviation (square root of the variance) is large, say greater than about 1.5, the contrast value is relatively reliable. Note that the variance of the weights depends on the cell size. It can be seen that both $1/N(B_j \cap \overline{D}) \rightarrow 0$ and $1/N(\overline{B}_j \cap \overline{D}) \rightarrow 0$, hence as unit cell size approaches zero, $s^2(w_j^+) \rightarrow 1/N(B_j \cap D)$ and $s^2(w_j^-) \rightarrow 1/N(\overline{B}_j \cap D)$, see equations (5.13) and (5.14). Bonham-Carter et al. (1989) discuss this and other aspects of the variances of weights and contrast in detail.

Weights and contrasts were calculated for all the proximity, geochemical and geophysical input maps using the cumulative form as described above. The weights and contrasts for the geological map, a categorical scale map, was calculated using a noncumulative form. The actual calculations were done using the program WEIGHTS. A detailed explanation of using WEIGHTS for calculating weights to determine the optimum threshold between 'anomaly' and 'background' that maximize the spatial association between the deposits and each predictor pattern is found in Appendix (B-1). The source code, compiled program and digital files used for the calculations are found in Appendix C. A complete listing of the calculated weights and contrasts determined for each multiclass evidence map are found in Appendix (Table A-3). The thresholds used

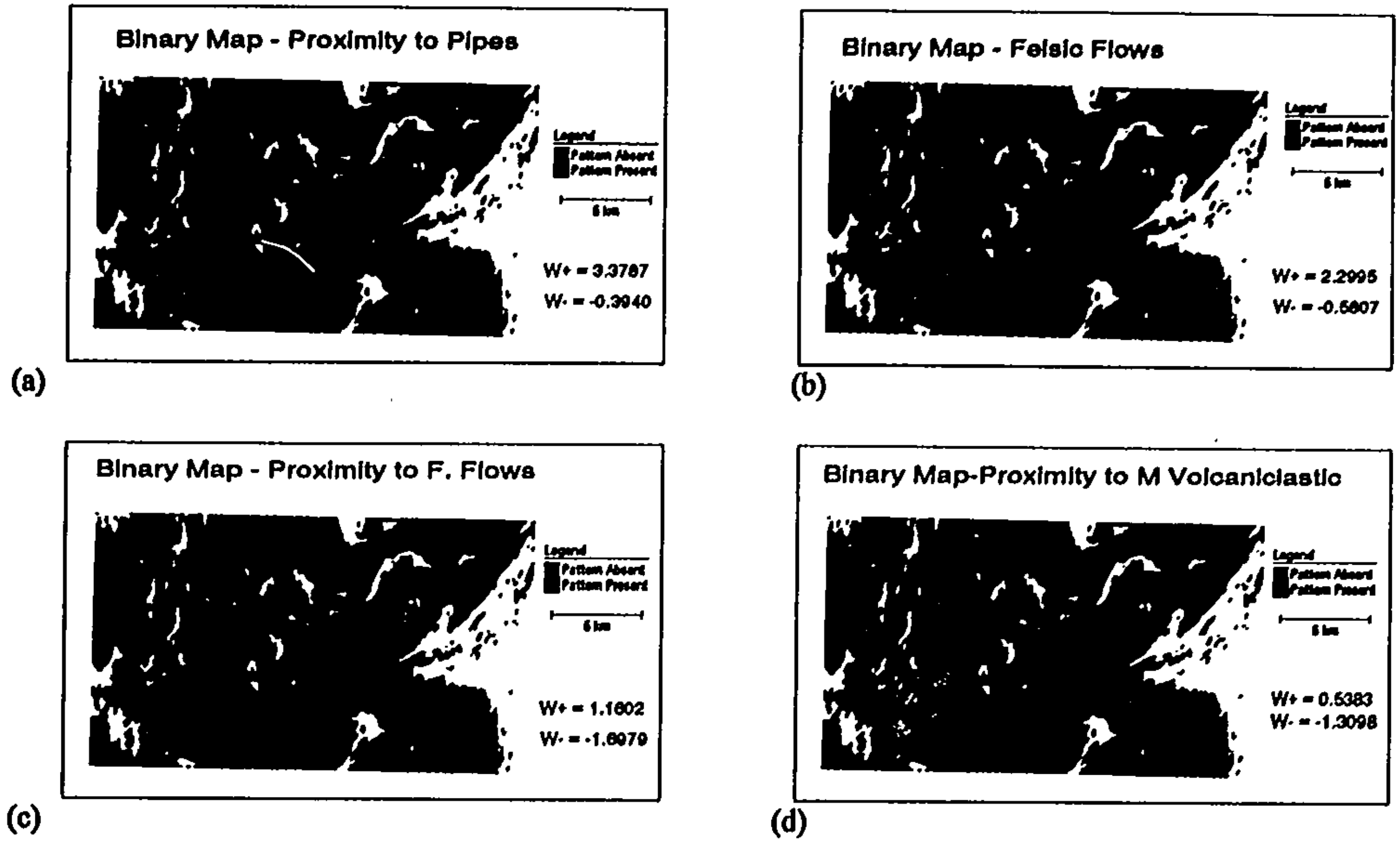

Figure 5.2 (a) - (w). Binary evidence maps. A description of the maps shown in this figure (name in brackets) and the name of the multiclass evidence map that they are associated with is given in Table 5.3. (a) binary evidence map for proximity to "pipe" alteration (NALTPPCB), (b) binary evidence map showing presence and absence of felsic flows (FFLOWB), .(c) binary evidence map for proximity to felsic flows (GEOL2C2B), (d) binary evidence map showing proximity to mafic volcaniclastic rocks (GEOL5C2B)

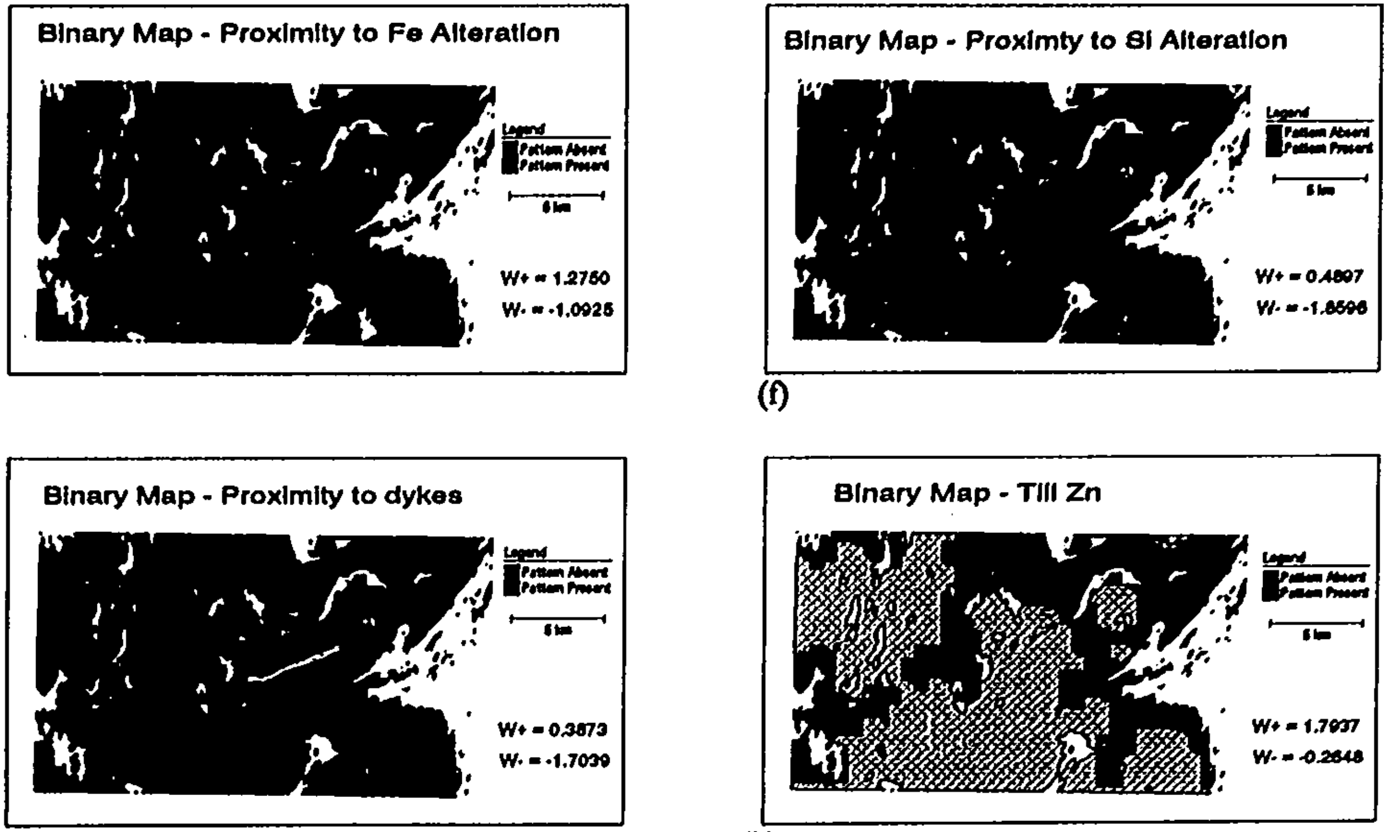

(e) (f) (g) (h)

Figure 5.2 (Cont'd) (e) binary evidence map for proximity to Fe alteration (NALTFECB), (f) binary evidence map for proximity to Si alteration (NALTSICB), (g) binary evidence map for proximity to synvolcanic dykes (DYKEBUFB), (h) binary evidence map for favourable concentration of Zn in till (KRGLNZNB).

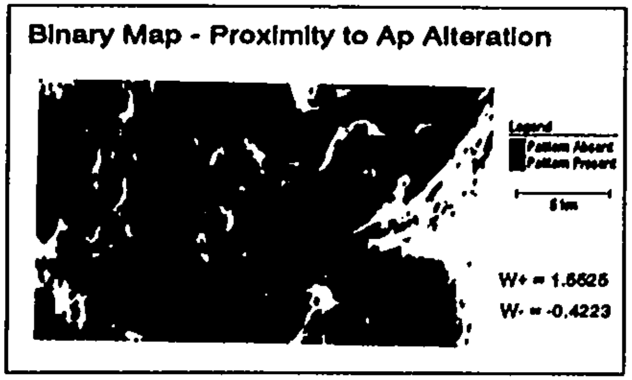

(i)

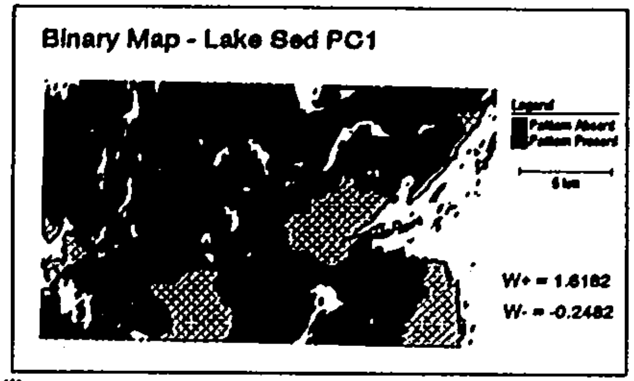

(j)

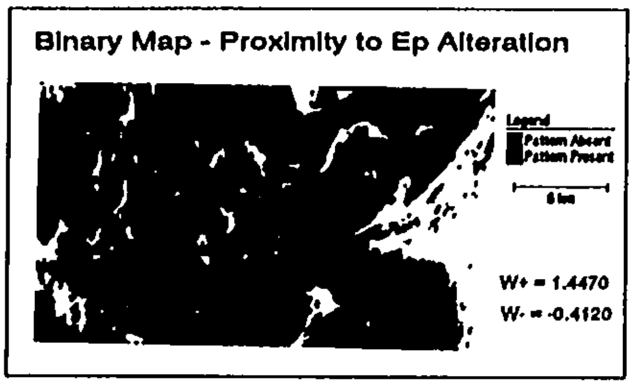

(k)

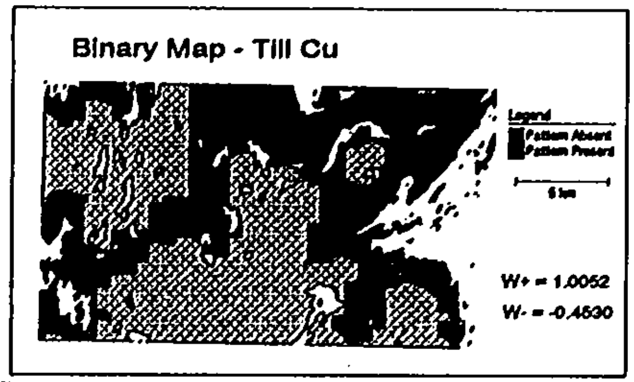

(l)

Figure 5.2 (Cont'd). (i) binary evidence map for proximity to amphibole alteration (NALTAPCB), (j) binary evidence map showing areas with favourable PC1 scores for lake sediment geochemistry (LKPC1NCB), (k) binary evidence map for proximity to epidote alteration (NALTEPCB), (l) binary evidence map for favourable concentration of Cu in till (KRGLNZNB).

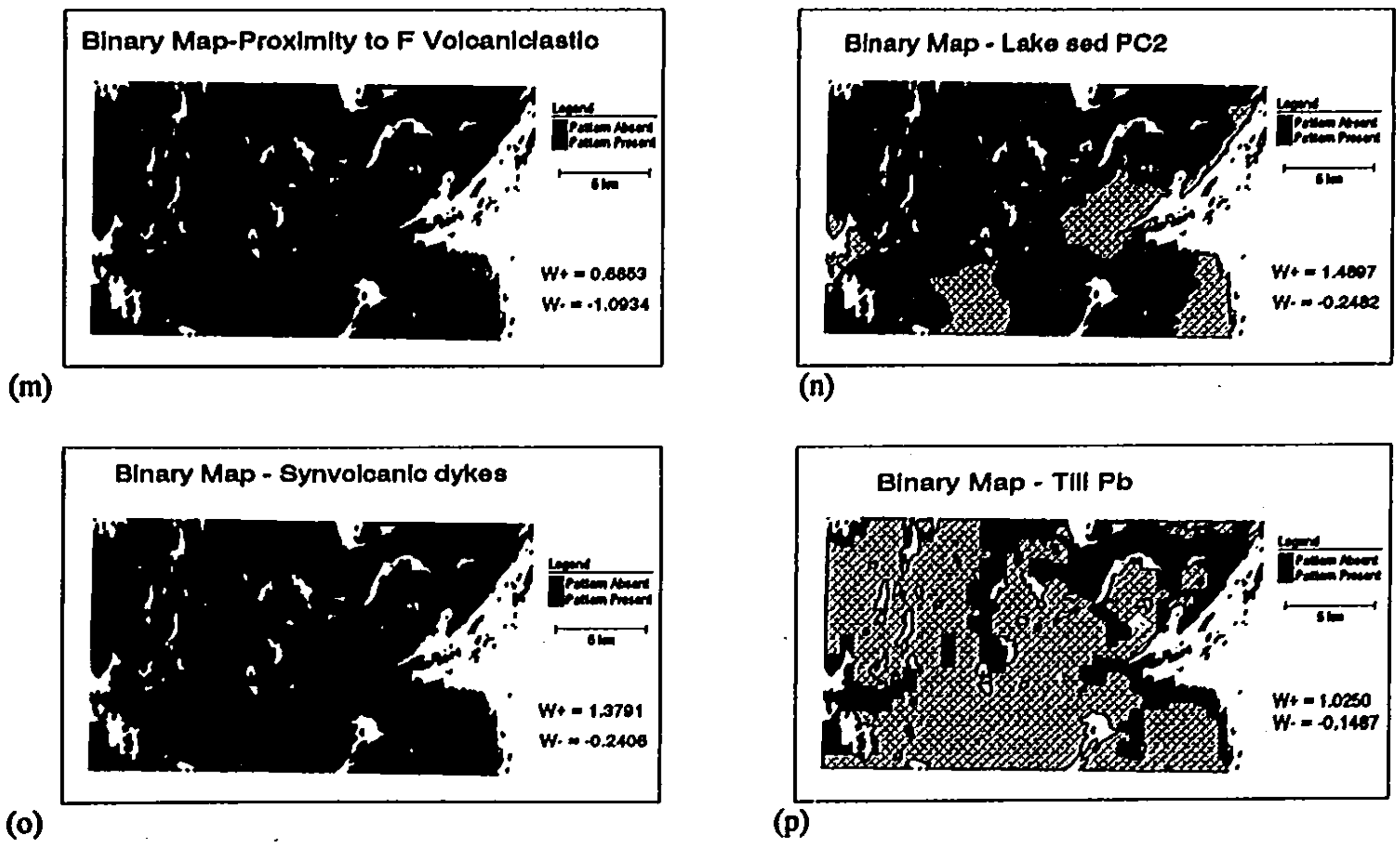

Figure 5.2 (Cont'd). (m) binary evidence map for proximity to felsic volcaniclastics (GEOL4C2B), (n) binary evidence map showing areas with favourable PC2 scores for lake sediment geochemistry (LKPC2NCB), (o) binary evidence map showing the presence of synvolcanic dykes (SYNDYKB), (p) binary evidence map for favourable concentration of Pb in till (KRGLNZNB).

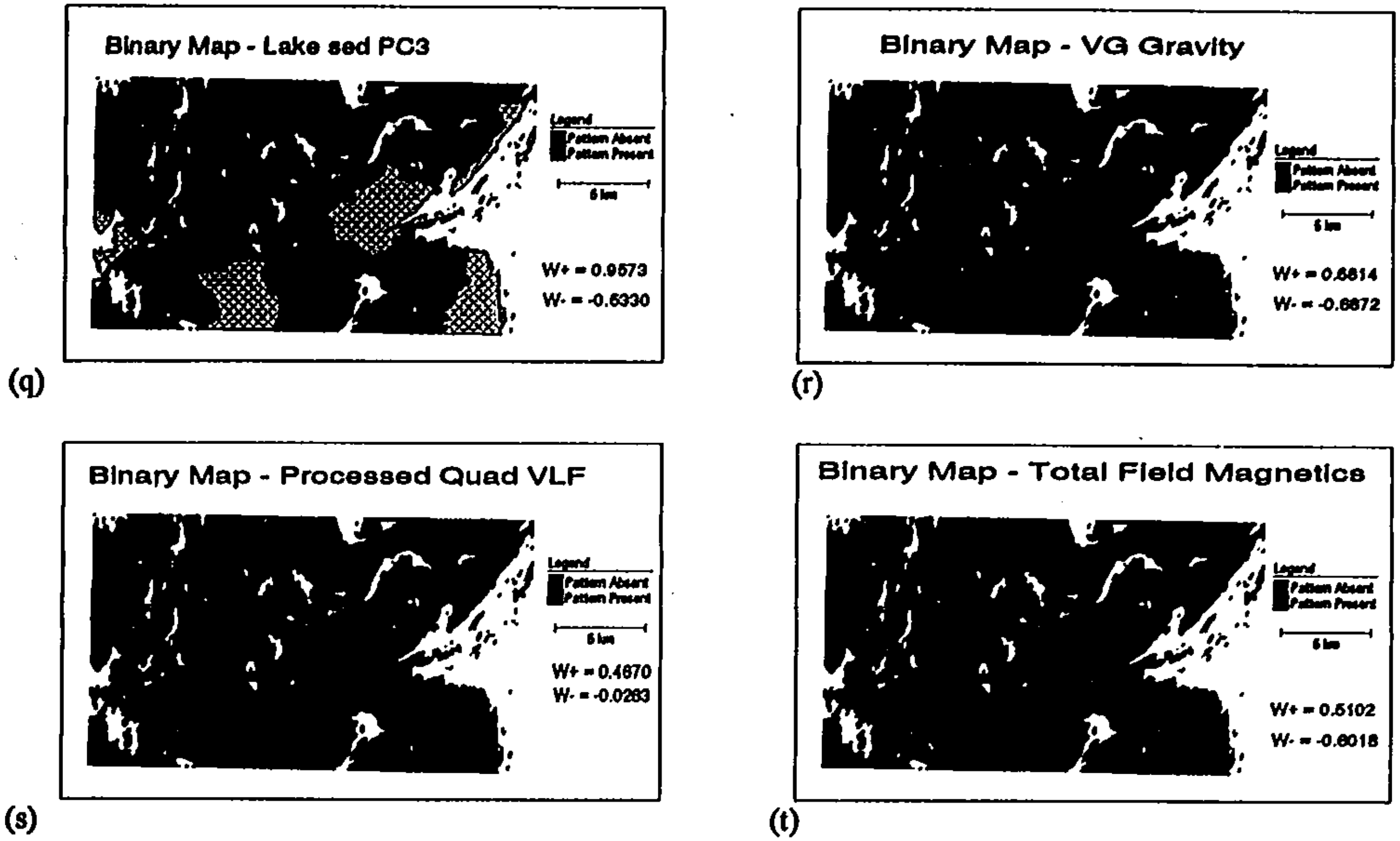

(q) (r) (s) (t)

Figure 5.2 (Cont'd)., (q) binary evidence map showing areas with favourable PC3 scores for lake sediment geochemistry (LKPC3NCB), (r) binary evidence map showing areas with favourable vertical gradient gravity signature (GRVNC25B), (s) binary evidence map showing areas with farvourable quarature VLF signature (NPBLF25B), (t) binary evidence map showing areas with favourable total field magnetic signature (MGNTCMB).

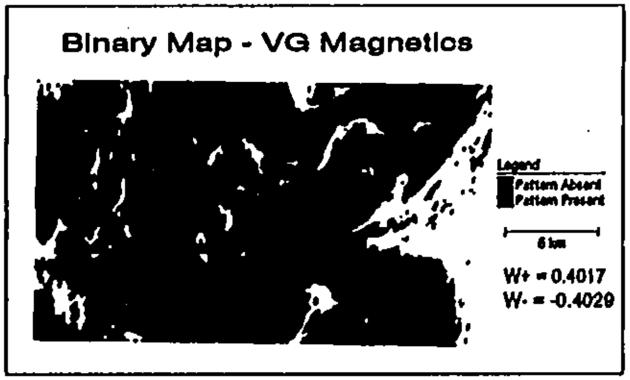

(u)

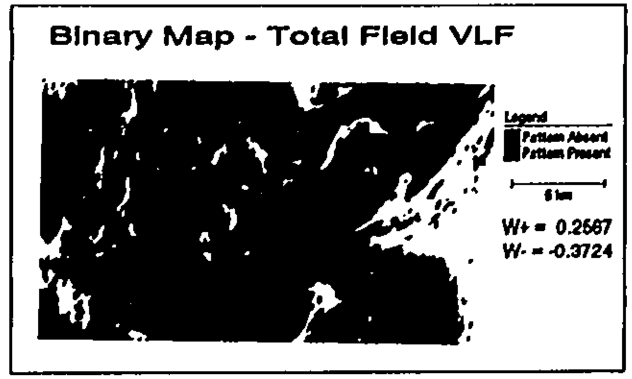

(v)

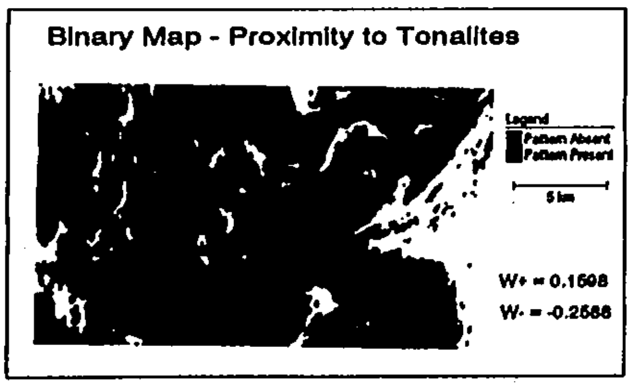

(w)

Figure 5.2 (Cont'd)., (u) binary evidence map showing areas with favourable vertical gradient magnetic signature (MGNVCMB), (v) binary evidence map showing areas with farvourable total field VLF signature (SLVLF25B), (w) binary evidence map showing proximity to subvolcanic sills (SILLBUFB).

in this study to reclassify the multiclass evidence maps to binary ones are also shown in Table A-3.

Based on the resulting calculated optimum thresholds two modifications were made to what was used as evidence maps. Two units, the felsic flows, hosting 7 of the 15 deposits, and the synvolcanic dykes, hosting 4 of the 15 deposits, showed the strongest spatial association to the deposits. The generalized geological map was replaced by two binary maps representing these two units. It is also noted that no statistical correlation was found between the deposits and proximity to zones mapped as pyrite alteration, so this map was omitted from the weights of evidence study. The resulting binary evidence maps (still 23) are shown in Figure 5.2. The weights and contrasts that were used to threshold these maps are listed in Table 5.3, where the maps are ordered from largest to smallest contrast values. In general the maps derived from the geological and alteration map tend to have the greatest contrast values, indicating that they are the best predictors of the known deposits, whereas the geophysical predictor maps have the least predictive capability.

5.3.2 Conditional Independence

At this stage pairwise conditional independence tests were carried out so that if any maps violated the conditional independence assumption they could be eliminated from the model. The results, summarized in Table 5.4, show that there are no χ^2 values greater than 5.4 meaning that for a probability level of 98%, there is no reason to reject

Map	W+	s(W+)	W-	s(W-)	C	C/s(C)	Binary Map	Description of Evidence Map
NALTPPC2	3.3787	0.7393	-0.394	0.3225	3.7728	0.8066	NALTPPCB (M1)	Areas mapped as alteration pipes with 10 buffers 0.25 km wide surrounding areas
FFLOW	2.2995	0.4764	-0.5807	0.3593	2.8802	4.8263	FFLOWB (M2)	Areas mapped as felsic flows only
GEOL2C2	1.1602	0.3024	-1.6979	0.7109	2.8581	3.6996	GEOL2C2B (M3)	Areas mapped as felsic flows with 10 buffers 0.25 km wide extending from contacts
NALTFEC2	1.275	0.3319	-1.0925	0.5049	2.3675	3.9183	NALTFECB (M5)	Areas mapped as Fe alteration with 10 buffers 0.25 km wide extending from contacts
NALTSIC2	0.4897	0.2798	-1.8596	1.0046	2.3493	2.2528	NALTSICB (M6)	Areas mapped as Si alteration with 10 buffers 0.25 km wide extending from contacts
DYKEBUF1	0.3873	0.2786	-1.7039	1.0054	2.0911	2.0044	DYKBUFB (M7)	Areas mapped as synvolcanic dykes with 10 buffers 0.25 km wide extending from contacts
KRGLNZN2	1.7937	0.5821	-0.2648	0.3083	2.0585	3.1252	KRGLNZNB (M8)	Kriged ln concentrations of Zn in C horizon tills (<63 µm size fraction)
NALTAPC2	1.5525	0.4617	-0.4223	0.3397	1.9749	3.4451	NALTAPCB (M9)	Areas mapped as amphibole alteration with 10 buffers 0.25 km wide extending from contacts
LKPC1NC	1.6182	0.5095	-0.3371	0.3228	1.9553	3.2416	LKPC1NCB (M10)	Pricipal Component 1 scores mapped on catchment basin map
NATLEPC2	1.447	0.4566	-0.412	0.3398	1.859	3.266	NALTEPCB (M11)	Areas mapped as epidote alteration with 10 buffers 0.25 km wide extending from contacts
GEOL5C2	0.5383	0.2910	-1.3098	0.7127	1.8481	2.4001	GEOL5C2B (M4)	Areas mapped as mafic volcaniclastic rocks with 10 buffers 0.25 km wide extending from contacts
KRGLNCU2	1.0052	0.3408	-0.8189	0.453	1.8241	3.2177	KRGLNCUB (M12)	Kriged ln concentrations of Cu in C horizon tills (<63 µm size fraction)
GEOL4C2	0.6853	0.3051	-1.0934	0.583	1.7797	2.7029	GEOL4C2B (M13)	Areas mapped as felsic volcaniclastics with 10 buffers 0.25 km wide extending from contacts
LKPC2NC	1.4897	0.5617	-0.2482	0.3084	1.7379	2.7121	LKPC2NCB (M14)	Principal Component 2 scores mapped on catchment basin map
SYNDYK	1.3791	0.5556	-0.2406	0.3084	1.6198	2.549	SYNDYKB (M15)	Areas mapped as synvolcanic dykes
LKPC3NC	0.9573	0.3798	-0.533	0.3845	1.4903	2.7577	LKPC3NCB (M17)	Principal Component 3 scores mapped on catchment basin map
GRVNC25V	0.6814	0.3342	-0.6872	0.4538	1.3686	2.4284	GRVNC25B (M18)	Vertical gradient gravity map
MGNTCM25	0.5102	0.316	-0.7415	0.507	1.2517	2.0953	MGNTCMB (M20)	Total field magnetics
KRGLNPB2	1.0250	0.6231	-0.1487	0.2959	1.1737	1.7015	KRGLNPBB (M16)	Kriged ln concentrations of Pb in C horizon tills (< 63 µm size fraction)
MGNVCM25	0.4017	0.3477	-0.4029	0.4162	0.8046	1.4835	MGNVCMB (M21)	Vertical gradient magnetics
SLVLF25	0.2567	0.3281	-0.3724	0.4562	0.6301	1.1213	SLVLF25B (M22)	Total field VLF
NPVLF25	0.4670	1.0461	-0.0263	0.2748	0.4933	0.4561	NPVLF25B (M19)	Processed quadrature VLF data map
SILLBUF	0.1598	0.327	-0.2588	0.4573	0.4187	0.5622	SILBUFB (M23)	Areas mapped as subvolcanic sills with 10 buffers 0.50 km wide extending from contacts

Table 5.3. Weights determined for predictor maps that define optimal association between known mineral deposits and map pattern.

MAP	M1	M2	M3	M4	M5	M6	M7	M8	M9	M10	M11	M12	M13	M14	M15	M16	M17	M18	M19	M20	M21	M22	M23
M1	0.00	0.94	0.16	0.27	0.16	0.44	0.0	0.63	0.13	0.30	0.08	0.54	0.39	0.13	0.39	0.04	0.71	0.04	0.39	0.54	0.08	3.23	0.54
M2		0.00	0.44	0.02	0.01	0.26	0.60	0.05	0.03	0.18	0.94	0.84	2.56	1.64	0.18	1.89	3.23	0.55	0.02	0.03	0.00	0.94	0.03
M3			0.00	0.38	0.36	0.00	0.88	0.14	0.07	0.61	0.16	0.29	2.76	0.07	0.64	0.10	0.22	0.22	2.76	0.07	0.16	0.16	0.07
M4				0.00	0.04	0.71	0.88	0.20	0.00	0.09	0.27	0.47	0.19	0.47	0.19	0.07	0.16	0.16	0.19	0.47	0.27	0.27	0.49
M5					0.00	0.71	0.88	0.14	1.80	0.00	0.08	0.29	0.00	0.29	0.00	1.18	0.04	1.18	0.64	1.80	1.25	0.16	0.29
M6						0.00	0.00	0.14	0.04	0.01	0.00	0.78	0.01	0.01	0.01	0.26	1.36	0.26	0.01	0.78	0.32	0.44	0.78
M7							0.00	0.11	0.06	0.06	0.00	0.11	0.11	0.02	0.06	0.19	0.19	0.36	0.11	0.19	0.00	0.00	0.06
M8								0.00	0.16	0.00	0.00	0.00	0.02	0.00	0.20	0.16	0.05	0.74	0.35	0.05	0.63	0.63	0.00
M9									0.00	0.17	0.54	0.04	1.07	0.94	1.07	0.31	2.81	2.81	0.04	0.15	0.13	0.13	0.94
M10										0.00	0.39	0.04	0.01	0.04	0.33	1.15	0.01	0.23	0.01	0.17	0.39	0.30	0.17
M11											0.00	0.54	0.39	0.54	0.39	0.71	0.71	0.71	0.39	0.54	0.08	0.08	0.54
M12												0.00	2.09	0.04	2.09	2.81	0.31	0.31	0.04	0.15	0.13	0.54	0.04
M13													0.00	1.07	0.33	0.23	1.72	1.72	0.33	0.17	0.39	0.39	0.17
M14														0.00	1.07	0.00	0.31	0.31	0.23	0.15	0.13	0.18	0.15
M15															0.00	1.15	1.72	1.72	0.01	1.07	0.39	0.39	0.17
M16																0.00	0.19	0.00	0.04	0.00	0.04	0.04	0.00
M17																	0.00	5.10	0.23	2.81	0.04	0.71	2.18
M18																		0.00	0.01	2.81	0.04	0.04	0.31
M19																			0.00	0.17	0.30	0.39	0.17
M20																				0.00	0.13	0.54	0.15
M21																					0.00	0.08	0.54
M22																						0.00	0.54
M23																							0.00

Table 5.4 Chi-square values for pairwise conditional independence tests. With 1 degree of freedom and probability level of 98%, tabled chi-square = 5.4, larger than any observed value, so CI hypothesis in not rejected at this level

the hypothesis that conditional independence exists for any of the pairs of maps. At least on a pairwise basis, there are no serious problems introduced by conditional dependence.

5.3.3 Map Combination

The weighted binary maps are now combined to create a posterior probability map by applying Equation (5.9). This process is readily carried out with the built-in GIS modelling language. It can also be carried out using a combination of GIS generated files and the external program PREDICTR. For a detailed description of these methods see Appendix B (B-2(a) for applying weight of evidence modelling using SPANS modelling language and B-2(b) for using the external program PREDICTOR). The digital maps and files required for this process are found in Appendix C.

For regions of maps where no data are available, such as areas outside the catchment basins in the lake sediment geochemical maps, the weight is assigned the value 0. The final probability map is shown in Figure 5.3. The posterior probabilities were classified by percentiles so that the 20 categories in the legend represent the 5th, 10th, 15th ... >95th percentiles. The prior probability using a unit cell area of 1 km^2 is 0.0560. All areas that show posterior probabilities greater than the prior are characterized by combined evidence that is favourable for deposits, whereas values less than the prior are relatively unfavourable. The ranking of regions by posterior probability produces a favourability map that is based on a statistical model and assumes that the known

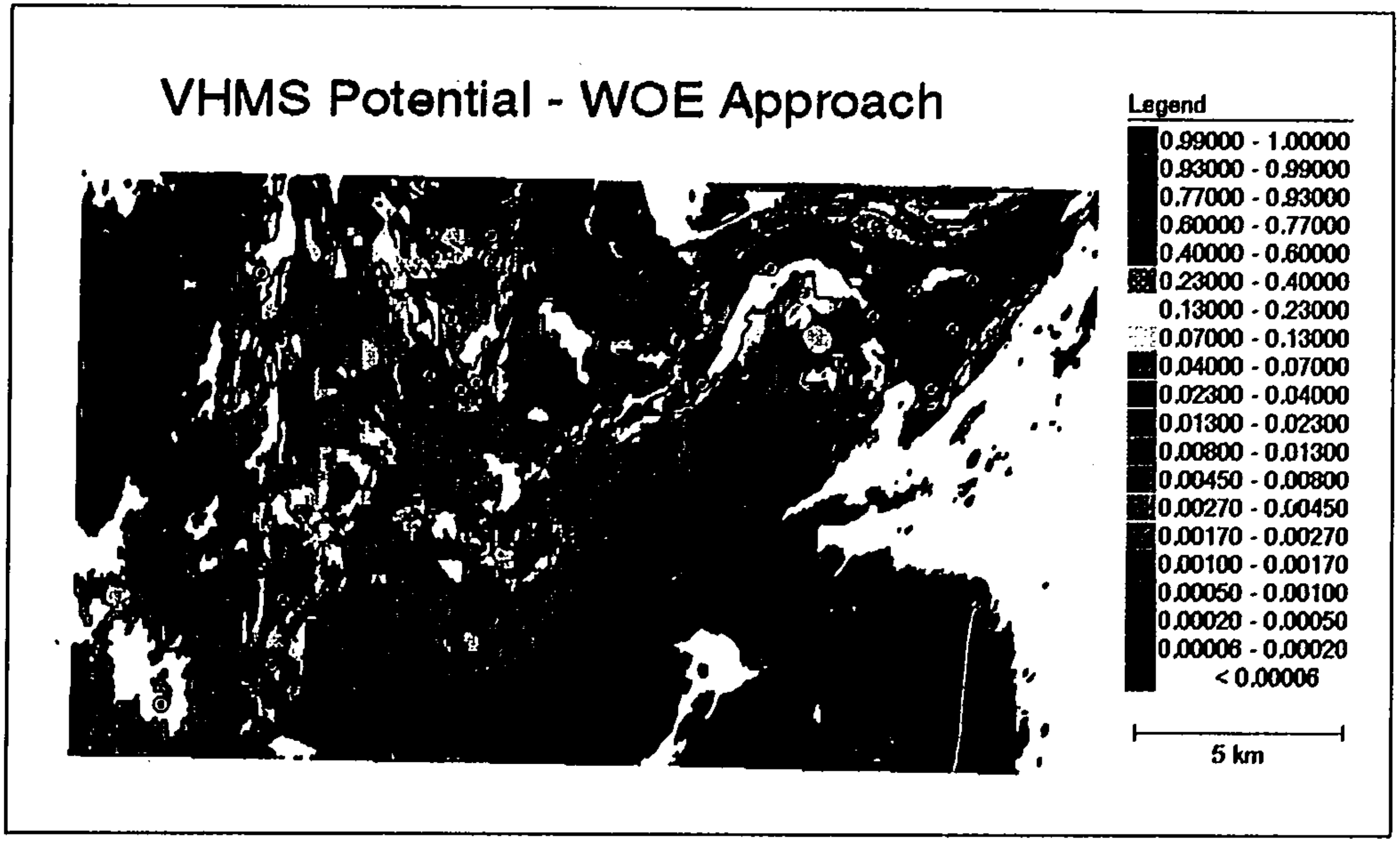

Figure 5.3. Posterior probability map for VHMS deposits generated using weights of evidence modelling approach.

deposits are an adequate sample of deposits (known and undiscovered) in the region.

5.4 Error Considerations

Though the pairwise conditional independence tests showed that there were no pairs of maps that obviously violated the assumption of conditional independence. A simple test test can be performed that measures the overall goodness-of-fit. In general if the predicted number of deposits is much larger than the observed number of deposits it can be assumed that there is some kind of repetitiveness in the data. The predicted number of deposits is calculated by summing the probability times the area of a polygon for all polygons (see Equation 5.14). For this study the predicted number of deposits is 36, more than double the number of observed deposits. Also, the overall goodness-of-fit can be evaluated using the Kolmogorov-Smirnov test as described in Section 5.2, Equations 5.13 to 5.16. The results of this test are shown in Figure 5.4. It is noted that the K-S statistic is 3.725 at a probability of 0.98. To accept the two-tailed null hypothesis, stating that the theoretical and observed distributions are the same, the K-S statistic must not exceed $1.36\sqrt{n}$ for $\alpha = 0.05$, where n is the total number of observations. In this study the total number of observations were 6994 (total number of unique conditions) so the K-S statistic should not not be greater than 0.0163. Thus, although there are no serious pairwise violations, the multiple interactions of such a large number of predictor maps results in a failure of the overall

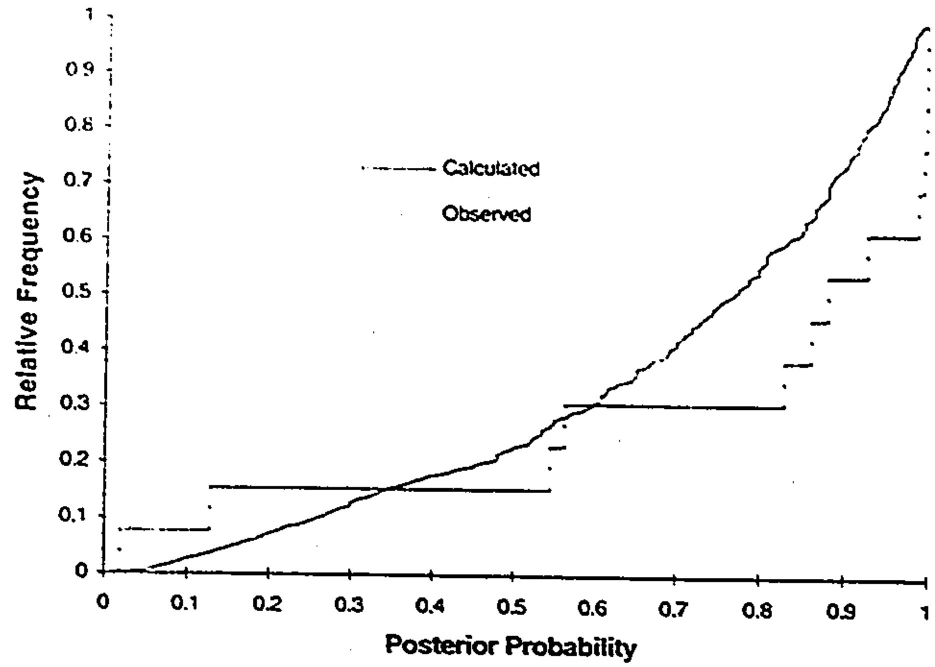

a)

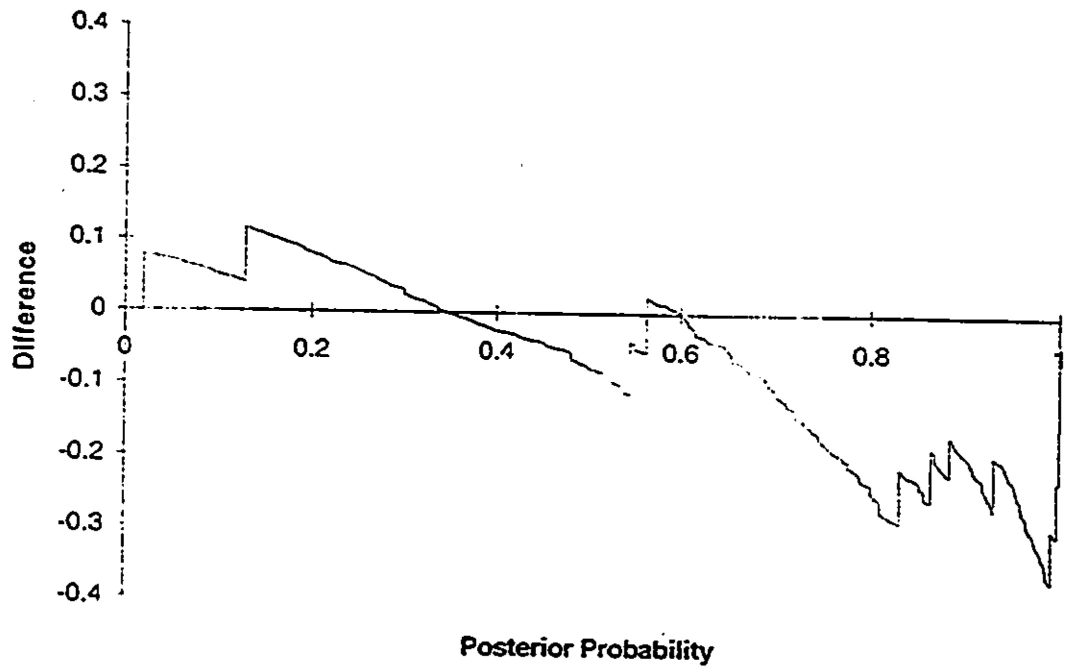

b)

Figure 5.4. a) Graphic representation of goodness-of-fit showing the distribution of observed versus theoretical frequencey distribution of deposits. b) the maximum difference is 0.3725 at a posterior probability of 0.98

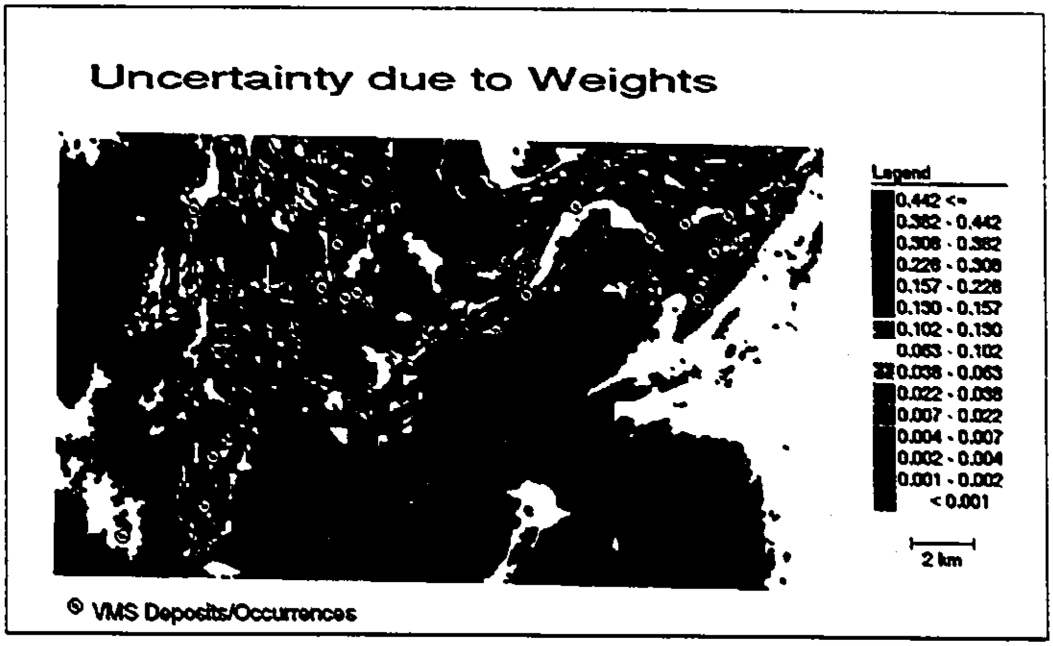

Figure 5.5 (a). Uncertainty of posterior probabilites due to variances with the estimates of the weights

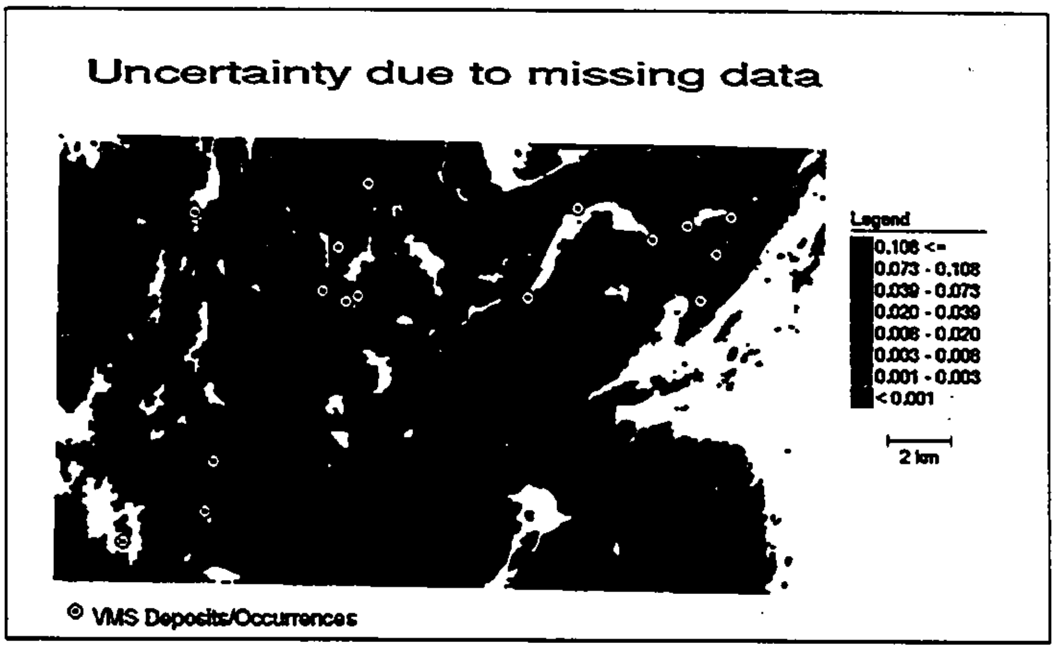

Figure 5.5 (b). Uncertainty of the posterior probability due to missing data.

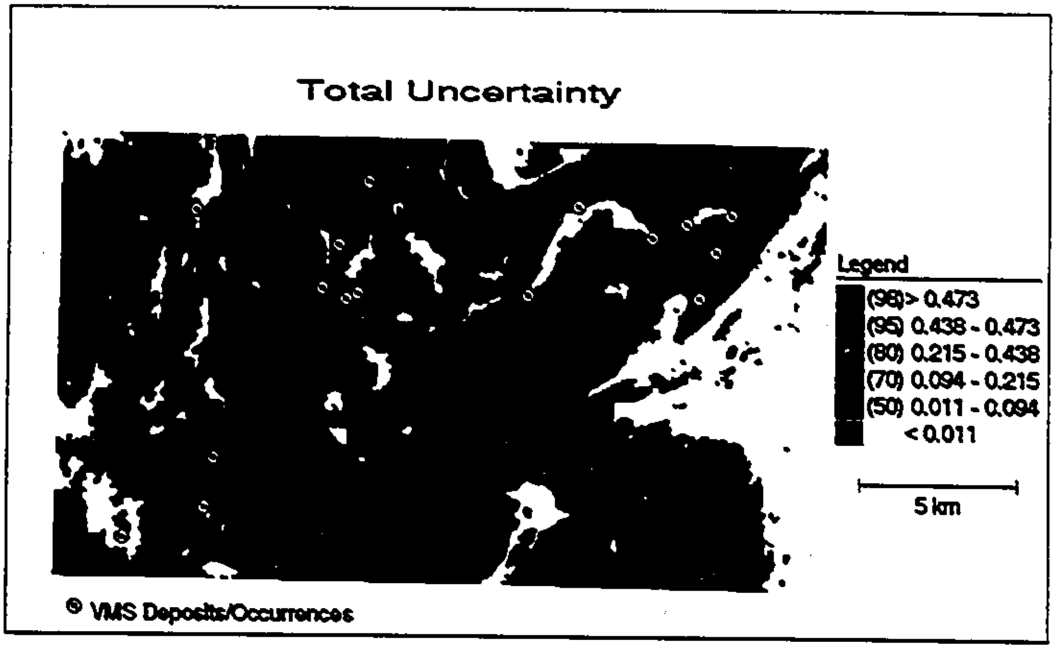

Figure 5.5 (c). The total uncertainty is the variance due to weights plus the sum of the variances due to the missing data.

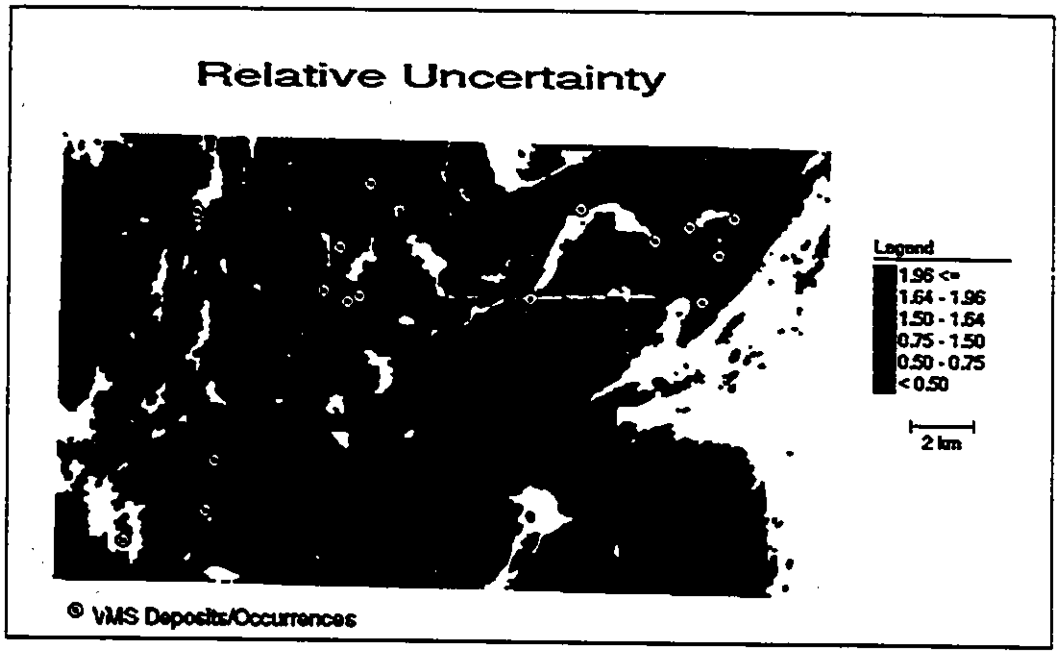

Figure 5.5 (d). Relative uncertainty of the posterior probability. The legend values represent t-values. Values greater than 1.645 indicate that the posterior probability is greater than 0 with a probability of 95%. The favourability in the various blue regions are relatively uncertain.

goodness-of-fit test. This is not unexpected, because many of the maps carry somewhat similar information. For example, the lake sediment chemistry and the till chemistry both reflect concentrations of Cu, Pb and Zn. Although the posterior probabilities are too large, it is likely that the ranking of areas by favourability is little affected by the violation of CI. In fact, the logistic regression approach, which does not require statistical independence, shows a favourability pattern very similar to that generated by the weights of evidence method. The logistic regression approach is discussed in Chapter 6.

Uncertainty of the posterior probability is due to many factors, but two important sources of error are; 1) uncertainty due to variances with the estimates of the weights and 2) variances due to missing data in one or more of the predictor maps. These uncertainties can be calculated using equations (5.18), (5.19), and (5.20). The total uncertainty for a unique overlap condition is the variance due to weights plus the sum of the variances due to missing data. These three variances are plotted in Figures 5.5 (a) - (c).

The posterior probability can be divided by its standard deviation due to uncertainties in the weights and due to missing data, in effect applying a test to determine whether the posterior probability is greater than zero (t-value). A t-value greater that 1.645 indicates that the corresponding posterior probability is greater than 0 with a probability of 95%. Areas in the relative uncertainty map, shown in Figure 5.5(d), that have values less than 1.645 (blue colours) are regions where the favourability estimates are relatively uncertain.

6. Integration Modelling Using Logistic Regression

6.1 Introduction

The use of regression analysis for estimating mineral resource potential has been described by Agterberg and Robinson (1972) where stepwise regression on 55 geological and geophysical variables was carried out in the Abitibi Volcanic belt in the Canadian Shield, to estimate the potential of 10 km cells (100 km^2) containing copper deposits. A retrospective study of the same area using the same methods was carried out by Agterberg and David (1979) following the discovery of 7 new deposits. The use of logistic regression for evaluating mineral potential was originally suggested by Tukey (1972) and applications carried out by Agterberg (1974) and Chung and Agterberg (1980).

The logistic regression model is different from the linear regression model in that the dependent variable in logistic regression is binary or dichotomous. The conditional mean or the expected value of the dependent value Y given the value x_{ij} of the i-th independent variable in the j-th cell for the logistic equation must be formulated to be bounded between 0 and 1. Also, the analysis of residuals in logistic regression is based on a binomial distribution instead of the normal distribution as in linear regression.

A FORTRAN computer program, LOGIST, for performing logistic regression was published by Chung (1978). The LOGIST program was modifed by Agterberg (1989), and called LOGDIA, so that frequencies of more than one discrete event in larger cells could be estimated and to provide a number of regression diagnostics. Finally, the program LOGDIA was modified so that when evidence was observed for polygons with unequal area, instead of equal-area cells, these could be weighted according to the size of the polygons (Agterberg, 1992). For this thesis, the LOGPOL program was modified to accept input from the GIS for up to 30 predictor variables and 10,000 weighted observations.

Weighted logistic regression was applied to the western half of the Chisel-Anderson area to predict VMS potential in an earlier study using a total of nine regional scale geological, geochemical and geophysical evidence maps (Agterberg, 1992; Reddy et al. (1991). These studies were preliminary in nature and emphasized method development.

The main advantages of using weighted logistic regression are 1) that the scores are confined to values between 0 and 1 so that they can be interpreted as probabilities, 2) when predictor variables are binary their coefficients can easily be interpreted and 3) it is not necessary for the predictor variables to be conditionally independent, an assumption of weights of evidence modelling. One of the key reasons for including this method in this study is to help evaluate the effects of conditional dependence that were observed in the weights of evidence method.

6.2 Weighted Logistic Regression Analysis Theory

Logistic regression methodology and diagnostics are presented in detail by Cox (1966) and Pregibon (1991). A simplified but lucid description of logistic regression is found in Hosmer and Lemeshow (1989). The algorithm used in LOGPOL is described in Agterberg (1990,1992) and summarized below.

The logistic model can be expressed as

$$P = \frac{\exp(\beta_0 + \beta_1 x_1 + \beta_2 x_2 + \ldots + \beta_n x_n)}{1 + \exp(\beta_0 + \beta_1 x_1 + \beta_2 x_2 + \ldots + \beta_n x_n)} \tag{6.1}$$

where,

P = the predicted probability of a mineral deposit occurring in a unit cell

β_i = unknown coefficients or parameters to be estimated, and

x_i = independent binary and/or continuous variables (with i=1,2,...,n)

Applying a logit (log-odds) transformation, the quantity P becomes

$$logit\ (P) = \ln\left[\frac{P}{1-P}\right] = \beta_0 + \beta_1 x_1 + \beta_2 x_2 + \ldots \beta_n x_n \tag{6.2}$$

Using matrix notation the values of *logit P* can be represented as a column vector

$$Y = \begin{bmatrix} x_{11} & x_{12} & x_{13} & \cdots & x_{1n} \\ x_{21} & x_{22} & x_{23} & \cdots & x_{2n} \\ & & \vdots & & \\ x_{i1} & x_{i2} & x_{i3} & \cdots & x_{\epsilon} \end{bmatrix} \cdot \begin{bmatrix} \beta_0 \\ \beta_1 \\ \vdots \\ \beta_i \end{bmatrix} \tag{6.3}$$

$Y = X\beta$, or in the (nxp) matrix X, where x_{ij} is the j-th observation for the i-th predictor variable and β_i is an unknown coefficient of the column vector β which is to be estimated.

In this study the area was not subdivided into equal-area cells and calculations performed on each cell; rather, the 23 evidence maps were represented as binary patterns, as used in the weights of evidence approach (see Chapter 5), and combined to generate a single map consisting of polygons of unequal area where each polygon is classified to represented a unique combination of the overlain input maps. This map, known as a unique conditions map, has j $(j=1,2,3...n)$ unique condition classes, where more than one polygon may have the same class. The study area is also described in terms of unit cells. These unit cells are allotted a small area generally used to represent the area of a deposit.

A value m_i is determined that represents the number of deposits in the j-th unique condition class. Two cases are of interest; where there are no deposits present for a unique condition class and where there are 1 or more deposits present. For the purpose of determining weights for performing the logistic regression calculations it is convenient to separate out the unique condition classes that have associated deposits and relabel them as m_j (j=1,2,3...n_d) where n_d is the number of unique conditions classes that have one or more deposits. The value m_j then, is the number of deposits for a unique condition class. Another value, t_i (i=1,2,3...n), representing the number of unit cells of the i-th unique condition not containing a deposit, is determined for all n unique condition classes. It will generally not be an integer value because it is the total area of the unique conditions class with the unit cell used as the unit of area. The values m_i and t_i are used to construct a weight vector as described below.

In practice the input for logistic regression is a table where the top portion represents unique conditions that have unit cells with deposits and the bottom portion represents unique conditions that have unit cells that do not contain deposits (usually all unique conditions). The total number of rows will be $N = n_d + n$ (number of unique conditions containing a deposit plus the total number of unique conditions). The two portions are identified by a column vector Y that contains a 1 if the record is a unique condition associated with a deposit (top n_d rows) and a 0 if it is a unique condition that has unit cells that have no deposits (bottom n rows).

Each row in the input table will consist of 23 values for the predictor variables (evidence maps), an element of the column vectos Y and a weight w_j. The first n_d rows will have a value of 1 for Y, and w_j will be the number of deposits per unique condition class. For the last n rows, Y will have the value of 0 and w_j will be equal to t_i.

A partial listing of the actual input data is shown in Table 6.1. The complete table has 7009 records with each record containing 25 fields. The complete input table is in the appendix of digital files (Appendix C) under the file name lucrep.inp.

Fitting the model requires obtaining estimates of the vector $\beta' = (\beta_0, \beta_1, \ldots \beta_k)$. The method of estimation used is maximum likelihood. There will be $k + 1$ likelihood equations which are obtained by differentiating the log-likelihood function with respect to the $k + 1$ coefficients. The likelihood equations that result may be expressed as

$$\sum_{i=1}^{n} [y_i - p_i] = 0 \tag{6.4}$$

and

$$\sum_{i=1}^{n} x_{ij} [y_i - p_i] = 0 \tag{6.5}$$

The estimated variances and covariances of the estimated coefficients are obtained from the matrix of second partial derivatives of the log-likelihood function. The partial derivatives can be expressed as

$$\frac{\partial^2 L(\beta)}{\partial \beta_j^2} = -\sum_{i=1}^{n} x_i^2 P_i (1 - P_i) \tag{6.6}$$

and

$$\frac{\partial^2 L(\beta)}{\partial\beta_j\,\partial\beta_u} = -\sum_{i=1}^{n} x_{ij}x_{iu}P_i(1-P_i) \tag{6.7}$$

for $j,u = 0,1,2,\ldots,p$ where p is the number of variables.

The matrix, $I(\beta)$, with dimensions (p+1) x (p+1) and containing the negative of the terms given by equations 6.6 and 6.7, is called the information matrix. The variances and covariances of the estimated coefficients are obtained from the inverse of this matrix.

For an $N \times N$ diagonal matrix V with nonzero elements $V_{jj} = w_j \cdot \hat{Y}_j \cdot (1-\hat{Y}_j)$, where $\hat{Y}_j$ is an estimated value of the probability P_j and using the maximum likelihood method to estimate coefficients, a column vector of scores $S = Y - \hat{Y}$ is made to converge until the relation $X'S = 0$ is satisfied.

When the input observations can be regarded as statistically independent, the goodness-of-fit can be evaluated by using the χ^2-*test* and the deviance statistic. Also these statistics depend on the unit cell size used for expressing the areas of the unique conditions (Agterberg, 1992) with both statistics increasing as the unit cell size decreases. It is noted in this study that the input observations are not statistically independent. As an alternative goodness-of-fit test the Kolmogorov-Smirnov test can be used. It has an advantage in that it does not require grouping of the observations into arbitrary categories as is done with the χ^2-*test*. In practice, the unique condition areas

Table 6.1. Example of input for weighted logistic regression. Note that the first 15 records have Y = 1 indicating it is a unit cell containing a deposit. The columns M_1 to M_{23} are references to input maps listed in Table 5.6. A value of 1 indicates the pattern is present and a value of 0 indicates the pattern is absent.

M_1	M_2	M_3	M_4	M_5	M_6	M_7	M_8	M_9	M_{10}	M_{11}	M_{12}	M_{13}	M_{14}	M_{15}	M_{16}	M_{17}	M_{18}	M_{19}	M_{20}	M_{21}	M_{22}	M_{23}	Y	W
1	0	1	1	1	0	0	0	0	0	1	1	0	1	1	1	0	0	1	0	1	0	1	1	1.00
1	1	1	1	0	1	0	0	1	0	0	0	0	0	1	0	1	1	0	1	0	0	1	1	1.00
1	1	1	1	1	1	0	0	0	0	0	1	0	1	1	1	1	1	1	1	1	0	1	1	1.00
1	0	1	1	1	1	0	0	0	0	0	0	1	1	0	0	0	0	1	0	1	0	0	1	1.00
1	0	0	1	1	0	0	0	0	0	0	1	1	1	1	1	0	0	0	0	1	0	1	1	1.00
1	0	1	1	1	1	0	1	0	1	0	0	0	1	0	0	0	0	1	0	1	0	1	1	1.00
1	1	1	1	1	0	0	0	0	0	0	1	0	1	0	1	0	0	1	0	1	0	1	1	1.00
0	0	1	1	1	0	0	0	1	1	0	1	0	0	1	0	0	1	1	0	1	1	1	1	1.00
1	1	1	0	1	1	0	1	0	1	0	1	0	0	1	1	1	1	1	1	1	0	0	1	1.00
1	0	1	1	1	1	1	1	0	0	0	0	1	1	1	1	0	0	1	1	1	0	1	1	1.00
1	1	1	1	1	1	1	1	1	0	0	1	0	0	1	1	1	0	0	0	1	0	0	1	1.00
1	0	1	0	1	1	1	0	1	0	0	1	0	1	1	1	1	1	1	1	1	1	1	1	1.00
1	1	1	1	1	1	0	0	1	0	0	1	0	1	1	1	1	1	1	0	1	0	0	1	1.00
1	0	0	1	1	1	1	0	0	1	0	0	1	1	0	0	0	0	0	0	1	0	1	1	1.00
1	1	1	0	1	0	0	0	0	0	0	1	0	0	1	1	0	0	1	0	1	0	1	1	1.00
0	0	0	0	0	0	0	0	0	0	0	0	0	0	0	0	0	0	0	0	0	0	1	0	528.12
0	0	0	0	0	0	0	0	0	0	0	0	0	0	0	0	0	0	0	0	0	0	0	0	460.94
0	0	0	0	0	0	0	0	0	0	0	0	0	1	0	0	0	0	0	0	0	0	1	0	417.65
0	0	0	0	0	0	0	0	0	0	0	0	0	0	0	0	0	0	0	0	0	0	1	0	375.26
0	0	0	0	0	0	0	0	0	0	0	0	0	0	0	0	0	0	0	0	0	0	1	0	253.45
1	0	0	1	1	0	0	0	0	0	0	0	0	0	0	0	0	0	0	0	1	0	0	0	204.40
0	0	0	0	0	0	0	0	0	0	0	1	0	0	0	0	0	0	0	0	0	0	1	0	200.24
0	0	0	0	0	1	0	0	0	0	0	0	0	0	0	0	0	0	0	0	0	0	1	0	192.63
1	0	0	1	1	0	0	0	0	0	0	0	0	0	0	0	0	0	0	0	1	0	1	0	190.05
0	0	0	0	0	0	0	0	0	0	0	0	0	0	0	0	0	0	0	0	0	0	0	0	181.50
0	0	0	0	0	0	0	0	0	0	0	1	0	0	0	0	0	0	0	0	0	0	0	0	181.00
0	0	0	0	0	0	0	0	0	0	0	0	1	0	0	0	0	0	0	0	0	0	0	0	166.15
0	0	0	0	0	0	0	0	0	0	0	0	0	0	0	0	0	0	0	0	0	0	0	0	165.23
0	0	0	0	0	0	0	0	0	0	0	1	0	0	0	0	0	0	0	0	0	0	0	0	159.04
1	0	1	1	1	1	0	1	0	0	0	1	0	0	0	0	1	0	0	0	1	0	1	0	.01
0	0	1	1	1	0	0	0	0	1	0	1	0	0	0	0	0	0	1	0	1	1	0	0	.01
0	0	1	1	0	1	0	0	1	0	0	1	0	0	0	0	0	0	1	0	1	1	1	0	.01
1	0	0	1	1	1	0	1	0	0	0	0	0	0	0	0	0	0	0	0	1	0	1	0	.01
1	1	1	0	0	0	0	0	0	1	0	0	0	0	0	0	0	0	0	0	1	0	1	0	.01
1	0	1	0	1	1	0	0	0	0	0	1	1	0	0	0	1	0	1	0	1	0	0	0	.01
1	0	1	1	1	0	0	0	0	1	0	1	0	0	0	0	0	0	1	0	1	1	0	0	.01

are ranked in order of their probabilities and the cumulative frequency distributions for the expected number of deposits and observed number of deposits determined for each area.

The expected frequency is calculated as

$$f_{ei} = \frac{A_k p_k}{\sum_{k=1}^{n} A_k p_k}$$

where A_i is the area of the i-th polygon with an estimated probability p_i.

6.3 Application

6.3.1 Evidence Maps

The same 23 binary evidence maps used in the weights of evidence method (Table 5.2), were used for this application of weighted logistic regression. This was to facilitate comparison with the weights of evidence model although it is noted that the multiclass maps could be used. This also made it possible to use the same unique conditions table built in SPANS for the weights of evidence method (see Appendix B-2(c)) as input for the FORTRAN computer program PREDICTR (Appendix B-2(c) for application and Appendix C for digital listing). Included in PREDICTR is a subroutine for weighted logistic regression. This subroutine is a version of the FORTRAN computer program LOGDIA (Agterberg, 1989) modified to allow weighting of the unique conditions according to their areas and to output the results in a format that is directly usable for SPANS.

6.3.2 Initial Parameters

The convergence level was set to 0.001. At the beginning of the iterative process of making the scores converge to 0.001 all the coefficients were set equal to zero. This generally leads to satisfactory results in fewer than 10 iterations (Agterberg, 1992). In weights of evidence modelling, the weights can be estimated for patterns with missing data (lake sediment geochemistry, till geochemistry) by omitting areas that are unknown from the weight calculations. In logistic regression, the portions of maps that have areas that are classified as "unknown" cannot be omitted because coefficients for all patterns are estimated simultaneously and significant loss of information would result. For this study the unknown areas in the lake sediment geochemistry maps and the till geochemistry maps were modified so that they were classified as "pattern not present" so that these maps could still be included in the model.

6.3.3 Results

Logistic regression coefficients were calculated for cell sizes of 1 km^2, 0.5 km^2, 0.1 km^2 and 0.01 km^2. The coefficients are listed in Table 6.2 a-d with the weights, their standard deviations, and contrasts of the weights from the weights of evidence method are also included for comparison. The coefficients change because the independent variables are weighted according to the area of the unique condition expressed in numbers of unit cells. Since the total study area is 335.28 km^2 the number of 1 km^2 unit

Table 6.2. Logistic regression coefficients, weights, contrast, with standard deviations and studentized C for models using a) 1.0 km^2 unit cells b) 0.5 km^2 unit cells c) 0.1 km^2 unit cells and d) 0.01 km^2 unit cells

a)

Map	B	s(B)	W+	s(W+)	W-	s(W-)	C	C/s(C)
Constant	-10.8910	2.8347						
DYKEBUFB	0.6359	1.4656	0.479	0.277	-1.844	1.004	2.323	2.231
FFLOWB	2.4389	1.0481	2.360	0.462	-0.584	0.358	2.943	5.033
GEOL2C2B	0.6715	1.0907	1.208	0.298	-1.715	0.710	2.923	3.798
GEOL4C2B	1.4483	1.0684	0.714	0.302	-1.112	0.582	1.826	2.786
GEOL5C2B	1.0249	1.5907	0.704	0.280	-2.089	1.003	2.793	2.683
KRGLNCUB	0.5360	1.0370	0.584	0.337	-0.906	0.586	1.490	2.203
KRGLNPBB	-0.5567	1.0685	0.909	0.546	-0.468	0.512	1.377	1.838
KRGLNZNB	0.3566	1.0280	0.991	0.547	-0.307	0.388	1.298	1.935
LKPC1NCB	1.6788	1.2492	1.403	0.501	-0.320	0.323	1.723	2.891
LKPC2NCB	1.6601	0.9975	1.266	0.553	-0.232	0.309	1.498	2.366
LKPC3NCB	2.7318	1.5857	0.733	1.063	-0.036	0.275	0.770	0.701
SILLBUFB	-0.2324	1.0889	0.259	0.326	-0.376	0.454	0.635	1.136
SYNDYKB	2.5160	1.0463	1.495	0.546	-0.242	0.307	1.647	2.631
GRVNC25B	0.2244	0.8209	0.456	0.328	-0.550	0.453	1.006	1.799
MGNTCMB	-0.0690	1.0722	0.628	0.314	-0.825	0.505	1.453	2.442
MGNVCMB	0.4287	0.9548	0.599	0.329	-0.643	0.453	1.242	2.219
NALTAPCB	0.0652	1.3932	1.351	0.444	-0.401	0.339	1.753	3.141
NALTEPCB	-0.2097	1.4601	1.468	0.448	-0.414	0.338	1.883	3.354
NALTFECB	1.4625	0.9143	1.409	0.329	-1.124	0.504	2.533	4.209
NALTPPCB	1.5393	1.3517	3.254	0.665	-0.393	0.321	3.647	4.937
NALTSICB	0.9038	1.5283	0.591	0.278	-1.981	1.003	2.572	2.471
NPVLF25B	0.7660	1.1725	1.216	0.761	-0.103	0.283	1.319	1.624
SLVLF25B	1.0831	0.7901	0.305	0.311	-0.544	0.507	0.850	1.429

NALTPPCB Favourable areas associated with alteration pipes
FFLOWB Areas mapped as felsic flows only
GEOL2C2B Favourable areas associated with felsic flows
NALTFECB Favourable areas associated with Fe alteration
NALTSICB Favourable areas associated with Si alteration
DYKBUFB Favourable areas associated with synvolcanic dykes
KRGLNZNB Favourable areas associated with Zn in C horizon tills (<63 μm)
NALTAPCB Favourable areas associated with amphibole alteration
LKPC1NCB Favourable areas associated with Pricipal Component 1 scores
NALTEPCB Favourable areas associated with epidote alteration
GEOL5C2B Favourable areas associated with mafic volcaniclastic rocks
KRGLNCUB Favourable areas associated with Cu in C horizon tills (<63 μm)
GEOL4C2B Favourable areas associated with felsic volcaniclastics
LKPC2NCB Favourable areas associated with Principal Component 2
SYNDYKB Favourable areas associated with synvolcanic dykes
LKPC3NCB Favourable areas associated with Principal Component 3
GRVNC25B Favourable areas associated with Vertical gradient gravity map
MGNTCMB Favourable areas associated with Total field magnetics
KRGLNPBB Favourable areas associated with Pb in C horizon tills (<63 μm)
MGNVCMB Favourable areas associated with Vertical gradient magnetics
SLVLF25B Favourable areas associated with Total field VLF
NPVLF25B Favourable areas associated with Processed quadrature VLF
SILLBUFB Favourable areas associated with Areas mapped as subvolcanic sills

b)

Map	B	s(B)	W+	s(W+)	W-	s(W-)	C	C/s(C)
Constant	-10.9404	2.4345						
DYKEBUFB	0.5575	1.2946	0.465	0.272	-1.825	1.002	2.290	2.206
FFLOWB	2.0881	0.9056	2.161	0.414	-0.573	0.356	2.735	5.011
GEOL2C2B	0.6834	0.9905	1.156	0.287	-1.696	0.709	2.852	3.730
GEOL4C2B	1.5475	0.9956	0.690	0.295	-1.097	0.580	1.787	2.748
GEOL5C2B	0.9282	1.4435	0.681	0.273	-2.069	1.001	2.750	2.649
KRGLNCUB	0.4800	0.9165	0.555	0.326	-0.884	0.582	1.438	2.157
KRGLNPBB	-0.0145	0.9618	0.522	-0.454	0.506	1.308	0.727	1.800
KRGLNZNB	0.3516	0.9144	0.933	0.522	-0.298	0.383	1.230	1.900
LKPC1NCB	1.4583	1.0524	1.314	0.472	-0.312	0.320	1.626	2.853
LKPC2NCB	1.5430	0.8982	1.191	0.524	-0.226	0.305	1.417	2.337
LKPC3NCB	2.5564	1.4310	0.701	1.030	-0.035	0.271	0.736	0.691
SILLBUFB	-0.2866	0.9918	0.252	0.321	-0.369	0.451	0.621	1.123
SYNDYKB	2.2010	0.9093	1.337	0.521	-0.238	0.304	1.575	2.609
GRVNC25B	0.1976	0.7334	0.443	0.322	-0.540	0.450	0.983	1.777
MGNTCMB	-0.1246	0.9832	0.608	0.308	-0.812	0.503	1.420	2.410
MGNVCMB	0.4419	0.8591	0.581	0.323	-0.632	0.450	1.213	2.190
NALTAPCB	0.2127	1.2017	1.288	0.425	-0.394	0.336	1.682	3.105
NALTEPCB	-0.0970	1.2815	1.395	0.427	-0.406	0.336	1.801	3.317
NALTFECB	1.4163	0.8208	1.340	0.314	-1.109	0.502	2.449	4.135
NALTPPCB	1.4693	1.1624	2.804	0.525	-0.385	0.319	3.189	5.193
NALTSICB	0.8396	1.3944	0.573	0.273	-1.961	1.002	2.534	2.441
NPVLF25B	0.6787	1.0229	1.163	0.733	-0.101	0.280	1.264	1.611
SLVLF25B	0.8932	0.7005	0.297	0.306	-0.535	0.503	0.832	1.412

NALTPPCB Favourable areas associated with alteration pipes
FFLOWB Areas mapped as felsic flows only
GEOL2C2B Favourable areas associated with felsic flows
NALTFECB Favourable areas associated with Fe alteration
NALTSICB Favourable areas associated with Si alteration
DYKBUFB Favourable areas associated with synvolcanic dykes
KRGLNZNB Favourable areas associated with Zn in C horizon tills (<63 μm)
NALTAPCB Favourable areas associated with amphibole alteration
LKPC1NCB Favourable areas associated with Pricipal Component 1 scores
NALTEPCB Favourable areas associated with epidote alteration
GEOL5C2B Favourable areas associated with mafic volcaniclastic rocks
KRGLNCUB Favourable areas associated with Cu in C horizon tills (<63 μm)
GEOL4C2B Favourable areas associated with felsic volcaniclastics
LKPC2NCB Favourable areas associated with Principal Component 2
SYNDYKB Favourable arers associated with synvolcanic dykes
LKPC3NCB Favourable areas associated with Principal Component 3
GRVNC25B Favourable areas associated with Vertical gradient gravity map
MGNTCMB Favourable areas associated with Total field magnetics
KRGLNPBB Favourable areas associated with Pb in C horizon tills (< 63 μm)
MGNVCMB Favourable areas associated with Vertical gradient magnetics
SLVLF25B Favourable areas associated with Total field VLF
NPVLF25B Favourable areas associated with Processed quadrature VLF
SILLBUFB Favourable areas associated with Areas mapped as subvolcanic sills

c)

Map	B	s(B)	W+	s(W+)	W-	s(W-)	C	C/s(C)
Constant	-11.9140	2.0820						
DYKEBUFB	0.4682	1.1494	0.454	0.268	-1.810	1.000	2.264	2.186
FFLOWB	1.7305	0.7848	2.032	0.384	-0.565	0.354	2.597	4.971
GEOL2C2B	0.7016	0.9053	1.117	0.279	-1.681	0.707	2.799	3.680
GEOL4C2B	1.6426	0.9124	0.673	0.290	-1.085	0.578	1.758	2.719
GEOL5C2B	0.8365	1.3233	0.664	0.268	-2.053	1.000	2.716	2.623
KRGLNCUB	0.4308	0.8131	0.534	0.318	-0.866	0.578	1.400	2.121
KRGLNPBB	-0.0313	0.8596	0.815	0.504	-0.443	0.501	1.258	1.770
KRGLNZNB	0.4075	0.8154	0.891	0.504	-0.289	0.379	1.181	1.873
LKPC1NCB	1.2441	0.8613	1.252	0.452	-0.305	0.317	1.557	2.822
LKPC2NCB	1.3139	0.7880	1.139	0.505	-0.221	0.302	1.359	2.311
LKPC3NCB	2.2856	1.2678	0.677	1.006	-0.035	0.268	0.712	0.684
SILLBUFB	-0.3461	0.9107	0.247	0.317	-0.363	0.448	0.611	1.112
SYNDYKB	1.9138	0.7846	1.288	0.504	-0.234	0.302	1.521	2.589
GRVNC25B	0.1337	0.6500	0.433	0.317	-0.533	0.448	0.966	1.760
MGNTCMB	-0.0821	0.8983	0.593	0.303	-0.802	0.501	1.395	2.385
MGNVCMB	0.4501	0.7773	0.567	0.317	-0.623	0.448	1.190	2.168
NALTAPCB	0.2095	1.0080	1.242	0.411	-0.388	0.334	1.630	3.076
NALTEPCB	0.0121	1.1350	1.342	0.412	-0.400	0.334	1.742	3.286
NALTFECB	1.3573	0.7302	1.291	0.304	-1.097	0.500	2.388	4.078
NALTPPCB	1.4856	0.9917	2.558	0.460	-0.379	0.317	2.937	5.259
NALTSICB	0.8301	1.2828	0.559	0.268	-1.945	1.000	2.505	2.418
NPVLF25B	0.4336	0.8603	1.124	0.712	-0.099	0.278	1.223	1.600
SLVLF25B	0.6930	0.6189	0.291	0.302	-0.527	0.501	0.818	1.399

NALTPPCB Favourable areas associated with alteration pipes
FFLOWB Areas mapped as felsic flows only
GEOL2C2B Favourable areas associated with felsic flows
NALTFECB Favourable areas associated with Fe alteration
NALTSICB Favourable areas associated with Si alteration
DYKBUFB Favourable areas associated with synvolcanic dykes
KRGLNZNB Favourable areas associated with Zn in C horizon tills (<63 μm)
NALTAPCB Favourable areas associated with amphibole alteration
LKPC1NCB Favourable areas associated with Pricipal Component 1 scores
NALTEPCB Favourable areas associated with epidote alteration
GEOL5C2B Favourable areas associated with mafic volcaniclastic rocks
KRGLNCUB Favourable areas associated with Cu in C horizon tills (<63 μm)
GEOL4C2B Favourable areas associated with felsic volcaniclastics

LKPC2NCB Favourable areas associated with Principal Component 2
SYNDYKB Favourable areas associated with synvolcanic dykes
LKPC3NCB Favourable areas associated with Principal Component 3
GRVNC25B Favourable areas associated with Vertical gradient gravity map
MGNTCMB Favourable areas associated with Total field magnetics
KRGLNPBB Favourable areas associated with Pb in C horizon tills (< 63 μm)
MGNVCMB Favourable areas associated with Vertical gradient magnetics
SLVLF25B Favourable areas associated with Total field VLF
NPVLF25B Favourable areas associated with Processed quadrature VLF
SILLBUFB Favourable areas associated with Areas mapped as subvolcanic sills

d)

Map	B	s(B)	W+	s(W+)	W-	s(W-)	C	C/s(C)
Constant	-14.0539	1.9929						
DYKEBUFB	0.4378	1.1123	0.452	0.267	-1.806	1.000	2.258	2.182
FFLOWB	1.6445	0.7587	2.006	0.379	-0.564	0.354	2.569	4.960
GEOL2C2B	0.7193	0.8860	1.109	0.278	-1.678	0.707	2.787	3.669
GEOL4C2B	1.6608	0.8840	0.669	0.289	-1.082	0.577	1.751	2.712
GEOL5C2B	0.8005	1.2918	0.660	0.267	-2.049	1.000	2.709	2.617
KRGLNCUB	0.4113	0.7901	0.529	0.316	-0.863	0.577	1.392	2.114
KRGLNPBB	-0.0270	0.8298	0.807	0.500	-0.441	0.500	1.248	1.764
KRGLNZNB	0.4453	0.7923	0.882	0.500	-0.289	0.378	1.171	1.867
LKPC1NCB	1.1705	0.8096	1.239	0.448	-0.304	0.316	1.543	2.815
LKPC2NCB	1.2152	0.7463	1.127	0.500	-0.220	0.302	1.347	2.306
LKPC3NCB	2.1812	1.2190	0.672	1.001	-0.034	0.267	0.706	0.682
SILLBUFB	-0.3511	0.8880	0.246	0.316	-0.362	0.447	0.608	1.110
SYNDYKB	1.8654	0.7522	1.277	0.500	-0.233	0.302	1.510	2.585
GRVNC25B	0.1031	0.6278	0.431	0.316	-0.531	0.447	0.962	1.756
MGNTCMB	-0.0391	0.8734	0.590	0.302	-0.800	0.500	1.390	2.380
MGNVCMB	0.4524	0.7563	0.564	0.316	-0.622	0.447	1.185	2.163
NALTAPCB	0.1466	0.9504	1.232	0.409	-0.387	0.333	1.619	3.069
NALTEPCB	0.0381	1.1022	1.330	0.409	-0.399	0.333	1.729	3.279
NALTFECB	1.3302	0.7011	1.280	0.302	-1.094	0.500	2.374	4.065
NALTPPCB	1.5278	0.9359	2.511	0.448	-0.378	0.316	2.889	5.265
NALTSICB	0.8437	1.2533	0.556	0.267	-1.942	1.000	2.498	2.413
NPVLF25B	0.3332	0.8105	1.116	0.708	-0.098	0.277	1.214	1.598
SLVLF25B	0.6491	0.5999	0.290	0.302	-0.526	0.500	0.815	1.396

NALTPPCB Favourable areas associated with alteration pipes
FFLOWB Areas mapped as felsic flows only
GEOL2C2B Favourable areas associated with felsic flows
NALTFECB Favourable areas associated with Fe alteration
NALTSICB Favourable areas associated with Si alteration
DYKBUFB Favourable areas associated with synvolcanic dykes
KRGLNZNB Favourable areas associated with Zn in C horizon tills (<63 μm)
NALTAPCB Favourable areas associated with amphibole alteration
LKPC1NCB Favourable areas associated with Pricipal Component 1 scores
NALTEPCB Favourable areas associated with epidote alteration
GEOL5C2B Favourable areas associated with mafic volcaniclastic rocks
KRGLNCUB Favourable areas associated with Cu in C horizon tills (<63 μm)
GEOL4C2B Favourable areas associated with felsic volcaniclastics
LKPC2NCB Favourable areas associated with Principal Component 2
SYNDYKB Favourable areas associated with synvolcanic dykes
LKPC3NCB Favourable areas associated with Principal Component 3
GRVNC25B Favourable areas associated with Vertical gradient gravity map
MGNTCMB Favourable areas associated with Total field magnetics
KRGLNPBB Favourable areas associated with Pb in C horizon tills (< 63 μm)
MGNVCMB Favourable areas associated with Vertical gradient magnetics
SLVLF25B Favourable areas associated with Total field VLF
NPVLF25B Favourable areas associated with Processed quadrature VLF
SILLBUFB Favourable areas associated with Areas mapped as subvolcanic sills

cells would be 335.28, the number of 0.5 km^2 unit cells would be 770.56 and the number of 0.01 km^2 unit cells would be 33528 unit cells. If a unique condition contains more than 1 deposit it would be weighted according to the number of deposits, however, it can be seen from Table 6.1 that each deposit has a unique set of independent variables associated with it (see 1st 15 rows).

The coefficients appear to be approaching a limiting value as the unit cell size decreases as shown by Agterberg (1992). The constant term (row 0 in Table 6.2(a) - 6.2(d)) can be compared to the prior logit in weights of evidence. The prior logits for the four different unit cell sizes are shown in Table 6.3.

The prior logits are smaller than the constant term in the logistic regression model by a factor of 1.82 for the 0.01 km^2 unit cells to a factor of 3.5 for the 1.0 km^2 unit cells. The reason for this difference is not understood.

The 23 coefficients can be compared to the contrast (W^+ - W^-) because they affect the results only if they are present. The negative weight does not have an equivalent term in logistic regression analysis. The coefficients can also be compared to

Table 6.3. Prior logit for different unit cell sizes calculated in the weights of evidence modelling

Unit Cell Size	1.0 km^2	0.5 km^2	0.1 km^2	0.01 km^2
Prior Logit	-3.0615	-3.7778	-5.4053	-7.7119
SD Prior Logit	0.4642	0.2611	0.2588	0.2583

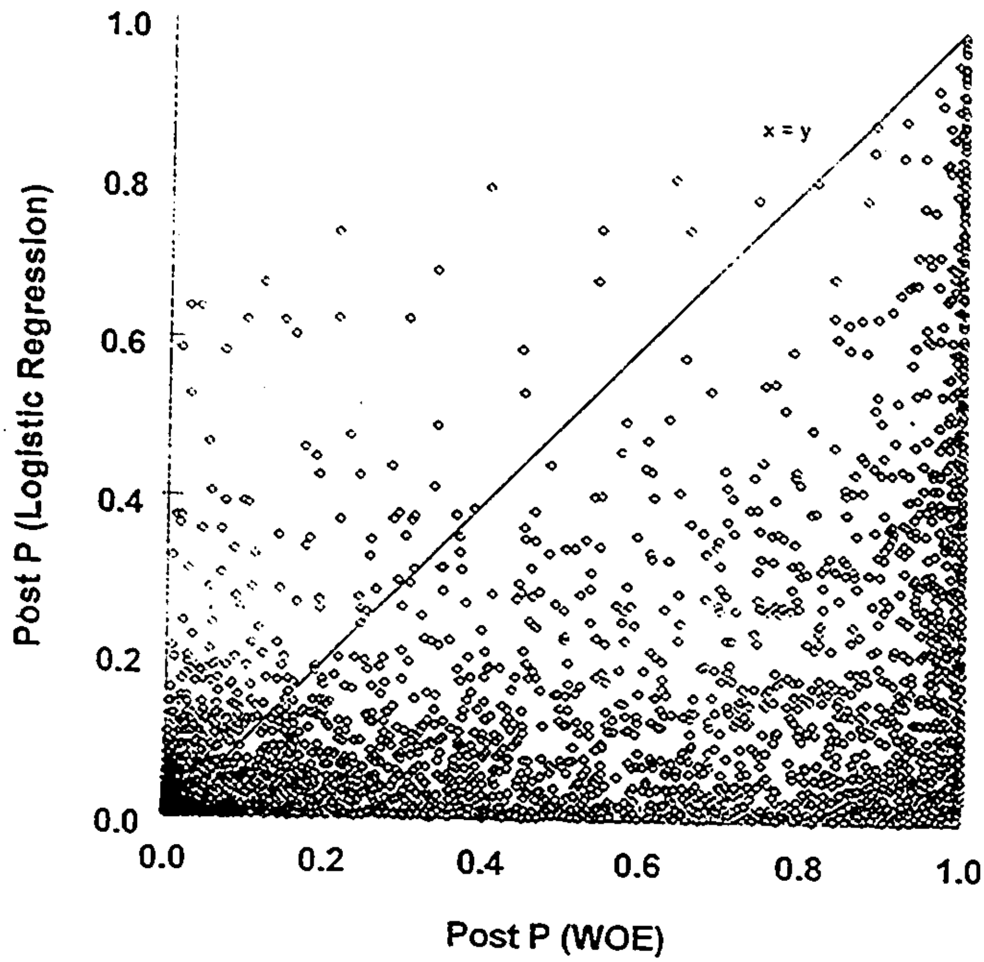

Figure 6.1. Plot of posterior probability generated by the weights of evidence method versus the posterior probability generated by the area weighted logistic regression method. The logistic regression results tend to be much lower than those from the weights of evidence method.

the C (Contrast) value since C is a measure of the significance of that particular piece of evidence as is the coefficient.

Comparing the coefficients to the weights and contrasts shows significant discrepancies in their size and rank. As observed in the weights of evidence method the overall test for conditional independence showed that the patterns seem to be interrelated (there is a violation of the assumption of conditional independence). The differences observed between the weights and coefficients and the relatively large standard deviations of the coefficients provide further evidence of multicollinearity in the system. Evidence maps that have coefficients much less than W+ or C are suggestive that conditional independence is a problem in the weights of evidence method. There are not many coefficients that can be truly identified as much smaller than W+ in Table 6.2 because of the large standard deviations associated with the coefficients, however, the kriged till geochemsitry maps for Pb (KRGLNPBB) and Zn (KRGLNZNB), the alteration maps for epidote (NALTEPCB) and amphibole (NALTAPCP) and the total field magnetic map (MGNTCMB) are all highly suspect (see Table 6.2).

Further evidence that there is a lack of conditional independence is suggested by the differences in the size of the posterior probabilities between the logistic regression method and the weights of evidence method. The posterior probabilities calculated using the weights of evidence method, using a unit cell size of 0.10 km^2, range from 0.000 to 0.998 (Figure 5.3). For the larger probabilities, they are many in the order of 20 times larger than those determined using logistic regression for the same unit cell size (see Figure 6.2). The large differences between the posterior probabilities for these two methods are further illustrated in Figure 6.1. In general there is not a very strong correlation (Pearsons R = 0.632) between the two results but the plot does emphasize that the posterior probabilities generated by the area weighted logistic regression method are much smaller than those generated by the weights of evidence method.

The Chi-square values for pairwise conditional independence tests, shown in Table 5.3, suggest that there are no pairs of maps that are obviously dependent. This makes it difficult to investigate this matter further, though one approach would be to systematically eliminate evidence maps until the results from the two methods were in better agreement.

Figure 6.2 shows the logistic posterior probability map (unit cell size = 0.1 km^2) which appears to have very similar distribution of areas indicating high favourability as the map showing results of the weights of evidence method (Figure 5.3).

6.4 Error Considerations

6.4.1Goodness-of-fit

Of interest is to evaluate how well the model does at predicting deposits with respect to known deposits. In general a model is good if the number of predicted deposits is close to the number of observed or actual deposits, which in this case is 15. The

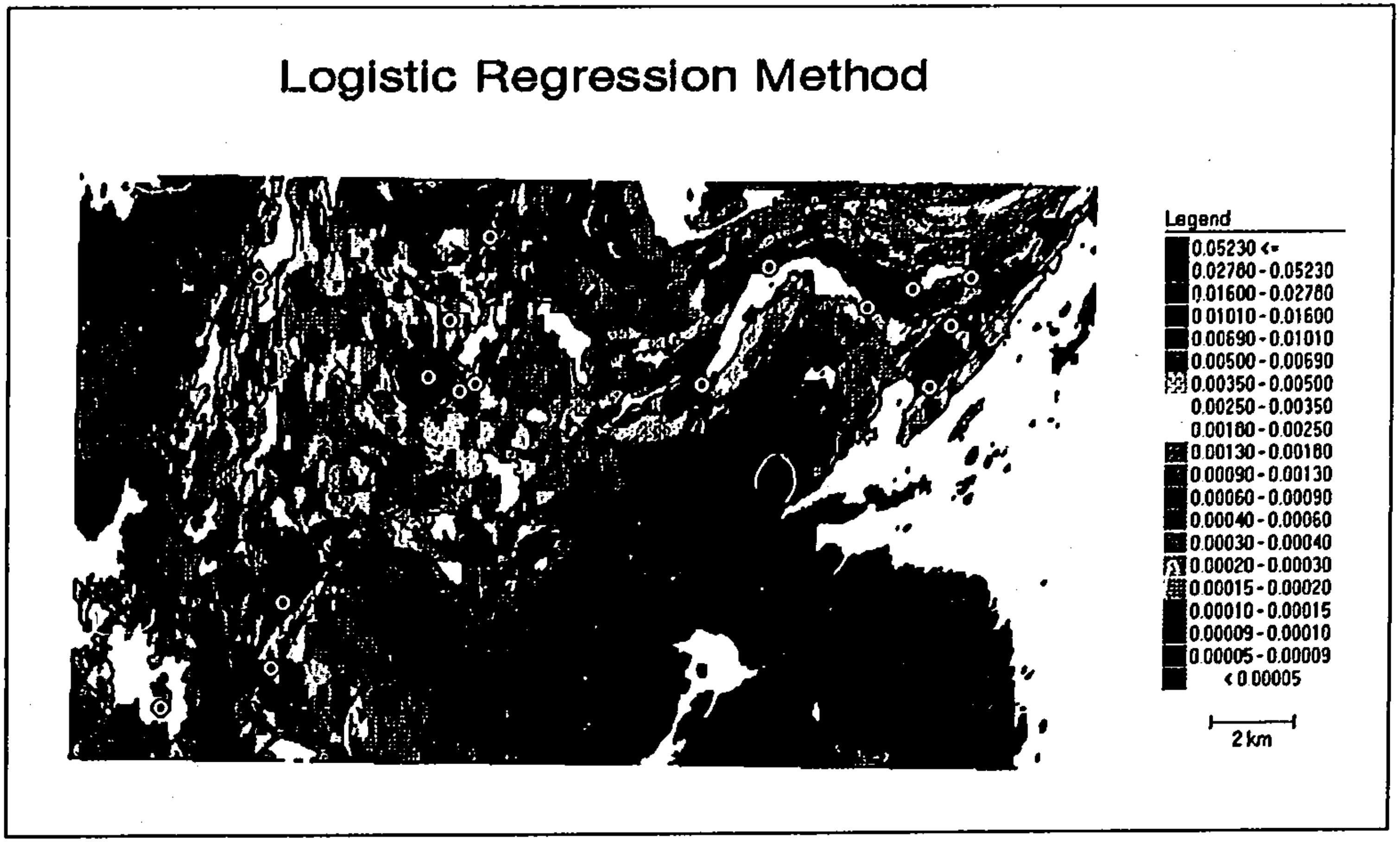

Figure 6.2. Posterior probability map for VHMS deposits generated by the area weighted logistic regression method.

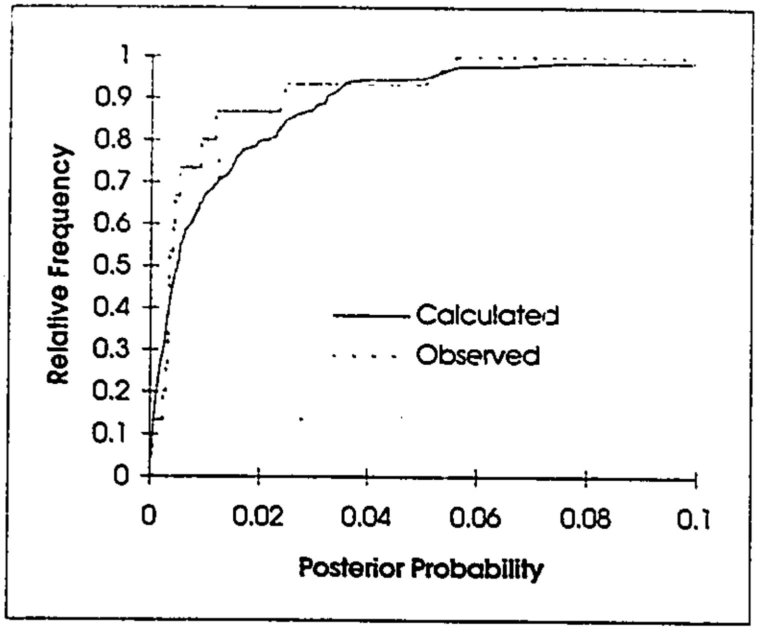

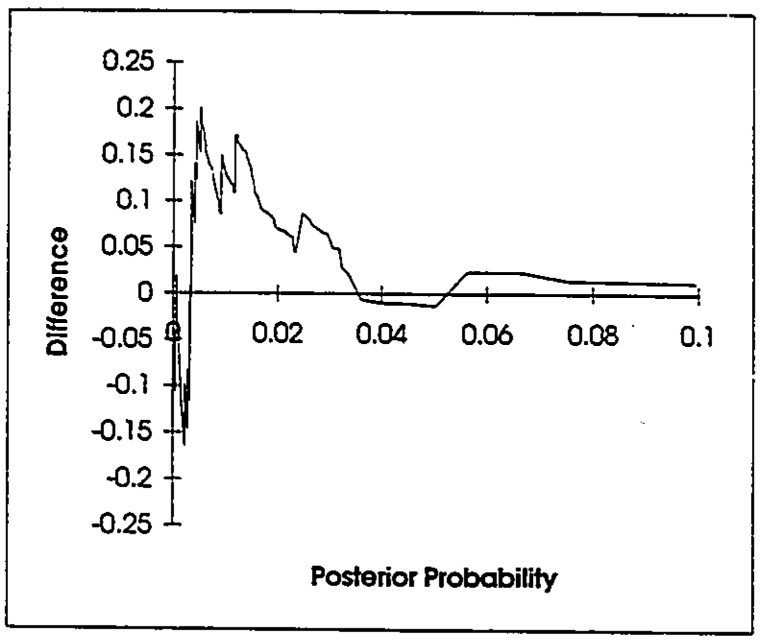

Figure 6.3 (a) - (c). Graphic representation of degree of fit for the logistic regression method. (a) Results for unit cell size of 0.01 km^2. Maximum difference is 0.201 at a posterior probability of .002

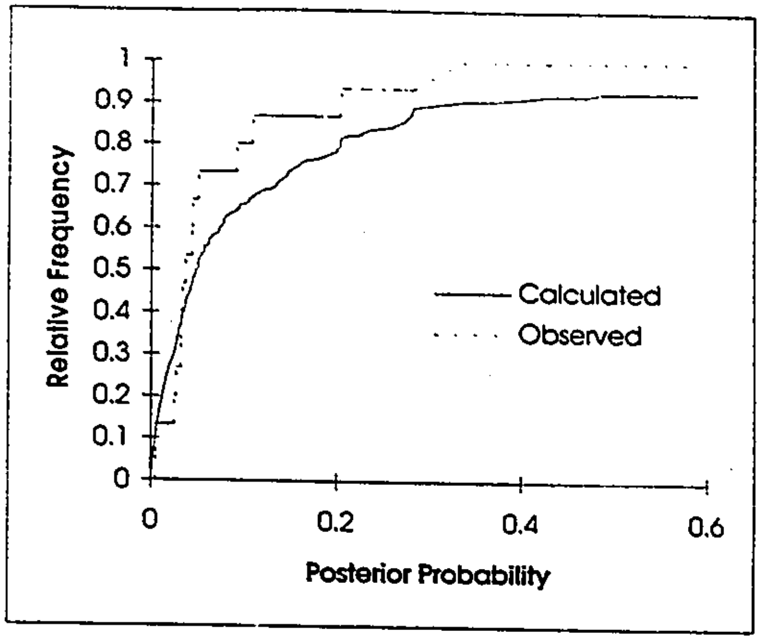

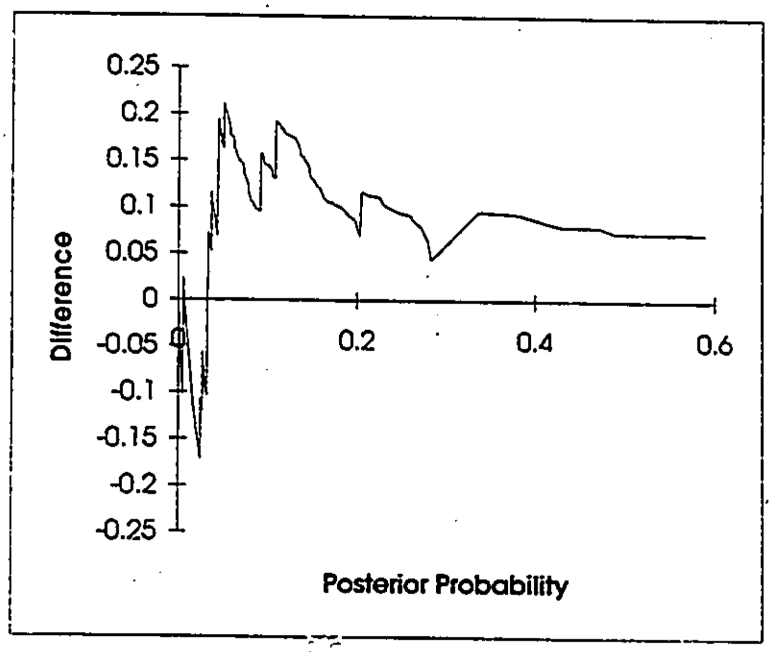

(b) Results for unit cell size of 0.1 km^2. Maximum difference between observed and calculated is 0.211 at probability 0.0052

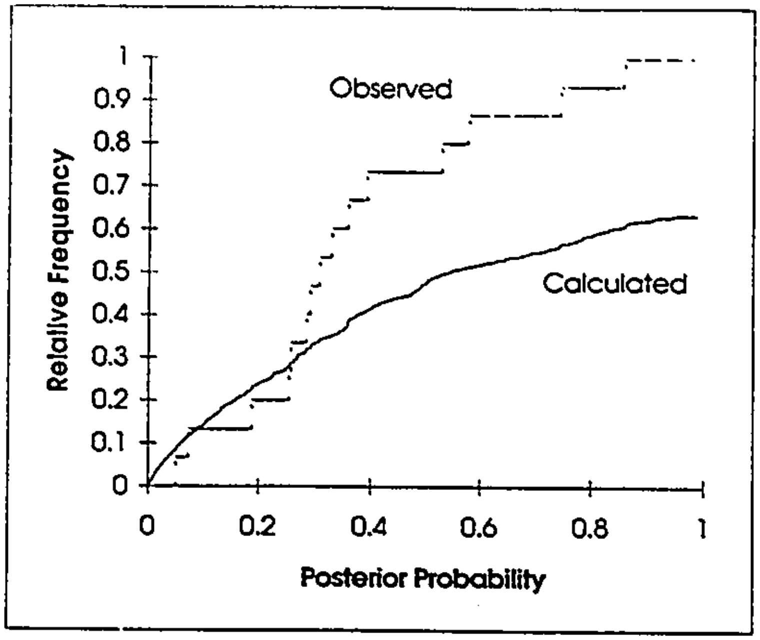

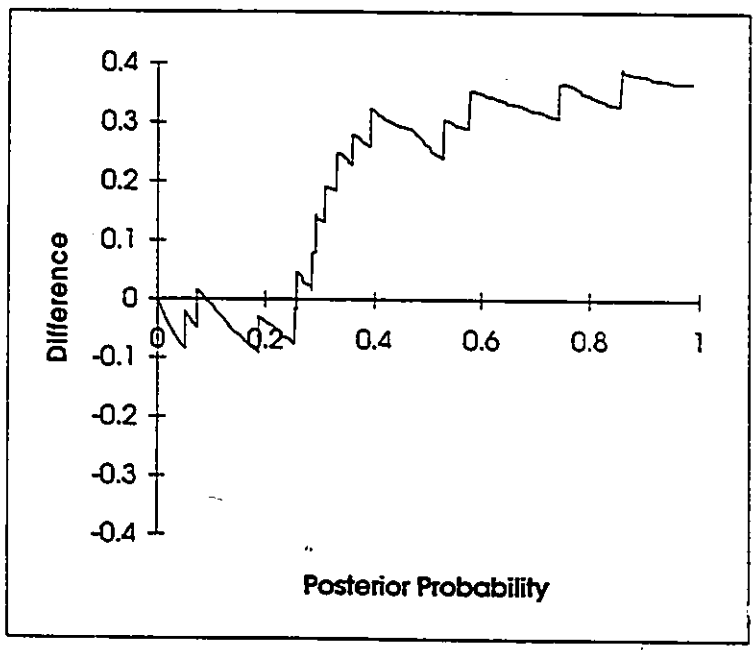

(c) Maximum difference for unit cell size of 1.0 km^2 is 0.392 at a probability of 0.85.

observed and expected number of deposits determined for logistic regression and weights of evidence methods using different unit cell sizes is summarized in Table 6.4. It can be seen that the difference between the observed and the expected decreases with decreasing unit cell size in applications of the logistic model while increasing with the weights of evidence model. The degree of fit for the logistic regression method is shown graphically in Figure 6.3. The posterior probability is plotted in the horizontal direction.

Table 6.4. Observed and expected number of deposits determined for logistic regression and weights of evidence methods using different unit cell sizes

Unit Cell Size	Observed	Weights of Evidence	Logistic Regression
1.0 km^2	15	34.66	9.49
0.5 km^2	15	53.2	11.38
0.1 km^2	15	149.59	13.93
0.01 km^2	15	651.21	14.87

The cumulative observed and theoretical frequencies are plotted in the vertical direction. The theoretical values for the frequency of a deposit are determined by multiplying the area of a unique condition by the posterior probability associated with that same unique condition. The observed frequencies are obtained by counting the number of deposits per unique condition. Both the observed frequencies and theoretical frequencies can be modified to relative frequencies by dividing by total number of deposits.

An appropriate statistical test to evaluate the goodness-of-fit of theoretical

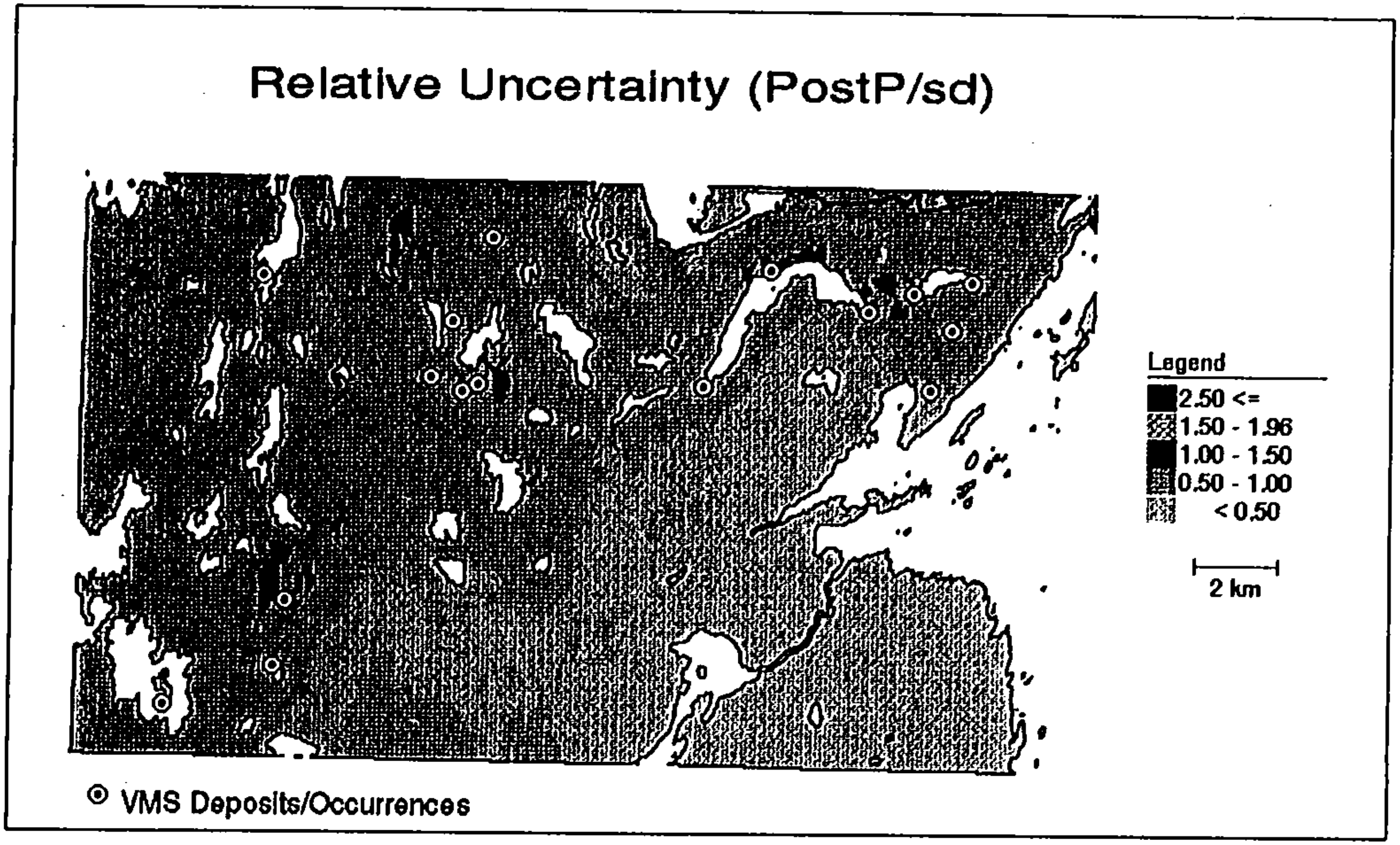

Figure 6.4. Relative uncertainty map, determined by dividing the posterior probabilities by their standard deviations, for posterior probabilities generated by the area weighted logistic regression method. Values greater that 1.645 indicate a relatively low uncertainty.

distribution to an observed distribution is the Kolmogorov-Smirnov ,K-S, statistic, which is for the maximum difference between the two distributions. The two-tailed null hypothesis states that the observed distribution is equal to the theoretical distribution. In order not to reject this hypothesis, the absolute value of the largest difference should not exceed $1.36/\sqrt{n}$(Davis, 1986, p. 102) for $\alpha = 0.05$, where n is the number of observations (6994 unique conditions). In this study the K-S statistic should not exceed 0.0163. It can be seen from figure 6.2 that the maximum differences for models using different cell sizes are all greater than the 0.0163, increasing as cell size increases, suggesting that the logistic model does not provide a good fit.

6.4.2 Uncertainty map

The corresponding relative uncertainty map (t-value map), determined by dividing the posterior probabilities by their standard deviations, is shown in Figure 6.4. In an approximate significance test based on the normal distribution in standard form, a relative uncertainty of less than 1.645 indicates that the corresponding posterior probability is not greater than 0 with a probability of 95%. For this study area where there is low uncertainty (a t-value greater that 1.645) is near the Stall lake deposit (north central shore of Stall Lake, see Figure 1.2).

7. Integration Modelling Using Fuzzy Logic

7.1 Introduction

The fuzzy logic approach is appealing, because it is straightforward to understand and implement. It can be used with data from any measurement scale and the weighting of evidence is controlled entirely by the deposit expert. This is in contrast to the data-driven approaches such as weights of evidence or logistic regression that use the locations of known deposits to estimate weights or coefficients (see Chapter 5 and 6). Very often a knowledge driven alternative is necessary because areas that are being actively explored have very few, or even no known deposits.

In this approach spatial objects on a map are considered as members of a set. For example, the spatial objects could be areas on a map and the set defined as "areas containing a VHMS deposit". In classical set theory, an object is a member of a set if it has a membership value of 1, or not a member if it has a membership value of 0. In fuzzy set theory, membership can take on any value between 0 and 1 reflecting the degree of certainty of membership. Fuzzy set theory employs the idea of a membership function, that expresses the degree of membership with respect to some attribute of interest. With maps, generally the attribute of interest is measured over discrete intervals (whatever the measurement scale), and the membership function can be expressed as a table relating map classes to membership values. Fuzzy membership can also be thought of in terms of support for a proposition or hypothesis. In this study, the goal is to identify ground favourable for VHMS deposits. The maps to be used as evidence to support or refute the proposition are all expressed on a common information metric--namely fuzzy membership on the [0,1] scale.

Membership functions are established for each of the map layers that are to be combined. Thus we might have membership functions for aeromagnetic data, for lithological units, for geochemical data and so on. Maps are combined by using fuzzy operators on the membership functions. All of the Boolean operators have fuzzy counterparts, and many others have been proposed. The final result is an output map showing the combined membership function, after applying a classification to create discrete classes for display.

7.2 Fuzzy Logic Theory

A fuzzy set F is a set of ordered pairs defined as follows.

$$F = \{x, \mu_F(x) | x \in A\}$$

where A is a collection of objects and $\mu_F(x)$ is the membership function or the degree of compatibility of x in F. In a geological context, suppose that A is a "space " of objects reflecting aeromagnetic intensity values and each object x has a membership function value $\mu_F(x)$ indicating the possibility that it is associated with a VHMS deposit then the membership function for A with respect to aeromagnetic intensity might be represented as shown in Table 7.1.

Table 7.1. Hypothetical example of membership values expressed as a table.

Class number	Areomagnetic Intensity, x	Membership ($\mu_F(x)$)
1	> 3000	0.35
2	500 - 3000	0.20
3	< 500	0.25

This implies that given the aeromagnetic data alone, the possibility that a particular location on the map contains a VHMS deposit is given by the set of values from the membership function. Although membership values lie in the range (0,1), the membership function is not the same as a probability density function. For example, the aeromagnetic intensity >3000 implies that the possibility of a VHMS deposit at that location is 0.35. However, the possibility that a map polygon is favourable for VHMS deposits is not a probability so the (1-possibility) does not imply improbability, nor is there an implication of probability of a deposit per unit area, as in probabilistic approaches such as weights of evidence. The membership scale is therefore a ranking and magnitude of membership and is treated on a relative basis (Bonham-Carter, 1994a; An et al., 1991) The word favourability or potential is thus used instead of the more formal term, probability.

Choosing membership function values is a subjective and often difficult task.

Nevertheless, it does permit an unambiguous and quantitative expression of expert judgement.

Fuzzy operators are used to combine fuzzy sets. For example, if a particular location on the map has a possibility of being a VHMS deposit of 0.35 from magnetic evidence and 0.05 from ground EM, fuzzy combination of these two numbers could take on a variety of values in the range (0,1) depending on the operator. Fuzzy operators can be applied to any number of input maps or layers of evidence.

The five most commonly used fuzzy operators and the effect that they have on combining membership functions are summarized in Figure 7.1, and further explained in An et al. (1991) and Bonham-Carter (1994a).

For this study the fuzzy "GAMMA" operator, the fuzzy "OR" and the fuzzy "AND" were employed. On output, the fuzzy OR results in taking the maximum value of the 2 or more input membership values, whereas the fuzzy AND results in the minimum of the input values. Thus the OR is an optimistic operator, and the AND is a conservative operator. In some situations, it is desirable that the combination of two favourable pieces of evidence is more favourable than either one taken individually, an "increasive" effect. The fuzzy GAMMA operator allows the degree of AND and OR to be parameterized, even permitting an "increasive" effect for large values of gamma, as illustrated in Figure 7.1. The advantage of the GAMMA operator is that when evidence is conflicting (one or more data sets indicating strong possibilities and others very weak

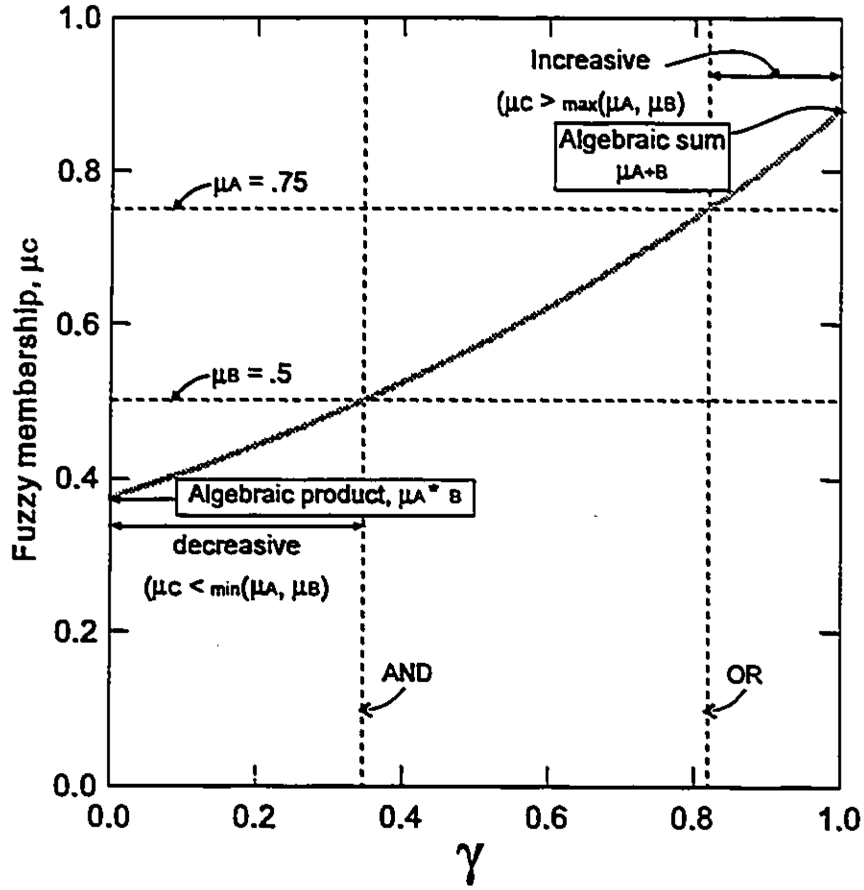

fuzzy AND

$\mu_{COMB} = \min(\mu_A, \mu_B, \mu_C \ldots)$

fuzzy OR

$\mu_{COMB} = \max(\mu_A, \mu_B, \mu_C \ldots)$

fuzzy ALGEBRAIC PRODUCT

$\mu_{COMB} = \prod_{i=1}^{n} \mu_i$

fuzzy ALGEBRAIC SUM

$\mu_{COMB} = 1 - \prod_{i=1}^{n} (1 - \mu_i)$

fuzzy GAMMA OPERATOR

$\mu_{COMB} = (\text{FUZZY ALGEBRAIC SUM})_{\gamma} * (\text{FUZZY ALGEBRAIC PRODUCT})_{1-\gamma}$

Figure 7.1. A graph of fuzzy membership, μ_c, obtained by combining two fuzzy memberships, μ_A and μ_B, versus γ. This shows the effect of variations in γ for the case of combining two values, $\mu_A = 0.75$ and $\mu_B = 0.5$. When $\gamma = 0$, the combination the combination equals the fuzz algebraic product; when $\gamma = 1$, the combination equals the fuzzy algebraic sum. When $0.8 < \gamma < 1$, the combination is larger than the largest input membership value (in this case 0.75), and the effect is therefore "increasive". When $0 < \gamma < 0.35$, the combination is smaller than the smallest input membership value (0.5) in this case and the effect is therefore "decreasive". When $0.35 < \gamma < 0.8$, the combination is neigher increasive nor decreasive, but lies whithin the range of the input membership values. The limits 0.8 and 0.35 are data dependent. **(from Bonham-Carter, 1994).**

possibilities), the resulting aggregation can produce possibilities somewhere between the extremes, with the degree of compensation controlled by the magnitude of the gamma parameter. This variability in choosing the type of fuzzy operator allows the modeller to mimic the decision-making processes typical of an exploration geologist.

7.3 Weighting the Evidence

The evidence maps used in this model are the same as used in the two data driven methods described in Chapters 5 and 6 and summarized in Table 4.5 and 5.2. In the fuzzy logic approach the evidence maps are not reduced to a binary format but rather a membership function was assigned to each map so that each class on the map has a value between 0 and 1. The values are subjective and based on "expert" opinion. The experts in this study were primarily geoscientists who were involved in the EXTECH project (see Chapter 1). In practice, membership functions are represented as fields on the GIS map attribute tables. These tables can be edited, allowing the modeller to experiment with different assumptions. Membership functions are summarized in Table A2 (Appendix A), along with the belief functions used for the Dempster-Shafer method treated in the next chapter.

An example of the actual attribute table associated with the proximity to synvolcanic dykes is shown in Table 7.2. The table consists of 10 header records describing the file to the GIS system followed by 10 data records, one for each class on the map. The table has three attribute fields. The first is the keyfield, linking the record to the map class, the second is the membership function, and the third is a descriptive text field.

Assigning the membership values was a very subjective process and relied totally on the expert's knowledge and experience. In general this was a new concept for the geoscientists involved and required several attempts to develop a membership function. As might be expected, a first attempt resulted in defining what was favourable versus unfavourable, similar to the binary evidence maps used in the data driven methods discussed in Chapters 5 and 6. It is noted that the statistical relationships between deposits and the different evidence maps determined in the weights of evidence were not used to influence these decisions. For example, being within 2 km of a synvolcanic dyke intrusion was favourable while being further away was unfavourable. Determining whether being within 250 m of a subvolcanic intrusion was more favourable than being within 500 m was more difficult for the expert and actually specifying a numeric membership value proved to be hardest.

In Table 7.2, regions where a dyke is present (Class 1), have been assigned a fuzzy membership of 0.8, reflecting the importance of such regions with respect to the heat conditions favourable for VHMS deposits. The region just off a dyke, but within 250 m of the contact are assigned an even more favourable value, 0.95. This region was assigned a higher membership value because VHMS deposits are not typically hosted within the dykes themselves. Then with increasing distance from the contact, the membership value decreases, and beyond 2 km the value is set to 0.1 reflecting that low favourability of the dykes contributing to the heat factor beyond that distance. It should be noted that the input maps are assigned memberships with respect to a series of intermediate propositions. For example, the membership function for proximity to synvolcanic dykes is with respect to the proposition "area with heat factor favourable for VHMS". The heat factor then becomes evidence for the proposition "area favourable for VHMS deposits". In this way the evidence is structured hierarchically, and can be represented by an inference network.

Map classes where the variable in question is 'unknown' were assigned a fuzzy membership value corresponding to the 50th percentile, to minimize the bias introduced in areas of missing data, see for example the membership functions for Zn, Cu and Pb in till in Table A2 (Appendix A).

7.4 Integration - Intermediate maps

After each evidence layer has been weighted by assigning membership functions, the input maps are combined in stages. This not only solves the problem of being limited

Table 7.2. Membership function for proximity to synvolcanic dykes map (Figure 4.7), shown as a map attribute table.

```
ID zdykcon
TITLE Fuzzy memberships for dyke contacts
MAPID dykebuf1
WINDOW nc 5808 7704 142208 12080
TABTYPE 1
NRECORD 10
 1  4   5.00 Class   Map class value
 2  0   6.20 Zheat   Fuzzy membership for distance from dykes
 3 35  15.0 Leg      Legend on map
DATA
 1 0.80 'On Dyke'
 2 0.95 '0.00 - 0.25 km'
 3 0.75 '0.25 - 0.50 km'
 4 0.65 '0.50 - 0.75 km'
 5 0.55 '0.75 - 1.00 km'
 6 0.50 '1.00 - 1.25 km'
 7 0.45 '1.25 - 1.50 km'
 8 0.40 '1.50 - 1.75' km'
 9 0.35 '1.75 - 2.00' km'
10 0.10 '> 2.00 km'
```

to "stacking" a maximum of 15 maps in a single pass (in the SPANS GIS used for the study), but also emphasises the spatial patterns in the intermediate maps, facilitating the interpretation of results. The inference network that summarizes the combination process is shown in Figure 7.2.

7.4.1 Geochemical Factor

Figure 7.3 shows the portion of the inference net defining how the geochemical evidence was combined to create the fuzzy geochemical factor map, which expresses the

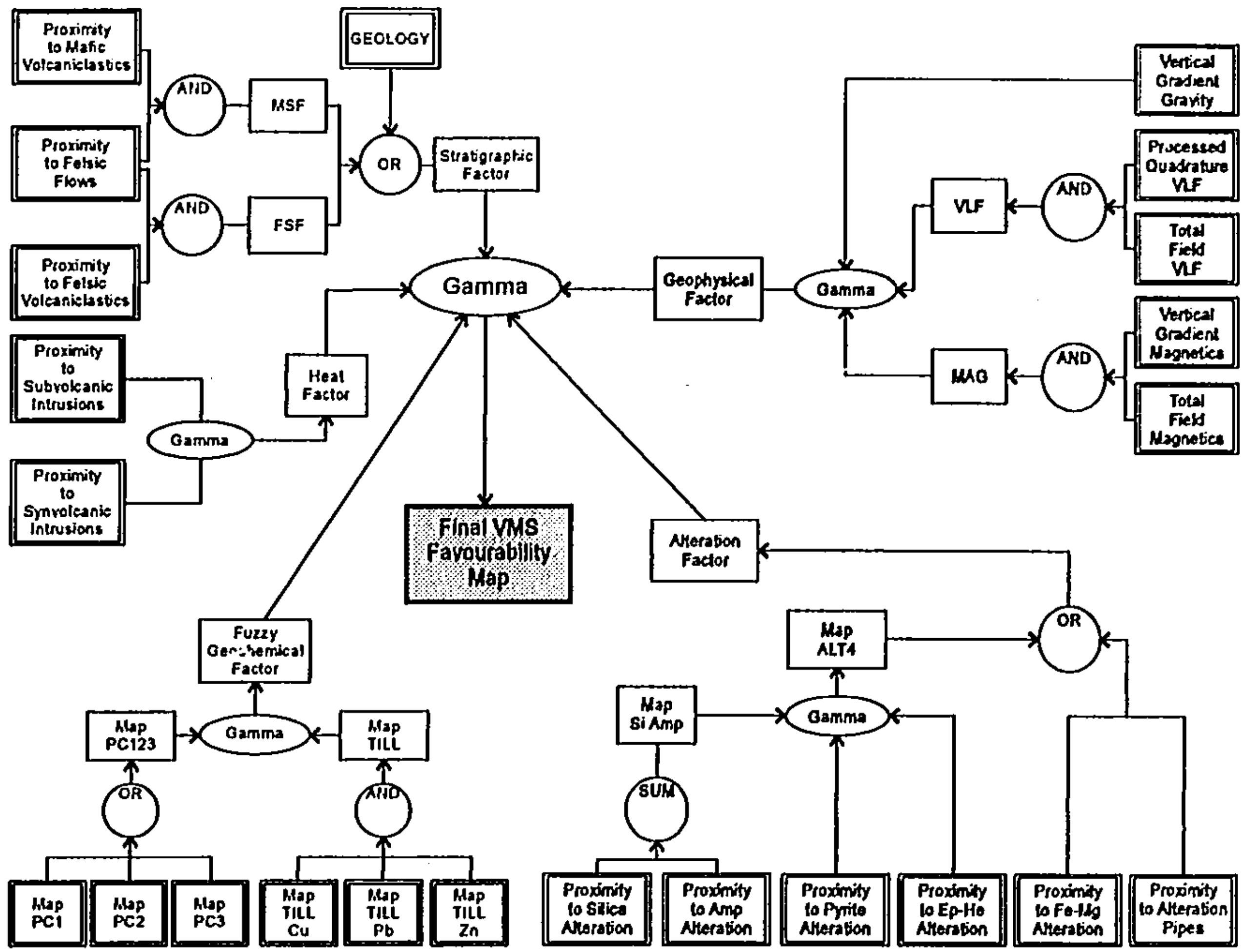

Figure 7.2. Inference net summarizing how all the evidence maps are combined to arrive at the final favourability.

spatial variation in overall geochemical evidence favourable for VHMS deposits. Since PC-1 (lake sediments) was explained as being related to Cu-rich deposits, PC-2 related to Zn-rich deposits and PC-3 as being related to both types, it was unnecessary for all three components to be coincident for favourable VHMS conditions. Following this reasoning the three PC maps were combined using a fuzzy OR, resulting in a new combined PC map, consisting of the maximum fuzzy membership value from PC-1, PC-2 or PC-3. Thus if any one of the PC maps is favourable, the result is also favourable.

Areas with anomalous concentrations of Cu *and* Pb *and* Zn in the till were considered to be the best till geochemical targets. To represent this situation, the till geochemical maps were combined using a fuzzy AND. An intermediate map, labelled TILL in Figure 7.3, was created that took the minimum membership value of the three maps at each spatial location. On this map, elevated membership function values occur only where all three elements are anomalous. It is noted that this decision rule could easily be modified to a fuzzy OR. Fuzzy AND is much more restrictive and conservative, fuzzy OR is more generous and optimistic.

Finally, if both favourable lake sediment chemistry and favourable till chemistry are coincident, these areas would be considered more favourable than if only one of these two conditions existed. This strategy was executed by combining the intermediate maps PC123 and TILL (on Figure 7.3) using the gamma operator, with γ=0.95. The resulting fuzzy geochemical factor is shown in Figure 7.4.

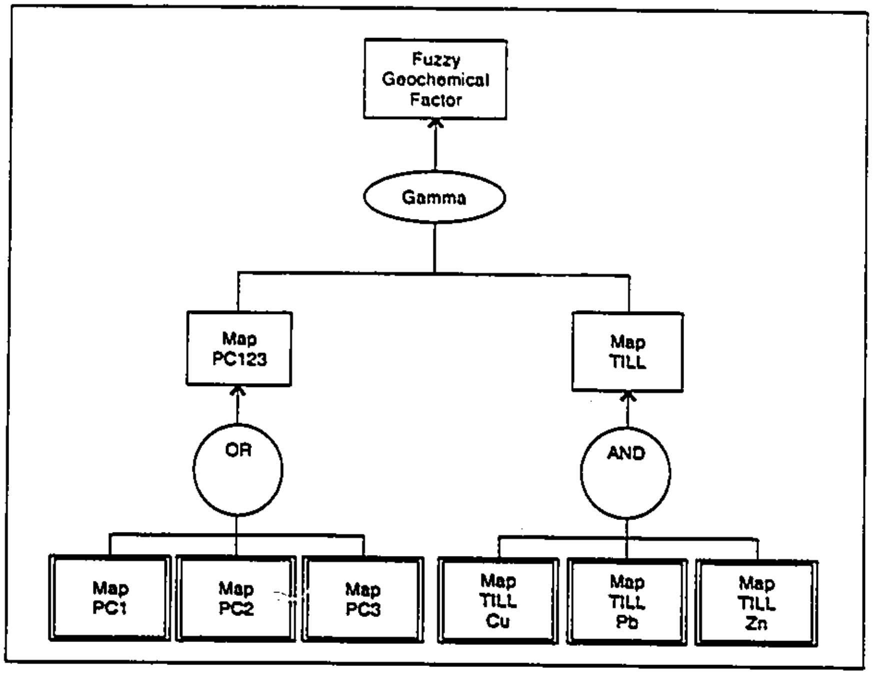

Figure 7.3. Inference net showing how geochemical evidence was combined to create the geochemical factor map

Figure 7.4. Fuzzy geochemical factor map.

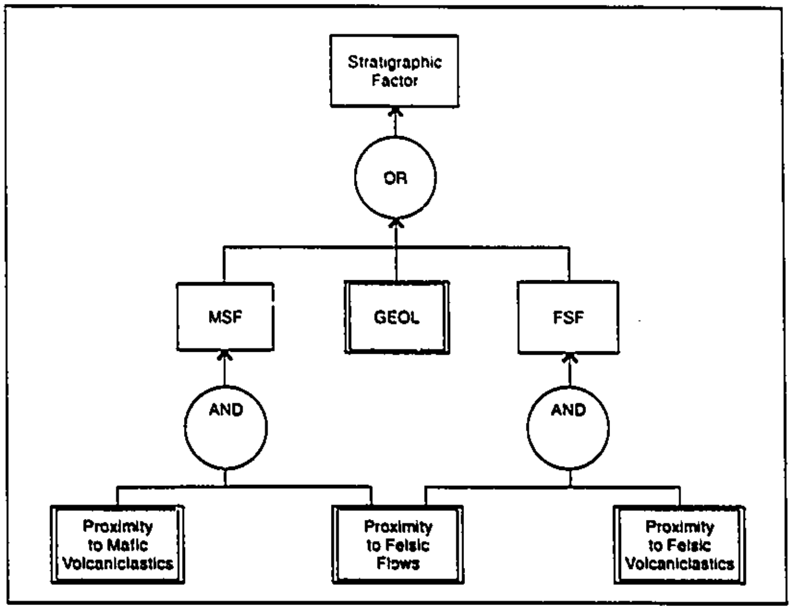

Figure 7.5. Inference net showing how stratigraphic evidence was combined to create the stratigraphic factor map

Figure 7.6. Fuzzy stratigraphic factor map.

7.4.2 Stratigraphic Factor

The inference net related to the stratigraphy is shown in Figure 7.5. To model areas that are close to both felsic flows and volcaniclastic units a fuzzy AND was used. This results in intermediate map, labelled FSF in the figure, which assigns a high membership value to areas that are close to both felsic flows and felsic volcaniclastics. MSF in Figure 7.5 is a map showing favourable proximity to both felsic flows *and* mafic volcaniclastics. Maps MSF and FSF are then combined with GEOL (fuzzy memberships for presence of individual lithologies) using a fuzzy OR (Figure 7.5). This ensures that in situations where there is a close proximity to one of the favourable contacts and the presence of a favourable host lithology that this will receive a higher membership value than where there is a close proximity to a favourable contact and the presence a less favourable host lithology. This may occur if a stratigraphic sequence consists of a thick unit of mafic flows (less favourable for hosting VHMS) overlain by a thin unit of less than 25 meters of felsic volcaniclastics followed by a unit of felsic flows. Being within 50 m of the favourable contact between the felsic volcaniclastics is normally assigned a high favourability, however, in this case 100 m from the contact falls within the mafic flow unit. Using a fuzzy OR operator results in the lower membership value of the mafic flow being assigned to the final map when the lithologic map and proximity map to favourable contacts are combined. The stratigraphic factor map (Figure 7.6), is thus assigned the highest membership values to areas close to the contact between felsic volcaniclastics and felsic flows, and still within a favourable host unit of felsic flows.

7.4.3 Heat Factor

The heat factor map is really an extension of the stratigraphic factor, but focuses on the geological constraints on the source of heat driving the hydrothermal system. The maps of proximity to subvolcanic intrusions and synvolcanic dykes were combined using the gamma operator (Figures 7.7 and 7.8). Because a high value of the gamma parameter was used ($\gamma = 0.95$), areas that are close to both subvolcanic intrusions and synvolcanic dykes can have combined membership values larger than either one taken individually, an increasive effect.

7.4.4 Alteration Factor

The six evidence maps showing proximity to the various types of alteration are combined as shown by the inference net in Figure 7.9. The fuzzy SUM operator was used to combine the Si and amphibole evidence maps to ensure that areas in close proximity to both types of alteration, had a resulting membership value that was higher than either of the two input maps. The resulting map (SIAMP) was then combined with the pyrite and epidote-hematite evidence map using the gamma operatator to produce an intermediate map that has high membership values where there are coincident zones of alteration

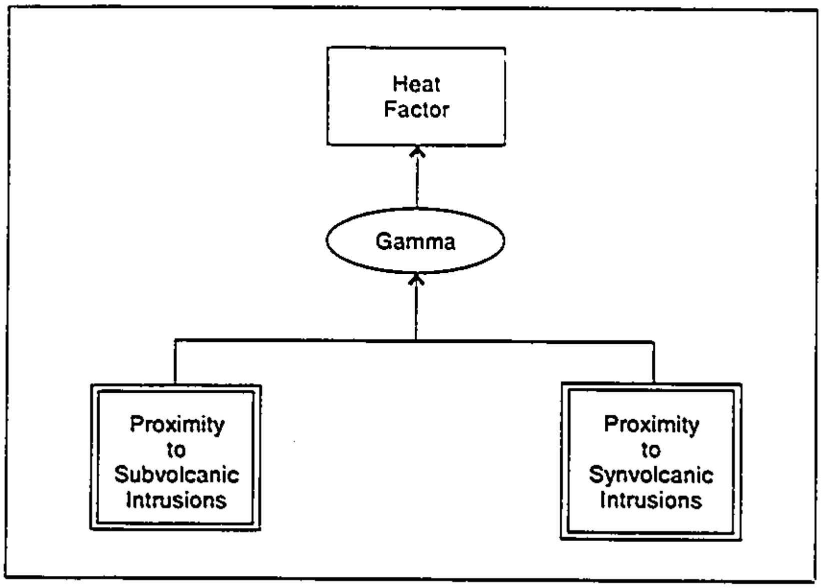

Figure 7.7. Inference net showing how evidence maps related to the heat source factor were combined to produce the heat factor map

Figure 7.8. Fuzzy heat factor map.

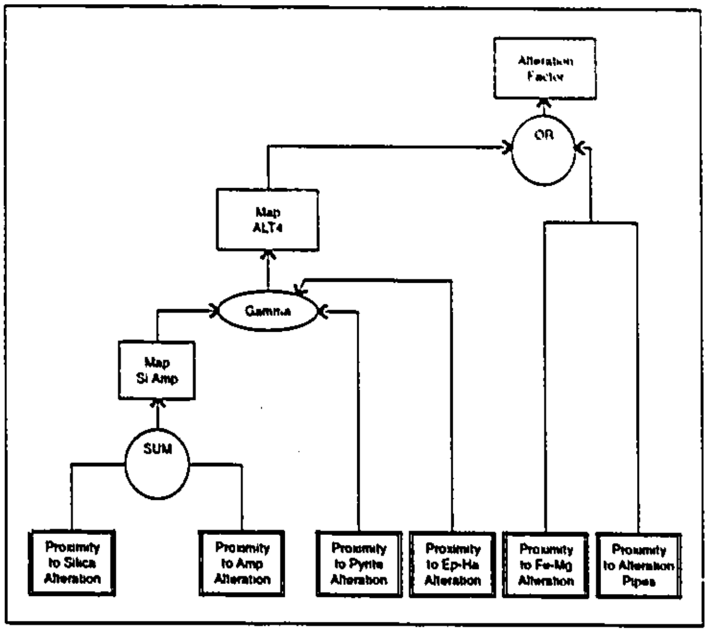

Figure 7.9. Inference net for combining evidence maps related to alteration.

Figure 7.10. Fuzzy alteration factor map.

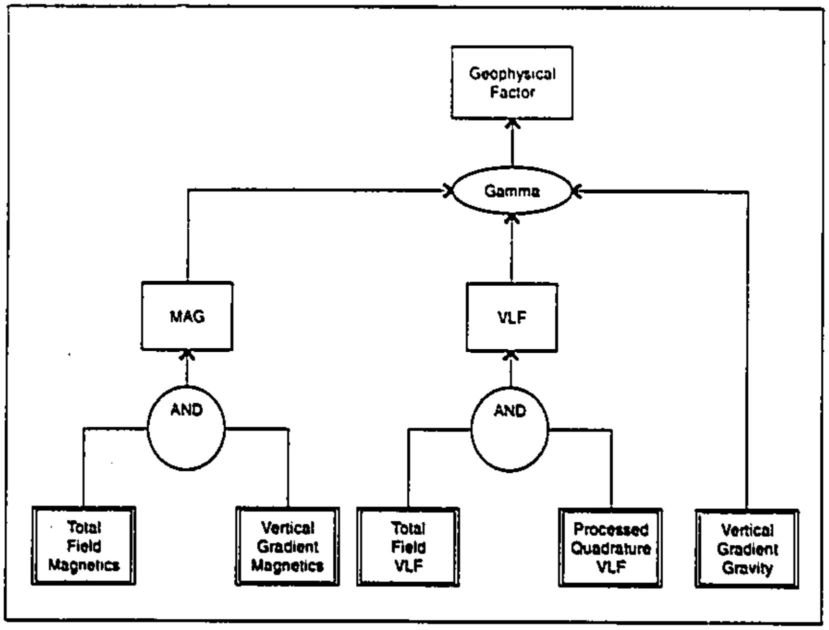

Figure 7.11. Inference net showing how geophysical evidence was combined to create the geophysical factor map

Figure 7.12. Fuzzy geophysical factor map.

(ALT4). Because the Fe-Mg metasomatism map and the Alteration Pipe map are important evidence independent of the others, a fuzzy OR was used to combine these maps with ALT4 to retain the high membership values assigned to them, as shown in the resulting alteration factor map in Figure 7.10.

7.4.5 Geophysics Factor

Geophysical evidence was combined using the scheme in Figure 7.11. The total field and quadrature VLF maps were combined using a fuzzy AND resulting in the map 'VLF', with elevated memberships only where both total field and quadrature anomalies occur together. Similarly the total field mag and vertical gradient mag were combined using a fuzzy AND. Since the highest membership values were assigned to the moderate magnetic responses in the two magnetic evidence maps, the resulting intermediate map (MAG) shows the highest membership values where the intermediate magnetic responses are coincident.

Finally VLF, MAG and the vertical gradient of gravity were combined using the gamma operator ($\gamma = 0.95$), see Figure 7.12. On this map, zones with high conductivity, moderate magnetic response and a regionally high gravity response are the most favourable.

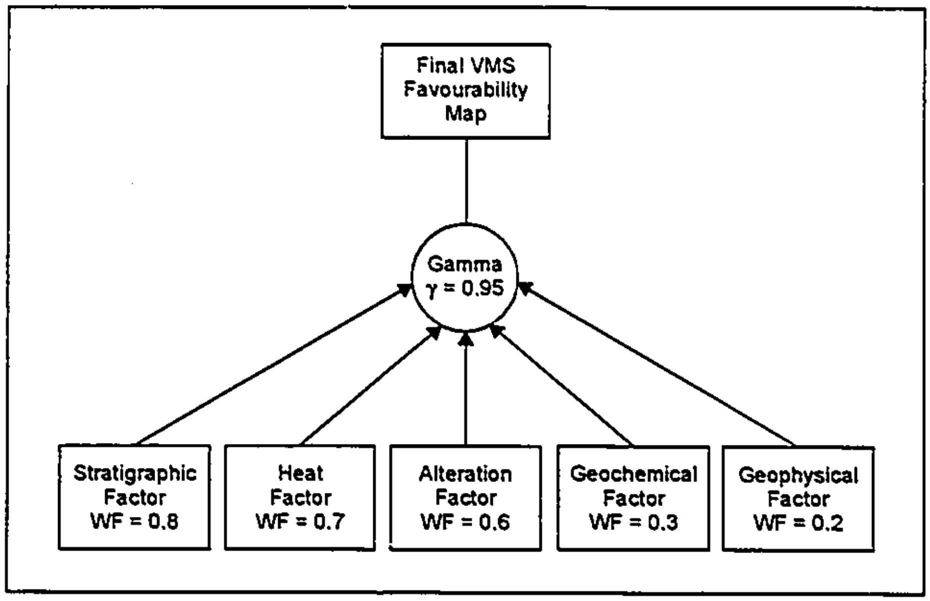

Figure 7.13. Inference net for final favourability map for VHMS deposits.

7.4.6 Final Favourability Map for VHMS

The five intermediate factor maps - heat, alteration, stratigraphic, geophysical and geochemical factors - were combined to generate the final favourability map, as shown in Figures 7.13 and 7.14. It is noted that an additional "weighting factor" (Figure 7.13) in the range [0,1] was used as a multiplier to modify the membership values of each intermediate map and provide a flexible method of changing the influence of each of the

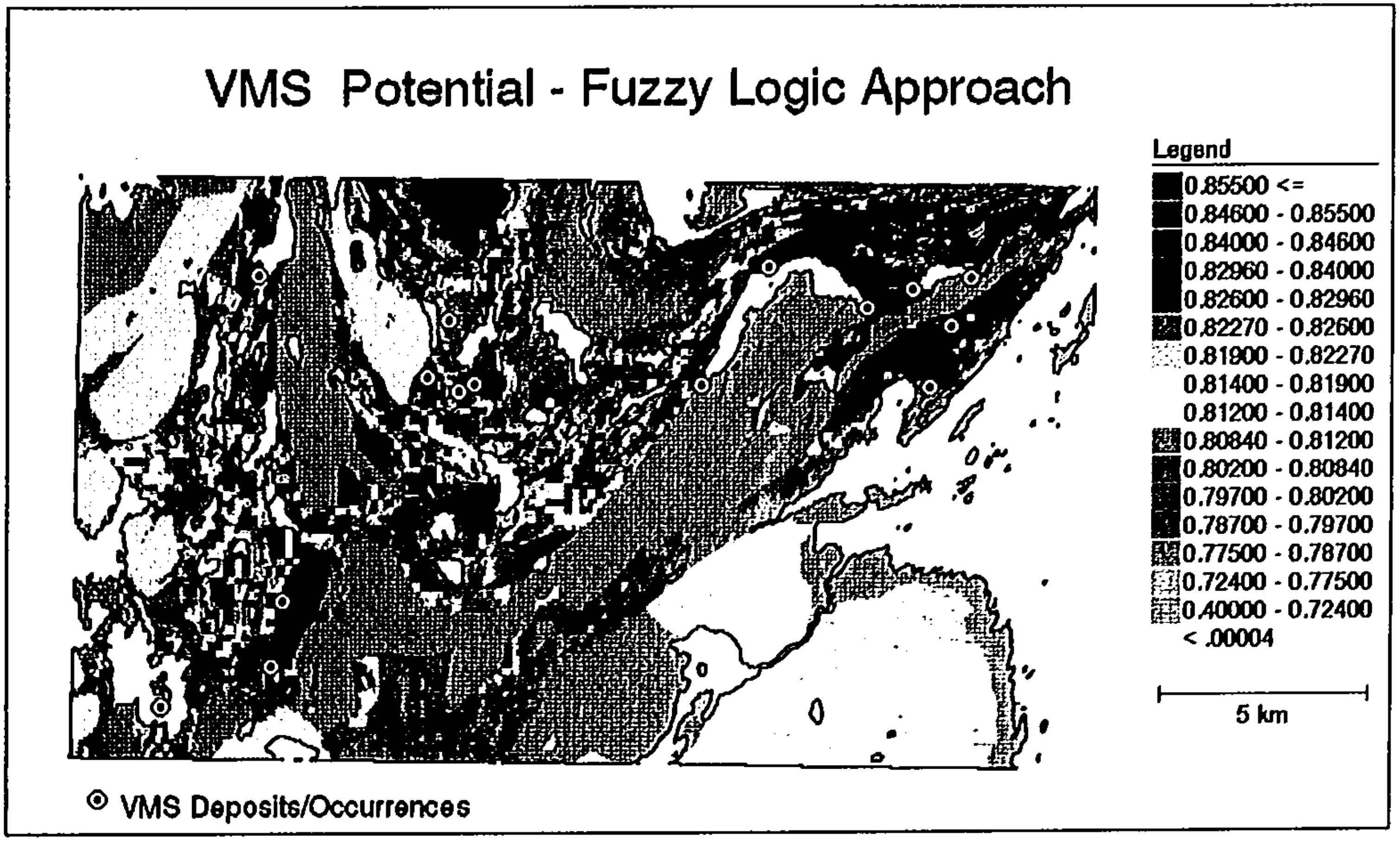

Figure 7.14. Final favourability map generated using the fuzzy logic method.

component factors. This is an overall weighting to express the expert's opinion as to the relative importance of each factor, that enables the modeller to make changes interactively with the GIS modelling language. To a certain degree, these weights also reflect the confidence the expert has in the data. For example, the low weighting factor assigned to the geochemical factor reflects the fact that there is incomplete coverage in the till survey and that the lake sediment samples were collected at a low density. Similarly the relatively low weighting factor for the geophysical data reflects that the data was collected at regional rather than local scales. The stratigraphic factor has a relatively high weighting factor reflecting the detail and information content expressed in the 1:20000 bedrock geology map.

The final favourability map is shown in Figure 7.14. The legend shows the membership function values for the areas identified by the corresponding colour. The breakpoints were determined by dividing the membership function into 20 quantile classes. Of the 15 VHMS deposits known before the modelling, 9 deposits have membership values in the top 10th percentile and 12 in the top 20th percentile. The new discovery at Photo Lake falls in the top 20th percentile.

Table 7.3 summarizes the 15 VHMS deposits and how they are related to the five factor maps and the final favourability map. For each factor map, the membership values are classified into 20 quantiles as was done on the final favourability map. The break points for classifying the data are defined at values that represent 5, 10, 15..., 95 percent of the data. In Table 7.3 a value of 95 means that the membership values at that point were in the 95th percentile (top five percent), a value of 90 means that the membership value at that point was greater than or equal to the 90th percentile but less than the 95th percentile and so on. Classifying the data into percentiles independently for each map allows a direct comparison between maps because ranks are being compared not absolute membership values.

Independently evaluating each factor map and how it is related to known deposits

Table 7.3. Summary of membership values at VHMS locations represented as percentiles so maps can be compared directly. Photo Lake was not used in the modelling but was discovered after the modelling was completed.

Deposit	Heat Factor	Stratigraphic Factor	Geochemical Factor	Alteration Factor	Geophysical Factor	Overall
Morgan Lake	50	35	5	15	90	65
Bomber Zone	95	80	45	70	85	90
Rain Drop	45	80	65	85	70	85
Pot	45	80	75	70	90	75
North Chisel	35	45	90	25	75	50
Chisel	40	95	90	95	85	95
Lost	60	95	95	85	85	90
Ghost	35	95	5	70	90	90
Joannie	70	45	75	85	55	85
Anderson	95	80	35	85	85	95
Stall	75	80	95	95	95	95
Rod	95	80	95	60	85	95
Ram Zone	75	45	90	95	65	90
Linda 1	75	80	85	85	90	95
Linda 2	35	80	85	95	20	80
Photo Lake	45	90	70	70	95	80

helps to assess how much each factor is contributing towards the final favourability. The eight deposits (Bomber Zone, Chisel, Lost Ghost, Anderson, Stall, Rod and Linda1) that fall in areas that have favourabilities above the 90th percentile on the final map also fall in highly favourable areas on each of the five factor maps with the exception of the Chisel, Lost and Ghost deposits on the heat factor map. The heat factor is a result of combining maps showing proximity to subvolcanic tonalite sills (Figure 4.6) and synvolcanic dykes (Figure 4.7). Inspecting these figures shows that though the Chisel, Lost and Ghost deposits are very close to synvolcanic dykes, they are between 2 and 3 km from subvolcanic sills. Because the membership function for these maps (see Table A-2, Appendix A) assigns membership values that decrease as distance increases from the dyke and sills, the sill map contributes very little when the maps are combined to create the heat factor map. The heat factor map also shows relatively low favourabilites for a number of other deposits (Rain Drop, Pot, North Chisel, Linda 2 and Photo Lake). Again, inspecting Figures 4.6 and 4.7 these deposits tend to be moderate distances (1-2 km) from both subvolcanic sills and synvolcanic dykes which would result in moderate membership values when they are combined. These results suggest that perhaps the membership values for moderate distances from heat sources should be increased.

The North Chisel and Morgan Lake deposits are associated with areas of moderate favourability indicating that they are in areas that do not conform very well to the exploration model. However, it is noted that the Morgan Lake deposit is in an area with a very high geophysical favaourability and the North Chisel deposit is in an area with a very high geochemical favourability.

7.5 Error Considerations

The fuzzy logic approach to integrating spatial data does not have a formal method for calculating variance or other measures of error. To a certain degree, uncertainty is built into the membership functions. Patterns on the predictor maps that are assigned membership values that range between 0.4 and 0.6, that is their degree of importance is neither strong nor weak, would be expected to have the largest uncertainty. Patterns that are assigned membership values that are closer to 1 or closer to 0 reflect that the patterns have a large degree of certainty that they are significant predictors or insignificant predictors respectively.

Another problem associated with the fuzzy logic method is dealing with areas where there is no data. In this study both the till geochemistry maps and the lake sediment geochemistry maps had areas where no data was collected. Assigning an area with no data a membership value of zero implies that the area is unfavourable when in fact it is unknown. One approach is to assign a membership value of 0.5 to areas where there is no data suggesting that it is neither favourable or unfavourable. Checking the membership functions assigned to the lake sediment geochemistry maps in Table A-2

(Appendix A), shows this was the approach used in this case. For the till geochemistry, the same membership value that was used for data that fell within the 50th percentile (0.65) was assigned to the areas of the map with no data. Of course a more drastic approach would be to eliminate these areas from the study.

The Dempster-Shafer approach, another knowledge-driven combination method, is more flexible than fuzzy logic for representing uncertainty in the data. The Dempster-Shafer output consists of favourability maps for "support" (conservative estimates), "plausibility" (optimistic estimates) and "ignorance" (uncertainty). This method is discussed in the following chapter.

8. Dempster-Shafer Model

8.1 Introduction

Dempster-Shafer belief theory is an alternative mechanism for knowledge representation and map combination. It is a knowledge-driven approach, with some advantages and disadvantages as compared with fuzzy logic. With the fuzzy logic approach, each evidence map is associated with a membership function that expresses the importance of the evidence on a scale between 0 and 1. For the Dempster-Shafer approach, each evidence map is associated with two independent "belief" functions that represent the information content of evidence, also on a scale from 0 to 1. The upper belief function (known as the "plausibility") can be considered as an optimistic assessment that the evidence supports a proposition, whereas the lower belief function (known as the "support") is a conservative estimate. The interval between the plausibility function and the support function is the uncertainty or ignorance. Disbelief is defined as one minus the plausibility. These relationships are summarized in Figure 8.1.

The advantage of this approach is that it allows the user to represent uncertainty in the knowledge representation because the interval between support and plausibility (also known as the "evidential interval") can be considered as a confidence band. Missing data can be modelled by defining the plausibility as 1, the support as 0, so that the uncertainty is 1. Evidence from two or more maps is combined using Dempster's rule (discussed below) of combination. The combined support, plausibility, disbelief and uncertainty can each be separately mapped, although only two of these quantities are independent. This contrasts with the fuzzy logic output, consisting only of a single map, the combined fuzzy membership.

The Dempster-Shafer method has been discussed in a mineral exploration context using a hypothetical dataset by Chung and Moon (1991) and Chung and Fabbri (1993). An (1992), An et al. (1994a) and An et al. (1994b) applied the method to combine a variety of geophysical datasets to predict base metal and iron formation deposits in an area north and west of this present study area.

8.2 Belief Function Theory

A detailed theoretical exposition and a formalization of the belief function approach can be found in Dempster (1968) and Shafer (1976). The discussion here is simplified and informal. A simple numerical example is given to illustrate Dempster's rule of combination.

Each map to be used as evidence to evaluate a proposition (e.g. "this cell contains a VHMS deposit") is associated with a pair of belief functions, the support function and the plausibility function. In practice, these functions can be held in map attribute tables (similar to the fuzzy membership tables discussed in Chapter 7), where each class on the map is associated with a support value and a plausibility value. Suppose we have map A,

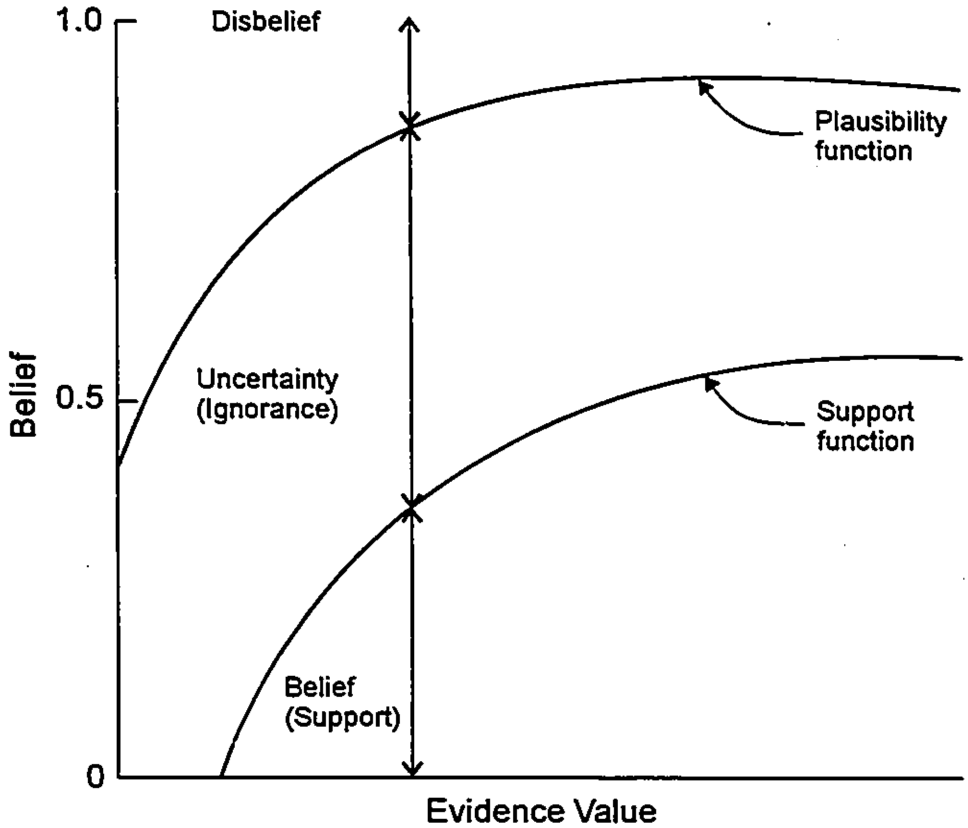

Figure 8.1. Each evidence map in the Dempster-Shafer approach is associated with two independent "belief" functions; the upper belief function (plausibility) and the lower belief function (support) The interval between the plausibility and support functions is the uncertainty or ignorance. Disbelief is defined as one minus the plausibility.

we will simply denote the value of the support due to A as Sup_A, and the plausibility due to A as Pls_A, where these are functions that vary with the value (map class) of A, and therefore can be mapped in their own right as lookup operations from map A. For a given value of map A, the ignorance or uncertainty is denoted as Unc_A, calculated as Pls_A - Sup_A, and the disbelief, Dis_A is 1 - Pls_A. Thus the sum $Sup_A + Unc_A + Dis_A = 1$. The disbelief is the belief that the proposition is false, i.e. that a cell does not contain a VHMS deposit. Note that plausibility is greater than or equal to support. Where plausibility and support are equal, the uncertainty is zero, and Sup + Dis = 1, as in the probability approach. These relationships are illustrated graphically on Figure 8.2.

For each map used as evidence, two independent functions must be estimated, usually either the support and disbelief, or the support and plausibility, but in some cases the uncertainty may be chosen with one of the other values. An et al. (1994a) and Chung and Fabbri (1993) discuss an estimation procedure and the one used in this study is discussed below.

Given two maps A and B, with the support and disbelief fur. ·:ons for each, Dempster's rule of combination for estimating the combined support and disbelief (and therefore uncertainty) is

$$Spt_C = \frac{Spt_A Spt_B + Spt_A Unc_B + Spt_B Unc_A}{\beta} \tag{8.1}$$

$$Dis_C = \frac{Dis_A Dis_B + Dis_A Unc_B + Dis_B Unc_A}{\beta} \tag{8.2}$$

$$Unc_C = \frac{Unc_A Unc_B}{\beta} \tag{8.3}$$

where the denominator for all three equations, defined as,

$$\beta = 1 - Spt_A Dis_B - Dis_A Spt_B \tag{8.4}$$

is a normalizing factor that ensures that Spt + Dis + Unc = 1.

An example of estimating belief functions and combining them applying equations 8.1 - 8.4 is given in the next section.

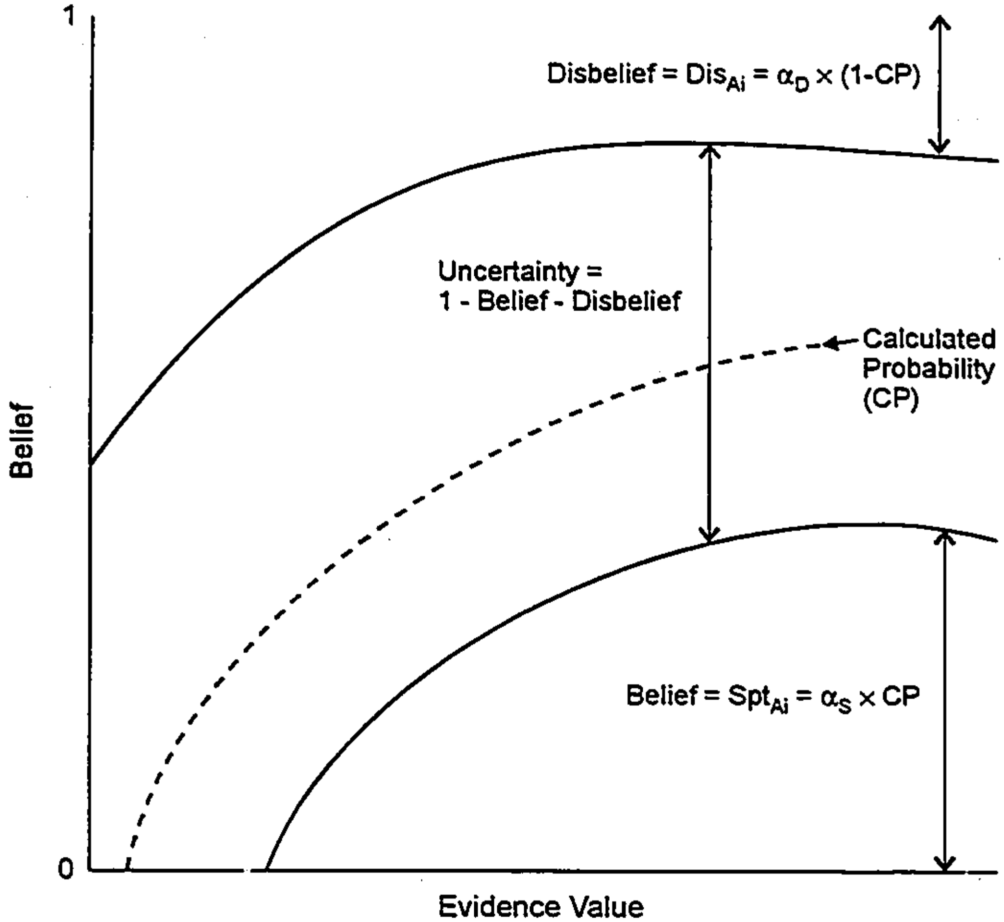

Figure 8.2. Approach to estimating Dempster-Shafer belief functions. For each class on an evidence map a probability that a small unit area (pixel) contains a deposit is estimated using the ratio of the number of pixels containing a deposit to the total number of pixels. The support function and disbelief functions are then calculated using constants α_S and α_D. See text for further explanation.

8.3 Application

8.3.1 Assigning Belief functions

The same 23 input maps used in the fuzzy logic approach were combined using the Dempster-Shafer method. The assignment of the belief function values was made subjectively for each input map. In practice, two problems are encountered at this stage. The first difficulty is the conceptualization of belief and disbelief. There is a tendency to think of disbelief as one minus the belief. It is often difficult to quantify an opinion indicating the difference between disbelief and uncertainty. The second problem, more on the pragmatic side, is that if two maps being combined both have large support values, the combined support becomes close to 1. Further combination with other maps with high support values results in values even closer to 1 (and disbelief and uncertainty approaching zero), making the results difficult to interpret.

In the present application, we have information about the locations of known deposits. It was decided, therefore, to use this information to guide the estimation of belief functions, using an ad hoc approach. Because the number of deposits is relatively small, the estimates are over-ridden by subjective opinion, using the exploration model. For the i-th class of input map A, the probability that a small unit area (pixel) contains a deposit, $P(D|A_i)$, is estimated by the ratio of the number of pixels containing a deposit by the total number of pixels:

$$P(D|A_i) = \frac{N(D \cap A_i)}{N(A_i)} \tag{8.5}$$

This probability is considered to represent an "average" belief, somewhere between the support and plausibility. The lower belief function (support) value for the i-th map class is then calculated by multiplying the probability by a constant, α_S, in the range [0,1]:

$$Spt_{A_i} = \alpha_S \, P(D|A_i) \tag{8.6}$$

The magnitude of α_S is dependent on the certainty the expert associates with the calculated probability. The larger the constant the smaller the uncertainty. The disbelief, which is related to the upper belief function (plausibility) by Dis = 1 - Pls, is calculated by multiplying one minus the probability by a second constant, α_D, also in the range [0,1].

$$Dis_{A_i} = \alpha_D * (1 - P(D|A_i)) \tag{8.7}$$

In this case, the larger the constant, the larger the uncertainty. This approach is illustrated in Figure 8.2.

In practice, the constants α_S and α_D were kept relatively small, in the order of .01-

.001, to avoid the problem of obtaining combined belief functions that approach unity. The same values were used for all maps. The calculated probabilities (see Table A2 of Appendix A) for maps of continuous variables have been manually smoothed to show a continuous function assuming that gaps found in the distribution are caused by the small number of known deposits. The belief function values are also listed in Table A2 (Appendix A) .

To illustrate how the belief functions are determined, using the above method, an example using the copper in till evidence map (Figure 4(a), is described below. All the sample calculations are done using the data for map class 2, which represents Cu concentrations above the 95th percentile.

Information about how many deposits are associated with each class on the map and what the area of each class is, can be determined using the GIS. This process is described in Appendix B-1 as part of determining the weights for evidence maps using the weights of evidence method. This information is summarized in Table 8.1.

The second class (95th precentile) has an area of 11 km^2 and 2 deposits (assumed to have an area of one unit cell). Applying equation 8.5 the probability of that class containing a deposit is

$$P(D|A) = N(D \cap A_i) / N(A_i)$$
$$=2/11$$
$$=0.182$$

Similar calculations are made for each class to determine the "calculated probability" as shown in column 4 in Table 8.1. It is noted that in general the probabilities increase going from the classes with lower concentrations of Cu to those with higher concentrations. It is assumed that if a large number of deposits were available for the area a much smoother probability function would be obtained. Using the calculated probabilities as a guide a smoothed probability function is estimated by the expert to reflect this assumption (see Table 8.1, column 5). It is emphasized that the calculated probabilities are just a guide to and can be over-ridden by the expert's opinion. Choosing an α_s and α_D as discussed above the support and disbelief function can now be calculated.

Table 8.1. Summary of map classes and associated deposits for the Cu in till evidence map (see sample calculations below)

Map Class (ppm ln Cu in Till)	Area (km²)	Number of Deposits	Calculated Probability	Smoothed Probability	Support $\alpha = 0.09$	Disbelief $\alpha = 0.01$	Uncertainty	Plausibility
6.34 - 6.90 (>98th %ile)	2	0	0	0.3	0.027	0.0070	0.966	0.993
5.91 - 6.34 (>95th %ile)	11	2	0.182	0.2	0.018	0.0080	0.974	0.992
5.63 - 5.91 (>90th %ile)	19	3	0.158	0.1	0.009	0.0090	0.982	0.991
5.34 - 5.63 (>80th %ile)	39	5	0.128	0.05	0.004	0.0095	0.986	0.990
5.20 - 5.34 (>70th %ile)	14	0	0	0.04	0.003	0.0096	0.987	0.990
4.98 - 5.20 (>50th %ile)	25	1	0.04	0.02	0.001	0.0098	0.989	0.990
0.00 - 4.98 (<50th %ile)	22	2	0.08	0.01	0.0009	0.0099	0.989	0.989
No Data	134	2	0.01	0.01	0.0009	0.0099	0.989	0.989

Using equation 8.6 and 8.7 we obtain

$$Spt_{A_t} = \alpha_s P(D|A_t)$$
$$= 0.090 \; X \; 0.20$$
$$= 0.018$$

and

$$
\begin{aligned}
Dis_A &= \alpha_D * (1 - P(D|A_i)) \\
&= 0.01 \; X \; (1 - 0.20) \\
&= 0.0080
\end{aligned}
$$

for the 95 percentile class. These functions are recorded in column 6 and 7 in Table 8.1. Notice that as the support decreases the disbelief increases. The uncertainty and plausibility are calculated using the following relationships.

$$
\begin{aligned}
Unc_A &= 1 - Spt_{A_i} - Dis_{A_i} \\
&= 1 - 0.018 - 0.0080 \\
&= 0.974
\end{aligned}
$$

and

$$
\begin{aligned}
Pls_{A_i} &= Spt_{A_i} + Unc_{A_i} \\
&= 0.018 + 0.974 \\
&= 0.992
\end{aligned}
$$

When the belief functions have been determined for all the evidence maps the objective is to combine them to create a new map. An example of combining two hypothetical evidence maps, A and B, at a location for which support and disbelief values are given (see Table 8.2), is shown below. Applying Equations 8.1 - 8.4 we obtain

$\beta = 1 - 0.02 - 0.035 = 0.9450,$

$Spt_C = ((0.05 \times 0.10) + (0.05 \times 0.50) + (0.10 \times 0.60)) / 0.945 = 0.0952,$

$Dis_C = ((0.35 \times 0.40) + (0.35 \times 0.50) + (0.40 \times 0.60)) / 0.945 = 0.5873,$

$Unc_C = (0.60 \times 0.50) / 0.945 = 0.3175,$

and the

$Pls_C = 1 - 0.5873 = 0.4127.$

Dempster's rule is applied recursively, so that the combination map C can now be combined with other maps in pairwise fashion.

Table 8.2. Illustration of Dempster's rule of combination. At one pixel, the support and disbelief values for maps A and B are supplied (bold). Map C is the combination of maps A and B. Values in italics are calculated.

	Support	**Disbelief**	**Uncertainty**	**Plausibility**
Map A	**0.0500**	**0.3500**	*0.6000*	*0.6500*
Map B	**0.1000**	**0.4000**	*0.5000*	*0.6000*
Map C	*0.0952*	*0.5873*	*0.3175*	*0.4127*

8.3.2 Maps of combined belief functions

The 23 input maps (not binary) as already described and listed in Table 4.5, were combined using Equations 8.1 - 8.4 and the values in Table A2 (Appendix A) held as map attribute tables. The output consists of four maps, showing the combined support, disbelief, plausibility and uncertainty associated with the proposition "favourable location for VHMS deposits", see Figure 8.3-8.6.

Figure 8.3 shows the spatial distribution of support. Elevated support is found associated with known deposits in the area as expected. Of particular interest are the areas that show strong support but are not associated with known deposits. The zones showing uniform values of weak support in the southeast, northwest and northeast are underlain by geological units that are post-Amisk in age and considered unsuitable for VHMS deposits. All post-Amisk rocks were assigned a constant high disbelief, low belief and low uncertainty, effectively masking out this region.

In general, disbelief (Figure 8.4) is low for areas showing high support. The spatial distribution of uncertainty is shown in Figure 8.5. As expected, areas of high support and low disbelief also have low uncertainty values. A northeast-southwest trending area of high

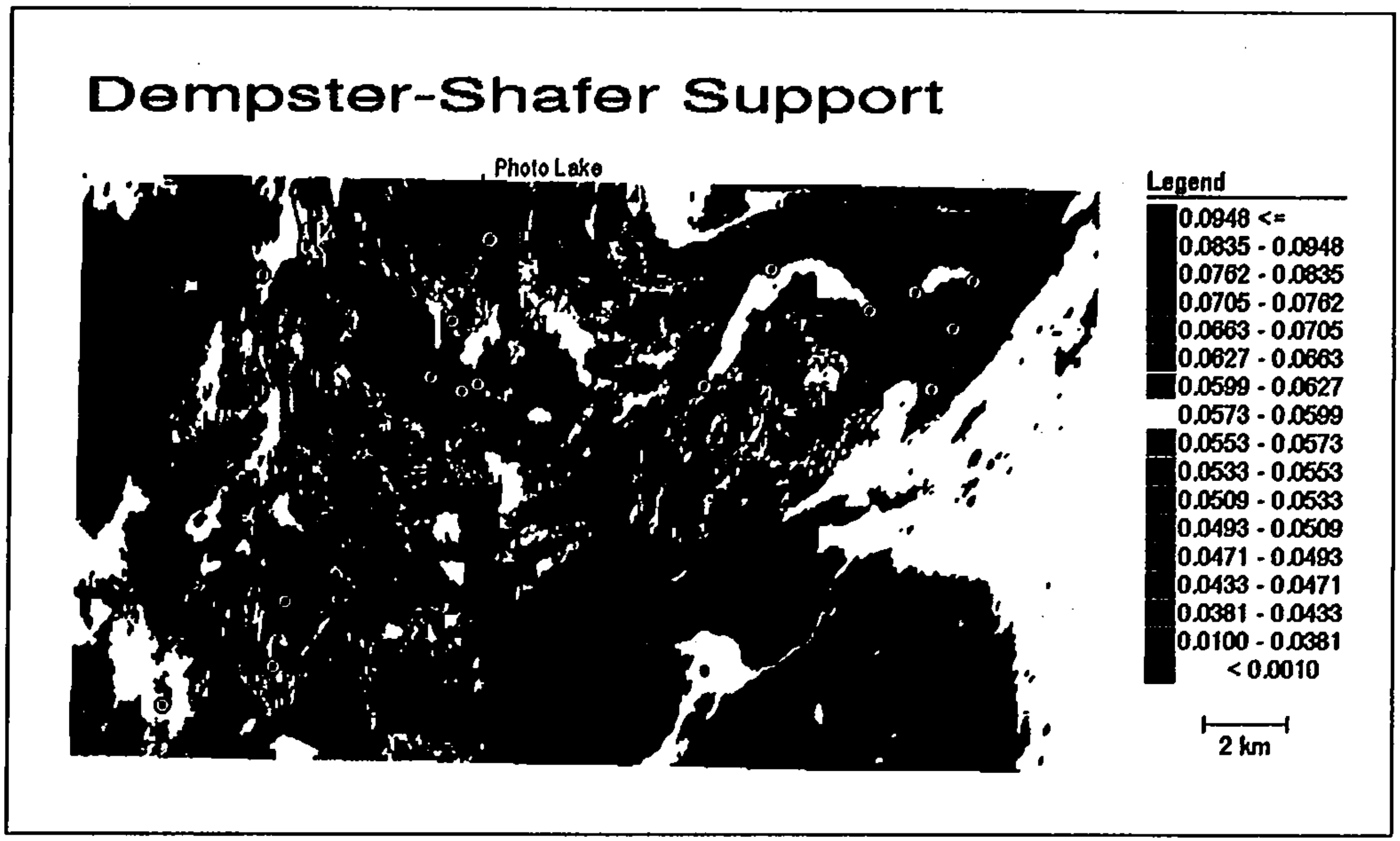

Figure 8.3. Spatial distribution of the lower belief function (support) as calculated using the Dempster-Shafer method. This can be compared to the disbelief, uncertainty and plausibility maps (Figures 8.4 - 8.6)

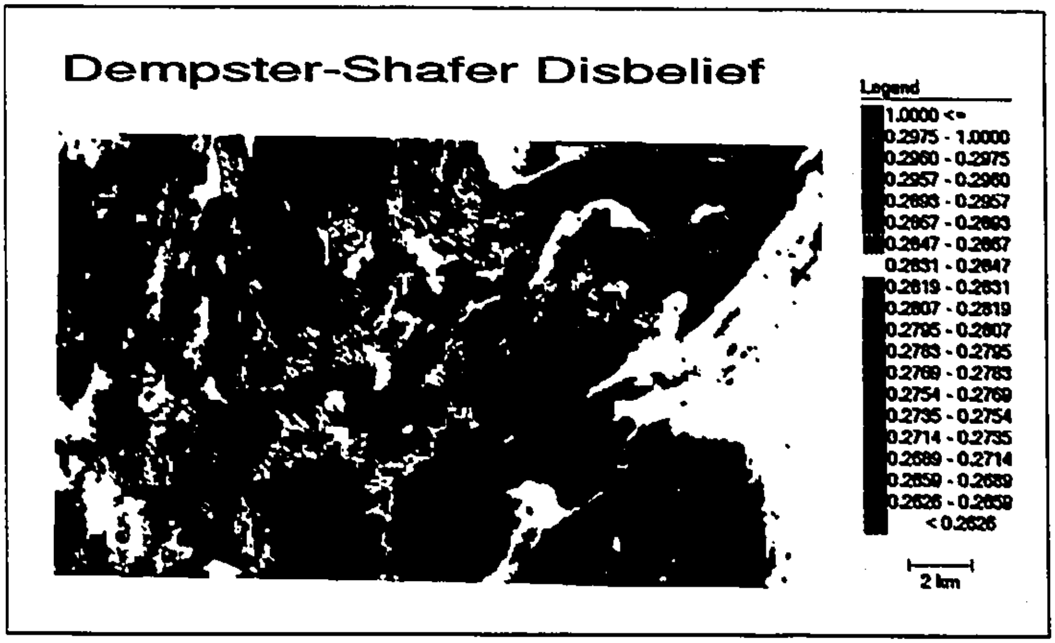

Figure 8.4. The spatial distribution of the disbelief function. In general disbelief is low for areas showing high support.

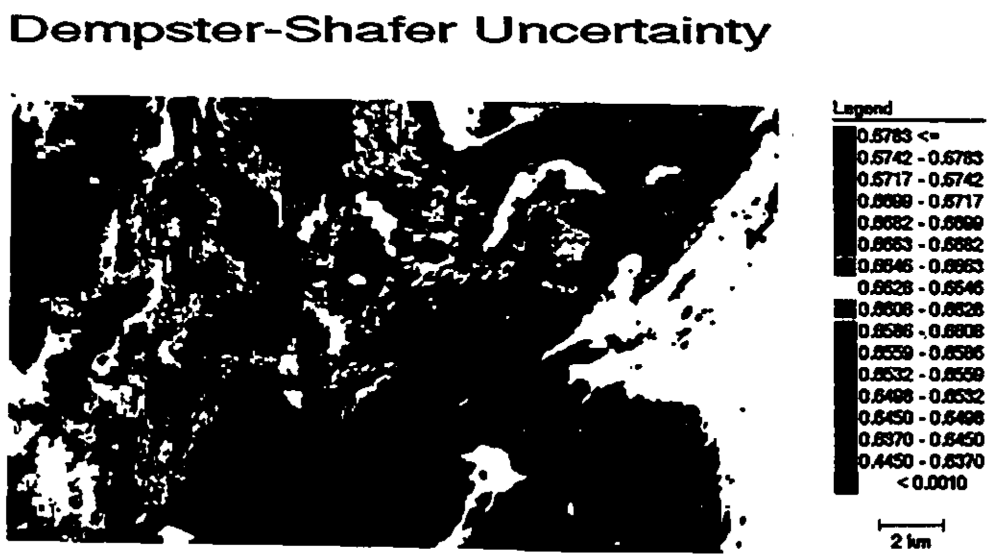

Figure 8.5. The spatial distribution of the uncertainty. Areas of high support and low disbelief have low uncertainty values.

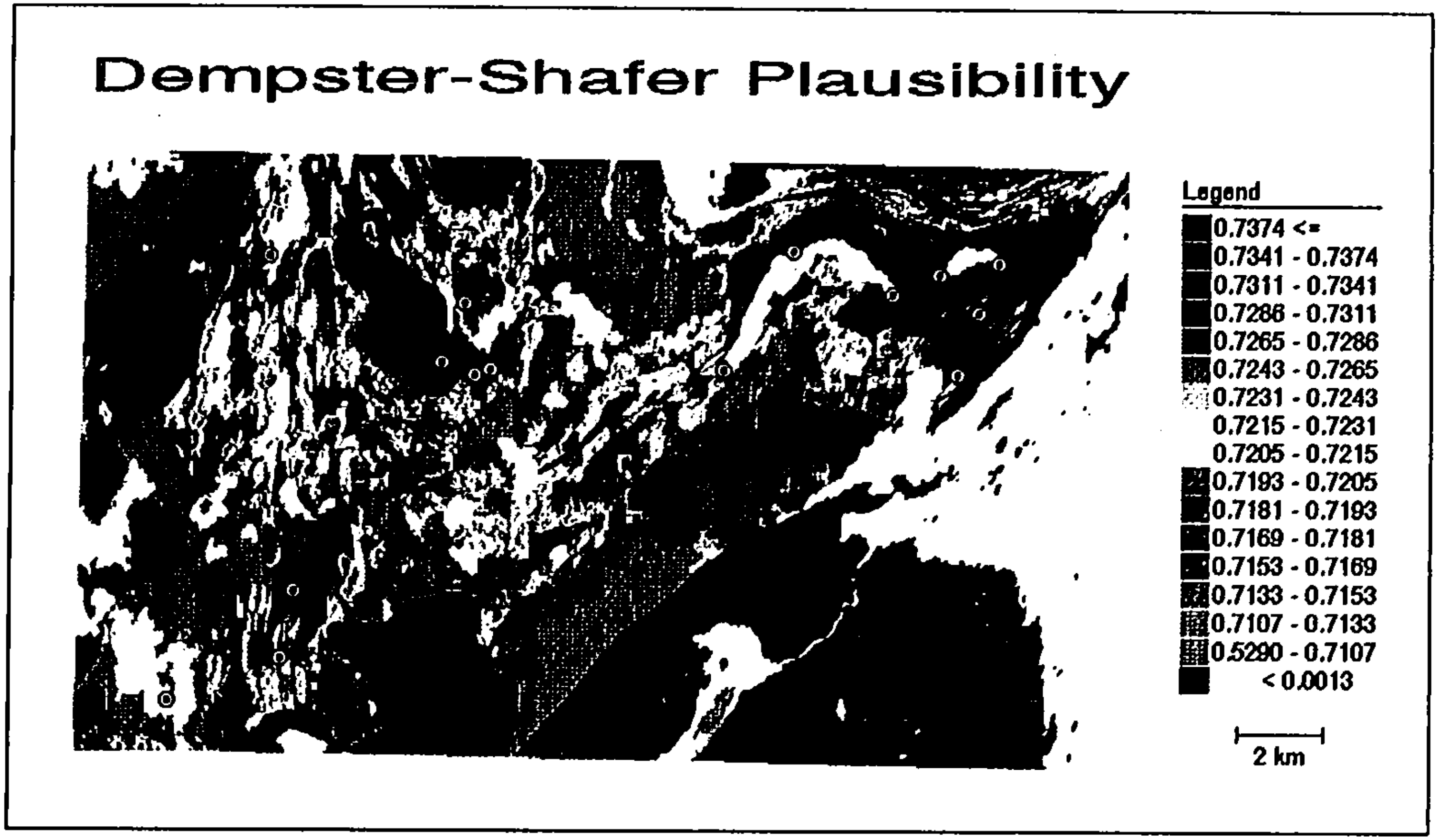

Figure 8.6. The plausibility map, the most optimistic assessment that an area will contain a deposit, is in general correlated with the support map.

uncertainty located north of the Wekusko pluton is due mainly to missing data on the lake-sediment and till maps. The plausibility map, see Figure 8.6, which can be considered the most optimistic assessment that an area will contain a deposit, is in general correlated with support, as might be expected from our method of estimating the belief functions. Two areas of elevated plausibility (but modest support) are situated on the northwest flank of the Wekusko pluton. These two areas, seen distinctly as zones of strong disbelief (Figure 8.4), result from the combination of elevated uncertainty with moderate support.

8.4 Error Considerations

The main advantage of the Dempster-Shafer model compared to the fuzzy logic model, both being knowledge driven models, is that the Dempster-Shafer approach allows the user to represent the uncertainty as the interval between support and plausibility. It is noted that this is not a measured value but a subjective value based on the expert's opinion and what value is assigned to the support and plausibility.

The areas on evidence maps where there was missing data, such as the case in the lake sediment geochmemistry and till geochemistry layers, could be effectively modelled by assigning these areas a plausibility value of 1 and a support value of 0, so that the uncertainty is 1. The two roughly rectangular areas that have no lake sediment geochemistry on the south side of the Sneath Lake Pluton, are clearly distinguishable on the plausibility map, Figure 8.6, characterized by values in the top 15th percentile.

Visual inspection of the favourability maps for VHMS in the Snow Lake area generated by four different methods all seem to have similar spatial patterns. A more formal comparison of the final maps are discussed in the next chapter.

9. Comparison of Favourability Maps

9.1 Introduction

A cursory visual inspection the final potential maps by the four methods, fuzzy logic, Dempster-Shafer, weights of evidence and area weighted logistic regression, shows a broad similarity between the results. In general, areas with known mineral deposits are associated with moderate to very high favourability. Areas geologically unrelated to VHMS deposits have been assigned a relatively low favourability by all four methods. However, there are some areas where the maps differ, and the next section describes the results of inter-map comparisons. To determine an overall measure of the correlation between the potential maps, pairwise comparisons were made using an area-weighted Spearman's rank correlation coefficient, and to identify specific areas of difference, a matrix overlay was performed.

9.2 Application

9.2.1 Spearman's rank correlation coefficients

Each of the five potential maps (support and plausibility maps from Dempster-Shafer were used) were classified using 5% quantiles, thereby normalizing each map to a uniform distribution with 20 classes. The resulting map classes were then treated as ordinal-scale numbers, and Spearman's rank correlation coefficient calculated as a global measure of similarity. Because the maps were in a vector polygon structure, an area-weighted Spearman's rank correlation coefficient was calculated using the following expression

$$r_s = \frac{\sum_{i=1}^{n} T_i(R_x - \overline{R_x})\,(R_y - \overline{R_y})}{\sqrt{\sum_{i=1}^{n} T_i(R_x - \overline{R_x})^2 \sum_{i=1}^{n} T_i(R_y - \overline{R_x})^2}} \tag{9.1}$$

where R_x and R_y are the area-weighted ranks of map x and map y respectively and T_i is the area of the i-th polygon. The bar indicates the mean value of the ranks which is the middle value, an integer if n is odd, a half integer if n is even, see Bonham-Carter (1994a, ch.8).

Two sets of coefficients are shown in Table 9.1. The values in brackets were calculated using only the Amisk volcanic strata excluding the tonalite sills and Post Amisk strata which are generally recognized as a geologically unsuitable environment for VHMS (Bailes,1992) and score very low in terms of favourablility by all methods used in this study. The values with no brackets were calculated based on the total study area. A value of 1 indicates a perfect positive correlation, a value of 0 indicates no correlation and a value of -1 indicates a perfect negative correlation. In all cases the correlation coefficients calculated using the whole study area show a stronger positive correlation than those just using the Amisk volcanic strata. This results from the strong influence of the relatively large area (143 km^2 or 42% of total area) underlying the non-Amisk volcanic strata that have a rather uniform low favourabiliy.

Comparing the resulting coefficients based on the total area, it is seen that the strongest correlation is between the weights of evidence posterior probability map and the logistic regression favourability map ($r = 0.871$). This also shows that in terms of relative favourability, the differences between these two methods despite the known violation of conditional independence as discussed in chapters 5 and 6. This is not surprising as both methods are "data-driven" and have results based on the measured correlation between known deposits and patterns on predictor layers. The second strongest correlation is between the weights of evidence maps and the Dempster-Shafer support map. This is presumably because the belief functions were estimated using guidelines from probability calculations, and weights of evidence is a also based on similar calculations.

However, it is still somewhat surprising that the two maps agree so well when one considers that the weights of evidence input maps are binary, whereas the Dempster-Shafer input maps are multi-class. The next largest coefficient is between Dempster-Shafer support and Dempster-Shafer plausibility. Again, this is to be expected, due to the method of estimating the belief functions. The two lowest coefficients are between

Dempster-Shafer plausibility and fuzzy logic and Dempster-Shafer plausibility and logistic regression. This is not unexpected as some of the favourable zones on the plausibility map are also associated with a high level of uncertainty.

9.2.2 Matrix Overlay

To see where the actual differences and similarities between maps occur, a matrix overlay operation was performed between each pair of potential maps. A matrix overlay operation is carried out by assigning the classes of the output map in a matrix (Figure 9.1), with the rows being the classes of input map 1, and the columns being the classes of input map 2. Where the classes (ranks) are the same for both input maps, the output is assigned to class value 10 (see diagonal in Figure 9.1). Note that output classes less than 10 are used if the class of input map 1 is less than the class of input map 2, but output classes greater than 10 are used for the converse situation. The result is to show the location and extent of differences in favorability between the input maps.

The resulting comparative maps are shown in Figure 9.2. It is interesting to note the differences at locations of known VHMS deposits are small for any of the map comparisons, indicating that all methods did approximately the same at predicting the known deposits. When comparisons are made between a knowledge driven approach and a data driven approach, the differences seem to be the most pronounced. The comparison of the difference between the weights of evidence probability map and fuzzy logic

	Fuzzy Logic	Weights of Evidence	DS Support	DS Plausibility	Logistic Regression
Fuzzy Logic	1	(0.677) 0.702	(0.667) 0.791	(0.498) 0.696	(0.587) 0.733
Weights of Evidence		1	(0.811) 0.851	(0.557) 0.711	(0.815) 0.871
DS Support			1	(0.757) 0.896	(0.727) 0.798
DS Plausibility				1	(0.493) 0.631
Logistic Regression					1

Table 9.1. Weighted Spearman's rank correlation coefficients for VHMS potential map pairs. The values in brackets are calculated excluding the tonalite sills and Post Amisk stratigraphy.

Map1

Map2 Value Rankings	1	2	3	4	5	6	7	8	9	10	11	12	...
1	10	11	11	12	12	13	13	14	14	15	15	16	
2	9	10	11	11	12	12	13	13	14	14	15	15	
3	9	9	10	11	11	12	12	13	13	14	14	15	
4	8	9	9	10	11	11	12	12	13	13	14	14	
5	8	8	9	9	10	11	11	12	12	13	13	14	
6	7	8	8	9	9	10	11	11	12	12	13	13	
7	7	7	8	8	9	9	10	11	11	12	12	13	
8	6	7	7	8	8	9	9	10	11	11	12	12	
9	6	6	7	7	8	8	9	9	10	11	11	12	
10	5	6	6	7	7	8	8	9	9	10	11	11	
11	5	5	6	6	6	7	8	8	9	9	10	11	
12	4	5	5	6	6	7	7	8	8	9	9	10	
⋮													

LEGEND

1 Map 1 ≥ Map 2 By 18 Ranks
2 Map 1 ≥ Map 2 By 16 Ranks
3 Map 1 ≥ Map 2 By 14 Ranks
4 Map 1 ≥ Map 2 By 12 Ranks
5 Map 1 ≥ Map 2 By 10 Ranks
6 Map 1 ≥ Map 2 By 8 Ranks
7 Map 1 ≥ Map 2 By 6 Ranks
8 Map 1 ≥ Map 2 By 4 Ranks
9 Map 1 ≥ Map 2 By 2 Ranks
10 Map 1 = Map 2
11 Map 1 ≤ Map 2 By 2 Ranks
12 Map 1 ≤ Map 2 By 4 Ranks
13 Map 1 ≤ Map 2 By 6 Ranks
14 Map 1 ≤ Map 2 By 8 Ranks
15 Map 1 ≤ Map 2 By 10 Ranks
16 Map 1 ≤ Map 2 By 12 Ranks
17 Map 1 ≤ Map 2 By 14 Ranks
18 Map 1 ≤ Map 2 By 16 Ranks
19 Map 1 ≤ Map 2 By 18 Ranks
20 Map 1 ≤ Map 2 By 20 Ranks

Figure 9.1. Overlay matrix for intermap comparisons. When this matrix is applied to two input maps, the output is assigned to a class value 10 when the classes on both maps are the same (see diagonal). Output classes are less than 10 if the class of input map 1 is less than the class of input map and are greater than 10 for the converse situation.

favourability map (Figure 9.2(b)) and the weights of evidence probability map and Dempster-Shafer support map (Figure 9.2(a)) shows that the fuzzy logic approach and Dempster-Shafer approach consistently assign higher favourabilities to similar areas than the weights of evidence approach. Comparing the results of the logistic regression approach to the fuzzy logic approach (Figure 9.2(d)) and to the Dempster-Shafer support map it is noticed that large areas have been assigned higher favourabilites by the knowledge driven approaches than the data driven logistic regression approach.

Comparison of the results from the two data driven approaches or the two knowledge driven approaches show smaller differences. Figure 9.2(e), illustrating the differences between the relative favourabilities assigned by the weights of evidence approach to the relative favourabilities assigned by logistic regression method, both data driven methods, shows only a few small areas that have large differences as does Figure 9.2(c) which shows the comparison between the fuzzy logic and Dempster-Shafer support methods; two knowledge driven methods.

9.2.3 Favourability at known deposit locations

Table 9.2 summarizes the favourability at known deposit locations for each of the four methods used in this study to combine spatial evidence. For each favourability map, the actual values (probabilities for weights of evidence and area weighted logistic regression methods, membership values for the fuzzy logic method and belief function

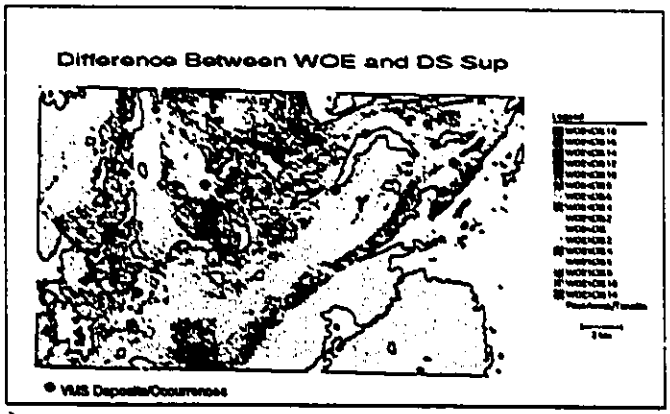

(a)

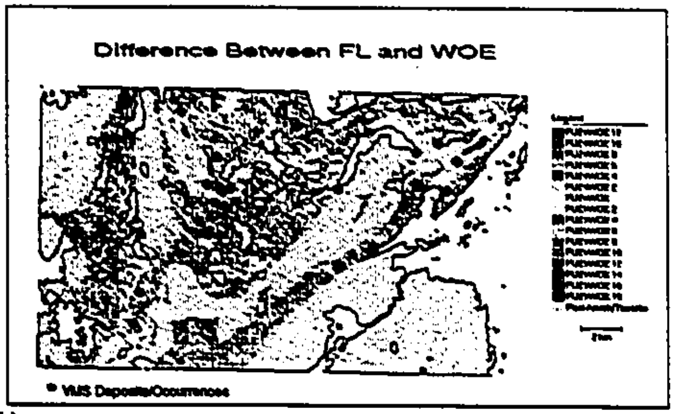

(b)

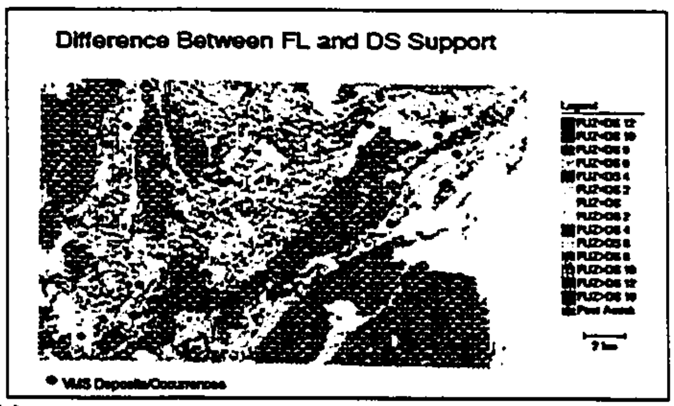

(c)

Figure 9.2 (a)-(f). Comparisons between pairs of favourability maps. (a) difference between weights of evidence and Dempster-Shafer support (b) difference betwwen fuzzy logic and weights of evidence methods (c) difference between fuzzy logic and Dempster-Shafer support.

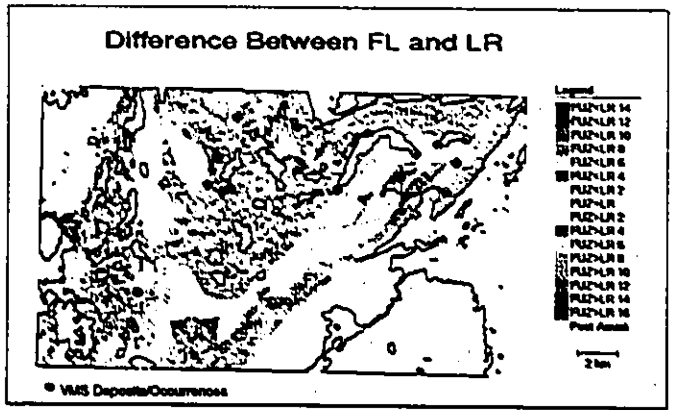

(d)

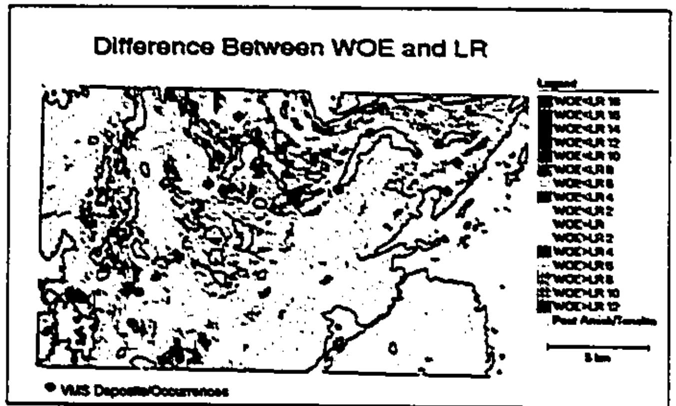

(e)

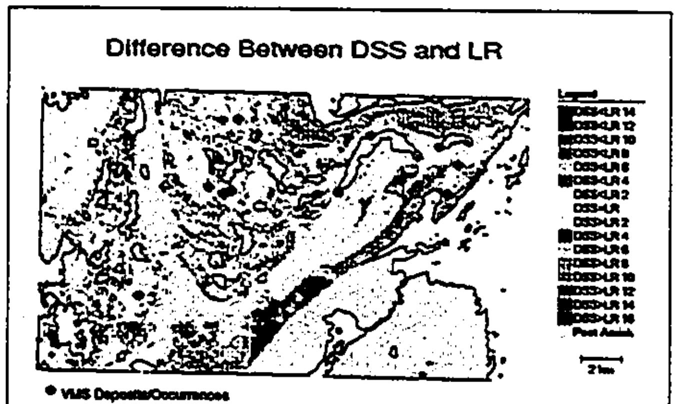

(f)

Figure 9.2 (cont'd). (d) difference between fuzzy logic and area weighted logistic regression (e) difference between weights of evidence and area weighted logistic regression (f) difference between area weighted logistic regression and Dempster-Shafer support.

values for Dempster-Shafer) are classified into 20 quantiles. The break points for classifying the data are defined at values that represent 5, 10, 15..., 95 percent of the data. In Table 9.2 a value of 95 means that the map values at that point were in the 95th

Table 9.2. Summary of favourability at deposit locations for each combination method. Photo Lake was not used in the model and was discovered after the completion of the model. The numbers represent the percentile that the favourability value fell in at each deposit location. The shaded rows are deposits that have favourability values in the top 5th percentile for all models.

Deposit	Weights of Evidence	Logistic Regression	Fuzzy Logic	Dempster-Shafer Support
Morgan Lake	45	70	65	65
Bomber Zone	75	75	90	90
Rain Drop	85	95	85	95
Pot	85	95	75	75
North Chisel	65	90	50	65
Chisel	95	95	95	95
Lost	90	95	90	95
Ghost	75	90	90	80
Joannie	85	95	85	85
Anderson	95	95	95	95
Stall	95	95	95	95
Rod	15	95	95	95
Ram Zone	95	70	90	95
Linda 1	95	95	95	95
Linda 2	90	95	80	95
Photo Lake	85	85	80	80

percentile (top five percent), a value of 90 means that the map value at that point was greater than or equal to the 90th percentile but less than the 95th percentile and so on. Classifying the data into percentiles independently for each map allows a direct comparison between maps because ranks are being compared not absolute values.

The results are very consistent, with all the deposits falling in areas of high favourabilities, generally above the 25 percentile, for each method. Though the Morgan Lake deposit does not fall in highly favourable areas, it is consistently in areas of moderate favourability for each method. The North Chisel and Rod deposits are assigned much lower favourabilities than the other methods by the weights of evidence method, including the other data driven method, area weighted logistic regression.

This overall consistency of results between methods, indicates that despite the known violation of conditional independence, it does not make a major impact on the ranks of the final favourability. However, the conditional dependency in the weights of evidence model may explain some of the differences.

10. Discussion and Summary

Four methods for combining spatial data have been developed for use with geoscience data and successfully implemented in a GIS environment during this study. The fuzzy logic method and Dempster-Shafer belief theory can be described as "knowledge-driven" approaches and the weights of evidence method and logistic regression method as "data-driven". Some distinct advantages and disadvantages are associated with each method.

Because the weights of evidence approach uses statistical measures to characterize the spatial associations between known deposits and map patterns to establish a weight for the evidence layer, a training site with known deposits is required to implement this method. The Snow Lake study area had a total of 15 known VHMS type deposits or a density of approximately 1 per 18 km^2, which is not a large sample but reasonable for a mining camp. The advantage is that the weights assigned to the evidence layers are, objective not based on the expert's knowledge and experience.

Area weighted logistic regression also requires a training site with known deposits. Scores are estimated based only on presence or absence of predictor patterns. As with the weights of evidence approach, the importance of a predictor layer is objective and not based on the expert's knowledge and experience. As well, the scores are confined to values between 0 and 1 so that they can be interpreted as probabilities, and it is less restrictive statistically in the sense that the predictor variables do not need to be conditionally independent.

The fuzzy logic approach tends to be much more flexible than the other three mehods used in this study in representing the expert's thought processes assisted with the use of inference nets constructed with fuzzy operators. It has the advantage of being able to evaluate the influence of different types of evidence by constructing intermediate maps. In this study, the geochemical, stratigraphic, heat, alteration and geophysical factor maps were such intermediate maps. The concept of a fuzzy membership function used to express the varying importance of each layer of evidence was intuitively simple for the expert, generally not familiar with numerical methods, to work with.

The Dempster-Shafer belief theory is more flexible than fuzzy logic for representing uncertainty in the data, but is more restrictive in the expressiveness of the combination rules. The Dempster-Shafer method produces outputs that include a conservative estimate of the favourablility (support), an optimistic estimate of favourability (plausibility) and related uncertainties (ignorance). Conceptually this approach is more difficult with some confusion arising when assigning support and disbelief function values.

Exploration Targets vs Drill Targets

It is important to keep in mind that the mineral favourability maps generated in this study were not intended to be used for defining drill targets but rather to define specific areas that warranted further detailed exploration. The source data used in this study included airborne geophysics flown with 500m line spacings or more, lake sediment geochemical survey at densities of 1 sample per 6 km^2 and geological mapping at 1:20,000 scale which do not provide sufficient detail to define a drill target. However these more regional data can be used very effectively for excluding areas that lack the general geological and geophysical characteristics determined from the exploration model.

The "best" method

All four of the methods have successfully identified areas containing known deposits as having high potential. Table 10.1 shows how deposits are linked with areas of favourability for the four different methods. For each favourability map, the actual values (probabilities for weights of evidence and area weighted logistic regression methods, membership values for the fuzzy logic method and belief function values for Dempster-Shafer) are classified into 20 quantiles. The break points for classifying the data are defined at values that represent 5, 10, 15..., 95 percent of the data. In Table 10.1 a value of 95 in the first column means that the map values at that point are in the 95th

Favourability Percentile	Fuzzy Logic		Dempster-Shafer Support		Weights of Evidence		Area Weighted Logistic Regression	
	Cumm. Area km²	Deposits*	Cumm. Area km²	Deposits*	Cumm. Area km²	Deposits*	Cumm. Area km²	Deposits*
>= 95	5.7 (2.15%)	1,4,5,6,7	10.2 (3.8%)	1,4,9,8,7,5,6,11, 12	6.9 (2.6%)	1,4,5,7,9	11.2 (4.1%)	1,2,4,5,6,7,8,10, 11,12
>= 90	16.6 (6.18%)	14,2,3,9,	20.8 (7.7%)	14	13.6 (5.1%)	2,8	17.4 (6.4%)	3,15
>= 85	26.1 (9.7%)	11,10	31.8 (11.8%)	10	21.2 (7.9%)	11,12,10,16	23.8 (8.8%)	16
>= 80	38.9 (13.3%)	8,16	43.0 (16.0%)	3,16	27.1 (10.1%)		29.9 (11.1%)	
>= 75	45.4 (16.9%)	12	54.5 (20.3%)	12	32.2 (12.0%)	14,3	37.4 (13.9%)	14
>= 70	56.5 (21.0%)		66.2 (24.6%)		38.6 (14.3%)		45.4 (16.9%)	13,9
>= 65	65.3 (24.3%)	13	78.4 (29.2%)	13,15	46.1 (17.2%)	15	53.0 (19.7%)	
>= 60	76.6 (28.5%)		91.3 (33.9%)		61.6 (22.9%)		64.2 (23.9%)	
>=55	88.1 (32.8%)		103.6 (38.5%)		70.9 (26.4%)		74.7 (27.7%)	
>= 50	102.7 (38.2%)	15	117.0 (43.5%)		84.3 (31.3%)		88.3 (32.8%)	
>= 45	108.6 (40.4%)		132.4 (49.25)		98.2 (36.5%)	13	103.9 (38.6%)	
>= 40	124.3 (46.2%)		142.8 (53.1%)		108.3 (40.3%)		117.8 (43.8%)	
>= 35	138.23 (51.4%)		156.5 (58.2%)		124.2 (46.2%)		121.2 (47.6%)	
>= 30	143.1 (53.2%)		173.0 (64.3%)		137.2 (51.0%)		134.5 (52.6%)	
>= 0	268.8 (100%)		268.8 (100%)		268.8 (100%)	6	268.8 (100%)	

* See Table 2.2 for deposit name lookup.

Table 10.1. Summary of areas (cumulative area in percent) predicted to be favourable for each method and the number of deposits predicted to be in favourable areas.

percentile (top five percent) and is the first map class, a value of 90 means that the map value at that point is greater than or equal to the 90th percentile but less than the 95th percentile and is the second map class, and so on. For each of the four methods the number of deposits in each map class and the area of the map class are recorded. The value in brackets is the cumulative area in percent.

Each method has at least 11 of the 16 known deposits for the area falling within the regions indicated as the top 20th percentile with respect to favaourability for VHMS mineralization. All four methods have also shown areas with high potential but no known mineralization (see below).

Deciding which approach is best is really a subjective decision and depends largely on how comfortable the users are with the conceptual aspects of each method. However, some general guidelines should be considered. As mentioned above, if no suitable training site is available, a data driven approach is not possible. On the other hand if a clearly defined exploration model is not developed a knowledge-driven approach may not be appropriate. Two other criteria may also be used to evaluate the effectiveness of each method; the number of known deposits predicted to be in favourable areas and the size of the predicted favourable area. Given a specific deposit type and a large geological environment to explore for it, one of the initial goals for an exploration project is to reduce the amount of area to a reasonable size for a more detailed study. If a method for assigning potential to areas for exploration does not restrict the amount of area defined as favourable to a reasonable amount, it could be considered less effective. Similarly if a method fails to predict areas as favourable where known deposits exist it also could be considered less effective.

Table 10.1 shows that for each method at least 11 of the 15 deposits known at the time of the modelling, fell within areas predicted to be in the top 20th percentile. Also included in the top 20th percentile are the four largest deposits (Chisel, Stall, Anderson and Linda 2). The amount of area predicted to be in the top 20th percentile increases slightly from 10.1 percent of total area (27.1 km^2) for the weights of evidence approach to 16.0% of the total area (43.0 km^2) for the Dempster-Shafer belief theory. Though the logistic regression approach does slightly better at limiting the amount of favourable area it does not represent a significant benefit.

Based on the results from this study, it appears that what is used for evidence is more critical than the actual spatial combination rule used. This implies that even for data driven models, careful consideration should be given at the beginning of the project to understanding the deposit model and identifying critical evidence.

GIS vs. Light table

Much effort and time has been spent on creating a digital georeferenced spatial data base, learning a GIS, and developing methods for combining spatial datasets. It is difficult to evaluate whether the results produced through this study are better or worse than what could have been produced using traditional methods as the real test would be whether more deposits were found, which, of course is not possible to evaluate. However, some very distinct advantages have become apparent as a result of using GIS and integration models.

- Having all the available data as a georeferenced digital data base allowed easy updating of information, such as geological maps, as new data were collected. Problems associated with trying to overlay maps at different scales and projections were eliminated. The digital data base was also a very effective filing system, allowing the data be organized and accessible.

- Processing the data to generate derived information such as kriging geochemical data or extracting important geological units was quick and made modifications easy to incorporate in a new model

- Accommodating modifications in the integration model to generate new favourability maps could also be done very quickly.

- Querying several layers of evidence at a location within the study area allowed better understanding of the results.

- One of the most significant advantages resulting from developing the exploration model (the first step in the process described in this study) and representing it as evidence maps and constructing inference nets to combine the evidence. This forced the user to become intimate with the geological characteristics associated with the deposits and become familiar with their interrelationships and how they affected the results. This of course could be done without a GIS but the GIS facilitated this process.

Predictor maps

One of the most critical steps in this project was establishing what criteria would be used as evidence for the presence of VHMS type deposits and generating representative "evidence" maps. Results will undoubtably be affected if different types of evidence are used. It is important to note that the 23 evidence maps used in this study, listed in Table 4.5, were selected based on one possible exploration model. The results obtained in this study should not be interpreted as the only possibility. One of the advantages of using a GIS as a tool for implementing integration methods is that different inputs can be used to reflect different models and results relatively quickly.

This study had access to bedrock mapping at a 1:20,000 scale. The availability of lithologic information at this level of detail is exhibited by the presence of 6 predictor maps related to stratigraphic data; four for the stratigraphic factor and two for the heat factor. Typically, areas being selected for regional exploration programs do not have bedrock coverage at this level of detail. This may necessitate alternative means to obtain the stratigraphic information required by this exploration model, such as using radiometric data to identify younger from older intrusive bodies. The lack of detailed maps may also demand that certain evidence not be included. For example in this study the presence of rhyolite flows was an important piece of evidence that was mapped on the 1:20000 scale map but was grouped into a general "Felsic Volcanic" unit on the 1:50000 compilation map. If only the 1:50000 compilation map was available this evidence could not be used.

The detail of data may also influence the importance the expert assigns to a certain piece of evidence and the weighting by the data-driven approach. In this study the geophysical data was collected at a moderately detailed level, 800 m line spacing for magnetic data, 500 m line spacing for VLF data and a 2 km grid for gravity. Though geophysical data is very important in the exploration for VHMS deposits the resolution of the data available in this study was not sufficient to identify well defined anomalies. This resulted in less emphasis being put on the geophysical data.

The evidence maps listed in Table 5.3 are ranked with respect to the calculated contrast value ($C = W^+ - W^-$). The contrast value defines the strength of the association between known mineral deposits and a map pattern. In general stratigraphic evidence is ranked highest followed by alteration evidence, geochemical evidence, heat source evidence and finally geophysical evidence. It may seem surprising that the geophysical data appears to have the least significance. The explanation may be related to the resolution of the data. The rather coarse resolution of the data allows broad anomaly patterns to be defined and there will be a much smaller points per pattern area ratio. On the other hand tight, well defined buffer zones around selected contacts defining stratigraphic evidence, results in a much larger points per area ratio. How the evidence is ranked for the fuzzy logic approach is very dependent on the inference network and fuzzy operators used. In this study the overall weights for the 5 evidence factors generally defines the general order of significance. An overall weighting factor of 0.8 was assigned to the stratigraphic factor, 0.7 to the heat factor, 0.6 to the alteration factor, 0.3 to the geochemical factor and 0.2 to the geophysical factor. It can be seen that the expert's ranking is similar to the empirically derived ranking from the weights of evidence method. This ranking also reflected the expert's general confidence in the data. It is difficult to see how the evidence is ranked in the Dempster-Shafer approach due to the nature of the combination rules.

Areas of Interest for Exploration

In general, selecting areas for further detailed exploration, is simply a matter of identifying areas that have a high favourability but no known deposits. However, the selection process can be approached in different ways and influenced by several factors. Each favourability map can be examined independently and targets selected on the merit of each method or the maps can be combined to form a "composite" picture. Depending on the exploration geologist's confidence in the different methods, one or more methods can be ignored. Whether the top 5th percentile, 10th percentile or a lower value is selected as the level that defines the "most" favourable regions will depend largely on budget restrictions.

Figure 10.1 summarizes the VHMS potential predicted by the four integration methods. Virtually all the coloured regions are potentially interesting but of particular interest are those areas that prove to have high potential by two or more methods.

In order to discuss particular zones of high potential, some regions have been outlined and numbered in Figure 10.1. The different classes on the map were made by combining the results from the four favourability maps. The first class (red colour) indicates where all four methods have a favourability in the upper 20th percentile. The next four classes (blues) are where three or more methods have a favourability in the 20th percentile. This is to facilitate discussion but it must be emphasized that any of the coloured areas on Figure 10.1 is worthy of examination. Area 4 and area 6 already contain known deposits, however, they are discussed here because it is useful to recognize the evidence associated with these known deposits and because the favourable areas seem to be extensive enough to warrant the possibility of finding further deposits.

The characteristics associated with these seven selected areas are discussed below. It is of interest to mention that the GIS was an invaluable tool for investigating these areas. It allowed the user to interactively select locations on the target map and obtain a summary of the inputs from the evidence maps and the modelling results. These areas are not ranked in order of importance.

Area 1

This is a narrow north-south trending zone 1-3 km south of Cook Lake on the west side of the Richard Lake pluton.

The stratigraphy for this area is of particular significance. The primary lithology is a felsic flow unit which has been recognized by Bailes (1987) as being a facies equivalent to part of the intact sequence of Amisk Group metavolcanic rock underlying the Chisel, Lost and Ghost deposits. These rocks have been separated from the Chisel Lake area by Richard Lake Pluton and the north-trending Varnson Lake fault and are complexly folded. Its proximity to the Richard Lake Pluton, less than 0.5 km, allows for a favourable heat environment. It is noted that this area is also adjacent to synvolcanic dykes, however, it is a fault contact making it difficult to determine how close the felsic flow unit was to the dykes before the faulting. This illustrates a general weakness in the modelling approach used here. Generating buffers around contacts to determine proximity to different features, does not take into account faults, unconformities, the

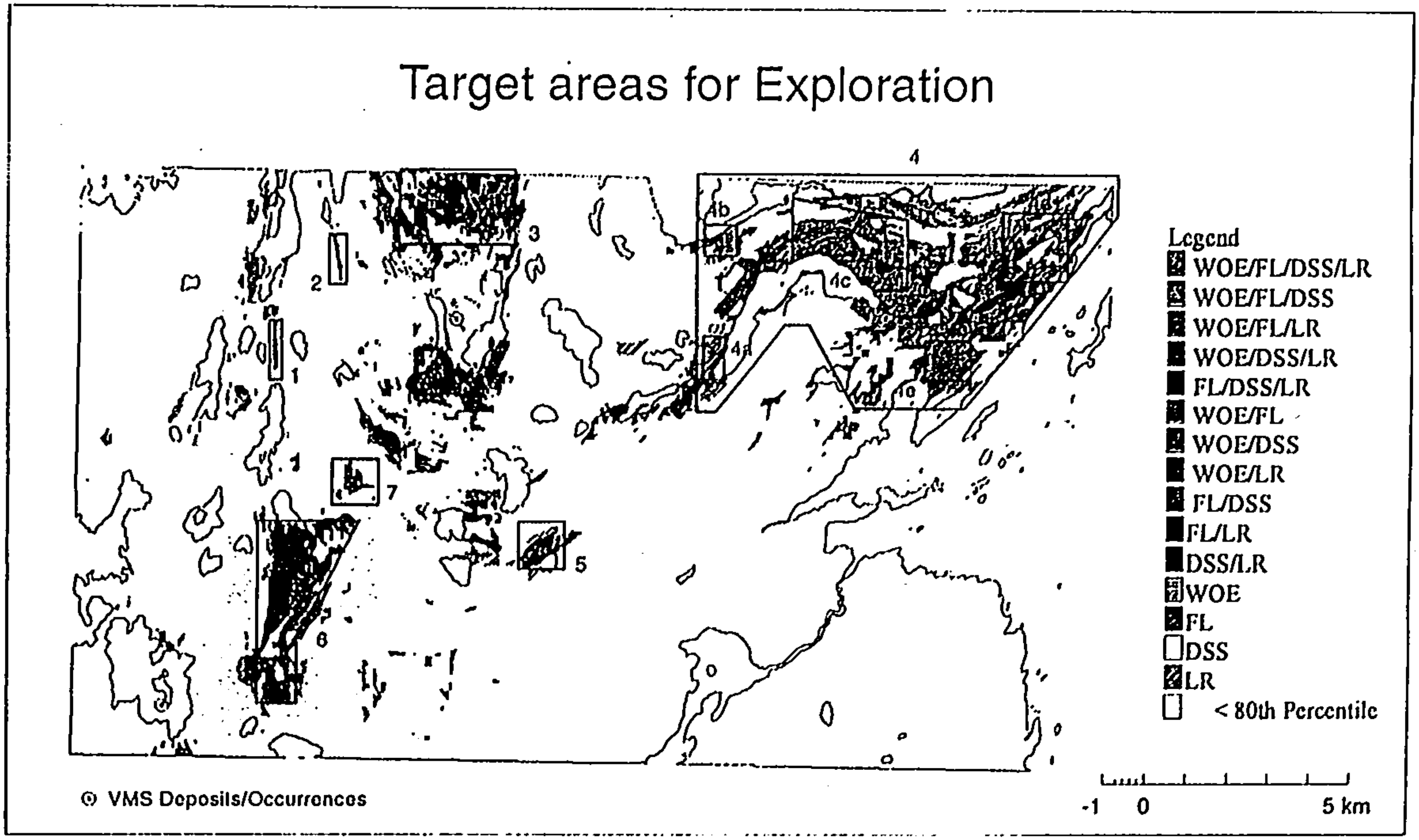

Figure 10.1. Summary of areas predicted by the four different methods to have high favourability for VHMS deposits. Seven areas that are of interest for further investigation have been identified and are discussed in text. WOE=weights of evidence, FL= fuzzy logic, DSS=Dempster-Shafer support, LR=area weighted logistic regression

presence of late intrusions, dip of contacts or other features that could alter the interpretation of the distance. The alteration factor is beneficial due to the presence of strong to weak Fe-Mg metasomatism. There is a strong magnetic and total field VLF signature for this area. Geochemical evidence is weak as no till samples were collected in this area and the lake sediment geochemical signature was not substantial.

Area 2

This area is located 0.5 km east of Cook Lake, in a small wedge between Richard Lake Pluton and Chisel Lake Pluton.

The presence of felsic flows, also recognized as possibly being part of the volcanic stratigraphy underlying the Chisel, Lost and Ghost deposits (Bailes, 1987) make this a favourable zone stratigraphically. The felsic units are immediately adjacent to the Richard Lake Pluton and synvolcanic dykes potential heat sources, however, as with Area 1, they are fault contacts so the true distance is not known and the heat factor may not be as significant as modelled. Strong Fe-Mg alteration is present and again no till samples were taken in this area while the lake sediment geochemistry has background levels. The geophysical signature showed strong magnetic responses and moderate VLF and gravity responses.

Area 3

This region is located at the northern limit of the study area centred between Snow Lake and Cook Lake.

An abundance of felsic flows and felsic volcaniclastic units make this a stratigraphically interesting area. Though it is rather distant from a subvolcanic tonalite, a moderately favourable potential with respect to a heat source is indicated by proximal synvolcanic dykes. Alteration in this area is characterized by strong and extensive Fe-Mg metasomatism. Till geochemistry shows anomalies in Pb and Cu and lake sediment geochemistry resulted in high PC1 scores (Cu) for this zone. The geophysical factor is typified by high magnetic responses, low VLF responses and high gravity responses.

Photo Lake

Photo lake is massive sulphide deposit in the order of 800,000 tons, discovered in 1994 by Hudson Bay Mining after drilling an airborne EM anomaly. Details of the deposit are being withheld on request of Hudson Bay Mining. (Bailes, pers. comm.)

It is of interest to note that the favourability modelling for this project and the selection of target areas, including AREA 3 which includes the Photo Lake deposit, was completed and presented at the Geological Survey of Canada's Forum in January, 1994. The new discovery at Photo Lake was unknown to the author until September, 1994.

Area 4

This a large area covering approximately 25 square km (7% of study area) to the north and west of Anderson Lake. It includes the past producing Anderson, Stall and Rod mines as well as the large (13MT) sub-economic Linda deposit. Despite this high density of deposits this whole area is generally characterized by favourable evidence and contains relatively large zones of favourabiity with no known deposits which are indicated on Figure 41 and summarized below.

The area labelled 4a is at the south end of Anderson Lake just north of the Joannie deposit. This area contains felsic flows and is close to both felsic and mafic volcaniclastic lithologies favourable for VHMS deposits. Tonalite sills and synvolcanic dykes are within 0.75 km providing good potential for heat sources. Till geochemistry indicates background levels of Pb and Zn, however, lake sediment geochemistry gives PC1 (Cu) and PC2 (Zn) scores above the 90th percentile. This zone is also proximal to Fe-Mg and Si alteration. High magnetic and gravity characterize this area.

Units of fragmental rhyolite flows and proximal mafic volcaniclastics comprise a favourable stratigraphic environment. Potential heat sources are within 2 km (tonalite sills) and 1 km (synvolcanic dykes). Till geochemistry indicates anomalous Cu and Pb concentrations above the 90th percentile and lake sediment geochemistry does not indicate any anomaly. Alteration is present in the form of Fe-Mg metasomatism. The geophysical factor is represented by a high magnetic response and high gravity response.

The area marked 4c is a continuous zone of high favourability extending for over 2 km between the Anderson deposit and the Stall deposit north of Anderson Lake. The lithology in this area is dominated by an abundance of felsic flows (Anderson Rhyolites). These rocks are stratigraphically close to both the tonalite sills and synvolcanic dykes making them favourable with respect to being close to a heat source. Alteration is ubiquitous, dominated by chlorite-biotite rich rocks. Completely altered rocks characteristic of alteration pipes are also present. Geochemical responses are variable with the lake sediment PC1 (Cu) being the most favourable indicator. Generally, magnetic responses are high while VLF and gravity responses are moderate.

The sub-area 4d is located to the north-west of Stall Lake. Units of rhyolite flows proximal to mafic volcaniclastic units and within 2 km of potential heat sources make the stratigraphy favourable. Fe-Mg and Si alteration has been mapped in this area. PC1(Cu) scores above the 90th percentile range are present and Zn concentrations in the till are present above the 80th percentile. Geophysical responses are variable but are generally high for magnetics and moderate for VLF and gravity.

The area labelled 4e is located 2 km south of Stall Lake between the Linda 1 and Linda 2 deposits. The area is underlain predominately by an aphyric phase of the Anderson Rhyolite proximal to heat sources. A number of alteration pipes characterized by pervasive staurolite/sericite/biotite alteration have been mapped. Small amounts of

Fe-Mg alteration have also been mapped. Till geochemistry is not favourable however, lake sediment geochemistry shows a moderately high PC2 (Zn) signature. The geophysical factor is typified by a high magnetic response and low VLF and gravity response.

Area 5

Area 5 is located north of Sneath Lake in the south central part of the study area. The presence of rhyolite flows and proximity to heat sources make this area stratigraphically favourable. Fe-Mg alteration has been mapped in the area and Si alteration 1.5 km to the north-east. No till samples were taken in the area and lake sediment geochemistry shows a moderately strong PC2 (Zn) signature for the area. The magnetic signature is high and both VLF and gravity show moderately high responses.

Area 6

Area 6 is a large region to the north-east of Morgan Lake extending for approximately 5 km between Hirst Lake in the south to Daly Lake in the north. This zone contains the Pot Lake and Tear Drop occurrences.

The general wedge shape of this area reflects the underlying rhyolites (Daly Lake Rhyolites). Small amounts of felsic volcaniclastic units are also present. Tonalite sills and synvolcanic dykes are both within 1 km of the area. Alteration is present in the form of Fe-Mg metasomatism and is proximal to Si alteration mapped to the west. No till samples were collected in the area and lake sediment geochemistry generally showed background values though PC3 (Mo) had a moderately strong signature. The magnetic response for the area was generally high while the VLF and gravity responses were variable.

Area 7

Area 7 is located to the north-east of Daly Lake. This is a favourable stratigraphic zone, underlain by felsic flows mapped and close to a possible heat source. It is proximal to Si and Fe-Mg alteration. Till geochemistry showed background concentrations of Cu, Pb and Zn and the lake sediment geochemistry showed a strong PC1 (Cu) signature for this area. Regional geophysical data indicated high magnetic responses and moderately high VLF and gravity responses.

Finally, the only real test to determine if the process and methods used in this study have been truly successful in facilitating the exploration geologist in the quest for unknown deposits, is for the selected areas of interest to be followed up with detailed studies and drilling.

It is hoped that in our world where mineral resources are becoming harder to find that this study will help those who are interested and willing in taking advantage of these new technologies in their search for new resources

REFERENCES

Agterberg, F.P. (1992a). Computer applications in geology. Encyclopedia of Earth System Science, v. 1, pp. 565-579.

Agterberg, F.P. (1992b). Combining indicator patterns in weights of evidence modelling for resource evaluation:Nonrenewable Resources, v.1, no.1, p. 35-50.

Agterberg, F.P., (1989a). Systematic approach to dealing with uncertainty of geoscience information in mineral exploration. In: Proceedings 21st APCOM Symposium, Las Vegas, March 1989, p. 165-178.

Agterberg, F.P. (1989b). LOGDIA - FORTRAN 77 program for logistic regression with diagnostics. Computers and Geoscience Vol. 15 No. 4, p. 599-614.

Agterberg, F.P. (1974). Automatic contouring of geological maps to detect target areas for mineral exploratoin : Jour. Math. Geol., v6, no. 4, p. 373-395.

Agterberg, F.P. and David, M., (1979). Statistical exploraton, In: A. Weiss (Editor), Computer mentods for the 80's, The American Institute of Mining and Metallurgical and Petroleum Enginerrs: New Yourk, p. 90-115.

Agterberg, F.P. and Robinson, S.C (1972). Mathematical problems of geology: Proceedings of the 38th Session of the International Statistical Institute , Washington, D.C. I.S.I. Bull., v. 44, p. 567-596.

Agterberg, F.P., Bonham-Carter, G.F. and Wright, D.F. (1990). Statistical pattern integration for mineral exploration: In Computer Applications in Resource Estimation Prediction and Assessment for Metals and Petroleum, Eds. Gaßl, G. and Merriam, D.F., Pergamon Press, Oxford-New York, p. 1-21.

Agterberg, F.P., Chung, C.F., Fabbri, A.G., Kelly, A.M. and Springer, J.S. (1972). Geomathematical evaluation of copper and zinc potential of the Abitibi area, Ontario and Quebec. Geol. Surv. Can., Paper 71-41, 55p.

Ahrens, L.H. (1954). Lognormal distribution of the elements. Geochim. Cosmochim. Acta v. 5, p. 49 - 73

An, P., (1992). Spatial reasoning techniques and integration of geophysical and geological information for resource exploration, Unpublished Ph.D. dissertation, The University, Winnipeg, 162 p.

An, P., Moon, W.M., and Rencz, A. (1991). Application of fuzzy set theory for integration of geological, geophysical and remote sensing data: Canadian Journal of Exploration Geophysics, v. 27, p. 1-11.

An, P., Moon, W.M. and Bonham-Carter, G.F. (1992). On a knowledge-based approach of integrating remote-sensing, geophysical and geological information, Proceedings IGARSS'92, p. 34-38.

An, P., Moon, W.M. and Bonham-Carter, G.F. (1994a). Uncertainty management in integration of exploration data using the belief function. Nonrenewable Resources, v.3, no. 1, p. 60-71

An, P., Moon, W.M. and Bonham-Carter, G.F. (1994b). An object-oriented knowlege representation structure for exploraton data integration: Nonrenewable Resources, v. 3, no. 2, p. 132-145.

Aronoff, S. (1989). Geographic Information Systems: A management perspective., WDL Publications, Ottawa. 294 p.

Bailes, A. H. (1990a). Chisel-Anderson Project (NTS 63K/16SE). In: Report of Activites 1990, Manitoba Energy and Mines, Mineral Division, pp. 43-48.

Bailes, A. H., (1990b). Geology of the Chisel-Morgan-Anderson Lake area. Manitoba Energy and Mines, Minerals Division, Preliminary Map 1990S-1, 1:20,000.

Bailes, A.H. and Galley, A.G. (1989). Geological setting of and hydrothermal alteration below the Chisel Lake massive Zn-Cu sulphide deposit, Manitoba Energy and Mines, Minerals Division, Report of Field Activities, p. 31-37.

Bailes, A.H. and Galley, A.G. (1991). Geological Setting of base metal mineralization in Anderson area. In: Report of Activities 1991, Manitoba Energy and Mines, Minerals Division, pp. 8-13.

Bailes, A.H. and Galley, A., (1992a). Chisel-Anderson-Morgan Lakes Preliminary Map 1992 S-1: Manitoba Energy and Mines. 1:20,000.

Bailes, A.H. and Galley, A. (1992b). Wekusko Lake (North) Preliminary Map 1992 S-2: Manitoba Energy and Mines. 1:20,000.

Bailes, A.H. and Galley, A.G. (in Prep). Stratigraphic setting of Early Proterozoic volcanic-hosted massive base metal sulfide deposits, Snow Lake, Manitoba; In: G.F. Bonham-Carter and G.E.M Hall eds., Volcanic-hosted massive sulphide deposits of the Snow Lake greenstone belt: an integrated study. GSC EXTECH 1 Publication

Bailes, A.H. and Galley, A.G. (1993). Geology of the Anderson-Stall volcanic-hosted massive sulphide area, Snow Lake, Manitoba (parts of NTS 63K16SE and 63J13SW; Geological Survey of Canada, Open File 2776, scale 1:10000.

Bailes, A.H. (1993). Snow Lake mapping projects (NTS 63K/16SE and 63J13SW); In: Manitoba Energy and Mines, Minerals Division, Report of Activities, 1993, p. 93-95.

Bailes, A.H. (1992). Wekusko Lake (North) project (NTSJ13/13SW); In: Manitoba Energy and Mines, Minerals Division, Report of Activities, 1992, p. 56-64.

Bailes, A.H. and Galley, A.G. (1992). Geology of the Kormans Lake area (NTS 63J13SW); In: Manitoba Energy and Mines, Minerals Division, Report of Activities, 1992, p. 65-74.

Bailes, A.H. (1988). Chisel-Morgan Lakes project; In: Manitoba Energy and Mines, Mineral Division, Report of Activities, 1988, p.53-61.

Bishop, M.M., Fienberg, S.E., and Holland, P.W. (1975). Discrete multivariate analysis: theory and practice. MIT Press, Cambridge, Massachusetts, 587 p.

Bonham-Carter, G.F. (1994a). Geographic systems for geoscientists: modelling with

GIS: Pergamon Press, Oxford, 398 p.

Bonham-Carter, G.F. (1994b). When to use the weights of evidence method for map data: Proceedings of Workshop on Spatial Modelling, Macaulay Land Research Institute, Aberdeen Scotland, September 1-2, 1994.

Bonham-Carter, G.F., Reddy, R.K.T. and Galley, A.G. (1994). Knowledge-driven modeling of volcanogenic massive sulphide potential with a geographic information system; In: Kirkham, R.V., Sinclair, W.D., Thorpe, R.I. and Duke, J.M. eds., Mineral Deposit Modeling: Geological Association of Canada, Special Paper 40.

Bonham-Carter, G.F., Agterberg, F.P. and Wright, D.F. (1988). Integration of geological datasets for gold exploration in Nova Scotia. Photogrammetry and Remote Sensing, v. 54, no. 11, p. 1585-1592.

Bonham-Carter, G.F., Agterberg, F.P. and Wright, D.F. (1989). Weights of evidence modelling: A new approach to mapping mineral potential: In Statistical Applicaitons in the Earth Sciences, ed. F.P. Agterberg and G.F. Bonham-Carter, Geological Survey of Canada, Paper 89-9, p. 171-183.

Bonham-Carter, G.F. and Agterberg, F.P. (1990). Application of a microcomputer-based geographic information system to mineral potential mapping: In Microcomputers in Geology, v.2, eds. Hanley, T. and Merriam, D.F., Pergamon Press, Oxford, p. 49-74.

Bonham-Carter, G.F. and Hall, G.E.M. (in prep.). Volcanic-hosted massive sulphide deposits of the Snow Lake greenstone belt: an integrated study. Geological Survey of Canada. EXTECH 1 Publication.

Botbol, J.M. (1971). An application of characteristic analysis to mineral exploration, Proc. 9th Intn. Sym. on Techniques for Decision-making in the mineral industry, CIMM, Special Volume 12, pp. 92-99.

Burrough, P.A. (1987). Principles of Geographical Information Systems for Land Resources Assessment. Clarendon Press, Oxford Press, Oxford, 193 p.

Cathles, L.M. (1983). An analysis of the hydrothermal system responsible for massive sulphide deposition in the Hokuroku basin of Japan: Economic Geology Monograph 5, p. 439 - 487.

Campbell, An.N., Hollister, V.F. and Duda, R.0. (1982). Recognition of a hidden mineral deposit by an artificial intelligence program: Science, v. 217 (3), p. 927-929.

Chrisman, N.R. (1991). The error component in spatial data. In: D.J. Maguire, M.F. Goodchild and D.W. Rhind (editors), Geographical Information Systems: Principles and Applications (2 volumes). Longman Scientific and Technical, London, v. 1: 165-174.

Chung, C.F. and Fabbri, A.G. (1993). The representation of geoscience information for data integration, Nonrenewable Resources, v. 2, no.2, p. 122-139.

Chung, C.F. and Moon, W.M. (1991). Combination rules of spatial geoscience data for mineral exploration: Geoinformatics, v. 2, no.2, p. 159-169.

Chung, C.F. and Agterberg, F.P. (1980). Regression models for estimating mineral resources from geological map data. Mathematical Geology, vol. 12, no. 5, p. 473-488.

Chung, C.F. (1983). SIMSAG: Integrated computer system for use in evaluation of mineral and energy resources, Journal of Mathematical Geology, Vol. 15 pp. 47-58.

Chung, C.F. (1978). Computer program for the logistic model to estimate the probability of occurrence of discrete events: Geol. Survey Canada, Paper 78-11, 23 p.

Coats, C.J.A., Clark, L.A., Buchan, R. and Brummer, J.J. (1970). Geology of the copper-zinc deposits of Stall Lake Mines Ltd. , Snow Lake area, N. Manitoba,; Economic Geology, v. 65, p. 970-984.

Coppock, J.T and Rhind, D.W. (1991). The history of GIS. In: D.J. Maguire, M.F. Goodchild and D. W. Rhind (editors), Geographical Information Systems: Principles and Applications (2 volumes) Longman Scientific and Technical, London, v. 1: 21-43.

Cox, D.R. (1966). Some procedures connected with the logistic qualitative respose curve; In: David, F.N., (Editor), Research papers in statistics, v.9, no. 3, p.

705-724.

Davis, J.C. (1986). Statistics and data analysis in geology. John Wiley and Sons, New York. 646 p.

Davis, F.W. and Simonett, D.S. (1991). GIS and remote sensing. In: D.J. Maguire, M.F. Goodchild and D. W. Rhind (editors), Geographical Information Systems: Principles and Applications (2 volumes) Longman Scientific and Technical, London, v. 1: 191-213.

Defense Mapping Agency, (1981). Product specifications for digital terrain elevation data (DTED). Defense Mapping Agency, Aerospace Center, St. Louis Air Force Station, Missouri., Stock No. SPECXDTED.

Dempster, A.P. (1968). A generalization of Bayesian inference: Journal Royal Statistical Society, series B, v.30, p.205-247.

Duda, R.O., Hart, P.E., Nilsson, N.J., Reboh, R., Slocum, J. and Sutherland, G.L. (1977). Development of a computer-based consultant for mineral exploration, Annual Report, SRI International Projects 5821 and 6415, p. 202

Dunn, R. and Pilsworth, D. (1994). The Canadian economy. In: 1993 Canadian mineral yearbook, Ed. E. Godin, Natural Resources Canada.

Englund, E. and Sparks, A. (1988). Geo-Eas (Geostatistical Environmental Assessment Software) User's Guide, United States Environmental Protection Agency, Systems Laboratory, P.O. Box 93478, Las Vegas, NV 89193-3478

ESRI, (1994). Understanding GIS. The ARC/INFO method. Environmental Research Systems Institute (ESRI), California

Fabbri, A. (1985). Image Processing of Geological Data. Van Nostrand Reinhold Company, 244 p.

Fedikow, M.A., Athayde, P. and Galley, A.G. (1993). Mineral deposits and occurrences in the Wekusko Lake area, NTS 63J/13: Manitoba Energy and Mines, Mineral Deposit Series Report No. 14, 460 p.

Fedikow, M.A., Athayde, P. and Galley, A.G. (1993b). MDS Map 14, Mineral Deposits and Occurrences in the File Lake area, Manitoba (NTS 63J/13). To accompant Report No. 14, Mineral Deposits Series, Manitoba Department of Mines and Energy. 1:50000

Fedikow, M.A., Ostry, G., Ferreira, K.J. and Galley, A.G., (1988), Mineral deposits and occurrences in the File Lake area, NTS 63K/16: Manitoba Energy and Mines, Mineral Deposit Series Report No. 5, 277 p., MDS Map No. 5, 1:50000

Fedikow, M.A.F., Athayde, P. and Galley, A.G., 1993: Mineral Deposits and Occurrences in the Wekusko Lake area, NTS 63J/13, Manitoba Energy and Mines, Geological Services, Mineral Deposit Series, Report No. 14.

Fisher, P.F. (1991). Spatial data sources and data problems.In: D.J. Maguire, M.F. Goodchild and D.W. Rhind (editors), Geographical Information Systems:

Principles and Applications (2 volumes). Longman Scientific and Technical, London, v. 1: 175-189

Friske, P. (in prep). Lake sediment geochemistry for the Snow Lake area. In: G.F. Bonham-Carter and G.E.M Hall eds., EXTECH 1: A Multidisiplinary Approach to Massive Sulphide Research in the Rusty Lake-Snow Lake Greenstone Belt, Manitoba. GSC Bulletin 426

Friske, P.F., McCurdy, M.W., Day, S.J.A., Gross, H., Lynch, J.J., and Durham, C.C. (1995). National Geochemical Reconnaissance lake sediment and water data, Snow Lake area, Manitoba (NTS 63J/13W and 63K/16E), Geological Survey of Canada Open File 3015.

Friske, P.W.B. and Hornbrook, E.H.W. (1991). Canada's National Geochemical Reconnaissance programme, Transactions Institute of Mining and Metalurgy, v. 100, p. B47-B56.

Froese, E. and Moore, J.M. (1980). Metamorphism in the Snow Lake area, Manitoba, Geological Survey of Canada, Paper 78-27, 16 p..

Garrett, R.G. (1974). Field data acqusition mehods for applied geochemical surveys at the Geological Survey of Canda, Paper Geological Survey of Canada 74-52, 36p.

Galley, A.G., Bailes, A.H. and Kistler,G. (1993). Geological setting and hydrothermal evolution for the Chisel Lake and North Chisel Zn-Pb-Ag-Au massive sulphide deposit, Snow Lake, Manitoba; Exploration and Mining Geology, v. 2, p. 271-295.

Galley, A. G. (1993). Characteristics of semi-conformable altertation zones associated with volcanic massive sulpide districts., Journal of Geochemical Exploration , v. 48, pp. 175-200.

Gobert, G. and Nielsen, E. (1991). Till geochemistry of the Snow Lake File Lake area (NTS 63K/16 and 63J/13); In: Manitoba Energy and Mines, Mineral Division, Report of Activities 1991, p. 47-48.

Goodacre, A.K., Grieve, R.A.F. and Halpeny, J.F. (1987). Observed gravity valuesof Canada: Geological Survey of Canada, Canadian Geophysical Atlas, Map 1, Scale 1:10,000,000.

Goodacre, A., Bonham-Carter, G.F., Agetrberg, F.P. and Wright, D.F. (1993). A statistical analysis of spatial associations of seismicity with drainage patterns and magnetic anomalies in western Quebec: Tectonophysics, v. 217, p.205-305.

Grant, F.S. and West, G.F. (1965). Interpretation theory in applied geophysics; McGraw Hill, Inc. N.Y., 583 p.

Harris, D.P. (1984). Mineral resources appraisal. Oxford University Press, NY, 1994

Hetu, R. (1991). Airborne Geophysical Survey of the Snow Lake area, Manitoba. Geological Survey of Canada Open File 2300.

Heuvelink, G.B.M. (1993). Error propogation in quantitative spatial modelling, CIP-Gegevens Koninklijke Bibliotheek, Den Haag, 151 p.

Hoffman, P.F. (1990). Subdivision of the Churchill Province and extent of the Trans-Hudson orogen, In: Lewry J.F. and Stauffer, M.R. eds., The Early Proterozoic Trans-Hudson Orogen of North America: Geological Association of Canada, Special Paper 37, p. 15-39.

Hoffman,P.F. (1988). United Plates of America, the birth of a craton: Early Proterozoic assembly and growth of Prot-Laurentia: Ann. Rev. Earth Planetary Sci., v. 16, p. 542-603

Hosmer, D.W. and Lemeshow, S. (1989). Applied Logistic Regression. Wiley, New York. 307p.

Isaaks, E.H. and Srivastava, R.M. (1989). An introduction to Applied Geostatistics, Oxford University Press, New York.

Jensen, S.K. and Domingue, J.O. (1988). Extracting topographic structure from digital elevation data for geographic information system analysis: Photogrammetric Engineering and Remote Sensing, v.54(11), p. 1593-1600.

Kaszycki, C.A., Gobert, G. and Nielsen, E. (1992). Till composition associated with volcanogenic massive sulphide deposits, Snow Lake and Rusty Lake areas, Manitoba: Geochemistry, Mineralogy and Regional Trends. In: Program with Abstracts, GSC Minerals Colloquium, Ottawa, 1992, p. 2

Kaszycki, C.A. (1989). Surficial geology and drift prospecting, Northwestern Manitoba. GSC Open File 2133, p. 131 - 154

Katz, S.S., (1991). Emulating the Prospector expert system with a raster GIS: Computers and Geosciences, v. 17, p. 1033-1050

Keefer, B.J., Smith, J.L. and Gregoire, T.G. (1988). Simulating manual digitizing error with statistical models. Proceedings of GIS/LIS '88. ACSM, Falls Church, pp. 475-483.

Knox-Robinson, C.M., (1994). Archean lode gold mineralisation potential of portion of the Yilgarn Block Western Australia: Developemnt and implementation of methodology for the creation of the regional-scale prospectivity maps using conventional geologicl map data and a geographic infroation systiem (GIS), Unpublished Ph.D. disseration, University of Western Australia, Perth., p. 178

Lam, N.S. (1983). Spatial interpolation methods: a review. The American Cartographer, v.10(2), p. 128 -149.

Lucas, S.B, Green, A., Hajnal, Z., White, D., Lewrey, J. Ashton, K., Weber, W. and Clowes, R. (1993). Deep seismic profile across a Proterozioic collision zone: surprises at depth; Nature, v. 363, p. 339-342.

Lydon, J.W. (1984). Volcanogenic massive sulphide deposits Part 1: a descriptive model; Geoscience Canada. v.11, p. 195-202.

Lydon, J.W. (1988). Volcanogenic massive sulphide deposits Part 2: genetic models;

Geoscience Canada, v. 15, p. 43-65.

Maffini, G.M., Arno, M. and Bitterlich, W. (1989). Observations and comments on the generation of error in digital GIS data. In: M.F. Goodchild and Gopal (editors) Accuracy of spatial databases. Taylor and Francis, Basingstoke, p. 55-67.

Maguire, D.J. (1991). An overview and definition of GIS. In: D.J. Maguire, M.F. Goodchild and D. W. Rhind (editors), Geographical Information Systems: Principles and Applications (2 volumes) Longman Scientific and Technical, London, v. 1: 9-20.

Sammet, H. (1990). The design and analysis of spatial data structures: Addison-Wesley Publishing Company, New York - Amsterdam, 493 p.

Martin, P.L. (1966). Structural analysis of the Chisel Lake orebody; Bulletin of the Canadian Institute of Mining and Metallurgy , v. 59, p. 630-636.

McCammon, R.B. (1989). Prospector-II - The redesign of Prospector: AI Systems in Government, March 27-31, 1989, Washington, D.C. pp. 88-92.

McCammon, R.B., Botbol, J.M., Sinding-Larssen R., and Bowen, R.W. (1983). Characteristic analysis - 1981: Final program and a possible discovery. Mathematical Geology, v. 15 p. 59

Miles, W. (1994). Personal communication, Geophysical Data Centre, Geological Survey of Canada, Ottawa.

Pregibon, D., (1981). Logistic regression diagnostics: Annals of Statistics, v. 9, n. 3, p. 705-724.

Reddy, R.K.T., Bonham-Carter, G.F. and Wright, D.F. (1990). GIS for mapping mineral resouce potential: preliminary results of a base-metal study, Snow Lake area, Manitoba. Proceedings of GIS for the 1990's Conference, Ottawa, Canada Ontario, March 5-9, 1990, p.384-400.

Reddy, R.K.T., Agterberg, F.P. and Bonham-Carter, G.F. (1991). Application of GIS-based logistic models to base-metal potential mapping in Snow Lake area, Manitoba; In: Proceedings Canadian Conference on GIS, Ottawa, Canada, March 18-22, 1991, p. 607- 618.

Reddy, R.K.T. and Bonham-Carter, G.F. (1991). A decision-tree approach to mineral potential mapping in Snow Lake area, Manitoba: Canadian Journal of Remote Sensing, v. 17, p. 191-200.

Reddy, R.K.T., Bonham-Carter, G.F. and Galley, A.G. (1992). Developing a geographic expert system for regeional mapping of volcanogenic massive sulfide (VHMS) deposit potential: Nonrenewable Resources, v.1(2) , p. 112 - 124

Reddy, R.K., Bonham-Carter, G.F. and Wright, D.F. (1990). GIS for mapping mineral resource potential: Preliminary results of base-metal study, Snow Lake area, Manitoba, Proceedings of GIS for the 1990's conference, Ottawa, Canada, March 5-8, 1990, p. 384-400.

Rose, A.W., Hawkes, H.E. and Webb, J.S. (1981). Geochemistry in mineral exploration. Academic Press, London. 657 p.

Shafer, G., (1976). A Mathematical Theory of Evidence: Princeton University Press, New Jersey, 297 p.

Singer, D.A. and Kouda, R. (1988). Integrating spatial and frequency information in the search for Kuroko Deposits of the Hokuroko District, Japan, Economic Geology, Vol. 83, No. 1, pp. 18-29.

Singer, D.A., (1993). Basic concepts in three-part quantitaive assessments of undiscovered mineral resources, Nonrenewable Resources, v. 2(2), p. 69-81.

Sinha, A.K. and Palacky, G.J. (in prep.). Ground electro-magnetic and VLF-EM surveys at 4 sites near Snow Lake, Manitoba. In: G.F. Bonham-Carter and G.E.M Hall eds., Volcanic-hosted massive suiphide deposits of the Snow Lake greenstone belt: an integrated study. GSC EXTECH 1 Publication

SPANS (1993). GIS: Learning System. INTERA TYDAC Technologies Inc., Ottawa.

Studer, R.D. (1982). Geology of the Stall Lake copper deposit, Snow Lake, Manitoba; Canadian Institute of Mining and Metallurgy Bulletin, v. 75, p. 66-72.

Syme, E.C. and Bailes, A.H. (1993). Stratigraphic and tectonic setting of Early Proterozoic volcanogenic massive sulfide deposits, Flin Flon, Manitoba: Economic Geology, V. 88, p. 566-589.

Syme, E.C. (1990). Stratigraphy and geochemistry of the Lynn Lake and Flin Flon metavolcanic belts, Manitoba, In: Lewry, J.F. and Stauffer, M.R., eds., The Early Proterozoic Trans-Hudson Orogen of North America: Geological Association of Canada, Special Paper 37, p. 143-161.

Tomlinson, R.F. (1967). An introduction to the Geographic Information System for the Canada Land Inventory. Department of Forestry and Rural Development, Ottawa, Canada

Tukey, J.W. (1972). Discussion of paper by F.P. Agterberg and S.C. Robinson (1972), Proceedings of the 38th Session of the International Statistical Institute, Washington, D.C. 1971: I.S. I. Bull, v. 44, p. 596.

Walford, P.C. and Franklin, J.M. (1982). The Anderson Lake Mine, Snow Lake, Manitoba; In: Hutchinson,R.W., Spenc, C.D. and Franklin, J.M. eds., Geological Associaton of Canada, Special Paper 25, p. 481-523.

Watson, D.F. (1992). Contouring: A guide to the analysis and display of spatial data. Pergamon Press, Oxford, 321 p.

Watson, G.P., Rencz, A.N. and Bonham-Carter, G.F. (1989). Computers assist prospecting. Geos v. 18, v. 18(1), p. 8-15.

Zaleski, E. Froese,E. and Gordon, T.M. (1991). Metamorphic petrology of Fe-Zn-Mg-Al alteration at the Linda volcanogenic massive sulphide deposit, Snow Lake, Manitoba, Canadian Mineralogist, v. 20,p. 995-1017.

APPENDIX A

Data Tables

Table A1. Lookup table for 1:20000 Geological map

Chisel-Morgan-Anderson Analog Map Legend (1:20000)	Code	Digital Map Code	Simplified Digital Map Legend	Code
PROTEROZOIC				
Post Amisk Intrusive Rocks				
Ham Lake Pluton	30	1	Post Amisk Intrusive Rocks	1
a) up to 30% xenoliths	30a	2		1
Hornblende-phyric quartz diorite	29	3		1
Granodiorite, tonalite	28	4		1
a) equigranular, granodiorite	28a	5		1
b) hornblende-phyric tonalite	28b	6		1
c) hornblende-phyric tonalite with abundant xenoliths	28c	7		1
Pyroxenite, metagabbro	27	8		1
Mafic intrusive complex: Gabbro, diorite, quartz diorite	26	9		1
a) intrusion breccia	26a	10		1
b) dyke complex	26b	11		1
Chisel Lake Intrusion	25	12		1
a) lower and upper peridotite	25a	13		1
b) pyroxenite	25b	14		1
c) lower gabbro	25c	15		1
d) middle gabbro	25d	16		1
e) upper gabbro	25e	17		1
f) gabbro pyroxenite	25f	18		1
Amisk Intrusive Rocks				
Quartz-phyric tonalite, tonalite	24	19		8
a) quartz-phyric (3-8mm phenocrysts)	24a	20	Subvolcanic Tonalite Sills	8
b) quartz-phyric (10-20 mm phenocrysts)	24b	21		8
c) quartz-plagioclase-phyric	24c	22		8
d) equigranular	24d	23		8
e) fine grained (1 mm and less)	24e	24		8
f) abundant xenoliths	24f	25		8
g) intrusion breccia	24g	26		8
Fine grained tonalite/felsic intrusions	23	27		8
a) equigranular	23a	28		8
b) plagioclase-phyric	23b	29		8
Quartz porphyry, quartz-plagioclase porphyry	22	30	Synvolcanic Intrusive Rocks	9
a) phenocrysts smaller than 5mm	22a	31		9
b) phenocrysts greater than 5mm	22b	32		9
c) dyke complex	22c	33		9
d) breccia	22d	34		9
e) [illegible], pyroxene-phyric	22e	35		9
Diorite intrusions	21	36		9
a) plagioclase-phyric	21a	37		9
b) dyke complex	21b	38		9
Pyroxene and pyroxene-plagioclase-phyric diorite	20	39		9
a) pyroxene-plagioclase-quartz-phyric quartz diorite	20a	40		9
b) intrusion breccia	20b	41		9
Gabbro, Diorite, quartz diorite	19	42		9
a) fine to medium grained	19a	43		9
b) medium grained	19b	44		9
c) coarse grained	19c	45		9
d) plagioclase-phyric	19d	46		9
e) pyroxene-phyric, pyroxene-plagioclase-phyric	19e	47		9
f) quartz diorite, melatonalite, tonalite	19f	48		9
g) magnetiferous diorite, quartz diorite, tonalite	19g	49		9
AMISK GROUP				
Sedimentary Rocks				
Parisian Formation: Paraconglomerate, minor greywacke	18	50	Missi Turbidite Assemblage	7
a) greywacke, mudstone	18a	51		7
Greywacke, siltstone, mudstone	17	52		7
Heterolithologic Volcanic Breccia				
Mixed mafic and felsic heterolithologic volcanic breccia	16	53	Mixed Volcaniclastic Rocks	6
a) mainly mafic fragments	16a	54		6
b) mainly felsic fragments	16b	55		6
Heterolithologic mafic volcanic breccia	15	56		6
Felsic Volcaniclastic Rocks				
Felsic volcanic breccia and minor wacke	14	57	Felsic Volcaniclastic Rocks	4
a) contains 10-30% mafic volcanic breccia and wacke	14a	58		4
b) related volcanic wacke and mudstone	14b	59		4
Dacite tuff, lapilli tuff	13	60		4
Mafic Volcaniclastic Rocks				
Mafic volcanic wacke	12	61		3
a) mainly porphyritic fragments	12a	62	Mafic Volcaniclastic Rocks	3
Mafic monolithologic volcanic breccia	11	63		3
a) aphyric	11a	64		3
b) plagioclase-phyric	11b	65		3
c) pyroxene-phyric, pyroxene-plagioclase-phyric	11c	66		3
Mafic tuff, lapilli tuff, tuff breccia, wacke	10	67		3

Table A1 (cont'd)

Felsic Flows	9			
Fine grained quartzo-feldspathic metamorphic rocks	9a	68	Felsic Flows	2
a) quartz-phyric	9b	69		2
b) fragmental	9c	70		2
c) plagioclase-phyric	9d	71		2
d) large quartz amygdules	8	72		2
Massive quartz-phyric rhyolite	7	73		2
Massive rhyolite lobes enveloped by breccia	7a	74		2
a) quartz-phyric	7b	75		2
b) quartz-plagioclase-phyric		76		2
Mafic Flows				
Fine grained mafic metamorphic rocks	6	77	Mafic Flows	3
a) porphyritic	6a	78		3
b) fragmental	6b	79		3
Pillow fragment Breccia	5	80		3
a) aphyric	5a	81		3
b) porphyritic	5b	82		3
Pyroxene-phyric flows, pyroxene-plagioclase-phyric flows	4	83		3
a) pillow fragment breccia	4a	84		3
b) amoeboid pillow breccia, thin pillowed flows	4b	85		3
Plagioclase-phyric flows	3	86		3
a) pillow fragment breccia	3a	87		3
b) amoeboid pillow breccia, thin pillowed flows	3b	88		3
Sparsely pyroxene-phyric flows, aphyric flows	2	89		3
a) pillow fragment breccia	2a	90		3
b) amoeboid pillow breccia, thin pillowed flows	2b	91		3
Aphyric flows	1	92		3
a) pillow fragment breccia	1a	93		3
b) amoeboid pillow breccia, thin pillowed flows	1b	94		3

Data Set	$\mu_A(x)$	SCP	Spt_A	Dis_A	Unc_A
Fe-Mg Alteration Buffers					
ON Alteration	0.75	0.4	0.0040	0.0006	0.9954
0.00 - 0.25 km	0.75	0.2	0.0020	0.0008	0.9972
0.25 - 0.50 km	0.60	0.1	0.0010	0.0009	0.9981
0.50 - 0.75 km	0.60	0.1	0.0010	0.0009	0.9981
0.75 - 1.00 km	0.55	0.07	0.0007	0.0009	0.9983
1.00 - 1.25 km	0.50	0.07	0.0007	0.0009	0.9983
1.25 - 1.50 km	0.45	0.05	0.0005	0.0009	0.9985
1.50 - 1.75 km	0.40	0.05	0.0005	0.0009	0.9985
1.75 - 2.00 km	0.35	0.02	0.0002	0.0009	0.9988
> 2.00 km	0.10	0.01	0.0001	0.0010	0.9989
Silica Alteration Buffers					
ON Alteration	0.70	0.20	0.0020	0.0008	0.9972
0.00 - 0.25 km	0.70	0.20	0.0020	0.0008	0.9972
0.25 - 0.50 km	0.65	0.15	0.0015	0.0008	0.9976
0.50 - 0.75 km	0.60	0.15	0.0015	0.0008	0.9976
0.75 - 1.00 km	0.50	0.10	0.0010	0.0009	0.9981
1.00 - 1.25 km	0.50	0.10	0.0010	0.0009	0.9981
1.25 - 1.50 km	0.45	0.08	0.0008	0.0009	0.9982
1.50 - 1.75 km	0.40	0.05	0.0005	0.0009	0.9985
1.75 - 2.00 km	0.35	0.02	0.0002	0.0009	0.9988
> 2.00 km	0.10	0.01	0.0001	0.0010	0.9989
Amphibole Alteration Buffers					
ON Alteration	0.70	0.10	0.0010	0.0009	0.9981
0.00 - 0.25 km	0.70	0.20	0.0020	0.0008	0.9972
0.25 - 0.50 km	0.65	0.20	0.0020	0.0008	0.9972
0.50 - 0.75 km	0.65	0.15	0.0015	0.0008	0.9976
0.75 - 1.00 km	0.55	0.15	0.0015	0.0008	0.9976
1.00 - 1.25 km	0.50	[illegible]	0.0010	0.0009	0.9981
1.25 - 1.50 km	0.45	0.10	0.0010	0.0009	0.9981
1.50 - 1.75 km	0.40	0.05	0.0005	0.0009	0.9985
1.75 - 2.00 km	0.35	0.05	0.0005	0.0009	0.9985
> 2.00 km	0.10	0.01	0.0001	0.0010	0.9989
Ep-Hm Alteration buffers					
ON Alteration	0.65	0.10	0.0001	0.0009	0.9981
0.00 - 0.25 km	0.65	0.20	0.0020	0.0008	0.9972
0.25 - 0.50 km	0.55	0.30	0.0030	0.0007	0.9963
0.50 - 0.75 km	0.55	0.20	0.0020	0.0008	0.9972
0.75 - 1.00 km	0.55	0.20	0.0020	0.0008	0.9972
1.00 - 1.25 km	0.50	0.15	0.0015	0.0008	0.9976
1.25 - 1.50 km	0.35	0.15	0.0015	0.0008	0.9976
1.50 - 1.75 km	0.30	0.10	0.0010	0.0009	0.9981
1.75 - 2.00 km	0.30	0.10	0.0010	0.0009	0.9981
> 2.00 km	0.10	0.05	0.0005	0.0009	0.9985

Data Set	$\mu_A(x)$	SCP	Spt_A	Dis_A	Unc_A
Alteration Pipes					
ON Alteration	0.90	0.80	0.0080	0.0002	0.9918
0.00 - 0.25 km	0.90	0.80	0.0080	0.0002	0.9918
0.25 - 0.50 km	0.70	0.50	0.0050	0.0005	0.9945
0.50 - 0.75 km	0.70	0.30	0.0030	0.0007	0.9963
0.75 - 1.00 km	0.65	0.50	0.0050	0.0005	0.9945
1.00 - 1.25 km	0.60	0.30	0.0030	0.0007	0.9963
1.25 - 1.50 km	0.55	0.20	0.0020	0.0008	0.9972
1.50 - 1.75 km	0.40	0.10	0.0010	0.0009	0.9981
1.75 - 2.00 km	0.35	0.10	0.0010	0.0009	0.9981
> 2.00 km	0.10	0.05	0.0005	0.0009	0.9985
Pb in Tills					
> 98th Percentile	0.80	0.50	0.0050	0.0005	0.9945
> 95th Percentile	0.76	0.30	0.0030	0.0007	0.9963
> 90th Percentile	0.73	0.20	0.0020	0.0008	0.9972
> 80th Percentile	0.70	0.06	0.0006	0.0009	0.9984
> 70th Percentile	0.67	0.05	0.0005	0.0009	0.9985
> 50th Percentile	0.65	0.04	0.0004	0.0009	0.9986
< 50th Percentile	0.10	0.02	0.0002	0.0008	0.9988
NO DATA	0.65	0.00	0.0000	0.0000	1.0000
Zn in Tills					
> 98th Percentile	0.80	0.20	0.0020	0.0008	0.9972
> 95th Percentile	0.76	0.20	0.0020	0.0008	0.9972
> 90th Percentile	0.73	0.15	0.0015	0.0008	0.9976
> 80th Percentile	0.70	0.10	0.0010	0.0009	0.9981
> 70th Percentile	0.67	0.08	0.0008	0.0009	0.9982
> 50th Percentile	0.65	0.07	0.0007	0.0009	0.9983
< 50th Percentile	0.10	0.05	0.0005	0.0009	0.9985
NO DATA	0.65	0.00	0.0000	0.0000	1.0000
Cu in Tills					
> 98th Percentile	0.80	0.30	0.0030	0.0007	0.9963
> 95th Percentile	0.76	0.20	0.0020	0.0008	0.9972
> 90th Percentile	0.73	0.10	0.0010	0.0009	0.9981
> 80th Percentile	0.70	0.05	0.0005	0.0009	0.9985
> 70th Percentile	0.67	0.04	0.0004	0.0009	0.9986
> 50th Percentile	0.65	0.02	0.0002	0.0008	0.9988
< 50th Percentile	0.10	0.01	0.0001	0.0009	0.9989
NO DATA	0.65	0.00	0.0000	0.0000	1.0000

Table A2. Fuzzy membership and Dempster-Shafer functions for each map used as evidence.

Data Set	$\mu_A(x)$	SCP	Spt_A	Dis_A	Unc_A
Generalized Geology					
Post Amisk Lithologies	0.00	-0.00	0.0000	1.0000	0.0000
Felsic flows	0.80	0.40	0.0040	0.0006	0.9954
Mafic flows	0.60	0.05	0.0005	0.0009	0.9985
Felsic volcaniclastic rocks	0.20	0.15	0.0015	0.0008	0.9976
Mafic volcaniclastic rocks	0.30	0.10	0.0010	0.0009	0.9981
Heterolithic volcaniclastic rocks	0.10	0.10	0.0010	0.0009	0.9981
Other sedimentary rocks	0.01	0.01	0.0001	0.0010	0.9989
Subvolcanic intrusions	0.00	0.005	0.0001	0.0009	0.9990
Synvolcanic intrusions	0.40	0.20	0.0020	0.0008	0.9972
Unmapped	0.00	0.00	0.0000	0.0000	1.0000
Proximity to Felsic Flows					
ON flow	0.20	0.40	0.0040	0.0006	0.9954
0.00 - 0.25 km	0.90	0.25	0.0025	0.0007	0.9967
0.25 - 0.50 km	0.85	0.10	0.0020	0.0009	0.9981
0.50 - 0.75 km	0.80	0.05	0.0005	0.0009	0.9985
0.75 - 1.00 km	0.70	0.045	0.0004	0.0009	0.9985
1.00 - 1.25 km	0.60	0.04	0.0004	0.0009	0.9986
1.25 - 1.50 km	0.40	0.03	0.0003	0.0009	0.9987
1.50 - 1.75 km	0.30	0.02	0.0002	0.0009	0.9988
1.75 - 2.00 km	0.20	0.01	0.0001	0.0010	0.9989
> 2.00 km	0.01	0.01	0.0001	0.0010	0.9989
Proximity to mafic volcaniclastics					
ON Unit	0.20	0.20	0.0020	0.0008	0.9972
0.00 - 0.25 km	0.90	0.20	0.0020	0.0008	0.9972
0.25 - 0.50 km	0.85	0.20	0.0020	0.0008	0.9972
0.50 - 0.75 km	0.80	0.20	0.0020	0.0008	0.9972
0.75 - 1.00 km	0.70	0.20	0.0020	0.0008	0.9972
1.00 - 1.25 km	0.60	0.20	0.0020	0.0008	0.9972
1.25 - 1.50 km	0.40	0.20	0.0020	0.0008	0.9972
1.50 - 1.75 km	0.30	0.20	0.0020	0.0008	0.9972
1.75 - 2.00 km	0.20	0.10	0.0010	0.0009	0.9981
> 2.00 km	0.01	0.01	0.0001	0.0010	0.9989
Proximity to Felsic Volcaniclastics					
ON Alteration	0.20	0.25	0.0020	0.0007	0.9967
0.00 - 0.25 km	0.90	0.25	0.0020	0.0007	0.9967
0.25 - 0.50 km	0.85	0.15	0.0010	0.0008	0.9976
0.50 - 0.75 km	0.80	0.10	0.0010	0.0009	0.9981
0.75 - 1.00 km	0.70	0.05	0.0005	0.0009	0.9985
1.00 - 1.25 km	0.60	0.02	0.0002	0.0009	0.9988
1.25 - 1.50 km	0.40	0.02	0.0002	0.0009	0.9988
1.50 - 1.75 km	0.30	0.015	0.0001	0.0009	0.9988
1.75 - 2.00 km	0.20	0.010	0.0001	0.0009	0.9989
> 2.00 km	0.01	0.005	0.0001	0.0009	0.9989

Data Set	$\mu_A(x)$	SCP	Spt_A	Dis_A	Unc_A
Lake Sed Geochem PC1					
No Data	0.50	0.60	0.000	0.000	1.000
> 98th Percentile	0.73	0.30	0.003	0.0009	0.9987
> 95th Percentile	0.70	0.20	0.002	0.0008	0.9972
> 90th Percentile	0.67	0.05	0.0005	0.0009	0.9985
> 80th Percentile	0.60	0.04	0.0004	0.0009	0.9986
> 70th Percentile	0.50	0.03	0.0003	0.0009	0.9987
> 50th Percentile	0.30	0.02	0.0002	0.0009	0.9988
< 50th Percentile	0.10	0.02	0.0002	0.0009	0.9988
Lake Sed Geochem PC2					
No Data	0.50	0.60	0.0000	0.0000	1.0000
> 98th Percentile	0.73	0.30	0.0030	0.0009	0.9987
> 95th Percentile	0.70	0.10	0.0020	0.0009	0.9981
> 90th Percentile	0.67	0.10	0.0020	0.0009	0.9981
> 80th Percentile	0.60	0.05	0.0005	0.0009	0.9985
> 70th Percentile	0.40	0.05	0.0005	0.0009	0.9985
> 50th Percentile	0.30	0.02	0.0002	0.0009	0.9988
< 50th Percentile	0.10	0.01	0.0001	0.0010	0.9989
Lake Sed Geochem PC3					
No Data	0.50	0.60	0.0000	0.0000	1.0000
> 98th Percentile	0.73	0.15	0.0010	0.0008	0.9976
> 95th Percentile	0.70	0.13	0.0010	0.0008	0.9978
> 90th Percentile	0.67	0.08	0.0008	0.0009	0.9982
> 80th Percentile	0.60	0.06	0.0006	0.0009	0.9984
> 70th Percentile	0.40	0.05	0.0005	0.0009	0.9985
> 50th Percentile	0.30	0.03	0.0003	0.0009	0.9987
< 50th Percentile	0.10	0.01	0.0001	0.0010	0.9989

Table A2 (cont'd)

Data Set	$\mu_A(x)$	SCP	Spt_A	Dis_A	Unc_A	Data Set	$\mu_A(x)$	SCP	Spt_A	Dis_A	Unc_A
Total Field VLF (%)						Airborne Total Field Magnetics					
1 -16.5461 - -3.5122	0.20	0.01	0.0001	0.00099	0.99891	1 Low	0.20	0.005	0.00005	0.00099	0.9989
2 -3.5122 - -2.7688	0.20	0.01	0.0001	0.00099	0.99891	2	0.20	0.01	0.0001	0.0009	0.9989
3 -2.7688 - -2.2215	0.20	0.02	0.0002	0.00098	0.99882	3	0.20	0.01	0.0001	0.0009	0.9989
4 -2.2215 - -1.7850	0.20	0.02	0.0002	0.00098	0.99882	4	0.20	0.010	0.0001	0.0009	0.9989
5 -1.7850 - -1.4185	0.20	0.02	0.0002	0.00098	0.99882	5	0.20	0.015	0.0015	0.00065	0.99856
6 -1.4185 - -1.1041	0.20	0.03	0.0003	0.00097	0.99873	6	0.20	0.015	0.0015	0.00065	0.99855
7 -1.1041 - -0.8426	0.20	0.03	0.0003	0.00097	0.99873	7	0.20	0.015	0.0015	0.00065	0.99856
8 -0.8426 - -0.6273	0.20	0.03	0.0003	0.00097	0.99873	8	0.20	0.02	0.0002	0.0009	0.99882
9 -0.6273 - -0.4409	0.20	0.04	0.0004	0.00096	0.99864	9	0.20	0.02	0.0002	0.0009	0.99882
10 -0.4409 - -0.2795	0.20	0.04	0.0004	0.00096	0.99864	10	0.20	0.02	0.0002	0.0009	0.99882
11 -0.2795 - -0.1269	0.20	0.04	0.0004	0.00096	0.99864	11	0.20	0.025	0.00025	0.00097	0.9987
12 -0.1269 - 0.0192	0.20	0.05	0.0005	0.00095	0.99855	12	0.20	0.025	0.00025	0.00097	0.9987
13 0.0192 - 0.1675	0.20	0.05	0.0005	0.00095	0.99855	13	0.20	0.025	0.00025	0.00097	0.9987
14 0.1675 - 0.3207	0.20	0.05	0.0005	0.00095	0.99855	14	0.20	0.030	0.0003	0.0009	0.9987
15 0.3207 - 0.4898	0.20	0.05	0.0005	0.00095	0.99855	15	0.20	0.030	0.0003	0.0009	0.9987
16 0.4898 - 0.6815	0.20	0.05	0.0005	0.00095	0.99855	16	0.20	0.030	0.0003	0.0009	0.9987
17 0.6815 - 0.9071	0.20	0.10	0.0010	0.00090	0.99810	17	0.20	0.030	0.0003	0.0009	0.9987
18 0.9071 - 1.1799	0.20	0.10	0.0010	0.00090	0.99810	18	0.20	0.030	0.0003	0.0009	0.9987
19 1.1799 - 1.5076	0.20	0.10	0.0010	0.00090	0.99810	19	0.20	0.04	0.0004	0.0009	0.9986
20 1.5076 - 1.9076	0.20	0.10	0.0010	0.00090	0.99810	20	0.20	0.05	0.0005	0.0009	0.9985
21 1.9076 - 2.4073	0.20	0.10	0.0010	0.00090	0.99810	21	0.70	0.10	0.0010	0.0009	0.9981
22 2.4073 - 3.0723	0.20	0.20	0.0020	0.0008	0.9972	22	0.70	0.15	0.0015	0.00085	0.9976
23 3.0723 - 4.0246	0.20	0.20	0.0020	0.0008	0.9972	23	0.70	0.15	0.0015	0.00085	0.9976
24 4.0246 - 5.9972	0.20	0.20	0.0020	0.0008	0.9972	24	0.20	0.2	0.0020	0.0008	0.9972
25 5.9972 - 24.6247	0.85	0.20	0.0020	0.0008	0.9972	25 High	0.20	0.2	0.0020	0.0008	0.9972
Processed VLF						Airborne Vertical Gradient Mag					
1 Low	0.20	0.02	0.0002	0.000980	0.99882	1 Low	0.20	0.01	0.00010	0.00099	0.99891
2	0.20	0.02	0.0002	0.000980	0.99882	2	0.20	0.01	0.00010	0.00099	0.99891
3	0.20	0.02	0.0002	0.000980	0.99882	3	0.20	0.02	0.00020	0.00098	0.99882
4	0.20	0.02	0.0002	0.000980	0.99882	4	0.20	0.02	0.00020	0.00098	0.99882
5	0.20	0.02	0.0002	0.000980	0.99882	5	0.20	0.02	0.00020	0.00098	0.99882
6	0.20	0.02	0.0002	0.000980	0.99882	6	0.20	0.02	0.00020	0.00098	0.99882
7	0.20	0.02	0.0002	0.000980	0.99882	7	0.20	0.02	0.00020	0.00098	0.99882
8	0.20	0.05	0.0005	0.000950	0.99855	8	0.20	0.03	0.00030	0.00097	0.99873
9	0.20	0.05	0.0005	0.000950	0.99855	9	0.20	0.03	0.00030	0.00097	0.99873
10	0.20	0.05	0.0005	0.000950	0.99855	10	0.20	0.03	0.00030	0.00097	0.99873
11	0.20	0.05	0.0005	0.000950	0.99855	11	0.20	0.03	0.00030	0.00097	0.99873
12	0.20	0.05	0.0005	0.000950	0.99855	12	0.20	0.03	0.00030	0.00097	0.99873
13	0.20	0.05	0.0005	0.000950	0.99855	13	0.20	0.04	0.00040	0.00096	0.99864
14	0.20	0.10	0.0010	0.00090	0.99810	14	0.20	0.04	0.00040	0.00096	0.99864
15	0.20	0.10	0.0010	0.00090	0.99810	15	0.20	0.04	0.00040	0.00096	0.99864
16	0.20	0.10	0.0010	0.00090	0.99810	16	0.20	0.04	0.00040	0.00096	0.99864
17	0.20	0.10	0.0010	0.00090	0.99810	17	0.20	0.05	0.00050	0.00095	0.99855
18	0.20	0.10	0.0010	0.00090	0.99810	18	0.02	0.05	0.00050	0.00095	0.99855
19	0.20	0.10	0.0010	0.00090	0.99810	19	0.20	0.05	0.00050	0.00095	0.99855
20	0.20	0.10	0.0010	0.00090	0.99810	20	0.20	0.10	0.0010	0.00090	0.99810
21	0.90	0.15	0.0015	0.00085	0.99765	21	0.90	0.10	0.0010	0.00090	0.99810
22	0.90	0.15	0.0015	0.00085	0.99765	22	0.90	0.10	0.0010	0.00090	0.99810
23	0.90	0.20	0.0020	0.0008	0.9972	23	0.90	0.15	0.0015	0.00085	0.99765
24	0.90	0.25	0.0025	0.00075	0.99675	24	0.20	0.15	0.0015	0.00085	0.99765
25 High	0.90	0.30	0.0030	0.00070	0.99630	25 High	0.20	0.15	0.0015	0.00085	0.99765

Table A2 (cont'd)

Data Set	$\mu_A(x)$	SCP	Spt_A	Dis_A	Unc_A	Data Set	$\mu_A(x)$	SCP	Spt_A	Dis_A	Unc_A
Airborne Vertical Gradient Gravity						Proximity to Subvolcanic Sills					
1 Low	0.30	0.001	0.00001	0.00099	0.99899	ON Sill	0.00	0.001	0.00001	0.00099	0.99899
2	0.30	0.01	0.00010	0.00099	0.99899	0.00 - 0.50 km	0.95	0.05	0.00050	0.00095	0.99855
3	0.30	0.01	0.00010	0.00099	0.99899	0.50 - 1.00 km	0.80	0.05	0.00050	0.00095	0.99855
4	0.30	0.01	0.00010	0.00099	0.99899	1.00 - 1.50 km	0.60	0.04	0.00040	0.00096	0.99864
5	0.30	0.01	0.00010	0.00099	0.99899	1.50 - 2.00 km	0.60	0.04	0.00040	0.00096	0.99864
6	0.30	0.02	0.00020	0.00098	0.99882	2.00 - 2.50 km	0.55	0.03	0.00030	0.00097	0.99873
7	0.30	0.02	0.00020	0.00098	0.99882	2.50 - 3.00 km	0.50	0.03	0.00030	0.00097	0.99873
8	0.30	0.02	0.00020	0.00098	0.99882	3.00 - 3.50 km	0.45	0.03	0.00030	0.00097	0.99873
9	0.30	0.02	0.00020	0.00098	0.99882	3.50 - 4.00 km	0.30	0.02	0.00020	0.00098	0.99882
10	0.30	0.02	0.00020	0.00098	0.99882	> 4.00 km	0.10	0.001	0.00001	0.00099	0.99899
11	0.30	0.03	0.00030	0.00097	0.99873						
12	0.30	0.03	0.00030	0.00097	0.99873						
13	0.30	0.03	0.00030	0.00097	0.99873	Proximity to synvolcanic dykes					
14	0.30	0.03	0.00030	0.00097	0.99873	ON Dyke	0.80	0.2	0.0020	0.0008	0.99720
15	0.30	0.03	0.00030	0.00097	0.99873	0.00 - 0.50 km	0.95	0.2	0.0020	0.0008	0.99720
16	0.90	0.03	0.00030	0.00097	0.99873	0.50 - 1.00 km	0.75	0.15	0.0015	0.00095	0.99765
17	0.90	0.03	0.00030	0.00097	0.99873	1.00 - 1.50 km	0.65	0.15	0.0015	0.00095	0.99765
18	0.90	0.05	0.00050	0.00095	0.99855	1.50 - 2.00 km	0.55	0.10	0.0010	0.00090	0.99810
19	0.90	0.05	0.00050	0.00095	0.99855	2.00 - 2.50 km	0.50	0.10	0.0010	0.00090	0.99810
20	0.30	0.1	0.0010	0.00090	0.99810	2.50 - 3.00 km	0.45	0.05	0.00050	0.00095	0.99855
21	0.30	0.1	0.0010	0.00090	0.99810	3.00 - 3.50 km	0.40	0.05	0.00050	0.00095	0.99855
22	0.30	0.15	0.0015	0.00095	0.99765	3.50 - 4.00 km	0.35	0.02	0.00020	0.00098	0.99882
23	0.30	0.15	0.0015	0.00095	0.99765	> 4.00 km	0.10	0.001	0.00001	0.00099	0.99899
24	0.30	0.20	0.0020	0.00080	0.99720						
25 High	0.30	0.20	0.0020	0.00080	0.99720						

Table A2 (cont'd)

Map Class for GEOLRC.MAP (Non-cumulative)	Area (km)	Deposits	W+	s (W+)	W-	s (W-)	C	s (C)	Stud (C)
1 Post Amisk	51	0							
2 Felsic Flows	**18**	**7**	**2.2995**	**0.4764**	**-0.5807**	**0.3593**	**2.8802**	**0.5968**	**4.8263**
3 Mafic Flows	70	3	-0.2774	1.0072	0.2482	0.2772	-1.6536	1.0447	-1.5829
4 Felsic Volcaniclastic Rocks	7	0							
5 Mafic Volcaniclastic Rocks	12	1	0.4213	1.0441	-0.0243	0.2749	0.4456	1.0796	0.4127
6 Mixed Volcaniclastic Rocks	13	0							
7 Other Sedimentary Rocks	21	0							
8 Subvolcanic Tonalite Sills	46	0							
9 Synvolcanic Intrusive Rocks	**21**	**4**	**1.3791**	**0.5556**	**-0.2406**	**0.3084**	**1.6198**	**0.6354**	**2.5490**
10 Unmapped	5	0							

Map Class for GEOL5C2.MAP (Cumulative)	Area (km)	Deposits	W+	s (W+)	W-	s (W-)	C	s (C)	Stud (C)
1 0.00 - 0.25 km	12	1	0.4213	1.0441	-0.0243	0.2749	0.4456	1.0796	0.4127
2 0.25 - 0.50 km	37	4	0.6949	0.5288	-0.1673	0.3090	0.8622	0.6124	1.4079
3 0.50 - 0.75 km	58	6	0.6550	0.4308	-0.2779	0.3407	0.9330	0.5493	1.6985
4 0.75 - 1.00 km	77	8	0.6711	0.3734	-0.4439	0.3851	1.1150	0.5364	2.0786
5 1.00 - 1.25 km	94	9	0.5761	0.3504	-0.5049	0.4155	1.0811	0.5435	1.9891
6 1.25 - 1.50 km	111	11	0.6143	0.3175	-0.8163	0.5065	1.4306	0.5978	2.3931
7 1.50 - 1.75 km	127	11	0.4669	0.3154	-0.7061	0.5072	1.1730	0.5973	1.9638
8 1.75 - 2.00 km	**141**	**13**	**0.5383**	**0.2910**	**-1.3098**	**0.7127**	**1.8481**	**0.7699**	**2.4005**
9 2.00 - 2.25 km	153	14	0.5294	0.2803	-1.9102	1.0044	2.4395	1.0428	2.3395
10 2.25 - 2.50 km	268	15							

Map Class for GEOL4C2.MAP (Cumulative)	Area (km)	Deposits	W+	s (W+)	W-	s (W-)	C	s (C)	Stud (C)
1 0.00 - 0.25 km	7	0							
2 0.25 - 0.50 km	32	3	0.5545	0.6063	-0.1011	0.2963	0.6556	0.6748	0.9715
3 0.50 - 0.75 km	53	6	0.7625	0.4333	-0.3043	0.3405	1.0667	0.5511	1.9356
4 0.75 - 1.00 km	74	8	0.7082	0.3742	-0.4574	0.3850	1.1656	0.5368	2.1712
5 1.00 - 1.25 km	94	11	0.7981	0.3207	-0.9211	0.5058	1.7192	0.5989	2.8704
6 1.25 - 1.50 km	**114**	**12**	**0.6853**	**0.3051**	**-1.0934**	**0.5830**	**1.7787**	**0.6581**	**2.7029**
7 1.50 - 1.75 km	132	12	0.5210	0.3027	-0.9648	0.5838	1.4858	0.6576	2.2593
8 1.75 - 2.00 km	150	13	0.4723	0.2902	-1.2375	0.7131	1.7098	0.7699	2.2207
9 2.00 - 2.25 km	165	13	0.3647	0.2889	-1.0941	0.7141	1.4588	0.7703	1.8938
10 2.25 - 2.50 km	268	15							

Table A3. Calculated weights and contrasts to determine thresholds for converting multiclass evidence maps to binary evidence maps. Bold records indicate the selected threshold. See Table 3.6 for descriptions of maps.

Map Class for GEOL2C2.MAP (Cumulative)	Area (km)	Deposits	W+	s (W+)	W-	s (W-)	C	s (C)	Stud (C)
1 0.00 - 0.25 km	18	7	2.2995	0.4764	-0.5807	0.3593	2.8802	0.5968	4.8263
2 0.25 - 0.50 km	56	12	1.5122	0.3251	-1.4154	0.5815	2.9277	0.6662	4.3948
3 0.50 - 0.75 km	81	13	1.1602	0.3024	-1.6979	0.7109	2.8581	0.7725	3.6996
4 0.75 - 1.00 km	104	13	0.8727	0.2963	-1.5653	0.7115	2.4380	0.7707	3.1634
5 1.00 - 1.25 km	125	13	0.6683	0.2929	-1.4275	0.7121	2.0958	0.7700	2.7219
6 1.25 - 1.50 km	145	14	0.5852	0.2811	-1.9744	1.0041	2.5596	1.0427	2.4548
7 1.50 - 1.75 km	163	14	0.4578	0.2795	-1.8152	1.0048	2.2730	1.0429	2.1794
8 1.75 - 2.00 km	177	14	0.3693	0.2784	-1.6721	1.0055	2.0414	1.0434	1.9566
9 2.00 - 2.25 km	187	14	0.3116	0.2778	-1.5578	1.0062	1.8693	1.0439	1.7908
10 2.25 - 2.50 km	268	15							

Map Class for SILLBUF.MAP (Cumulative)	Area (km)	Deposits	W+	s (W+)	W-	s (W-)	C	s (C)	Stud (C)
1 0.00 - 0.50 km	46	0							
2 0.50 - 1.00 km	107	7	0.1676	0.3909	-0.1267	0.3626	0.2943	0.5332	0.5518
3 1.00 - 1.50 km	154	10	0.1598	0.3270	-0.2588	0.4573	0.4187	0.5622	0.7447
4 1.50 - 2.00 km	188	11	0.0498	0.3107	-0.1255	0.5129	0.1753	0.5997	0.2924
5 2.00 - 2.50 km	215	12	-0.0034	0.2971	0.0138	0.5944	-0.0173	0.6645	-0.0260
6 2.50 - 3.00 km	233	12	-0.0881	0.2964	0.4595	0.6038	-0.5476	0.6726	-0.8141
7 3.00 - 3.50 km	246	15							
8 3.50 - 4.00 km	255	15							
9 4.00 - 4.50 km	262	15							
10 4.50 - 5.00 km	268	15							
	268	15							

Map Class for DYKEBUF1.MAP (Cumulative)	Area (km)	Deposits	W+	s (W+)	W-	s (W-)	C	s (C)	Stud (C)
1 0.00 - 0.25 km	21	4	1.3791	0.5556	-0.2406	0.3084	1.6198	0.6354	2.5490
2 0.25 - 0.50 km	98	8	0.3995	0.3688	-0.3195	0.3860	0.7189	0.5339	1.3467
3 0.50 - 0.75 km	141	10	0.2516	0.3280	-0.3680	0.4563	0.6196	0.5619	1.1026
4 0.75 - 1.00 km	174	14	0.3873	0.2786	-1.7039	1.0054	2.0911	1.0433	2.0044
5 1.00 - 1.25 km	199	15							
6 1.25 - 1.50 km	216	15							
7 1.50 - 1.75 km	225	15							
8 1.75 - 2.00 km	230	15							
9 2.00 - 2.25 km	234	15							
10 2.25 - 2.50 km	268								
11 > 2.5 km	268								

Table A3 (cont'd)

Map Class for LKPC1NC.MAP (Cumulative)	Area (km)	Deposits	W+	s (W+)	W-	s (W-)	C	s (C)	Stud (C)
PC1 SCORES									
1 2.292 - 3.280	2	0							
2 1.479 - 2.292	21	5	1.6182	0.5095	-0.3371	0.3218	1.9553	0.6032	3.2416
3 1.353 - 1.479	36	5	0.9742	0.4309	-0.2710	0.3233	1.2452	0.5795	2.1488
4 1.049 - 1.353	66	6	0.5198	0.4281	-0.2392	0.3410	0.7591	0.5473	1.3870
5 0.817 - 1.094	75	8	0.6965	0.3739	-0.4532	0.3850	1.1497	0.5367	2.1422
6 -0.289 - 0.817	143	13	0.5194	0.2908	-1.2902	0.7128	1.8096	0.7699	2.3505
7 <-0.289	225	15							
8 No Data	268	15							

Map Class for LKPC2NC.MAP (Cumulative)	Area (km)	Deposits	W+	s (W+)	W-	s (W-)	C	s (C)	Stud (C)
PC2 SCORES									
1 4.213 - 8.079	4	2	2.4956	0.9264	-0.1320	0.2844	2.6276	0.9691	2.7113
2 1.156 - 4.213	8	3	2.2050	0.7155	-0.2008	0.2956	2.4059	0.7742	3.1077
3 0.825 - 1.156	19	4	1.4897	0.5617	-0.2482	0.3084	1.7379	0.6408	2.7121
4 0.485 - 0.825	87	8	0.5334	0.3709	-0.3869	0.3855	0.9203	0.5350	1.7203
5 0.208 - 0.485	98	8	0.4004	0.3688	-0.3200	0.3860	0.7203	0.5339	1.3493
6 -0.194 - 0.208	131	10	0.3298	0.3290	-0.4459	0.4556	0.7758	0.5619	1.3805
7 <-0.194	224	15							
8 No Data	268	15							

Map Class for LKPC3NC.MAP (Cumulative)	Area (km)	Deposits	W+	s (W+)	W-	s (W-)	C	s (C)	Stud (C)
PC3 SCORES									
1 >1.352	7	1	0.9163	1.0713	-0.0420	0.2747	0.9583	1.1060	0.8665
2 1.162 - 1.352	59	8	0.9573	0.3798	-0.5330	0.3845	1.4903	0.5404	2.7577
3 1.031 - 1.162	85	8	0.5639	0.3715	-0.4005	0.3854	0.9644	0.5352	1.8018
4 0.878 - 1.031	132	8	0.0876	0.3648	-0.0915	0.3880	0.1791	0.5326	0.3363
5 0.682 - 0.878	163	11	0.1997	0.3122	-0.4040	0.5098	0.6037	0.5978	1.0100
6 0.005 - 0.682	224	15							
7 <0.005	268	15							
8 No Data									

Table A3 (cont'd)

Map Class for KRGLNCU2.MAP (Cumulative)	Area (km)	Deposits	W+	s (W+)	W-	s (W-)	C	s (C)	Stud (C)
ln Cu (Kriged)									
1 6.339 - 6.899	2	0							
2 5.913 - 6.339	13	2	1.1086	0.7678	-0.0981	0.2847	1.2067	0.8189	1.4736
3 5.636 - 5.913	32	5	1.1094	0.4856	-0.2890	0.3231	1.3985	0.5833	2.3974
4 5.339 - 5.636	71	10	1.0052	0.3408	-0.8189	0.4530	1.8241	0.5669	3.2177
5 5.202 - 5.339	86	10	0.7993	0.3364	-0.7423	0.4535	1.5416	0.5646	2.7304
6 4.983 - 5.202	112	11	0.6116	0.3175	-0.8145	0.5065	1.4261	0.5978	2.3857
7 0.000 - 4.983	134	13	0.5925	0.2918	-1.3625	0.7124	1.9550	0.7699	2.5393
8 No Data	268	15							

Map Class for KRGLNPB2.MAP (Cumulative)	Area (km)	Deposits	W+	s (W+)	W-	s (W-)	C	s (C)	Stud (C)
ln Pb (Kriged)									
1 4.277 - 5.118	0	0							
2 3.221 - 4.277	6	1	1.0689	1.0826	-0.0458	0.2747	1.1147	1.1169	0.9980
3 3.020 - 3.221	10	2	1.3567	0.7840	-0.1082	0.2846	1.4649	0.8341	1.7562
4 2.869 - 3.020	21	3	1.0250	0.6231	-0.1487	0.2959	1.1737	0.6898	1.7015
5 2.754 - 2.869	32	5	1.1160	0.4859	-0.2898	0.3231	1.4058	0.5835	2.4092
6 2.530 - 2.754	49	5	0.6360	0.4715	-0.2113	0.3237	0.8473	0.5719	1.4815
7 0.000 - 2.530	77	8	0.5125	0.3962	-0.3008	0.3612	0.8133	0.5361	1.5170
8 No Data	268	15							

Map Class for KRGLNZN2.MAP (Cumulative)	Area (km)	Deposits	W+	s (W+)	W-	s (W-)	C	s (C)	Stud (C)
ln Zn (Kriged)									
1 5.916 - 7.051	2	1	2.7491	1.3869	-0.0647	0.2746	2.8138	1.4138	1.9903
2 5.493 - 5.916	7	1	0.9209	1.0716	-0.0421	0.2747	0.9630	1.1063	0.8705
3 5.376 - 5.493	15	4	1.7937	0.5821	-0.2648	0.3083	2.0585	0.6587	3.1252
4 5.262 - 5.376	32	4	0.8739	0.5342	-0.1922	0.3088	1.0660	0.6170	1.7277
5 5.161 - 5.262	45	4	0.4840	0.5234	-0.1306	0.3092	0.6146	0.6079	1.0110
6 5.075 - 5.161	65	4	0.0942	0.5160	-0.0322	0.3100	0.1264	0.6019	0.2100
7 0.000 - 5.075	117	11	0.5579	0.3167	-0.7774	0.5067	1.3353	0.5976	2.2346
8 No Data	268	15							

Table A3 (cont'd)

Map Class for NALTSIC2.MAP (Cumulative)	Area (km)	Deposits	W+	s (W+)	W-	s (W-)	C	s (C)	Stud (C)
1 0.00 - 0.25 km	7	0							
2 0.25 - 0.50 km	36	4	0.7489	0.5303	-0.1754	0.3089	0.9243	0.6137	1.5061
3 0.50 - 0.75 km	65	6	0.5333	0.4283	-0.2434	0.3410	0.7767	0.5475	1.4188
4 0.75 - 1.00 km	91	8	0.4814	0.3701	-0.3623	0.3857	0.8438	0.5345	1.5786
5 1.00 - 1.25 km	116	10	0.4668	0.3308	-0.5573	0.4547	1.0241	0.5623	1.8212
6 1.25 - 1.50 km	139	11	0.3687	0.3141	-0.6141	0.5079	0.9828	0.5972	1.6457
7 1.50 - 1.75 km	159	14	0.4897	0.2798	-1.8596	1.0046	2.3493	1.0428	2.2528
8 1.75 - 2.00 km	174	14	0.3911	0.2787	-1.7105	1.0053	2.1016	1.0432	2.0145
9 2.00 - 2.25 km	185	14	0.3206	0.2779	-1.5769	1.0061	1.8974	1.0438	1.8179
10 2.25 - 2.50 km	268	15							

Map Class for NALTFEC2.MAP (Cumulative)	Area (km)	Deposits	W+	s (W+)	W-	s (W-)	C	s (C)	Stud (C)
1 0.00 - 0.25 km	15	5	2.0820	0.5429	-0.3630	0.3227	2.4451	0.6316	3.8714
2 0.25 - 0.50 km	63	11	1.2750	0.3319	-1.0925	0.5049	2.3675	0.6042	3.9183
3 0.50 - 0.75 km	102	11	0.7124	0.3192	-0.8760	0.5061	1.5884	0.5983	2.6547
4 0.75 - 1.00 km	133	11	0.4161	0.3147	-0.6607	0.5076	1.0768	0.5972	1.8030
5 1.00 - 1.25 km	158	13	0.4140	0.2895	-1.1643	0.7136	1.5783	0.7701	2.0496
6 1.25 - 1.50 km	176	14	0.3770	0.2785	-1.6859	1.0055	2.0628	1.0433	1.9772
7 1.50 - 1.75 km	190	15							
8 1.75 - 2.00 km	200	15							
9 2.00 - 2.25 km	210	15							
10 2.25 - 2.50 km	268	15							

Map Class for NALTPFC2.MAP (Cumulative)	Area (km)	Deposits	W+	s (W+)	W-	s (W-)	C	s (C)	Stud (C)
1 0.00 - 0.25 km	0	0	0.0000	0.0000	0.0000	0.0000	0.0000	0.0000	0.0000
2 0.25 - 0.50 km	3	4	0.0000	0.0000	0.0000	0.0000	0.0000	0.0000	0.0000
3 0.50 - 0.75 km	7	5	3.3787	0.7393	-0.3940	0.3215	3.7728	0.8066	4.6774
4 0.75 - 1.00 km	13	6	2.6436	0.5524	-0.4820	0.3394	3.1256	0.6483	4.8210
5 1.00 - 1.25 km	18	7	2.2937	0.4759	-0.5804	0.3594	2.8741	0.5964	4.8194
6 1.25 - 1.50 km	24	8	2.0947	0.4301	-0.6942	0.3835	2.7889	0.5763	4.8398
7 1.50 - 1.75 km	30	10	2.1204	0.3863	-1.0152	0.4520	3.1356	0.5946	5.2737
8 1.75 - 2.00 km	36	10	1.8639	0.3716	-0.9895	0.4521	2.8534	0.5852	4.8757
9 2.00 - 2.25 km	42	10	1.6453	0.3514	-0.9609	0.4522	2.6062	0.5789	4.5019
10 2.25 - 2.50 km	268	15							

Table A3 (cont'd)

Map Class for NALTAPC2.MAP (Cumulative)	Area (km)	Deposits	W+	s (W+)	W-	s (W-)	C	s (C)	Stud (C)
1 0.00 - 0.25 km	1	0							
2 0.25 - 0.50 km	10	2	1.4281	0.7894	-0.1106	0.2846	1.5387	0.8392	1.8336
3 0.50 - 0.75 km	16	3	1.3509	0.6398	-0.1700	0.2958	1.5209	0.7049	2.1576
4 0.75 - 1.00 km	20	3	1.0685	0.6250	-0.1520	0.2959	1.2205	0.6915	1.7649
5 1.00 - 1.25 km	24	5	1.4754	0.5017	-0.3262	0.3229	1.8015	0.5966	3.0196
6 1.25 - 1.50 km	27	6	1.5525	0.4617	-0.4223	0.3397	1.9749	0.5732	3.4451
7 1.50 - 1.75 km	29	6	1.4566	0.4571	-0.4130	0.3398	1.8696	0.5695	3.2826
8 1.75 - 2.00 km	31	6	1.3654	0.4530	-0.4031	0.3398	1.7685	0.5663	3.1227
9 2.00 - 2.25 km	34	6	1.2871	0.4498	-0.3938	0.3399	1.6809	0.5638	2.9813
10 2.25 - 2.50 km	268	15							

Map Class for NALTEPC2.MAP (Cumulative)	Area (km)	Deposits	W+	s (W+)	W-	s (W-)	C	s (C)	Stud (C)
1 0.00 - 0.25 km	1	0							
2 0.25 - 0.50 km	5	2	2.3412	0.8983	-0.1302	0.2845	2.4713	0.9423	2.6227
3 0.50 - 0.75 km	8	3	2.1822	0.7127	-0.2003	0.2956	2.3826	0.7716	3.0880
4 0.75 - 1.00 km	11	3	1.7405	0.6675	-0.1874	0.2957	1.9279	0.7301	2.6407
5 1.00 - 1.25 km	14	5	2.1496	0.5490	-0.3658	0.3226	2.5154	0.6368	3.9502
6 1.25 - 1.50 km	17	6	2.1540	0.5015	-0.4633	0.3395	2.6173	0.6056	4.3217
7 1.50 - 1.75 km	21	6	1.8856	0.4812	-0.4482	0.3396	2.3338	0.5890	3.9626
8 1.75 - 2.00 km	25	6	1.6609	0.46743	-0.4318	0.3397	2.0927	0.5778	3.6218
9 2.00 - 2.25 km	29	6	1.4470	0.4566	-0.4120	0.3398	1.8590	0.5692	3.2660
10 2.25 - 2.50 km	268	15							

Map Class for NALTPYC2.MAP (Cumulative)	Area (km)	Deposits	W+	s (W+)	W-	s (W-)	C	s (C)	Stud (C)
1 0.00 - 0.25 km	1	0							
2 0.25 - 0.50 km	12	1	0.3894	1.0427	-0.0228	0.2749	0.4122	1.0783	.3823
3 0.50 - 0.75 km	29	2	0.2241	0.7328	-0.0304	0.2852	0.2545	.7863	.3237
4 0.75 - 1.00 km	50	2	-0.3503	0.7217	0.0667	0.2860	-0.4170	.7763	-.5372
5 1.00 - 1.25 km	72	5	0.2226	0.4634	-0.0951	0.3246	0.3178	.5658	.5616
6 1.25 - 1.50 km	96	5	-0.0783	0.4593	0.0416	0.3258	-0.1199	.5631	-.2129
7 1.50 - 1.75 km	120	7	0.0449	0.3895	-0.0377	0.3635	0.0826	.5327	.1550
8 1.75 - 2.00 km	143	8	-0.0040	0.3638	0.0046	0.3690	-0.0087	.5326	-.0163
9 2.00 - 2.25 km	165	12	0.2824	0.2998	-0.6851	0.5859	0.9674	.6581	1.4700
10 2.25 - 2.50 km	268	15							

Table A3 (cont'd)

Map Class for SLVLF25.MAP (Cumulative - IN REVERSE)	Area (km)	Deposits	W+	s (W+)	W-	s (W-)	C	s (C)	Stud (C)
1 HIGH	268	15	-0.0780	0.2848	0.7497	0.7500	-0.8278	0.8023	-1.0318
2	250	13	-0.0093	0.2854	0.0627	0.7290	-0.0720	0.7829	-0.0919
3	235	13	0.0611	0.2859	-0.3258	0.7220	0.3869	0.7766	0.4983
4	219	13	0.1285	0.2865	-0.5789	0.7187	0.7074	0.7737	0.9143
5	206	13	0.1105	0.2980	-0.3495	0.5893	0.4600	0.6603	0.6965
6	193	12	0.0822	0.3110	-0.1964	0.5120	0.2787	0.5991	0.4652
7	182	11	0.1465	0.3117	-0.3183	0.5106	0.4648	0.5982	0.7769
8	171	11	0.1046	0.3264	-0.1812	0.4581	0.2858	0.5625	0.5080
9	162	10	0.1586	0.3270	-0.2573	0.4573	0.4159	0.5622	0.7398
10	154	10	0.2074	0.3275	-0.3181	0.4567	0.5255	0.5620	0.9350
11	147	10	0.3596	0.3140	-0.6047	0.5080	0.9643	0.5972	1.6147
12	140	10	-0.0773	0.3882	0.0729	0.3646	-0.1502	0.5326	0.2821
13	135	7	-0.0351	0.3886	-0.0317	0.3642	-0.0668	0.5326	-0.1255
14	129	7	-0.5711	0.5083	0.3286	0.3136	-0.8997	0.5973	-1.5064
15	123	4	-0.5218	0.5087	0.2865	0.3131	-0.8084	0.5974	-1.3532
16	118	4	-0.4622	0.5092	0.2404	0.3126	-0.7026	0.5975	-1.1759
17	111	4	-0.6927	0.5858	0.2874	0.2998	-0.9801	0.6581	-1.4894
18	104	3	-0.6020	0.5866	0.2312	0.2992	-0.8332	0.6585	-1.2653
19	95	3	-0.4923	0.5877	0.1732	0.2986	-0.6654	0.6592	-1.0094
20	86	3	-0.3413	0.5893	0.1072	0.2980	-0.4485	0.6604	-0.6791
21	74	3	-0.5855	0.7186	0.1306	0.2865	-0.7161	0.7737	-0.9256
22	62	2	-1.0591	1.0102	0.1445	0.2762	-1.2036	1.0473	-1.1493
23	49	1							
24	35	0							
25 LOW	21	0							

Table A3 (cont'd)

Map Class for NPVLF25.MAP (Cumulative - IN REVERSE)	Area (km)	Deposits	W+	s (W+)	W-	s (W-)	C	s (C)	Stud (C)
1 HIGH	268	15							
2	268	15							
3	268	15							
4	268	15							
5	268	15							
6	267	15							
7	266	15							
8	264	15							
9	259	14	-0.0372	0.2748	0.7563	1.0611	-0.7935	1.0961	-0.7239
10	250	14	-0.0001	0.2750	0.0008	1.0291	-0.0009	1.0653	-0.0008
11	236	13	-0.0173	0.2853	0.1207	0.7303	-0.1381	0.7840	-0.1761
12	210	13	0.1066	0.2863	-0.5050	0.7196	0.6115	0.7745	0.7896
13	176	11	0.1165	0.3114	-0.2643	0.5112	0.3809	0.5986	0.6363
14	135	7	-0.0777	0.3882	0.0733	0.3646	-0.1509	0.5326	-0.2834
15	93	7	0.3112	0.3929	-0.2103	0.3619	0.5215	0.5342	0.9762
16	59	4	0.1966	0.5177	-0.0629	0.3098	0.2595	0.6033	0.4302
17	35	3	0.4366	0.6032	-0.0847	0.2964	0.5213	0 6721	0.7757
18	21	2	0.5529	0.7425	-0.0633	0.2849	0.6162	0.7953	0.7747
19	11	1	0.4670	1.0461	-0.0263	0.2748	0.4933	1.0816	0.4561
20	6	0							
21	3	0							
22	1	0							
23	0	0							
24	0	0							
25 LOW	0	0							

Table A3 (cont'd)

Map Class for MGNTCM25.MAP (Cumulative - IN REVERSE)	Area (km)	Deposits	W+	s (W+)	W-	s (W-)	C	s (C)	Stud (C)
1 HIGH	268	15							
2	268	15							
3	268	15							
4	268	15							
5	268	15							
6	266	15							
7	262	15							
8	256	15							
9	248	15							
10	237	13	-0.0185	0.2853	0.1291	0.7305	-0.1476	0.7842	-0.1882
11	222	13	0.0495	0.2858	-0.2729	0.7228	0.3223	0.7773	0.4147
12	207	13	0.1241	0.2865	-0.5644	0.7189	0.6884	0.7739	0.8896
13	195	12	0.1030	0.2980	-0.3304	0.5895	0.4334	0.6605	0.6562
14	183	12	0.1670	0.2986	-0.4794	0.5878	0.6463	0.6593	0.9803
15	172	12	0.2346	0.2993	-0.6079	0.5866	0.8426	0.6585	1.2795
16	158	12	0.3245	0.3002	-0.7460	0.5854	1.0705	0.6579	1.6272
17	141	11	0.3569	0.3140	-0.6018	0.5080	0.9587	0.5972	1.6053
18	122	11	0.5102	0.3160	-0.7415	0.5070	1.2517	0.5974	2.0953
19	104	9	0.4683	0.3487	-0.4453	0.4159	0.9136	0.5427	1.6833
20	86	7	0.3996	0.3943	-0.2533	0.3616	0.6529	0.5350	1.2206
21	67	4	0.0579	0.5154	-0.0203	0.3101	0.0782	0.6015	0.1300
22	45	3	0.1817	0.5975	-0.0407	0.2967	0.2224	0.6671	0.3334
23	27	1	-0.4501	1.0187	0.0415	0.2754	-0.4916	1.0552	-0.4658
24	9	0							
25 LOW	2	0							

Table A3 (cont'd)

Map Class for MGNVCM25.MAP (Cumulative - IN REVERSE)	Area (km)	Deposits	W+	s (W+)	W-	s (W-)	C	s (C)	Stud (C)
1 HIGH	268	15							
2	264	14	-0.0557	0.2746	1.6154	1.1389	-1.6710	1.1716	-1.4263
3	258	13	-0.1102	0.2846	1.4158	0.7885	-1.5260	0.8383	-1.8204
4	252	13	-0.0840	0.2848	0.8428	0.7541	-0.9268	0.8061	-1.1498
5	245	12	-0.1381	0.2960	0.8979	0.6178	-1.0361	0.6851	-1.5124
6	235	12	-0.0979	0.2963	0.5298	0.6056	-0.6277	0.6742	-0.9310
7	226	12	-0.0553	0.2966	0.2581	0.5990	-0.3134	0.6684	-0.4688
8	216	11	-0.1003	0.3095	0.3428	0.5204	-0.4431	0.6055	-0.7319
9	206	11	-0.0490	0.3099	0.1487	0.5169	-0.1977	0.6026	-0.3281
10	196	11	0.0021	0.3103	-0.0059	0.5145	0.0080	0.6008	0.0133
11	186	10	-0.0405	0.3251	0.0864	0.4614	-0.1269	0.5644	-0.2248
12	174	10	0.0263	0.3257	-0.0507	0.4596	0.0770	0.5633	0.1367
13	164	9	-0.0185	0.3429	-0.0285	0.4205	-0.0470	0.5425	-0.0866
14	153	9	0.0551	0.3436	-0.0773	0.4193	0.1324	0.5421	0.2442
15	139	9	0.1560	0.3447	-0.1961	0.4180	0.3521	0.5418	0.6498
16	123	9	0.2853	0.3462	-0.3165	0.4169	0.6017	0.5419	1.1103
17	110	9	0.4017	0.3477	-0.4029	0.4162	0.8046	0.5424	1.4835
18	99	9	0.5236	0.3496	-0.4771	0.4157	1.0007	0.5431	1.8425
19	86	8	0.5477	0.3712	-0.3934	0.3854	0.9411	0.5351	1.7588
20	72	7	0.5855	0.3975	-0.3277	0.3610	0.9132	0.5370	1.7007
21	60	7	0.7966	0.4020	-0.3924	0.3605	1.1890	0.5400	2.2019
22	47	5	0.6819	0.4726	-0.2209	0.3236	0.9028	0.5728	1.5761
23	34	3	0.4735	0.6041	-0.0901	0.2964	0.5636	0.6729	0.8376
24	21	1	-0.2033	1.0238	0.0162	0.2752	-0.2196	1.0602	-0.2071
25 LOW	10	1	0.5919	1.0520	-0.0314	0.2748	0.6234	1.0873	0.5733

Table A3 (cont'd)

Map Class for GRVNC25V.MAP (Cumulative - IN REVERSE)	Area (km)	Deposits	W+	s (W+)	W-	s (W-)	C	s (C)	Stud (C)
1 HIGH									
2	268	15							
3	265	15							
4	252	15							
5	243	14	0.0313	0.2753	-0.3590	1.0204	0.3904	1.0569	0.3693
6	234	14	0.0732	0.2756	-0.6872	1.0148	0.7604	1.0515	0.7231
7	223	14	0.1228	0.2760	-0.9624	1.0112	1.0853	1.0482	1.0353
8	211	13	0.1008	0.2863	-0.4845	0.7199	0.5854	0.7747	0.7556
9	198	13	0.1705	0.2869	-0.7026	0.7174	0.8731	0.7726	1.1301
10	183	12	0.1690	0.2986	-0.4836	0.5878	0.6527	0.6593	0.9900
11	168	12	0.2576	0.2995	-0.6462	0.5862	0.9038	0.6583	1.3730
12	153	11	0.2699	0.3130	-0.5010	0.5089	0.7709	0.5974	1.2904
13	138	11	0.3806	0.3143	-0.6262	0.5078	1.0068	0.5972	1.6858
14	124	11	0.4974	0.3158	-0.7313	0.5071	1.2287	0.5974	2.0569
15	111	10	0.5124	0.3315	-0.5889	0.4545	1.1013	0.5625	1.9578
16	95	10	0.6814	0.3342	-0.6872	0.4538	1.3686	0.5636	2.4284
17	80	8	0.6229	0.3725	-0.4252	0.3852	1.0481	0.5359	1.9560
18	67	4	0.0700	0.5156	-0.0243	0.3101	0.0943	0.6017	0.1568
19	51	4	0.3474	0.5205	-0.1014	0.3095	0.4488	0.6055	0.7411
20	40	2	-0.1256	0.7253	0.0208	0.2856	-0.1464	0.7795	-0.1878
21	27	2	0.2693	0.7339	-0.0357	0.2851	0.3050	0.7874	0.3874
22	18	2	0.7010	0.7480	-0.0747	0.2849	0.7757	0.8004	0.9691
23	13	2	1.0941	0.7670	-0.0974	0.2847	1.1915	0.8181	1.4564
24	7	1	0.9455	1.0734	-0.0428	0.2747	0.9883	1.1080	0.8920
25 LOW	1	1	2.8389	1.4178	-0.0651	0.2746	2.9040	1.4441	2.0109

Table A3 (cont'd)

APPENDIX B

Implementing integration methods in a GIS - Detailed procedures using SPANS GIS.

Note: This section is meant to be used as a guide to help understand the details of the methods used in this study. It should also allow the user to reproduce the results obtained in this study using the digital data found in Appendix C. This manual is a summary of the authors working notes taken over the course of the study and has had no quality control testing. The author sincerely apologizes for any mistakes, omissions or obscure explanations.

Appendix B - 1: Determining optimum thresholds for creating binary evidence maps from multiclass evidence maps.

A. Objective

Both the weights of evidence and logistic regression method use binary evidence maps. Although neither method is restricted to the use of binary maps, their use can be beneficial in a few ways. Most geologists think of evidence as either "anomalous" or "background" so thresholding of multiclass maps into a binary form is appealing. In logistic regression when the predictor variables are binary the coefficients are easier to interpret and in weights of evidence the number of layers of evidence that can be used in the unique conditions modelling becomes much less restrictive. In determining how to convert a multiclass map into a binary map the question to be answered is, "Which pattern represents an anomaly with respect to a volcanic hosted massive sulphide deposit?". The pattern could be the distance from a geological contact or a linear structure, a lithological unit, or contoured geochemical data. This module descibes the process that was used to convert the multiclass maps to a binary form.

B. Method

Determining the threshold that maximizes the spatial association between the resulting binary map pattern and the point pattern can be carried out using geological judgement or statistically. The method used in this case is statistical where the weights and contrast (see Chapter 5) are calculated for each pattern on the map. In practice a clear answer as to what the threshold is, cannot always be obtained by calculating the weights and some subjective evaluation becomes necessary.

Though there are 23 evidence maps the process is the same for them all except for a small variation when using categorical data. The procedure will be described in detail for two examples; 1) bedrock geology, representing categorical type data and 2) distance from tonalite sills, representing ordinal or higher scale data types. A table showing the results of this process carried out on all the multiclass evidence maps is in Appendix A.

Assuming the multiclass evidence maps have been made the procedure involves 5 steps.

1. Calculate the areas of the different classes on the multiclass evidence map. These may be successive buffer zones representing distance intervals surrounding a fault or geological contact, lithologic units, catchment basins classified according to element

concentrations, or contour intervals for geochemical data.

2. Determine the number of points (deposits) that are associated with each map class so that we now know the area of each class and how many deposits are in each map class.

3. Use this information to calculate the weights and contrast for the different map classes.

4. Inspect the weights and contrasts and determine which map class (pattern) that indicates the strongest spatial association with the deposit pattern. Ideally this is where the contrast and W+ are the greatest.

5. Reclassify the multiclass evidence map to a binary map.

C. Files

Input:

geolrc.map - generalized bedrock geology at 1:20000 for Chisel-Anderon area.
dykebufl.map - areas mapped as sybvolcanic sills with 10 buffers 0.25 km wide extending from contacts
vhms1.tba - VMS type deposit locations in the Chisel-Anderson study area

Output files:

fflowb.map - binary map of felsic flows only
dykebufb.map - binary map
geolrc.wts - output from wts.exe containing calculated weights and contrasts for geolrc.map
dykebufl.wts - output from wts.exe containing calculated weights and contrasts for dykebufl.map
geolrc.rep - file containing area calculations for the classes in geolrc.map
dykebufl.rep - file containing area calculations for the classes in dykebufl.map
vhms1g.tba - ascii file containing VMS type deposits and appended classes from GEOLRC.MAP

Executable file:

wts.exe - FORTRAN program for calculating weights and contrasts

D. Procedure (Categorical level maps)

1. ANALYZE/MAP/AREA

Using this SPANS command, calculate the areas of the 10 different lithologies in GEOLRC.MAP. The user should respond "yes" to the query for a basemap cut (make sure basecmlk.map is being used as a basemap). The results are ascii and can be output to a file name of the users choice. A file containing the area information for map GEOLRC.MAP exists with the name geolrc.rep.

2. MODEL/POINTS/APPEND

This SPANS command appends the map classes from GEOLRC.MAP to the deposit point table VHMS1.TBB (the binary table file). This provides a means for determining how many deposits are associated with each map class, which are geological units in this case.

3. TRANFORM/EXPORT/LIBRARY/TABLE

The binary point file with the appended map classes from GEOLRC.MAP must be exported as an ascii file. This command creates an ascii file of the users choice. A file VHMS1G.TBA exists with this information.

4. WTS

In an OS/2 window execute the program wts.exe. Input to the program will be the two files VMS1A.TBA and GEOLRC.REP. Ouptput will be in a file named after the area file with a .wts extension (eg. GEOLRC.WTS) The output is shown below.

Name of file: area1n.WTS
total no of points 15
area of unit cell 1.000000 sq. kms
total area 268.881000 unit cells 268.881000 sq. kms.
The following table is cumulative, Areas in unit cells

class		area	points	W+	s(W+)	W-	s(W-)	C	s(C)	Stud(C)
1	1	51	0							
2	2	70	7	.6200	.3982	-.3395	.3609	.9595	.5374	1.7855
3	3	140	10	.2582	.3281	-.3751	.4562	.6333	.5619	1.1269
4	4	148	10	.2022	.3275	-.3120	.4568	.5142	.5620	.9150
5	5	160	11	.2203	.3124	-.4342	.5095	.6545	.5976	1.0951
6	6	174	11	.1328	.3115	-.2941	.5109	.4269	.5984	.7134
7	7	195	11	.0064	.3103	-.0174	.5143	.0239	.6007	.0397
8	8	242	11	-.2180	.3086	1.1081	.5429	-1.3261	.6245	-2.1236
9	9	263	15							

This table is also cumulative, but in reverse order
Areas in unit cells

class	area	points	W+	s(W+)	W-	s(W-)	C	s(C)	Stud(C)
1 1	268	15							
2 2	217	15							
3 3	198	8	-.3395	.3609	.6200	.3982	-.9595	.5374	-1.7855
4 4	128	5	-.3751	.4562	.2582	.3281	-.6333	.5619	-1.1269
5 5	120	5	-.3120	.4568	.2022	.3275	-.5142	.5620	-.9150
6 6	108	4	-.4342	.5095	.2203	.3124	-.6545	.5976	-1.0951
7 7	94	4	-.2941	.5109	.1328	.3115	-.4269	.5984	-.7134
8 8	72	4	-.0174	.5143	.0064	.3103	-.0239	.6007	-.0397
9 9	26	4	1.1081	.5429	-.2180	.3086	1.3261	.6245	2.1236
10 10	5	0							

The following table is non-cumulative
Areas in unit cells

class	area	points	W+	s(W+)	W-	s(W-)	C	s(C)	Stud(C)
1 Post Amisk	51	0							
2 Felsic Flows	18	7	2.2995	.4764	-.5807	.3593	2.8802	.5968	4.8263
3 Mafic Flows	70	3	-.2774	.5901	.0833	.2978	-.3606	.6610	-.5456
4 Felsic Volcanics	7	0							
5 Mafic Volcanics	12	1	.4213	1.0441	-.0243	.2749	.4456	1.0796	.4127
6 Mixed Volcanics	13	0							
7 Other Sediments	21	0							
8 Tonalite sills	46	0							
9 Synvolcanic sills	21	4	1.3791	.5556	-.2406	.3084	1.6198	.6354	2.5490
10 Unmapped	5	0							

Because the geological map data is categorical the non-cumulative table (last table) is of interest.

The unit cell size was chosen as 1 km^2, so that in the second class (Felsic Flows) there are 7 deposits out of a possible 15 while the area of the Felsic Flows is 18 km^2 out of a total of 268.8 km^2 (ie. total area of study). This gives the highest contrast (2.8802) indicating that the proportion of 7/15 is much larger than 18/268.8 and that the Felsic flows have more deposits associated with them due to chance. Similarly the Synvolcanic sills (class 9) and Mafic Volcaniclastics (unit 5) also have a higher proportion of points associated with them than due to chance, though not as high as the Felsic Flows. In fact, it could be argued that the W+ for the Mafic Volcaniclastics is not significant since the Studentized C is much less that 1.5. The other two units that have deposits associated with them, the Mafic Flows and the Tonalite Sills have negative values for W+ indicating that a larger proportion of points would be expected due to chance than were observed.

5. MODEL/RECLASSIFICATION/MAKE MAP/INTERACTIVE

A binary map can now be constructed by reclassifying the multiclass map using the above command. By convention a class of 2 is assigned to a map where the pattern in present, a class of 1 to map where the pattern is absent and a class of 0 to a map where the pattern is missing. In this case the Felsic Flows (already class 2) would be left as is, and all the units would be reclassed to class 1.

Ordinal or higher level maps

Note that the steps are exactly the same for maps with data at a higher measurement scale. The difference is that weights are calculated for cumulative areas (see discussion in Step 4 below)

1. ANALYZE/MAP/AREA

Using this SPANS command, calculate the areas of the 10 different lithologies in DYKEBUF1.MAP. The user should respond "yes" to the query for a basemap cut (make sure basecmlk.map is being used as a basemap). The results are ascii and can be output to a file name of the users choice. A file containing the area information for map DYKEBUF1.MAP exists with the name dykebufl.rep.

2. MODEL/POINTS/APPEND

This SPANS command appends the map classes from DYKEBUF1.MAP to the deposit point table VMS1.TBB (the binary table file). This provides a means for determining how many deposits are associated with each map class, which are geological units in this case. Create a new point file VMS2A.TBB

3. TRANFORM/EXPORT/LIBRARY/TABLE

The binary point file, VMS2A.TBB with the appended map classes from DYKEBUF1.MAP must be exported as an ascii file. This command creates an ascii file of the users choice. A file VMS2A.TBA exists with this information.

4. WTS

In an OS/2 window execute the program wts.exe. Input to the program will be the two files VMS2A.TBA and DYKEBUF1.REP. Output will be in a file named after the area file with a .wts extension (eg. DYKEBUF1.WTS) The output is shown below.

Name of file: dykebufl.WTS
total no of points 15
area of unit cell 1.000000 sq. kms
total area 268.881000 unit cells
268.881000 sq. kms.
The following table is cumulative
Areas in unit cells

class		area	points	W+	s(W+)	W-	s(W-)	C	s(C)	Stud(C)
1	0.25 km	21	4	1.3791	.5556	-.2406	.3084	1.6198	.6354	2.5490
2	0.50 km	98	8	.3995	.3688	-.3195	.3860	.7189	.5339	1.3467
3	0.75 km	141	10	.2516	.3280	-.3680	.4563	.6196	.5619	1.1026
4	1.00 km	174	14	.3873	.2786	-1.7039	1.0054	2.0911	1.0433	2.0044
5	1.25 km	199	14							
6	1.50 km	216	15							
7	1.75 km	225	15							
8	2.00 km	230	15							
9	2.25 km	234	15							
10	2.50 km	268	15							
11	>2.5km	268	15							

This table is also cumulative, but in reverse order
Areas in unit cells

class		area	points	W+	s(W+)	W-	s(W-)	C	s(C)	Stud(C)
1	1	268	15							
2	2	247	11	-.2406	.3084	1.3791	.5556	-1.6198	.6354	-2.5490
3	3	170	7	-.3195	.3860	.3995	.3688	-.7189	.5339	-1.3467
4	4	127	5	-.3680	.4563	.2516	.3280	-.6196	.5619	-1.1026
5	5	94	1	-1.7039	1.0054	.3873	.2786	-2.0911	1.0433	-2.0044
6	6	69	1							
7	7	52	0							
8	8	43	0							
9	9	38	0							
10	10	34	0							

The following table is non-cumulative
Areas in unit cells

class		area	points	W+	s(W+)	W-	s(W-)	C	s(C)	Stud(C)
1	1	21	4	1.3791	.5556	-.2406	.3084	1.6198	.6354	2.5490
2	2	77	4	-.0857	.5134	.0331	.3106	-.1188	.6000	-.1981
3	3	42	2	-.1866	.7242	.0321	.2857	-.2187	.7785	-.2809
4	4	33	4	.8386	.5331	-.1877	.3088	1.0263	.6161	1.6659
5	5	24	1	-.3176	1.0213	0.271	0.2753	-0.3447	1.0577	-0.3259
6	6	16	0							
7	7	9	0							
8	8	5	0							
9	9	3	0							
10	10	34	0							
11	0	0	0							

This map has 10 distance buffers spaced at 0.25 km intervals from contacts of synvolcanic dykes (classes 1 - 10) and a class representing distances greater than 2.5 km (class 11). Weights and contrasts can be calculated for each distance corridor successively, and the variation in contrast with distance can be determined. However, when there are not very many points, there could be many classes that will have no points occurring in them or a very few. The results are a very noisy and unreliable curve, with poor estimates. Though this is not particularly clear in this example, the non-cumulative table (last table) is an example of such calculations. The alternative is to calculate weights for cumulative distances and to examine the variation of the weights and contrast at successive cumulative distance intervals. This has been done in the first table above.

Ideally, the distance at which the highest contrast occurs should indicate the optimum distance at which the map should be thresholded into a binary map, that is the distance where the strongest association between t' : map pattern and the deposits exists. However, here as in many cases, there is not a clear maximum. The contrast at .25 km and at 1.00 km from the contact of synvolcanic dykes are very similar for this map. Making a decision as to which distance to choose in not always clear cut. It is noted that the W+ value at 0.25 km is relatively large (1.379) so that being within this distance there is a large upweighting effect, however, for the same distance W- is relatively small (-0.2406) so that being beyond this distance has a very little downweighting effect. At 1 km the situation is in reverse but because the penalty for being off the pattern (beyond 1 km) is very large the resulting contrast is slightly larger that at 0.25 km.

In this case it can be argued that using the distance of .25 km as a threshold reduces the area to be explored to only 21 km^2 and only involves 4 of the 15 deposits which may be too restrictive for a first evaluation. Since the association is even a little stronger at 1.00 km and allows a larger area to be favourable and involves 14 of the 15 deposits, this is a more suitable threshold. It is noted if the priority was to keep the area to be explored to a minimum to keep within a budget, this would not be a good argument.

5. MODEL/RECLASSIFICATION/MAKE MAP/INTERACTIVE

A binary map can now be constructed by reclassifying the multiclass map using the above command. By convention a class of 2 is assigned to a map where the pattern is present, a class of 1 to map where the pattern is absent and a class of 0 to a map where the pattern is missing. In this case map classes 1 through 4 (distances 0.0 - 1.00 km) would be assigned a class of 2 and map classes 5 - 11 (distances > 1.00 km) would be assigned a class value of 1. There are no areas of missing data.

Appendix B - 2(a): Applying weights of evidence modelling using SPANS modelling language: Map modelling

A. Objective

Using binary evidence maps and their associated weights, a posterior probability map indicating mineral favourability or potential can be generated using the weights of evidence model implemented in the SPANS modelling language.

B. Method (map modelling)

The theory of the weights of evidence model is discussed fully with references in Chapter 4. For this application it is assumed that the evidence maps have been reclassified into binary form and the weights for the patterns on the maps been established (See Appendix B - 1). The maps are coded as 2 = pattern present, 1 = pattern not present and 0 = pattern missing or unknown. Because there is a limit of 15 maps that can be included in the modelling equation and there is a total of 23 evidence maps that must be integrated in this model this approach requires two iterations. In general the steps are as follows:

1. Write an equation in the SPANS modelling language that identifies 15 or less of the binary evidence maps, assigns the weights (already determined) to the map patterns and performs the calculations to combine the weights with the prior probability to produce a posterior probability. The prior probability for this iteration is defined as the number of unit cells with and occurrence divided by total area in unit cells.

2. Execute the equation and produce a posterior probability map. This "intermediate" posterior probability map becomes the "prior probability map" for the next iteration.

3. Write a second equation in the SPANS modelling language that identifies the remaining evidence maps, assigns the appropriate weights and performs the weights of evidence calculations. This second equation must also identify the output map from the first iteration as it is used as the source of the prior probability. The output from this iteration is the final probability map.

4. Reclassify the final probability map if desired and add annotations.

C. Files

To carry out this method in SPANS the following files are required and are included in Appendix C. The maps have been reclassified into binary form and the W+ and W-values have calculated for each. By definition the maps are coded as 2 = map pattern present, 1 = map pattern absent and 0 = map pattern unknown.

Input files: Binary evidence maps and previously calculated weights (see Appendix B-1)

Binary Map	W+	s(W+)	W-	s(W-)	Description of Evidence Map
NALTPPCB.MAP	3.3787	0.7393	-0.394	0.3225	Areas mapped as alteration pipes with 10 buffers 0.25 km wide surrounding areas
FFLOWB .MAP	2.2995	0.4764	-0.5807	0.3593	Areas mapped as felsic flows only
geol2c2b.map	1.1602	0.3024	-1.6979	0.7109	Areas mapped as felsic flows with 10 buffers 0.25 km wide extending from contacts
geol3c2b.map	0.5383	0.2910	-1.3098	0.7127	Areas mapped as mafic volcaniclastic rocks with 10 buffers 0.25 km wide extending from contacts
naltfecb.map	1.275	0.3319	-1.0925	0.5049	Areas mapped as fe alteration with 10 buffers 0.25 km wide extending from contacts
naltsicb.map	0.4897	0.2798	-1.8596	1.0046	Areas mapped as si alteration with 10 buffers 0.25 km wide extending from contacts
dykebufb.map	0.3873	0.2786	-1.7039	1.0054	Areas mapped as synvolcanic dykes with 10 buffers 0.25 km wide extending from contacts
krglnznb.map	1.7937	0.5821	-0.2648	0.3083	Kriged ln concentrations of zn in c horizon tills (<63 μm size fraction)
naltapcb.map	1.5525	0.4617	-0.4223	0.3397	Areas mapped as amphibole alteration with 10 buffers 0.25 km wide extending from contacts
lkpc1ncb.map	1.6182	0.5095	-0.3371	0.3228	Pricipal component 1 scores mapped on catchment basin map
naltepcb.map	1.447	0.4566	-0.412	0.3398	Areas mapped as epidote alteration with 10 buffers 0.25 km wide extending from contacts
krglncub.map	1.0052	0.3408	-0.8189	0.453	Kriged ln concentrations of cu in c horizon tills (<63 μm size fraction)
geol4c2b.map	0.6853	0.3051	-1.0934	0.583	Areas mapped as felsic volcaniclastics with 10 buffers 0.25 km wide extending from contacts
lkpc2ncb.map	1.4897	0.5617	-0.2482	0.3084	Principal component 2 scores mapped on catchment basin map
syndykb.map	1.3791	0.5556	-0.2406	0.3084	Areas mapped as synvolcanic dykes
krglnpbb.map	1.0250	0.6231	-0.1487	0.2959	Kriged ln concentrations of pb in c horizon tills (< 63 μm size fraction)
lkpc3ncb.map	0.9573	0.3798	-0.533	0.3845	Principal component 3 scores mapped on catchment basin map
grvnc25b.map	0.6814	0.3342	-0.6872	0.4538	Vertical gradient gravity map
npvlf25b.map	0.4670	1.0461	-0.0263	0.2748	Processed quadrature vlf data map
ngntcmb.map	0.5102	0.316	-0.7415	0.507	Total field magnetics
ngnvcmb.map	0.4017	0.3477	-0.4029	0.4162	Vertical gradient magnetics
slvlf25b.map	0.2567	0.3281	-0.3734	0.4562	Total field vlf
sillbufb.map	0.1598	0.327	-0.2588	0.4573	Areas mapped as subvolcanic sills with 10 buffers 0.50 km wide extending from contacts

Output files: woepart1.map intermediate map from first equation
woevms1.map (user may be choose another name if desired)

D. Procedure

1. Build an equation in the file "eqaution.inp" that combines less than 15 of the evidence maps (this is a limit imposed by the SPANS GIS). In this application we have combined

13 of the 23 binary evidence maps in an equation named "woepart1". This equation is listed below. Note that colons in column 1 indicate a comment. The equation name is preceded by an upper case E and a space.

```
E woepart1 Combine first 13 of 23 binary maps
:Weights of evidence for Snow Lake VMS  type deposits only
:To be used with map modelling, not table modelling
: Because there are 23 binary input maps and only 15 maps can be used
: in a single model, the modelling has been done in 2 phases.
: This is part combines the first 13  binary evidence maps.
:calculate the log of the prior odds from prior probability
:The value 0.0558 = no of unit cells with occurrences/total area in unit cells
: no of occurrences=15, area=268.881 km*km
  lprioro = log(0.0558/ (1.0 - 0.0558)) ;
:assign weight to fi, where i  is the 1,2..13 maps used for prediction
:The W+ and W- values were calculated previously and inserted here
: map name in quotes; map classes are 2 = present, 1 = absent, 0 = unknown
   f1 = {2.2995 if class('fflowb') == 2 , -0.5807 if class('fflowb') == 1 , 0};
   f2 = {1.3791 if class('syndykb') == 2 , -0.2406 if class('syndykb') == 1 , 0};
   f3 = {0.5383 if class('geol5c2b') == 2 , -1.3098 if class('geol5c2b') == 1 , 0};
   f4 = {0.6853 if class('geol4c2b') == 2 , -1.0934 if class('geol4c2b') == 1 , 0};
   f5 = {1.1602 if class('geol2c2b') == 2 , -1.6979 if class('geol2c2b') == 1 , 0};
   f6 = {0.1598 if class('sillbufb') == 2 , -0.2588 if class('sillbufb') == 1 , 0};
   f7 = {0.3873 if class('dykebufb') == 2 , -1.7039 if class('dykebufb') == 1 , 0};
   f8 = {1.6182 if class('lkpc1ncb') == 2 , -0.3371 if class('lkpc1ncb') == 1 , 0};
   f9 = {1.4897 if class('lkpc2ncb') == 2 , -0.2482 if class('lkpc2ncb') == 1 , 0};
  f10 = {0.9573 if class('lkpc3ncb') == 2 , -0.5330 if class('lkpc3ncb') == 1 , 0};
  f11 = {1.0052 if class('krglncub') == 2 , -0.4530 if class('krglncub') == 1 , 0};
  f12 = {1.0250 if class('krglnpbb') == 2 , -0.1487 if class('krglnpbb') == 1 , 0};
  f13 = {1.7937 if class('krglnznb') == 2 , -0.2648 if class('krglnznb') == 1 , 0};
:add the weights together
  total =  f1 + f2 + f3 + f4 + f5 + f6 + f7 + f8 + f9 + f10 + f11 + f12 + f13;
:add the log prior odds
  lposto = lprioro + total ;
:convert log odds to odds, but make 0 if all the weights are zero
  posto = {exp(lposto) if total <> 0 , 0};
:convert posterior odds to posterior probability
  postp = posto / (1. + posto);
:make map "woepart1"
  postp;
```

2. MODELLING/OVERLAY/MAP

This is the sequence of SPANS functions that are used to execute the equation listed above. A dialogue box queries for an equation name, at which point the equation name "woepart1" is entered, an output map name, woepart1 was used here but a new name could be given, and a classification, classification 110 should be used. The classification assigns a map class number of between 1 and 100 depending on the calculated probability. A probability of .01 or less is assigned a map class value of 100, probability .02 or less is assigned 99 and so on so that a probability of 1.00 will be assigned a map class value of 1.

3. A second equation must now be constructed in the equation.inp file to combine the remaining 10 binary evidence maps. It is listed below.

```
E  woepart2 Combine the last binary maps to woe1
:Weights of evidence for Snow Lake - VMS type deposits only
:
:use classification 134
:To be used with map modelling, not table modelling
:
: This combines the last of the binary input maps to the results of
: equation woepart1. The results of equation woepart1 will be the prior
: probability for this part.
 pp = class('woepart1');
 pp1 = table('zfactor',pp,'memfun');
:calculate the log of the prior odds from prior probability
  lprioro = log(pp1/ (1.0 - pp1)) ;
:assign weight to fi, where i is the 1,2..13 maps used for prediction
:The W+ and W- values were calculated previously and inserted here
:The name in quotes is the map name; map classes are 2 for present, 1 for absent, 0 for
unknown
  f1 = {0.4897 if class('naltsicb') == 2 , -1.8596 if class('naltsicb') == 1 , 0};
  f2 = {1.2750 if class('naltfecb') == 2 , -1.0925 if class('naltfecb') == 1 , 0};
  f3 = {3.3787 if class('naltppcb') == 2 , -0.3940 if class('naltppcb') == 1 , 0};
  f4 = {1.5525 if class('naltapcb') == 2 , -0.4223 if class('naltapcb') == 1 , 0};
  f5 = {1.4470 if class('naltepcb') == 2 , -0.4120 if class('naltepcb') == 1 , 0};
  f6 = {0.2567 if class('slvlf25b') == 2 , -0.3734 if class('slvlf25b') == 1 , 0};
  f7 = {1.2595 if class('npvlf25b') == 2 , -0.0633 if class('npvlf25b') == 1 , 0};
  f8 = {0.5102 if class('mgntcmb') == 2 , -0.7415 if class('mgntcmb') == 1 , 0};
  f9 = {0.4017 if class('mgnvcmb') == 2 , -0.4029 if class('mgnvcmb') == 1 , 0};
 f10 = {0.6814 if class('grvnc25b') == 2 , -0.6872 if class('grvnc25b') == 1 , 0};
```

```
:add the weights together
  total =  f1 + f2 + f3 + f4 + f5 + f6 + f7 + f8 + f9 + f10 ;
:add the log prior odds
  lposto = lprioro + total ;
:convert log odds to odds, but make 0 if all the weights are zero
  posto = {exp(lposto) if total <> 0 , 0};
:convert posterior odds to posterior probability
  postp = posto / (1. + posto);
:make map "woevms1"
:  postp;
```

Note that in this equation the prior probability (variable pp1) is not a constant as in the first equation but the posterior probability determined by the combination of the first 13 evidence maps and mapped. Because SPANS cannot read a value linked to a map class directly, a lookup table must also be constructed that links the map class number to the appropriate probability. This file has been built and is called zfactor.tba and is partially listed below.

```
ID zfactor
TITLE Probability for map woepart1
MAPID zfactor
WINDOW nc 5808 7704 14208 12080
TABTYPE 1
NRECORD 101
 1  3 9.000000 0   class Class
 2  0 10.200000 0  prob Probability for woepart1 map classes
DATA
0     0.001
1     0.99
2     0.98
3     0.97
4     0.96
5     0.95
      .

 98    0.02
 99    0.01
 100   0.001
```

4. MODELLING/OVERLAY/MAP

The same sequence of SPANS functions are carried out here as in step 2, however, in this pass the equation name is woepart2 and the output map name is vmswoe1. The classification is labelled 134

Note. If no classification existed, a classification can be constructed by choosing the quantiles option in the dialog box. When this option is chosen, instead of a map being created a classification is generated having the number of quantiles as specified by the user. This step can then be executed using that classification.

5. VISUALIZE/ENTITIES/MAP

The final probability map vmswoe1 may now be displayed.

6. VISUALIZE/ANNOTATIONS/LEGEND

Various annotations can be added to map to enhance it including a legend, north arrow, title, and labels.

Appendix B - 2(b): Applying weights of evidence modelling using SPANS modelling language: Table modelling

A. Objective

The objective is the same as described in the map modelling approach (Appendix B - 2a), that is we want to combine the binary evidence maps and their associated weights, to produce a posterior probability map indicating mineral favourability or potential using the weights of evidence model and SPANS modelling language. In addition we wish to generate a table that has the final probabilities so that we can have more flexibility in analyzing them (doing an x-y plot of area vs probability or calculating expected probability, for example) and to reduce the number of computations required to be done by the GIS.

B. Method

This alternative method can be done in SPANS using what is known as unique conditions modelling combined with table modelling. The method used in table modelling is very similar to the map modelling method except for the extra step of building a unique conditions overlay table and map and slightly different syntax in the equation. Again there is a limit of overlaying 15 maps in SPANS so there has to be two iterations. The basic steps are as follows:

1. Calculate a unique conditions overlay, which produces a unique conditions map and an associated unique conditions table, for 15 or less of the binary evidence maps.

2. Write an equation in the SPANS table modelling language (instead of map modelling syntax) that reads the binary map classes from the unique conditions (instead of from the map directly), assigns the weights (already determined) based on the map pattern class recorded in the unique conditions table and performs the calculations to combine the weights with the prior probability to produce a posterior probability. The prior probability for this iteration is defined as the number of unit cells with an occurrence divided by total area in unit cells.

3. Execute the equation and produce a new table which has the results (posterior probability) of the model appended as a new field. This "intermediate" posterior probability becomes the "prior probability map" for the next iteration.

4. Calculate a second unique conditions overlay, which produces another unique conditions map and associated unique conditions table, using the remaining binary

evidence maps and the unique conditions map created in step 1.

5. Write a second equation in the SPANS table modelling language that identifies the remaining evidence maps, assigns the appropriate weights based on the map classes it finds in the second unique conditions file and performs the weights of evidence calculations. This second equation uses the table produced from the first equation to look up the prior probability.

6. Execute the equation and produce a new table which has the results of the model appended as a new field. This is the final posterior probability.

7. Reclassify the second unique conditions map based on the field containing the posterior probabilities in the table produced by the second equation to produce the final probability map and add annotations.

C. Files

Input files:

binary evidence maps as listed in Appendix B-2(a)

Output files:

woe1uniq.tba/tbb	unique conditions table resulting from unique conditions overlay
of	13 binary evidence maps
woe1uniq.map	unique conditions map linked to woe1uniq.tba/tbb
woetab1r.tba/tbb	table containing intermediate posterior probabilities resulting from first modelling equation
woe2uniq.tba/tbb	unique conditions table resulting from unique conditions overlay
of	remaining 10 binary evidence maps and woe1uniq.map
woetab2r.tba/tbb	table containing final probabilities and linked to map woe2uniq.map
woetab.map	final probability map

D. Procedure

1. MODELLING/OVERLAY/UNIQUE CONDITIONS

A dialogue box prompts for a list of maps to be used to create a unique overlay after executing these SPANS functions. For this application 13 of the binary evidence maps were selected. A second prompt requests a name for the output files. The results are a unique conditions map (woeluniq.map) and a corresponding unique conditions table (woeluniq.tba/tbb). The unique conditions table is partly listed below.

The rows in the table are the unique conditions. They correspond to unique combinations of the input maps (listed as fields in the table header). The unique conditions map, woeluniq, has 1011 unique conditions and each class is linked to the unique conditions table by a record number in field 2. The area of each unique conditions class is listed in field 1 and can be seen to be ordered in decreasing size. Note that each unique conditions class may have 1 to many polygons. This information is not recorded in the unique conditions table but may be obtained by creating an entities map using the SPANS function /TRANSFORM/DATA TYPES/MAP TO/ VECTORS.

```
ID woeluniq
TITLE woeluniq
MAPID woeluniq
WINDOW nc 0 0 0 0
TABTYPE 5
FTYPE free
KEYFIELD 2
KEYBASE 0
NRECORD 1011
 1  0 15.400000 0    area area
 2  4 7.000000 0 woeluniq woeluniq
 3  4 7.000000 0 dykebufb dykebufb
 4  4 7.000000 0   fflowb fflowb
 5  4 7.000000 0 geol2c2b geol2c2b
 6  4 7.000000 0 geol4c2b geol4c2b
 7  4 7.000000 0 geol5c2b geol5c2b
 8  4 7.000000 0 krglncub krglncub
 9  4 7.000000 0 krglnpbb krglnpbb
10  4 7.000000 0 krglnznb krglnznb
11  4 7.000000 0 lkpc1ncb lkpc1ncb
12  4 7.000000 0 lkpc2ncb lkpc2ncb
13  4 7.000000 0 lkpc3ncb lkpc3ncb
14  4 7.000000 0 sillbufb sillbufb
15  4 7.000000 0  syndykb syndykb
```

```
DATA
   21.2264    1 1 1  1 1 1 0 0 0 1 1 1 1 1
   11.6159    2 1 1  1 1 1 0 0 0 1 1 1 2 1
   11.4862    3 1 1  1 1 1 0 0 0 0 0 0 1 1
    8.7169    4 1 1  1 1 1 0 0 0 0 0 0 2 1
    8.4576    5 2 1  1 2 2 0 0 0 1 1 1 1 1
    7.2400    6 2 1  1 2 2 0 0 0 1 1 1 2 1
    7.2099    7 1 1  1 1 1 1 1 1 1 1 1 1 1
    6.5535    8 2 1  2 2 2 0 0 0 1 1 1 1 1

     .      . . . . . . . . . . . . . . .
     .      . . . . . . . . . . . . . . .

    0.0001   1004 2 1  1 1 2 1 0 1 1 0 0 2 1
    0.0001   1005 1 1  2 1 2 2 0 1 1 1 1 2 1
    0.0001   1006 1 1  1 2 1 1 0 2 0 0 0 1 1
    0.0001   1007 1 1  1 2 1 1 0 1 1 2 1 2 1
    0.0001   1008 2 1  1 2 2 2 0 0 1 2 1 2 2
    0.0001   1009 1 1  1 2 2 1 0 1 2 1 1 2 1
    0.0001   1010 2 2  2 2 2 1 2 1 0 0 0 2 1
    0.0001   1011 2 1  2 1 1 1 0 1 2 1 1 2 1
```

2. Build and equation in the file equation.inp that reads the unique conditions table (woe1uniq), extracts the class values for each map, assigns the appropriate weights and calculates the posterior probability using the weights of evidence method. The eqution is listed below.

```
E woetab1 Combine first 13 of 23 binary maps
:Weights of evidence for Snow Lake VMS
:   VMS type deposits only
:
:To be used with table modelling, not map modelling
:  PRIMARY TABLE = woe1uniq
:   Classification = 110
: Because there are 23 binary input maps and only 15 maps can be used
: in a single model, the modelling has been done in 2 phases.
: This is part combines the first 13  binary evidence maps.
:
:calculate the log of the prior odds from prior probability
```

```
:The value 0.0558 = no of unit cells with occurrences/total area in unit cells
: no of occurrences=15, area=268.881 km*km
  lprioro = log(0.0558/ (1.0 - 0.0558)) ;

:assign weight to fi, where i is the 1,2..13 maps used for prediction
:The W+ and W- values were calculated previously and inserted here
:The name in quotes is the map name; map classes are 2 for present, 1 for absent, 0 for
unknown
  f1 = {2.2995 if field('fflowb') == 2 , -0.5807 if field('fflowb') == 1 , 0};
  f2 = {1.3791 if field('syndykb') == 2 , -0.2406 if field('syndykb') == 1 , 0};
  f3 = {0.5383 if field('geol5c2b') == 2 , -1.3098 if field('geol5c2b') == 1 , 0};
  f4 = {0.6853 if field('geol4c2b') == 2 , -1.0934 if field('geol4c2b') == 1 , 0};
  f5 = {1.1602 if field('geol2c2b') == 2 , -1.6979 if field('geol2c2b') == 1 , 0};
  f6 = {0.1598 if field('sillbufb') == 2 , -0.2588 if field('sillbufb') == 1 , 0};
  f7 = {0.3873 if field('dykebufb') == 2 , -1.7039 if field('dykebufb') == 1 , 0};
  f8 = {1.6182 if field('lkpc1ncb') == 2 , -0.3371 if field('lkpc1ncb') == 1 , 0};
  f9 = {1.4897 if field('lkpc2ncb') == 2 , -0.2482 if field('lkpc2ncb') == 1 , 0};
  f10 = {0.9573 if field('lkpc3ncb') == 2 , -0.5330 if field('lkpc3ncb') == 1 , 0};
  f11 = {1.0052 if field('krglncub') == 2 , -0.4530 if field('krglncub') == 1 , 0};
  f12 = {1.0250 if field('krglnpbb') == 2 , -0.1487 if field('krglnpbb') == 1 , 0};
  f13 = {1.7937 if field('krglnznb') == 2 , -0.2648 if field('krglnznb') == 1 , 0};
:add the weights together
  total = f1 + f2 + f3 + f4 + f5 + f6 + f7 + f8 + f9 + f10 + f11 + f12 + f13;
:add the log prior odds
  lposto = lprioro + total ;
:convert log odds to odds, but make 0 if all the weights are zero
  posto = {exp(lposto) if total <> 0 , 0};
:convert posterior odds to posterior probability
  postp = posto / (1. + posto);
:write to table (woetab1r) new field with postp
  postp;
  result(postp);
```

Note that this equation is exactly the same as the equation written for the map modelling method with two exceptions. 1) instead of specifying a map class('   ') the table field name is specified. Since the field name is the same as the map name the only modification that is required it to change class('   ') to field('   '). 2) The statement 'result(postp)' is added at the end. This causes a new field showing the posterior probability to be added to the new table.

3. MODELLING/TABLE

This SPANS command opens a dialogue box that requests the name of an equation, a primary table and a new table. The equation name is WOETAB1 (see equation above), the primary table is WOE1UNIQ and the new table name is the users choice but one exists named WOETAB1R. The operations coded in the equation are now carried out using the information in the WOE1UNIQ table and the results (posterior probability) are written to table WOETAB1R along with all the information that was originally in WOE1UNIQ.

4. Build a second equation in the file equation.inp that reads the unique conditions table (WOE2UNIQ), extracts the class values for each map, assigns the appropriate weights and calculates the posterior probability using the weights of evidence method. The equation is listed below. Note that the prior probability is read from table W0ETAB1R which was calculated in step3.

```
E  woetab2 Final postp woe table modelling
:Weights of evidence for Snow Lake VMS
:    VMS type deposits only
:
:To be used with table modelling
: PRIMARY TABLE = woe2uniq
:
: This combines the last of the binary input maps to the results of
: equation woepart1. It calculates the post P and expected no of deps.
:
:
:
 pp  = field('woe1uniq');
 pp1 = table('woetab1r',pp,'postp');
:calculate the log of the prior odds from prior probability
  lprioro = log(pp1/ (1.0 - pp1)) ;

:assign weight to fi, where i  is the 1,2..13 maps used for prediction
:The W+ and W- values were calculated previously and inserted here
:The name in quotes is the map name; map classes are 2 for present, 1 for absent, 0 for
unknown
  f1 = {0.4897 if field('naltsicb') == 2 , -1.8596 if field('naltsicb') == 1 , 0};
  f2 = {1.2750 if field('naltfecb') == 2 , -1.0925 if field('naltfecb') == 1 , 0};
  f3 = {3.3787 if field('naltppcb') == 2 , -0.3940 if field('naltppcb') == 1 , 0};
```

```
  f4 = {1.5525 if field('naltapcb') == 2 , -0.4223 if field('naltapcb') == 1 , 0};
  f5 = {1.4470 if field('naltepcb') == 2 , -0.4120 if field('naltepcb') == 1 , 0};
  f6 = {0.2567 if field('slvlf25b') == 2 , -0.3734 if field('slvlf25b') == 1 , 0};
  f7 = {0.4670 if field('npvlf25b') == 2 , -0.0263 if field('npvlf25b') == 1 , 0};
  f8 = {0.5102 if field('mgntcmb') == 2 , -0.6018 if field('mgntcmb') == 1 , 0};
  f9 = {0.4017 if field('mgnvcmb') == 2 , -0.4029 if field('mgnvcmb') == 1 , 0};
 f10 = {0.6814 if field('grvnc25b') == 2 , -0.6872 if field('grvnc25b') == 1 , 0};
areax = field('area');
:add the weights together
  total =  f1 + f2 + f3 + f4 + f5 + f6 + f7 + f8 + f9 + f10 ;
:add the log prior odds
  lposto = lprioro + total ;
:convert log odds to odds, but make 0 if all the weights are zero
  posto = {exp(lposto) if total <> 0 , 0};
:convert posterior odds to posterior probability
  postp = posto / (1. + posto);
:make map
:  postp;
: calculate expected no. of deposits
expd = expd + (postp * areax);
:output table = woetab2r
result(postp,expd);
```

Inspection of this equation shows that the posterior probability is calculated and a second variable (expd) assigned the value of the accumulated product of the posterior probability times the class area. The final value in this field will contain the total number of predicted deposits, which should equal the total observed number of deposits. Where the predicted number is greatly in excess of the observed, some violation of the conditional independence assumption occurs.

5. MODEL/RECLASSIFICATION/BUILD MAP/BY TABLE

The final step is build a map showing the spatial distribution of the posterior probabilities contained in table WOETAB2R. This table is linked to the unique conditions map WOE2UNIQ.

The SPANS command above opens a dialogue box. The following entries should be made; WOE2UNIQ for map, WOETAB2R for table, 2 for map class field (field name is WOE2UNIQ), POSTP for value field, and 2 for classification.

The resulting map has some very slight differences mainly due to the precision of the data. The probabilities recorded in table WOETAB2R are recorded to four significant digits, while the lookup table ZFACTOR in the map modelling method contains break point to two significant digits.

Appendix B - 2(c): Applying weights of evidence modelling using unique condition files and external software PREDICTR

A. Objective

In the map modelling and table modelling applications of weights of evidence described above, it was required to write an equation in the SPANS modelling language "hard wiring" in previously calculated weights. The objective of this method is to utilize an external program that uses information in a unique conditions table exported from SPANS that allows weights, contrasts, posterior probabilities, uncertainty due to weights, uncertainty due to missing data and total uncertainty all in one pass. The results can be written to a new table, imported into SPANS and mapped back to the unique conditions map to show their spatial distribution.
It is noted that in order to establish optimal thresholds when making the binary evidence maps used in generating the unique conditions overlay it is useful to calculate the weights before applying this method.

B. Method

Assuming that the binary evidence maps exist, this method involves three basic steps.

1. A unique conditions table and map is generated that contains all the unique overlap conditions created by overlaying the 23 binary evidence maps. It is noted that for applications where there are more than 15 maps involved (a limit imposed by SPANS), such as this one, making the unique conditions file requires some extra processing as described in the procedure section below. A second table is generated that contains the mineral deposit locations and the class of the unique conditions map in which the deposit occurs.

2. The two tables generated in step 1 are exported as ascii files and used as input for the external program PREDICTR. This program calculates weights, posterior probabilities, and uncertainties then creates a new table containing the results.

3. The final step is to import the new table into SPANS and reclassify the unique conditions map with any or all of the new variables.

C. Files

Input files:
binary evidence maps as listed in Appendix B-2(a)

woe1uniq.tba	unique conditions table resulting from combining 13 binary evidence maps
woe1uniq.map	unique conditions map linked to table woe1uniq.tba
woe2uniq.tba	unique conditions table resulting from combining the remaining 10 binary evidence maps and woe1uniq.map
woe2uniq.map	unique conditions map linked to table woe2uniq.tba
woe2.tba	unique conditions table containing information from all 23 binary evidence maps resulting from "joining" woe1uniq.tba and woe2uniq.tba also linked to woe2uniq.map
woe2pnt.tba	VMS deposit locations with map classes from woe2uniq.map appended

Output files:

wts.dat	output file from PREDICTR containing weights for each map
weights.tba	output file from PREDICTR containing posterior probability and other calcualted variables

Executable file:

PREDICTR.EXE	FORTRAN program compiled under OS/2 operating system

D. Procedure

Step 1 - Creating a unique conditions table and map for all 23 binary evidence maps

1. MODELLING/OVERLAY/UNIQUE CONDITIONS

These SPANS commands open a dialogue box prompting the user to select maps to be used in the overlay; choose 15 or less of the binary evidence maps. For an output map name the user can choose a new one or use the existing WOE1UNIQ which contains information for 13 of the binary evidence maps.

2. MODELLING/OVERLAY/UNIQUE CONDITIONS

Same as step one except choose the remaining binary evidence maps and also include the unique conditions map generated in 1, this is very important as it is used as the key field (see Step 3). A new unique conditions table may be created or the existing unique conditions map and table named WOE2UNIQ may be used.

3. Combine the unique conditions tables WOE1UNIQ and WOE2UNIQ

This operation is done outside of SPANS using a relational database manager (RDMS). The operation to do this is commonly referred to as a "union" operation in RDMS. In practice the field in table WOE2UNIQ containing the map class of WOE1UNIQ is replaced by the corresponding set of unique overlap conditions defined in table WOE1UNIQ. The resulting file created here (created using the RDMS R- Base) is called WOE2. This is one of the files that will be used as input into the external program PREDICTR.

4. MODELLING/POINTS/APPEND CLASS

Append the unique conditions class from the unique conditions map WOE2UNIQ to the point table VMSDEP which contains only the locations of the known VMS deposits. This is necessary because the appended field indicates which unique conditions classes contain occurrence points. An existing file created using this command is CIPNTS.TBA

Step 2 - Using external FORTRAN program

5. Exit to an OS/2 window and run PREDICTR

At the OS/2 prompt, type PREDICTR. A series of inputs will be required as prompted by the program. The number of binary evidence maps is 23, the weights of evidence option is 4, and the unique conditions field the field labelled WOE2UNIQ.

Two output files are generated by the program, WTS.DAT and WEIGHTS.TBA. The WTS.DAT file contains summary data related to the evidence maps including the W+ and W- for each pattern. Below is a partial listing of the output file WEIGHTS.TBA. Note that the actual file has 6994 unique conditions and is in Appendix C as a digital file.

```
ID demp
TITLE Weights of Evidence
MAPID woe2
WINDOW ?
TABTYPE 5
FTYPE free
KEYFIELD 2
NRECORD 6994
1  0  15.400000 0     area area
2  4  7.000000 0     uniq unique conditions
3  4  7.000000 0     depos number of deposits
```

4 0 10.400000 0 postp posterior probability
5 0 10.400000 0 tpost Studentized post prob
6 0 10.400000 0 sdevw Uncertainty (weights)
7 0 10.400000 0 sdevm Uncertainty (missing)
8 0 10.400000 0 stot Total uncertainty
DATA

5.2812	1	0	.0000	.3905	.0000	.0000	.0000
4.6094	2	0	.0000	.3858	.0000	.0000	.0000
4.1765	3	0	.0000	.4177	.0000	.0000	.0000
3.7526	4	0	.0000	.4141	.0000	.0000	.0000
2.5345	5	0	.0000	.3829	.0000	.0000	.0000
2.0440	6	0	.0001	.5211	.0002	.0001	.0002
2.0024	7	0	.0000	.3926	.0000	.0000	.0000
.	.	.	.	.	.	.	.
.	.	.	.	.	.	.	.
.0001	6991	0	.0013	.4981	.0024	.0010	.0026
.0001	6992	0	.0041	.4696	.0083	.0029	.0088
.0001	6993	0	.2433	.6849	.3358	.1158	.3552
.0001	6994	0	.4579	.9927	.4467	.1148	.4612

Step 3 - Reclassifying unique conditions map

6. TRANSFORM/IMPORT/LIBRARY/TABLE

The file WEIGHTS.TBA must be imported into the internal SPANS data base so it can be used for further modelling applications.

7. ANALYZE/TABLE/HISTOGRAM

This command allows the user to examine the distribution of the posterior probability. The table name is WEIGHTS, field 1 (area) should be chosen for the x-axis and field 4 (posterior probability) should be chosen for the y-axis. Select the cumulative option for the x-axis and execute. The resulting plot is useful for determining break points for the classification. However, a classification was already established in the map modelling method (classification 2).

8. MODELLING/RECLASSIFICATION/BUILD MAP /FROM TABLE

Using the WEIGHTS table file, reclassify the unique conditions map WOE2UNIQ using any of the fields representing the posterior probability (field 4), studentized posterior probability (field 5), uncertainty due to weights (field 6), uncertainty due to missing data (field 7) or total uncertainty (field 8).

Appendix B - 3: Testing for Conditional Independence for weights of evidence modelling

A. Objective

When the weights of evidence model is used, conditional independence (CI) is assumed to exist. It is possible to check CI with statistical tests to show the magnitude of the problem, and identify the maps that are causing the difficulty. Based on the results, maps causing the problem may be rejected from the modelling or modified to reduce the problem.

B. Method

In practice there are two tests to determine whether the CI assumption is being violated; a pairwise test and an overall test.

The pairwise test should be run on all possible pairs of maps that are to be combined before the model is executed. In this method a chi-square test is used to determine if two binary patterns are conditionally independent with respect to a set of deposit points. If conditional independence exists the observed number of deposits in an overlap region where a pattern from two maps exist should be equal to the predicted number of deposits. The calculations for this test are explained in detail in chapter 5.

The overall test is performed after the final posterior probabilities have been calculated. If the total predicted number of deposits is much larger than the total observed number, it suggests that CI is being violated. This is not a formal test and in practice it appears that the predicted number of deposits is always somewhat larger that the number of observed deposits. A rule of thumb is that if the predicted number is larger than the observed number by greater that 10 percent it is a strong indicator that CI has been violated. Again the equations used in this test are discussed in chapter 4.

C. Files

Input:

woe2.tba	unique conditions table containing unique overlap conditions for all 23 binary evidence maps
woe2pnt.tba	point file containing locations of VMS deposits and associated map class of map WOE2UNIQ

Output:

user defined	data from program including chi-square pairwise test results a file name citest.dat already has been created

Executable file:

cippl.exe	program to calculate pairwise chi-square test on all map pairs (binary)

D. Procedure

1. In an OS/2 window type CIPPL to start the program. The number of binary maps is 23, the name of the unique conditions file is WOE2, the name to the point file containing the VMS deposit locations with the map classes of the unique conditions map appended to it is CIPNTS, the query to combine two maps should get a NO response,and the output file is the users choice. An output file named CIWOE2.DAT already exists.

The output file contains a summary table of the χ^2 values for testing conditional independence between all pairs of 23 binary evidence maps.

Note. When two maps are identified as causing a violation of CI a possible option for correcting the situation is to combine the dependent patterns together with Boolean operators. This program gives the option of using an AND operator to combine patterns leading to a single more restrictive showing only areas where both patterns are present or an OR operator leading to a single map showing areas where either pattern is present. In this study no maps were identified as violating the assumption of CI, however, if the user wished to combine two maps they would choose a YES response to the query if they wanted to combine two maps. They could then identify the maps and choose either an AND or OR operation.

Appendix B - 4: Applying area weighted logistic regression to predict VHMS favourability

A. Objective

The main objective is to use area weighted logistic regression to estimate the VMS potential for the Snow Lake area. Both weights of evidence modelling and weighted logistic regression are special cases of the so-called loglinear model and makes for an interesting comparison. All loglinear models result in weights (W+ or coefficients), posterior probabilities and corresponding estimate of uncertainty. These results were compared between the two methods with respect to different unit cell sizes. Further, since the logisitic model does not assume conditional independence, this method can be used to evaluate the effects of conditional independence that was observed in the weights of evidence method.

B. Method

Once the evidence maps are created the calculation of the scores and coefficients are done outside of SPANS as the coefficients in logistic regression are computed by means of a mathematically complicated iterative process and not suitable for the SPANS modelling language. This method requires three steps similar to weights of evidence model calculated using a unique conditions table described in Appendix B - 2(c).

1. A unique conditions table and map is generated that contains all the unique overlap conditions created by overlaying the 23 binary evidence maps. It is noted that for applications where there are more than 15 maps involved (a limit imposed by SPANS), such as this one, making the unique conditions file requires some extra processing as described in the procedure section below. A second table is generated that contains the mineral deposit locations and the class of the unique condition map in which the deposit occurs.

2. The two tables generated in step 1 are exported as ascii files and used as input for the external program PREDICTR. The area weighted logistic regression option is chosen.

3. Tables containing coefficients, variance-covariance matrix, expected and observed frequencies of deposits and posterior probabilities are output. The table containing the probabilities is imported into SPANS and used to reclassify the unique conditions map.

C. Files

Input files:

woe2.tba	unique conditions table containing information from all 23 binary evidence maps resulting from "joining" woe1uniq.tba and woe2uniq.tba also linked to woe2uniq.map
cipnts.tba	VMS deposit locations with map classes from woe2uniq.map appended

Output files:

logpol.inp	an intermediate file that contains input parameters including, level of convergence for scores to stop , maximum number of Iterations, number of explanatory variables etc. (see Agterberg, 1989 for complete details)
lucrep	data file for the logistic regression algorithm, it is a modified version of WOE2.TBA, missing data has been changed to not present.
lopol.out	output file showing number of iterations for scores to reach the specified level of convergence
logco.dat	calculated coefficients and variance-covariance matrix
logpol.tba	table containing posterior probabilities to be imported back into SPANS to reclassify unique conditions map
cumfre.tba	comparison of observed and predicted frequencies of deposits.

Executable file:

PREDICTR	FORTRAN program

D. Procedure

Step 1 - Creating a unique conditions table and map for all 23 binary evidence maps

1. MODELLING/OVERLAY/UNIQUE CONDITIONS

These SPANS commands open a dialogue box prompting the user to select maps to be used in the overlay; choose 15 or less of the binary evidence maps. For an output map name the user can choose a new one or use the existing WOE1UNIQ which contains information for 13 of the binary evidence maps.

2. MODELLING/OVERLAY/UNIQUE CONDITIONS

Same as step one except choose the remaining binary evidence maps and also include the unique conditions map generated in 1, this is very important as it is used as the key field (see Step 3). A new unique conditions table may be created or the existing unique conditions map and table named WOE2UNIQ may be used.

3. Combine the unique conditions tables WOE1UNIQ and WOE2UNIQ

This operation is done outside of SPANS using a relational database manager (RDMS). The operation to do this is commonly referred to as a "union" operation in RDMS. In practice the field in table WOE2UNIQ containing the map class of WOE1UNIQ is replaced by the corresponding set of unique overlap conditions defined in table WOE1UNIQ. The resulting file created here (created using the RDMS R- Base) is called WOE2. This is one of the files that will be used as input into the external program PREDICTR.

4. MODELLING/POINTS/APPEND CLASS

Append the unique conditions class from the unique conditions map WOE2UNIQ to the point table VMSDEP which contains only the locations of the known VMS deposits. This is necessary because the appended field indicates which unique conditions classes contain occurrence points. An existing file created using this command is CIPNTS.TBA

Step 2 - Using external FORTRAN program

5. Exit to an OS/2 window and run PREDICTR

At the OS/2 prompt, type PREDICTR. A series of inputs will be required as prompted by the program. The number of binary evidence maps is 23, the area weighted logistic regression option is 5, and the unique conditions field the field labelled WOE2UNIQ.

The user is prompted during the program to enter a unit cell size. A recommended cell size is suggested which is approximately 40 times smaller than the ratio of total area to number of deposits (a value of 0.55). This may be used for the first iteration.

Four output files are generated by the program, LOGPOL.OUT, LOGCO.DAT, LOGPOL.TBA and CUMFRE.TBA.

LOGPOL.OUT contains a summary of the input parameters such as the convergence level and number of independent variables (evidence maps). It also lists the coefficients for all the iterations before the scores reach the convergence level.

LOGCO.DAT contains the coefficients, their standard deviations and the variance-covariance matrix for the final solution. (The coefficients for this study are listed in Table 5.2)

LOGPOL.TBA is table linked to the unique conditions map WOE2UNIQ. It contains values calculated in PREDICTR including the posterior probability, the student t on the posterior probability, the standard deviation of the posterior probability the chi-square coefficient and the deviance coefficient.
NOTE: The chi-square coefficient and the deviance coefficient are measures related to the goodness of fit of the model. However, they are only useful when the observations are independent. In this case the observations are not independent and so they are not used in this study.

CUMFRE.TBA is a table comparing the expected and observed frequencies of deposits for each unique conditions class. This information can be used with the Kolmogorov-Smirnov test to determine if the model provides a good fit.

Step 3 - Reclassifying unique conditions map

6. TRANSFORM/IMPORT/LIBRARY/TABLE

The file LOGPOL.TBA must be imported into the internal SPANS data base so it can be used to reclassify the unique conditions map.

7. MODELLING/RECLASSIFICATION/BUILD MAP /FROM TABLE

Using the LOGPOL table file, reclassify the unique conditions map WOE2UNIQ using any of the fields representing the posterior probability (field 4), studentized posterior probability (field 5), or the standard deviation of the posterior probability (field 6).

9. EDIT/LIBRARY/TABLE min max total

Use this command to determine the maximum value in the last column (difference between cumulative calculated number of deposits and cumulative observed number of deposits) in table CUMFRE. This value can be used in the Kolmogorov-Smirnov test to determine the goodness of fit of the logistic regression model

Appendix B - 5: Applying fuzzy logic method to predict VHMS favourability

A. Objective

The goal, as with the weights of evidence and logistic regression approach, is to combine several layers of spatial evidence to predict mineral potential. However, the fuzzy logic approach is a knowledge driven method and can be useful when there is an absence of sufficient information about known mineral deposits. This approach is appealing because it is straightforward to understand and implement. It can be used with data from any measurement scale and allows the user to mimic the thought processes of the expert when combining the data.

B. Method

The theory of fuzzy sets is described in some detail with references in Chapter 6. In very general terms, the idea is to consider spatial objects on a map as members of a set. For this study, the spatial objects are the areas of the different classes on an evidence map and the set defined as areas containing a VMS deposit. In fuzzy set theory, membership can take on any value between 0 and 1, reflecting the degree of certainty of membership. Fuzzy set theory uses membership functions that express the degree of membership for some attribute of interest. Given an evidence map where the attribute of interest, such as concentration of Zn in tills, is measured in discrete intervals, a membership function can be constructed relating the map intervals or classes to a membership value. Maps and their associated membership values are combined using fuzzy operators.

This method was implemented in SPANS using the map modelling method though table modelling and unique conditions modelling could also have been used. Assuming that the evidence maps have been generated, the method is implemented using the following steps:

1. A table is constructed for each evidence map containing the associated membership function

2. Related evidence is grouped together to represent different factors. This is done primarily to facilitate the understanding of the influence each type of evidence has on the final outcome. It also helps avoid problems associated with an overlay limit of 15 maps imposed by SPANS.

3. Inference nets using various fuzzy operators are built for each factor reflecting how the

expert would combine the evidence maps.

4. An equation is built in the SPANS modelling language for carrying out the fuzzy calculations for each factor

5. These equations are executed resulting in intermediate factor maps. These can be evaluated to determine how much each factor is contributing to the final outcome. The values associated with the classes on each intermediate factor map is the membership value.

6. Finally, the intermediate factor maps are combined to make a final favourability map.

C. Files

Input Files:

23 multiclass evidence maps and an associated table containing a membership function (table name containing membership function is in brackets and has a .tba/.tbb extension)

Stratigraphic Factor Maps

GEOLRC (ZGEOL)	- Generalized geology map
GEOL2C2 (ZFFLOW)	- Areas mapped as felsic flows with 10 buffers 0.25 km wide extending from contacts
GEOL4C2 (ZFVOLC)	- Areas mapped as felsic volcaniclastic rocks with 10 buffers 0.25 km wide extending from contacts
GEOL5C2 (ZMVOLC)	- Areas mapped as mafic volcaniclastic rocks with 10 buffers 0.25 km wide extending from contacts

Alteration Factor Maps

NALTFEC2 (ZNALTFE)	- Areas mapped as Fe alteration with 10 buffers 0.25 km wide extending from contacts
NALTSIC2 (ZNALTSI)	- Areas mapped as Si alteration with 10 buffers 0.25 km wide extending from contacts
NALTAPC2 (ZNALTAP)	- Areas mapped as amphibole alteration with 10 buffers 0.25 km wide extending from contacts
NATLEPC2 (ZNALTEP)	- Areas mapped as epidote alteration with 10 buffers 0.25 km wide extending from contacts
NALTPPC2 (ZNALTPP)	- Areas mapped as alteration pipes with 10 buffers 0.25 km wide extending from contacts
NALTPYC2 (ZNALTPY)	- Areas mapped as pyrite alteration with 10 buffers 0.25 km wide extending form contacts

Heat Factor Maps

DYKEBUF1 (ZDYKCON)	- Areas mapped as synvolcanic dykes with 10 buffers 0.25 km wide extending from contacts

SILLBUF (ZSILCON) - Areas mapped as subvolcanic sills with 10 buffers 0.50 km wide extending from contacts

Geochemical Factor Maps

LKPC1NC (ZLKPC1) - Pricipal Component 1 scores mapped on catchment basin map
LKPC2NC (ZLKPC2) - Principal Component 2 scores mapped on catchment basin map
LKPC3NC (ZLKPC3) - Principal Component 3 scores mapped on catchment basin map
KRGLNCU2 (ZKTILCU) - Kriged ln concentrations of Cu in C horizon tills (<63 μm size fraction)
KRGLNZN2 (ZKTILZN) - Kriged ln concentrations of Zn in C horizon tills (<63 μm size fraction)
KRGLNPB2 (ZKTILPB) - Kriged ln concentrations of Pb in C horizon tills (< 63 μm size fraction)

Geophysical Factor Maps

GRVNC25V (ZVGRV) - Vertical gradient gravity map
NPVLF25 (ZPVLF) - Processed quadrature VLF data map
MGNTCM25 (ZTMAG) - Total field magnetics
MGNVCM25 (ZVMAG) - Vertical gradient magnetics
SLVLF25 (ZTVLF) - Total field VLF

Lookup table for converting map classes from 1 - 100 to a membership value between 0 and 1

zfactor.tba

Ouput Files:

Intermediate Factor Maps to be combined using equation FUZZYNC

STRTFACT - stratigraphic factor map (100 classes)
HEATXX - heat factor map (100 classes)
ALTERXX - alteration factor map (100 classes)
NCHMFACT - chemical factor map (100 classes)
GPFAC100 - geophysical factor map (100 classes)

Intermediate Factor maps that have been classified into 20 quantiles to view as an aid to intereptation

SGFAC - stratigraphic factor map (20 quantiles)
ALTERHET - heat factor map (20 quantiles)
ALTERALT - alteration factor map (20 quantiles)
GCFAC - geochemical factor map (20 quantiles)
GPFAC - geophysical factor map (20 quantiles)

Final favourability map

PMAY94

Equation Files:

In equation.inp the equations are

fuzzysnc - conbines maps related to stratigraphic factor
fuzzyhnc - combines maps related to heat factor
fuzzyanc - combines maps related to alteration factor
fuzzycnc - combines maps related to chemical factor
fuzzygnc - combines maps related to geophysical factor
fuzzync - combines the five intermediate maps created in the first five equations

D. Procedure

1. The fuzzy membership functions are entered as fields in .tba files using a text editor, then imported to internal .tbb files. The membership functions for all the evidence maps are listed in Table 1 in APPENDIX C. As an example the table for the geology map (zgeol.tba) is listed below. There are 10 records with four fields each. The first field is the class value of the map GEOLRC.MAP. The membership values, in the second field, has a value between 0 and 1 to reflect the relative importance of the different lithologies as possible hosts for VHMS deposits. Note that the felsic flows (record 2)are assigned a membership value of 0.8 indicating a very high potential for hosting VHMS deposits while the sedimentary unit (record 7) is assigned a membership value of 0.2 indicating a very low favourability. These values are very subjective and depend on the "experts" opinion. The third field is a probability function used by the Dempster-Shafer approach (see Chapter 7 and Appendix B-6) and the fourth field is a text field with the name of the unit, for reference.

```
ID zgeol
TITLE Name and membership functions
MAPID zgeol
WINDOW nc 5808 7704 14208 12080
TABTYPE 1
FTYPE free
KEYFIELD 1
KEYBASE 0
NRECORD 11
 1  3 9.0000000 0   class Class
 2  0 10.2000000 0  zstrat fuzzy membership for stratigraphic factor
 3  0 6.3000000 0  prob probability for Dempster Shaffer
```

```
4 55 35.000000 0    name name of unit
DATA
        1   0.00 0.00   "      Post Amisk Lithologies"
        2   0.80 0.40   "             Felsic flows"
        3   0.60 0.05   "              Mafic flows"
        4   0.20 0.15   "   Felsic volcaniclastic rocks"
        5   0.30 0.10   "    Mafic volcaniclastic rocks"
        6   0.10 0.10   "Heterolithic volcaniclastic rocks"
        7   0.10 0.01   "      Other sedimentary rocks"
        8   0.00 0.005  "      Subvolcanic intrusions"
        9   0.50 0.20   "      Synvolcanic intrusions"
       10   0.00 0.00   "              Unmapped "
```

2. The next step, to group the evidence into geologically related evidence, is optional but is very useful in helping to understand. In this case the data was grouped into five "factors"; stratigraphic, heat, alteration, geochemical and geophysical. The maps for each factor are listed in Part C above.

3. Constructing inference nets to help understand how the maps should be combined so as to best reflect the expert's thought process is also optional but extremely useful in keeping your data organized, translating the combination process into a modelling language and to help in understanding the results. The effects of using various fuzzy operators can be much better understood when a visual check can be made with an inference net. The inference nets and fuzzy operators used in this exercise are illustrated and discussed fully in Chapter 6.

4. Next, equations must be written in equation.inp that will do the model calculations. In practice, an equation is written for each factor. This produces 5 intermediate maps. Another equation must be written to combine these five intermediate maps to produce a final favourability map.

The first five equations are listed below. Note that the format is the same for each equation; read the map class for each map, look up the appropriate membership function associated with the map class from the table and finally perform the fuzzy operation to combine the maps.

```
E fuzzysnc Fuzzy Stratigraphic Factor
:map modelling version
:"Gamma value, usually in range (0.5,1.0)"
gamma = 0.95;
gamc = 1-gamma;
```

```
:get class values from map
m1 = class(geolrc);
m2 = class(geol2c2);
m3 = class(geol4c2);
m4 = class(geol5c2);
:get fuzzy membership values from tables;
z1 = table('zgeol',m1,'zstrat');
z2 = table('zfflow',m2,'zstrat');
z3 = table('zfvolc',m3,'zstrat');
z4 = table('zmvolc',m4,'zstrat');
:calculate favourable stratigraphy, zsc
prox24 = min(z2,z4);
prox25 = min(z2,z5);
zsc = max(prox24,prox25,z1);
: To query the model, remove colons from the following 7 lines and
: add a colon to the last line.
:"geolrc (simp geol)"
:"geol2c2 (fel flow)"
:"geol4c2 (fel vcls)"
:"geol5c2 (maf vcls)"
:"strat fac"
:result(m1,m2,m3,m4,zsc)
zsc;

E fuzzyhnc Fuzzy Heat Factor
:map modelling version
:get class values from map
:"Gamma value, usually in range (0.5,1.0)"
gamma = 0.95;
gamc = 1-gamma;
m4 = class(sillbuf);
m5 = class(dykebufl);
:get fuzzy membership values from tables;
z4 = table('zsilcon',m4,'zheat');
z5 = table('zdykcon',m5,'zheat');
:calculate favourable heat, zhc
za = 1-(1-z4)*(1-z5);
zb = z4 * z5;
zhc = fac2 * pow(za,gamma) * pow(zb,gamc);
: To query the model reove the colons from the following 5 lines
```

```
: and add a colon to the from of the last line
:"sillbuf (tonalites)"
:"dykebufl (syn dykes)"
:"heat fac"
:result(m4,m5,zhc)
zhc;

E fuzzyanc Fuzzy Alteration Factor
:map modelling version
gamma = 0.95;
gamc = 1-gamma;
:get class values from map
m6 = class(naltsic2);
m7 = class(naltfec2);
m8 = class(naltppc2);
m6a= class(naltapc2);
m7a= class(naltpyc2);
m8a= class(naltepc2);
:get fuzzy membership values from tables;
z6 = table('znaltsi',m6,'zalt');
z7 = table('znaltfe',m7,'zalt');
z8 = table('znaltpp',m8,'zalt');
z6a= table('znaltap',m6a,'zalt');
z7a= table('znaltpy',m7a,'zalt');
z8a= table('znaltep',m8a,'zalt');
: calculate algebraic sum of Si and Amp
prod=(1-z6)*(1-z6a);
as=1-prod;
: calculate gamma for as (SiAmp), py, ep
za1=1-(1-as)*(1-z7a)*(1-z8a);
zb1=as*z7a*z8a;
zc2=fac3 * pow(za1,gamma) * pow(zb1,gamc);
:calculate max (or) for zc2, fe, pp
zc3 = max(zc2,z7,z8);
:To query model remove colons from following 7 lines and add
: a colon to the front of the last line
:"naltsic2 (Si)"
:"naltfec2 (Fe-Mg)"
:"naltppc2 (Pipes)"
:"naltapc2 (ap)"
```

```
:"naltpyc2 (Pyrite)"
:"naltepc2 (ep)"
:"alteration fac"
:result(m6,m7,m8,m6a,m7a,m8a,zc3)
zc3;

E fuzzycnc Fuzzy Chemical Factor
:map modelling version
:"Gamma value, usually in range (0.5,1.0)"
gamma = 0.95;
gamc = 1-gamma;
:get class values from map
ml1 = class(lkpc1nc);
ml2 = class(lkpc2nc);
ml3 = class(lkpc3nc);
mt1 = class(krglncu2);
mt2 = class(krglnpb2);
mt3 = class(krglnzn2);
:get fuzzy membership values from tables;
zl1 = table('zlkpc1',ml1,'zlkpc1');
zl2 = table('zlkpc2',ml2,'zlkpc2');
zl3 = table('zlkpc3',ml3,'zlkpc3');
zt1 = table('zktilcu',mt1,'ztill');
zt2 = table('zktilpb',mt2,'ztill');
zt3 = table('zktilzn',mt3,'ztill');
:calculate the facourable chem factor, zcc
zlm = min(zl1,zl2,zl3);
ztm = max(zt1,zt2,zt3);
za = 1 - (1-zlm)*(1-ztm);
zb = zlm*ztm;
zcc =  pow(za,gamma) * pow(zb,gamc);
: To query the model remove the colons from the following 8 lines and add
: a colon to the last line
:"lkpc1nc"
:"lkpc2nc"
:"lkpc3nc"
:"krglncu2"
:"krglnpb2"
:"krglnzn2"
:"geochem fac"
```

```
:result(ml1,ml2,ml3,mt1,mt2,mt3,zcc)
zcc;

E fuzzygnc Fuzzy Geophysics Factor
:map modelling version
:"Gamma value, usually in range (0.5,1.0)"
gamma = 0.95;
gamc = 1-gamma;
:get class values from map
mtm = class(mgntcm25);
mvm = class(mgnvcm25);
mtv = class(slvlf25);
mpv = class(npvlf25);
mvg = class(grvnc25v);
:get fuzzy membership values from tables;
ztm = table('ztmag',mtm,'ztmag');
zvm = table('zvmag',mvm,'zvmag');
ztv = table('ztvlf',mtv,'ztvlf');
zpv = table('zpvlf',mpv,'zpvlf');
zvg = table('zvgrv',mvg,'zvgrv');
:calculate the favourable geophysics factor, zgc
za = 1 - (1-ztm) * (1-zvm) * (1-ztv) * (1-zpv) * (1-zvg);
zb = ztv*zpv*ztm*zvm*zvg;
zgc = fac5 * pow(za,gamma) * pow(zb,gamc);
zgc1 = {0.3 if (class('geolrc')==8 or class('geolrc')==1),zgc};
: To query the model remove the colons from the following 8 lines
: and add a colon to the front of the last line
:"mgntcm25 (TF Mag)"
:"mgnvcm25 (VG Mag)"
:"slvlf25 (TV VLF)"
:"npvlf25 (Qad VLF)"
:"grvnc25v (VG Grav)"
:"geophysical factor (zgc)"
:result(mtm, mvm, mtv, mpv, mvg, zgc1)
zgc1;
```

5. MODEL/OVERLAY/MAP

The above equations are applied using the above commands in SPANS. This exercise is carried out using the map modelling approach though table modelling could also have been used. This step is repeated five times, once for each equation. Besides asking for the equation name, which would be one of the five names given above, the user is also queried for a classification and an output map. At this point the user has a choice to either, 1) create an intermediate map that can be used directly with the equation FUZZYNC that combines the 5 intermediate favourability maps to create the final favourability map or 2) create an intermediate maps that can be viewed to help investigate the importance of each factor.

Choice 1. After executing the MODEL/OVERLAY/MAP commands a menu will query you for an equation name (eg. FUZZYSNC for the stratigraphic factor), next it will query you for a classification. Classification 112 is a scheme that has 100 classes between 0 and 1 so that the break points are 0.01, 0.02, 0.03... 0.99. Using this classification, maps will be assigned a map class of 1 if the combined membership value is > .99, 2 for a combined membership value of > 98 and less than or equal to 99 and so on. This allows a map to be generated that has up to 100 classes that can be used directly in the final map combination process (see step 6 below) with the use of a lookup table that links the map class value to an actual membership value. (SPANS does not assign a real value, such as a membership value, to a pixel but rather an integer class value that can be linked to a look up table). These maps are not useful for aiding in the interpretation as they are because when they are displayed it is by map class, with no link to the actual value that was calculated. To make them more useful a legend and colour scheme would have to be manually created. An output map name of your choice can be assigned, however, if it is desired to go straight to the final analysis the intermediate map names already completed are listed above.

Choice 2. If map is desired so that the results can be visualized in a way that can be helpful for interpretation, then when the choice for a classification scheme appears, a value should be entered that is not associated with an existing classification. Another query appears requiring the number of quanitles desired, an integer value should be entered here. For example, entering a value of 2 will give you a classification of two map classes that represent the combined membership values above the 50th percentile and below the 50th percentile, entering 4 for the number of quantiles will give you a classification where your map classes represent the combined membership values in terms of quartiles.

It is noted that completing these steps does not immediately create a useable map, it creates a classification and assigns it to the number you entered in the classification scheme box (hence why you use a number that is not associated with anything else). It is then necessary to rerun the model equation using the newly created classification. After the model is completed, using the commands

EDIT/LIBRARY/LEGENDS/FROM CLASSIFICATION

will allow you to create a legend that links the map class values to the actual calculated membership values. Make sure that the legend is assigned to the right map. This can be checked using

EDIT/LIBRARY/MAP INFORMATION

The map can then be displayed and investigated using the commands

VISUALIZE/ENTITIES/MAP

The names of intermediate maps that have been created based on 20 quantiles are listed above.

6. MODEL/OVERLAY/MAP

The final step is to combine the five intermediate factor maps using the equation listed below. Some differences in the equation should be noted.

i) At the beginning of the equation the variables fac1, fac2... fac5 have been assigned a value between 0 and 1. These values represent the overall weighting of each factor. In this study the stratigraphic factor was given the highest overall weighting while the geophysical factor was assigned the lowest overall weighting. These overall weights were chosen based on the experts opinion.

ii) a look up table (zfactor.tba) is used that relates the map class to an actual membership value. The intermediate factor maps do not have their own tables with membership values because when the evidence maps were combined in Step 5 to create the intermediate factor maps the results of each equation were in fact the membership values for the intermediate factor map (see Chapter 6 for details)

iii) note that following the comment line ": get rid of unwanted information" two lines have been added. The first line restricts the calculations to the base map and the second line assigns a value of 0 to the areas where there are Post Amisk lithologies.

```
E fuzzync VMS potential by fuzzy logic
:map modelling version
```

```
:"Weight 1: For the stratigraphic factor"
fac1 =0.8;
:"Weight 2: For the heat factor"
fac2 =0.7;
:"Weight 3: For the alteration factor"
fac3 = 0.6;
:"Weight 4: For the geochemical factor"
fac4 = 0.3;
:"Weight 5: For the geophysical factor"
fac5 = 0.2;
:"Gamma value, usually in range (0.5,1.0)"
gamma = 0.95;
gamc = 1-gamma;
:get class values from map
mf1 = class(strtfact);
mf2=class(heatxx);
mf3=class(alterxx);
mf4  = class(nchmfact);
mf5 = class(gpfac100);
:get fuzzy membership values from tables;
zsc = table('zfactor',mf1,'memfun');
zhc = table('zfactor',mf2,'memfun');
zac = table('zfactor',mf3,'memfun');
zcc = table('zfactor',mf4,'memfun');
zgc = table('zfactor',mf5,'memfun');
:combine the five factors to predict favourable VMS environment, xc
za = 1-(1-zsc)*(1-zhc)*(1-zac)*(1-zcc)*(1-zgc);
za = {za if class(lkznaa) <> 0, 1 - (1-zsc)*(1-zhc)*(1-zac)*(1-zgc)};
zb = zsc*zhc*zac*zcc*zgc;
zb = {zb if class(lkznaa) <> 0, zsc*zhc*zac*zgc};
xc = pow(za,gamma) * pow(zb,gamc);
:get rid of unwanted information
xc = {xc if class(basecm)==1,0};
xc = {xc if class(geolrc) <> 1, 0};
:To query the model remove the colons from the following 8 lines and
: add a colon to the front of the last line
:"Heat Factor zhc"
:"Stratigraphic Factor zsc"
:"Chem Factor zcc"
:"Geophysical Factor zgc"
```

```
:"Alteration Factor zac"
:"Final Potential xc"
:result(zhc,zsc,zcc,zgc,zac,xc);
xc;
```

Before running the model you are asked for a classification. The user may chose to use the classification already determined to group the results into 20 quantiles (number 115) or determine their own by using the quantiles option. A legend has been built for classification 115 and is called "pmay94" . A final map as been generated also called PMAY94

7. EDIT/LIBRARY/MAP INFORMATION
   Make sure that the PMAY94 legend is used by PMAY94 map

8. VISUALIZE/ENTITIES/MAP
   Display the final favourability map.

Appendix B - 6: Applying Dempster-Shafer method of map combination using SPANS table modelling language

A. Objective

It is the objective of this method to use the Dempster-Shafer belief theory as an alternative mechanism for knowledge representation and map combination to produce a mineral potential map. The main advantage of this approach with respect to fuzzy logic is that it allows the user to represent uncertainty in the knowledge representation. Evidence from two or more maps can be combined using Dempster's rule of combination resulting in maps showing belief, disbelief, plausibility and uncertainty. The main disadvantage is lack of flexibility in combining the evidence to reflect the expert's thought processes.

B. Method

The Dempster-Shafer belief theory is discussed in detail in Chapter 7. In practice the method is implemented in SPANS using table modelling. The same multiclass evidence maps used in the fuzzy logic approach are also used in this method. Again there is a limit of overlaying 15 maps in SPANS so the modelling has to be done in two passes. The basic steps are as follows:

1. Calculate a unique conditions overlay, which produces a unique conditions map and an associated unique conditions table for 15 or less of the multiclass evidence maps.

2. Make a table for each evidence map where the records in the table contain a map class and the probability that a deposit occurs in that map class.

3. Write an equation in the SPANS table modelling language that reads the map classes from the unique conditions table created in step 1, reads the associated probability that a deposit occurs in that class from the tables created in step 2 and uses Dempster's combination rules to calculate the belief, the disbelief and uncertainty.
NOTE: This equation calls a function outside of SPANS that implements Dempster's combination rules.

4. Execute the equation and produce a new table which has the results (belief, disbelief and uncertainty) of the model appended as new fields. These "intermediate" results will be used as the initial belief and disbelief values for the next iteration.

5. Calculate a second unique conditions overlay, which produces another unique conditions map and associated unique conditions table, using the remaining multiclass evidence maps and the unique conditions map created in step 1.

6. Write a second equation in the SPANS table modelling language that reads the map classes from unique conditions file created in step 5, reads the associated probability that a deposit occurs in that class from the tables created in step 2 and uses Dempsters combination rules to calculate the belief, disbelief and uncertainty. Because Dempster's combination rule is symmetric, these equations can be used repeatedly to combine any number of maps. Thus the output from step 4 becomes the input for this second pass.

7. Execute the equation and produce a new table which has the results of the model appended as a new field.

8. Reclassify the second unique conditions map based on the field containing the belief, disbelief or uncertainty.

C. Files

Input files:

23 multiclass evidence maps - see list in fuzzy logic method (Appendix B - 5)

23 tables, one for each evidence map, containing calculated probability for each map class - see list in fuzzy logic method (Appendix B - 5)

dsuniq1.tba	unique conditions table containing overlay information for 13 multiclass evidence maps
dsuniq1.map	unique conditions map showing unique overlap areas for 13 multiclass evidence maps
dsuniq2.tba	unique conditions table containing overlay information for remaining 10 multiclass evidence maps and dsuniq1.map
dsuniq2.map	unique conditions map showing unique overlap areas for remaining 10 multiclass evidence maps and dsuniq1.map

Output files:

disuniq1a.tba	unique conditions table with intermediate belief, disbelief and uncertainty results linked to unique conditions map DSUNIQ1
disuniq2a.tba	unique conditions table with final belief, disbelief and uncertainty results

	linked to the unique conditions map DSUNIQ2
dssup2.map	support map
dsdis2.map	disbelief map
dspls2.map	plausibility map
dsunc2.map	uncertainty map
*.wts	where * is the evidence map name, output file generated by WTS program.

Modelling equations:

equation.inp	the two equations are named DSNONC1 and DSNONC2
userf.c	source code for function called by the SPANS equations DSNONC1 and DSNONC2 that executes Dempster's combination rule, written in C language
userf.dll	compiled version of userf.c, must reside in the directory containing the SPANS program

D. Procedure

Step 1

1. MODELLING/OVERLAY/UNIQUE CONDITIONS

A dialogue box prompts for a list of maps to be used to create a unique overlay after executing these SPANS functions. For this application 13 of the binary evidence maps were selected. A second prompt requests a name for the output files. The results are a unique conditions map (dsuniq1.map already created) and a corresponding unique conditions table (dsuniq1.tba/tbb already created).

Step 2

2. OS/2 WINDOW

Run the WTS program as described in Appendix B-1. Use the non-cumulative table from the output file and calculate the probability that a deposit occurs in a given map class by dividing the number of deposits found in the map class by the total area of the map class. This is done for each of the 23 multiclass evidence maps. Note: These files are in the data base and have been named the same as the evidence map name with a .wts extension.

Use a text editor to create table files where each record contains the map class and the probability that an occurrence occurs in that class.

For an example, the evidence map NALTPPC2 showing proximity to alteration pipes is used here.

The resulting file from WTS is called NALTPPC2.WTS, and the non-cumulative table from this file is listed below.

The following table is non-cumulative
Areas in unit cells

class	area	points	W+	s(W+)	W-	s(W-)	C	s(C)	Stud(C)
1	0	1	-.9609	.4522	1.6453	.3614	-2.6062	.5789	-4.5019
2	3	3	7.0975	4.9135	-.2230	.2954	7.3205	4.9224	1.4872
3	4	1	1.6955	1.1498	-.0567	.2746	1.7522	1.1821	1.4822
4	5	1	1.3619	1.1093	-.0518	.2747	1.4136	1.1428	1.2370
5	5	1	1.2745	1.1006	-.0502	.2747	1.3246	1.1344	1.1677
6	5	1	1.2779	1.1009	-.0502	.2747	1.3281	1.1347	1.1705
7	5	2	2.2303	.8802	-.1287	.2845	2.3589	.9251	2.5500
8	5	0							
9	6	0							
10	226	5	-.9609	.4522	1.6453	.3614	-2.6062	.5789	-4.5019

The value in the points field is divided by value in the area field to obtain the calculated probability that an occurrence occurs in that map class.

This information is built into a table to be used by the modelling equation. This file is listed below.

```
ID znaltpp
TITLE Fuzzy memberships for alt pipe bufs
MAPID naltppc2
WINDOW nc 5808 7704 14208 12080
TABTYPE 1
FTYPE free
KEYFIELD 1
KEYBASE 0
NRECORD 10
 1 4 5.000000 0   class class
 2 0 6.200000 0    zalt fuzzy membership for alteration factor
 3 0 6.200000 0   prob probability function
 4 40 20.000000 0     leg legend
DATA
```

1	0.90	0.8	'Alteration Pipes'
2	0.90	0.8	'0.00 - 0.25 km'
3	0.70	0.5	'0.25 - 0.50 km'
4	0.70	0.3	'0.50 - 0.75 km'
5	0.65	0.2	'0.75 - 1.00 km'
6	0.60	0.15	'1.00 - 1.25 km'
7	0.55	0.10	'1.25 - 1.50 km'
8	0.40	0.08	'1.50 - 1.75 km'
9	0.35	0.06	'1.75 - 2.00 km'
10	0.10	0.02	'> 2.00 km'

Note that this file also has the fuzzy membership function included (field 2). The probability function (field 2) has been smoothed assuming that calculated probabilities would form a continuous function.
This process is repeated for all 23 evidence maps.

Step 3

3. Build an equation in the file equation.inp that reads the unique conditions table (woe1uniq.tba), extracts the class values for each map, assigns the appropriate probability and calculates the belief, disbelief and uncertainty using Dempster's combination rules. The equation is listed below.

```
E dsnonc1 DS Table Model (Pass1,Non-centred)
:read the map class from the appropriate field
x1= field('naltppc2');
x2= field('krglnzn2');
x3=field('lkpc1nc');
x4=field('geol2c2');
x5=field('geol5c2');
x6=field('naltfec2');
x7=field('naltsic2');
x8=field('dykebuf1');
x9=field('krglncu2');
x10=field('geol4c2');
x11=field('lkpc2nc');
x12=field('geolrc');
: assign appropriate calculated probabilities for each map class
p1=table('znaltpp',x1,'prob');
```

```
p2=table('zktilzn',x2,'prob');
p3=table('zlkpc1',x3,'prob');
p4=table('zfflow',x4,'prob');
p5=table('zmvolc',x5,'prob');
p6=table('znaltfe',x6,'prob');
p7=table('znaltsi',x7,'prob');
p8=table('zdykcon',x8,'prob');
p9=table('zktilcu',x9,'prob');
p10=table('zfvolc',x10,'prob');
p11=table('zlkpc2',x11,'prob');
p12=table('zgeol',x12,'prob');
"What is multiplier for belief?"
B=input;
"What is multiplier for disbelief"
D=input;
bel1=B*p1;
dis1 = D * (1-p1);
dis1 = {dis1 if p1 >0,0};
dis1 = {.98 if ( x12 == 7 or x12 == 1), dis1};
bel1 = {.02 if ( x12 == 7 or x12 == 1), bel1};
bel2=B*p2;
dis2 = D * (1-p2);
dis2 = {dis2 if p2 >0,0};
dis2 = {.98 if ( x12 == 7 or x12 == 1), dis2};
bel2 = {.02 if ( x12 == 7 or x12 == 1), bel2};
bel3=B*p3;
dis3 = D * (1-p3);
dis3 = {dis3 if p3 >0,0};
dis3 = {.98 if ( x12 == 7 or x12 == 1), dis3};
bel3 = {.02 if ( x12 == 7 or x12 == 1), bel3};
bel4=B*p4;
dis4 = D * (1-p4);
dis4 = {dis4 if p4 >0,0};
dis4 = {.98 if ( x12 == 7 or x12 == 1), dis4};
bel4 = {.02 if ( x12 == 7 or x12 == 1), bel4};
bel5=B*p5;
dis5 = D * (1-p5);
dis5 = {dis5 if p5 >0,0};
dis5 = {.98 if ( x12 == 7 or x12 == 1), dis5};
bel5 = {.02 if ( x12 == 7 or x12 == 1), bel5};
```

```
bel6=B*p6;
dis6 = D * (1-p6);
dis6 = {dis6 if p6 >0,0};
dis6 = {.98 if ( x12 == 7 or x12 == 1), dis6};
bel6 = {.02 if ( x12 == 7 or x12 == 1), bel6};
bel7=B*p7;
dis7 = D * (1-p7);
dis7 = {dis7 if p7 >0,0};
dis7 = {.98 if ( x12 == 7 or x12 == 1), dis7};
bel7 = {.02 if ( x12 == 7 or x12 == 1), bel7};
bel8=B*p8;
dis8 = D * (1-p8);
dis8 = {dis8 if p8 >0,0};
dis8 = {.98 if ( x12 == 7 or x12 == 1), dis8};
bel8 = {.02 if ( x12 == 7 or x12 == 1), bel8};
bel9=B*p9;
dis9 = D * (1-p9);
dis9 = {dis9 if p9 >0,0};
dis9 = {.98 if ( x12 == 7 or x12 == 1), dis9};
bel9 = {.02 if ( x12 == 7 or x12 == 1), bel9};
bel10=B*p10;
dis10 = D * (1-p10);
dis10 = {dis10 if p10 >0,0};
dis10 = {.98 if ( x12 == 7 or x12 == 1), dis10};
bel10 = {.02 if ( x12 == 7 or x12 == 1), bel10};
bel11=B*p11;
dis11 = D * (1-p11);
dis11 = {dis11 if p11 >0,0};
dis11 = {.98 if ( x12 == 7 or x12 == 1), dis11};
bel11 = {.02 if ( x12 == 7 or x12 == 1), bel11};
bel12=B*p12;
dis12 = D * (1-p12);
dis12 = {dis12 if p12 >0,0};
dis12 = {.98 if ( x12 == 7 or x12 == 1), dis12};
bel12 = {.02 if ( x12 == 7 or x12 == 1), bel12};
"input bel =1, dis =2, unc = 3"
switch=input;
userf(switch,bel1,bel2,bel3,bel4,bel5,bel6,bel7,bel8,bel9,bel10,bel11,bel12,
        dis1,dis2,dis3,dis4,dis5,dis6,dis7,dis8,dis9,dis10,dis11,dis12);
```

Note that the last line calls an external function (userf) which does the actual computation. The calculated belief, disbelief and uncertainties are passed back to the output table named when the MODEL/TABLE command is given.

Step 4

4. MODEL/TABLE

This SPANS command opens a dialogue box that requests the name of an equation, a primary table and a new table. The equation name is DSNONC1 (see equation above), the primary table is DSUNIQ1 and the new table name is the users choice but one exists named DSUNIQ1A. The new table has fields representing the calculated belief, disbelief and uncertainty that are linked to the unique conditions map DSUNIQ1. This map and table will be used to determine the initial belief and disbelief values for the next iteration (see steps/commands 5-8)

5. Repeat step 1 using remaining evidence maps (unique conditions dsuniq2.map and dsuniq2.tba already exist)

Repeat step 3 to combine the remaining evidence maps. The equation name is **dsnonc2.**

Note that the first map in the equation is dsuniq1. The belief, disbelief and uncertainty for this map are the values that were calculated in the first iteration and recorded in the unique conditions table dsuniq1.tba which is in turn linked to the unique conditions map dsuniq1.map.

Repeat step 4 (an unique conditions table dsuniq2a.tba already exists)

6. MODEL/RECLASS/BUILD MAP/FROM TABLE

Use the second unique conditions table (DSUNIQ2A) with the appended results and reclassify the unique conditions map DSUNIQ2 using the support, disbelief or uncertainty fields. These are the final results.

Appendix B - 7: Using area weighted Spearman's rank correlation coefficient to compare final favourability maps by pairs.

A. Objective

In this study favourability maps were generated using four different methods and visual inspection gives the impression that they are all similar. When comparing the spatial patterns between two maps it is useful to be able to quantify any spatial association. Because the results have been presented as quantiles the final favourability maps can be considered as ordinal in scale. The process described below presents a method for using a Spearman's rank correlation coefficient to measure the spatial association between the different maps by looking at them in pairs. Because the data comes from irregular polygons, an area-weighted form is used.

B. Method

1. The first step is to overlay the maps to be compared and identify the area and value of the two input maps that are associated with the new polygons resulting from the overlay (ie. a unique conditions overlay). If comparisons are to be made between a number of different pairs of maps all covering the same area, in practice, a single unique conditions overlay containing all the maps can be made and information selected for the pair of maps being compared as needed.

2. Use this information to calculate the area weighted Spearman's rank correlation coefficient using an external FORTRAN program. Details concerning how the calculations are actually carried out are given in Chapter 8.

C. Files

Input files:

basecmlk.map	- base map for Chisel-Anderson Study area
basefav1.map	- base map for Chisel-Anderson Study area for Amisk volcanics only
dsup2.map	- Dempster-Shafer support map for VHMS deposits
dspls2.map	- Dempster-Shafer plausibility map for VHMS deposits
pmay94.map	- fuzzy logic method favourability map for VHMS deposits
logreg.map	- logistic regression method favourability map for VHMS deposits
woevms1.map	- weights of evidence method favourability map for VHMS deposits

Output files:

uniqcor3.map - unique conditions map resulting from overlay of favourability maps using whole study area (using basecmlk.map as basemap)
uniqcor3.tba - ascii file containing overlay information for map uniqcor3.map
uniqmsk3.map - unique conditions map resulting from overlay of favourability maps just for areas of Amisk volcanics (using basefav1.map for basemap)
uniqmsk3.tba - ascii file containing overlay information for map uniqmsk3.map
*.cor - output files from the program where * is the user defined prefix

Executable files:
awsrcor.exe

D. Procedure

1. FILE/NEW STUDY AREA/BASEMAP

Make sure that the basemap is defined as basecmlk.map. When doing modelling, calculations are only performed for the area defined by the base map. The area underlying basecmlk.map includes the whole Chisel-Anderson study area

2. MODEL/OVERLAY/UNIQUE CONDITIONS

A dialogue box is displayed following the execution of the above SPANS commands and lists all the available maps in the directory (universe). Select the maps to be compared (dssup2.map, dspls2.map, woevms1.map, logreg.map and pmay94.map). Type in an output file name to be assigned to the unique conditions map and table. One already exists by the name of uniqcor3.tba/map.

3. TRANSFORM/EXPORT/LIBRARY/TABLE

Export the unique conditions table as the ascii version is required as input for the executable program that calculates the Spearman's rank correlation coefficient.

4. AWSRCOR

In an OS/2 window execute the program awsrcor.exe. The only input is the unique conditions table exported in 3. It will read and display the table header that contains the names of the maps used to build the unique conditions map and which fields in the table hold the map information. The user is then prompted to enter the field numbers of the two maps to be compared.

The default output file name is the unique conditions table name with the extension..cor. It should be renamed as it will be overwritten when the program is executed again. A sample of the output is listed below. Of particular interest is the Spearman's rank correlation coefficient listed on the last line.

Output is in file file mwelr.cor
Number of records = 24425
Sum of map 1 ranks = 289127.00
Sum of squares, map 1 ranks = 4023081.00
Sum of map 2 ranks = 250701.00
Sum of squares, map w ranks = 3178855.00
Sum of cross products = 3387069.00
Mean of ranks for map1,map2 = 11.84 10.26
Variance of ranks for map1,map2 = 24.59 24.80
Standard deviation for map1,map2 = 4.96 4.98
Covariance between ranks 1 and ranks 2 = 17.17
Correlation between map1 and map2 = .70
The area weighted r = .817

5. Repeat the steps 1-4 using basefav1.map as the basemap. This will compare the areas underlying the Amisk volcanic rocks only. This may be a more accurate comparison as the tonalite sills and Post Amisk rocks represent a large proportion of the study area that is uniformly low potential.

Note: Output files already exist for the various map pairs that have been compared

For area underlying Amisk Volcanics only

mflwe.cor	- comparison of fuzzy logic and weights of evidence
mfldss.cor	- comparison of fuzzy logic and Dempster-Shafer support
mfldsp.cor	- comparison of fuzzy logic and Dempster-Shafer plausibility
mfllr.cor	- comparison of fuzzy logic and logistic regression
mwedss.cor	- comparison of weights of evidence and Dempster-Shafer support
mwedsp.cor	- comparison of weights of evidence and Dempster-Shafer plausibility
mwelr.cor	- comparison of weights of evidence and logistic regression
mdssp.cor	- comparison of Dempster-Shafer support and plausibility
mdsslr.cor	- comparison of Dempster-Shafer support and logistic regression
mdsplr.cor	- comparison of Dempster-Shafer plausibility and logistic regression

For area underlying whole Chisel-Anderson study area

corflwe.cor	- comparison of fuzzy logic and weights of evidence
corfldss.cor	- comparison of fuzzy logic and Dempster-Shafer support
corfldsp.cor	- comparison of fuzzy logic and Dempster-Shafer plausibility

corfllr.cor	- comparison of fuzzy logic and logistic regression
corwedss.cor	- comparison of weights of evidence and Dempster-Shafer support
corwedsp.cor	- comparison of weights of evidence and Dempster-Shafer plausibilty
corwelr.cor	- comparison of weights of evidence and logistic regression
cordssp.cor	- comparison of Dempster-Shafer support and plausibilty
cordsslr.cor	- comparison of Dempster-Shafer support and logistic regression
cordsplr.cor	- comparison of Dempster-Shafer plausibility and logistic regression

APPENDIX C

Digital Database

SPANS DATA BASE LISTING

SPANS System Files

NAME	TYPE	DESCRIPTION
spans.dat	binary	SPANS internal database file containing information on map legends, map titles, windows, classifications, raster file headers, and browse files
palet.dat	binary	SPANS system file containing colour palette information
rgb.dat	rgb.dat	SPANS system file containing palette red, green, blue values
curparam.dat	binary	SPANS system file containing projection extents of "universe" for the study area

Multiclass evidence maps

NAME	TYPE	DESCRIPTION
geolrc.map	binary	generalized 1:20000 geology of the Chisel - Anderson study area.
flows.map	binary	areas mapped as felsic flows only
geol2c2.map	binary	areas mapped as felsic flows with 10 buffers 0.25 km wide extending from contacts
geol5c2.map	binary	areas mapped as mafic volcaniclastic rocks with 10 buffers 0.25 km wide extending from contacts
geol4c2.map	binary	areas mapped as felsic volcaniclastics with 10 buffers 0.25 km winde extending from contacts
naltfec2.map	binary	areas mapped as Fe alteration with 10 buffers 0.25 km wide extending from contacts
naltsic2.map	binary	areas mapped as Si alteration with 10 buffers 0.25 km wide extending from contacts
naltapc2.map	binary	areas mapped as amphibole alteration with 10 buffers 0.25 km wide
naltepc2.map	binary	areas mapped as epidote alteration with 10 buffers 0.25 km wide
naltppc2.map	binary	areas mapped as alteration pipes with 10 buffers 0.25 km wide surrounding areas
dykebufl.map	binary	areas mapped as synvolcanic dykes with 10 buffers 0.25 km wide
sillbuf.map	binary	areas mapped as subvolcanic sills with 10 buffers 0.50 km wide extending from contacts
krglnzn2.map	binary	kriged ln concentrations of Zn in C horizon tills (<63μm size fraction)
krglncu2.map	binary	kriged ln concentrations of Cu in C horizon tills (<63μm size fraction)
krglnpb2.map	binary	kriged ln concentrations of Pb in C horizon tills (<63μm size fraction)
lkpc1nc.map	binary	Principal Component 1 scores mapped on catchment basin map
lkpc2nc.map	binary	Principal Component 2 scores mapped on catchment basin map
lkpc3nc.map	binary	Principal Component 3 scores mapped on catchment basin map
grvnc25v.map	binary	vertical gradient gravity map - 25 classes

NAME	TYPE	DESCRIPTION
npvlf25.map	binary	processed quadrature VLF data map - 25 classes
slvlf25.map	binary	total field VLF - 25 classes
mgntcm25.map	binary	total field magnetics - 25 classes
mgnvcm25	binary	vertical gradient magnetics - 25 classes

Binary Evidence Maps (multiclass maps thresholded to define optimal association between known mineral deposits and map pattern

NAME	TYPE	DESCRIPTION
fflowb.map	binary	1:20000 geology map reclassified to felsic flows (class 2) and other (class 1)
geol2c2b.map	binary	area < 0.75 km (class 2) and area > 0.75 km (class 1) from felsic flows
geol5c2b.map	binary	area < 2.00 km (class 2) and area > 2.00 km (class 1) from mafic volcaniclastics
geol4c2b.map	binary	area < 1.50 km (class 2) and area > 1.50 km (class 1) from felsic volcaniclastics
naltfecb.map	binary	area < 0.50 km (class 2) and area > 1.50 km (class 1) from Fe alteration
naltsicb.map	binary	area < 1.75 km (class 2) and area > 1.75 km (class 1) form Si alteration
naltapcb.map	binary	area < 1.50 km (class 2) and area > 1.50 km (class 1) from amphibole alteration
naltepcb.map	binary	area < 2.50 km (class 2) and area > 2.50 km (class 1) from epidote alteration
naltppcb.map	binary	area < 0.75 km (class 2) and area > 0.75 km (class 1) from alteration pipes
dykebufb.map	binary	area < 1.00 km (class 2) and area > 1.00 km (class 1) from synvolcanic dykes
syndykb.map	binary	1:20000 geology map reclassified as synvolcanic dykes (class 2) and other (class 1)
sillbufb.map	binary	area < 0.75 km (class 2) and area > 0.75 km (class 1) from subvolcanic tonalite sills
krglnznb.map	binary	area > 90th percentile of ln Zn (class 2) and area < 90th percentile ln Zn
krglncub.map	binary	area > 80th percentile of ln Cu (class 2) and area < 90th percentile ln Cu
krglnpbb.map	binary	area > 80th percentile of ln Pb (class 2) and area < 80th percentile ln Pb
lkpc1ncb.map	binary	area > 95th percentile (class 2) and area < 95th percentile of lake sediment PC1 scores
lkpc2ncb.map	binary	area > 90th percentile (class 2) and aera < 95th percentile of lake sediment PC2 scores

NAME	TYPE	DESCRIPTION
lkpc3ncb.map	binary	area > 95th percentile (class 2) and area < 95th percentile of lake sediment PC3 scores
grvnc25b.map	binary	area of high gravity values (class 2) and area of low to moderate gravity values
npvlf25b.map	binary	area of high processed VLF values (class 2) and other (class 1)
slvlf25b.map	binary	area of high total field VLF values (class 2) and other (class 1)
mgntcmb.map	binary	area of moderate to high total field magnetic values (class 2) and other (class 1)
mgnvcmb	binary	area of moderate to high vertical gradient magnetic values (class 2) and other (class 1)

Files associated with modelling (not including evidence maps) Note: To get ascii versions of binary tables, use the commmad TRANSFORM/EXPORT/LIBRARY/TABLE

Weights of Evidence Modelling

NAME	TYPE	DESCRIPTION
woe2.tba	ascii	unique conditions table of all 23 binary evidence map overlap conditions to be used with extenal Fortran progam PREDICTR, result of "joining" woe1uniq.tba and woe2uiq.tba in a RDMS
cipnts.tba/tbb	ascii/binary	point file of all VMS deposits for the Chisel-Anderson area with the class number of the unique conditions map woe2uniq.map appended, to be used with PREDICTR
woe2uniq.map	binary	unique conditions map showing unique overlap areas of all 23 binary evidence maps, to be used with the external Fortran program PREDICTR and associated with unique conditions table woe2unq.tbb
weights.tbb	binary	table file containing results of weights of evidence modelling, used to reclassify woe2uniq.map
equation.inp	ascii	contains equations in SPANS modelling language to perform various modellin operations, for weights of evidence see equations WOEPART1 and WOEPART2
woe1uniq.tbb	binary	unique conditon table of 13 of 23 binary maps (see header for descripiton), useful for table modelling, intermediate table for generating woe2.tba
woe1uniq.map	binary	uniqe conditions map associatated with table woe1unq.tba
woe2uniq.tbb	binary	uniqe conditions table including the remaining 10 binary evdience maps not in woe1uniq.tba and the unique conditions map woe1uniq.map
woepart1.map	binary	resulting map after executing equation WOEPART1 in equation.inp, the classes range between 1 and 100, representing a probability between 0 and 1 as expressed in the lookup table zfactor.tba

NAME	TYPE	DESCRIPTION
zfactor.tbb	binary	lookup table used in map modelling and table modelling to link map classes to a probability (WOE and fuzzy logic approaches)
woevms1.map	binary	final probability map resulting from weights of evidence modelling
woetab1r.tbb	binary	unique conditions table of first 13 binary evidence maps and an intermediate posterior probability generated through table modelling
woetab2r.tbb	ascii	unique conditions table of remaining 10 binary evidence maps, woe1uniq.map, and the final posterior probability generated through table modelling
woe2pnt.tbb	binary	VHMS deposit locations with map classes from woe2uniq.map appended
predictr.exe	binary	FORTRAN program compiled in OS2 for modelling using SPANS output files
cippl.exe	binary	FORTRAN program compiled in OS2 for testing conditional independence using SPANS output files

Fuzzy Logic Modelling. Other files required are the multiclass evidence maps listed above. (see Appendix B-5, Chapter 6)

NAME	TYPE	DESCRIPTION
zgeol.tbb	binary	table containing fuzzy logic membership function and Dempster-Shafer probability function for evidence map GEOLRC
zfflow.tbb	binary	table containing fuzzy logic membership function and Dempster-Shafer probability function for evidence map GEOL2C2
zfvolc.tbb	binary	table containing fuzzy logic membership function and Dempster-Shafer probability function for evidence map GEOL4C2
zmvolc.tbb	binary	table containing fuzzy logic membership function and Dempster-Shafer probability function for evidence map GEOL5C2
znaltfe.tbb	binary	table containing fuzzy logic membership function and Dempster-Shafer probability function for evidence map NALTFEC2
znaltsi.tbb	binary	table containing fuzzy logic membership function and Dempster-Shafer probability function for evidence map NALTSIC2
znaltap.tbb	binary	table containing fuzzy logic membership function and Dempster-Shafer probability function for evidence map NALTAPC2
znaltep.tbb	binary	able containing fuzzy logic membership function and Dempster-Shafer probability function for evidence map NALTEPC2

NAME	TYPE	DESCRIPTION
znaltpp.tbb	binary	table containing fuzzy logic membership function and Dempster-Shafer probability function for evidence map NALTPPC2
znaltpy.tbb	binary	table containing fuzzy logic membership function and Dempster-Shafer probability function for evidence map NALTPYC2
zdykcon.tbb	binary	table containing fuzzy logic membership function and Dempster-Shafer probability function for evidence map DYKEBUF1
zsilcon.tbb	binary	table containing fuzzy logic membership function and Dempster-Shafer probability function for evidence map SILBUF
zlkpc1.tbb	binary	table containing fuzzy logic membership function and Dempster-Shafer probability function for evidence map LKPC1NC
zlkpc2.tbb	binary	table containing fuzzy logic membership function and Dempster-Shafer probability function for evidence map LKPC2NC
zlkpc3.tbb	binary	table containing fuzzy logic membership function and Dempster-Shafer probability function for evidence map LKPC3NC
zktilcu.tbb	binary	table containing fuzzy logic membership function and Dempster-Shafer probability function for evidence map KRGLNCU2
zktilpb.tbb	binary	table containing fuzzy logic membership function and Dempster-Shafer probability function for evidence map KRGLNPB2
zktilzn.tbb	binary	table containing fuzzy logic membership function and Dempster-Shafer probability function for evidence map KRGLNZN2
zvgrv.tbb	binary	table containing fuzzy logic membership function and Dempster-Shafer probability function for evidence map GRVNC25V
zpvlf.tbb	binary	table containing fuzzy logic membership function and Dempster-Shafer probability function for evidence map NPVLF25
ztvlf.tbb	binary	table containing fuzzy logic membership function and Dempster-Shafer probability function for evidence map SLVLF25
ztmag.tbb	binary	table containing fuzzy logic membership function and Dempster-Shafer probability function for evidence map MGNTCM25
zvmag.tbb	binary	table containing fuzzy logic membership function and Dempster-Shafer probability function for evidence map MGNVCM25
strtfact.map	binary	intermediate map showing fuzzy potential related to stratigraphic factor (100 classes) to be used in final modelling stage
heatxx.map	binary	intermediate map showing fuzzy potential related to heat factor (100 classes) to be used in final modelling stage

NAME	TYPE	DESCRIPTION
alterxx.map	binary	intermediate map showing fuzzy potential related to alteration factor (100 classes) to be used in final modelling stage
nchmfact.map	binary	intermediate map showing fuzzy potential related to geochemical factor (100 classes) to be used in final modelling stage
gpfac100.map	binary	intermediate map showing fuzzy potential related to geophysical factor (100 classes) to be used in final modelling stage
sgfac.map	binary	intermediate map showing fuzzy potential related to stratigraphic factor (20 quantiles) to be visualized for interpretation
alterhet.map	binary	intermediate map showing fuzzy potential related to heat factor (20 quantiles) to be visualized for interpretation
gcfac.map	binary	intermediate map showing fuzzy potential related to geochemical factor (20 quantiles) to be visualized for interpretation
gpfac.map	binary	intermediate map showing fuzzy potential related to geophysical factor (20 quantiles) to be visualized for interpretation
pmay94.map	binary	final favourability map for fuzzy logic method
equation.inp	ascii	contains equations in SPANS modelling language to perform various modellin operations, for fuzzy logic modelling see equations FUZZYSNC, FUZZYIINC, FUZZYANC, FUZZYCNC, FUZZYGNC, FUZZYNC

Area weighted logistic regresion method using PREDICTR.EXE (see Appendix B-4, Chapter 5)

NAME	TYPE	DESCRIPTION
woe2.tbb	binary	unique conditions table containing information from all 23 binary evidence maps resulting from "joining" woe1uniq.tba and woe2uniq.tba, it is linked with woe2uniq.map
cipnts.tbb	binary	VHMS deposit locations with map classes from unique conditions map woe2uniq.map appended
logpol.inp	ascii	an intermediate file that contains input parameters including, level of envergence for scores to stop, maximum number of iterations, number of explanitory variables etc. (see Agterberg, 1989 for complete details)
lucrep	ascii	data file for the logistic regression algorithm, it is a modified version of woe2.tba, missing data has been changed to not present

NAME	TYPE	DESCRIPTION
logpol.out	ascii	output showing number of iterations for scores to reach the specified level of convergence
logco.dat	ascii	table containing posterior probabilities to be imported back into SPANS to reclassify unique conditions map
cumfre.tba	ascii	comparison of observed and predicted frequencies of deposits
logreg.map	binary	map showing VHMS potential resulting from area weighted logistic regression method
logrunc.map	binary	map showing relative uncertainty (prob/sd) associated with area weighted regression method
logrstdv.map	binary	map showing standard deviations associated with probability determined using area weighted logistic regression
predictr.exe	binary	FORTRAN program to be used in OS/2 window to do area weighted logistic regression calculations

Dempster-Schafer method

Note: Files used in the Dempster-Shafer method that have already been listed in the fuzzy logic method above include

1) 23 multiclass evidence maps
2) 23 input tables (z*.tba), one for each evidence map, containing the calculated probability function used in the DS calculations

NAME	TYPE	DESCRIPTION
dsuniq1.tbb	binary	uniqe conditions table containing overlay information for 13 multiclass evidence maps, linked to dsuniq1.map
dsuniq1.map	binary	unique conditions map showing unique overlap areas for the 13 multiclass evidence in table dsuniq1.tba
dsuniq2.tbb	binary	unique conditions table containing overlay information for remaining 10 multiclass evidence maps and dsuniq1.map
dsuniq2.map	binary	unique condition map linked to unique conditions table dsuniq2.tba

NAME	TYPE	DESCRIPTION
dsuniq1a.tbb	binary	unique conditions table with intermediate belief, disbelief and uncertainty results linked to unique conditions map dsuniq1.map
dsuniq2a.tbb	binary	unique conditions table with the final belief, disbelief and uncertainty results linked to the unique conditions map dsuniq2.map
dssup2.map	binary	final "support" (belief) map
dsdis2.map	binary	final disbelief map
dspls2.map	binary	final plausibility map
dsunc2.map	binary	final uncertainty map
equation.inp	ascii	two related modelling equations are named dsnonc1 and dsnonc2
userf.c	ascii	source code for function called by SPANS equations dsnonc1 and dsnonc2 that executes Dempster's combination rule, written in C language
userf.dll	binary	compiled version of userf.c, must reside in the directory containing the SPANS program executable file

Comparison of Favourability maps

NAME	TYPE	DESCRIPTION
basecmlk.map	binary	base map for Chisel-Anderson study area
basefav1.map	binary	base map for Chisel-Anderson - Amisk volcanic rocks only
dssup2.map	binary	Dempster-Shafer support map
dspls2.map	binary	Dempster-Shaffer plausibility map
pmay94.map	binary	fuzzy logic favourability map
logreg.map	binary	logistic regression method favourability map
woevms1.map	binary	weights of evidence method favourability map
uniqcor3.map	binary	unique conditions map resulting from overlay of favourabiliy maps using whole study area (using basecmlk.map as base map)
uniqcor3.tbb	binary	unique conditions table

NAME	TYPE	DESCRIPTION
uniqmsk3.map	binary	unique conditions map resulting from overlay of favourability maps just for area underlying Amisk Volcanics
uniqmsk3.tbb	binary	ascii file containing overlay information for map uniqmsk3.map
corflwe.cor	ascii	output from program AWSRCOR.EXE comparing fuzzy logic and weight of evidence favorability maps
corfldss.cor	ascii	output from program AWSRCOR.EXE comparing fuzzy logic and Dempster-Shafer support favorability maps
corfldsp.cor	ascii	output from program AWSRCOR.EXE comparing fuzzy logic and Dempster-Shafer plausibility favorability maps
corfllr.cor	ascii	output from program AWSRCOR.EXE comparing fuzzy logic and area weighted logistic regression favourability maps
corwedss.cor	ascii	output from program AWSRCOR.EXE comparing weights of evidence and Dempster-Shafer support favourability maps
corwedsp.cor	ascii	output from program AWSRCOR.EXE comparing weights of evidence and Dempster-Shafer support favourability maps
corwelr.cor	ascii	output from program AWSRCOR.EXE comparing weights of evidence and area weighted logistic regression favourability maps
cordssp.cor	ascii	output from program AWSRCOR.EXE comparing Dempster-Shafer support and Dempster-Shafer plausibility favourability maps
cordsslr.cor	ascii	output from program AWSRCOR.EXE comparing Dempster-Shafer support and area weighted logistic regression favourability maps
cordsplr.cor	ascii	output from program AWSRCOR.EXE comparing Dempster-Shafer plausibility and area weighted logistic regression favourability maps
mflwe.cor	ascii	output from program AWSRCOR.EXE comparing fuzzy logic and weight of evidence favorability maps (for Amisk Volcanics only)
mfldss.cor	ascii	output from program AWSRCOR.EXE comparing fuzzy logic and Dempster-Shafer support favorability maps (for Amisk Volcanics only)
mfldsp.cor	ascii	output from program AWSRCOR.EXE comparing fuzzy logic and Dempster-Shafer plausibility favorability maps (for Amisk Volcanics only)
mfllr.cor	ascii	output from program AWSRCOR.EXE comparing fuzzy logic and area weighted logistic regression favourability maps (for Amisk Volcanics only)
mwedss.cor	ascii	output from program AWSRCOR.EXE comparing weights of evidence and Dempster-Shafer support favourability maps (for Amisk Volcanics only)

NAME	TYPE	DESCRIPTION
fuzwoe.mat	ascii	matrix overlay template for identifiying areas of similarity and differences between FL and WOE favourability maps
fuzwoe.map	binary	map showing similarites and differences between FL and WOE favourability maps
fuzdsup.mat	ascii	matrix overlay template for identifiying areas of similarity and differences between FL and DS support favourability maps
fuzdsup.map	binary	map showing similarites and differences between FL and DS support favourability maps
fuzdpls.mat	ascii	matrix overlay template for identifiying areas of similarity and differences between FL and DS plausibility favourability maps
fuzdpls.map	binary	map showing similarites and differences between FL and DS plausibiliy favourability maps
fuzlogr.mat	ascii	matrix overlay template for identifiying ereas of similarity and differences between FL and area weighted LR favourability maps
fuzlogr.map	binary	map showing similarites and differences between FL and area weighted logistic regresssion favourability map

NAME	TYPE	DESCRIPTION
woedsup.mat	ascii	matrix overlay template for identifiying areas of similarity and differences between WOE and DS support favourability maps
woedsup.map	binary	map showing similarites and differences between WOE and DS support favourability maps
woelogr.mat	ascii	matrix overlay template for identifiying areas of similarity and differences between WOE and area weighted LR favourability maps
woelogr.map	binary	map showing similarites and differences between WOE and area weighted LR favourability maps
suppls.mat	ascii	matrix overlay template for identifiying areas of similarity and differences between DS support and DS plausibility favourability maps
suppls.map	binary	map showing similarites and differences between DS support and DS plausibility favourability maps
dsslogr.mat	ascii	matrix overlay template for identifiying areas of similarity and differences between DS support and area weighted LR favourability maps
dsslogr.map	binary	map showing similarites and differences between DS support and area weighted LR favourability maps

Calculating Contrasts (see Appendix B-1)

NAME	TYPE	DESCRIPTION
wts.exe	binary	Fortran program using SPANS area analysis output files and map files to calcualte W+ and W- and contrasts. wts.for is source code.
geolrc.map	binary	geology map of Chisel-Anderson area
dykebuf1.map	binary	map showing buffers surrounding synvolcanic dyke
vhms1.tbb	binary	Point file with VHMS deposit locations
geolrc.rep	ascii	area analysis of geolrc.map (input for wts.exe)
dykebuf1.rep	ascii	area analysis of dykebuf1.map (input for wts.exe)
vhms1g.tbb	binary	deposit locations with map classes of geolrc.map appended (input for wts.exe)
vms2a.tbb	binary	deposit locations with map classes of dykebuf1.map appended (input for wts.exe)
geolrc.wts	ascii	output from wts.exe showing weights and contrasts for geolrc.map
dykebuf1.wts	ascii	output from wts.exe showing weights and contrasts for dykebuf1.map

List of "picture files" in standard .pcx format (may be viewed with any utility supporting this format such as COREL DRAW)

Picture file Name	Size (bytes)	Description
airpot.pcx	136,872	map of airborne Potassium (%) with overlay of subvolcanic tonalite sills contacts
allnet.pcx	43,586	Inference net showing links between evidence maps, combination rules and outcome maps used in fuzzy logic
altmod.pcx	65,075	map of simplified 1:20000 geology and cartoon of ideal alteration patterns for VHMS deposits
alterfac.pcx	77,898	intermediate map showing "alteration factor" in fuzzy logic modelling
altnet.pcx	22,785	inference net showing how 6 alteration evidence maps are combined in fuzzy logic modelling
belfun.pcx	10,437	figure showing ideal relationship between the Dempster-Shafer belief and disbelief functions
calfun.pcx	10,488	figure showing how Dempster-Shafer belief functions are related to the calculated probability function
chemfac.pcx	62,537	intermediate map showing "geochemical factor" in fuzzy logic modelling
chemnet.pcx	11,142	inference net showing how 6 geochemical evidence maps are combined in fuzzy logic modelling
cmprfrnt.pcx	41,094	front end slide for demo on comparing results of the four modelling methods
comb.pcx	48,367	slide of equations used for combining weights in weights of evidence modelling
conditio.pcx	58,752	slide of equations used for calculating conditional independence in weights of evidence modelling
define.pcx	50,386	slide giving definitions of W+ and W- used in weights of evidence method
dscomb.pcx	36,754	slide of equations used in Dempster-Shafer combination rules
dsdis2w.pcx	128,578	map of Chisel-Anderson area showing "disbelief" calculated by Dempster-Shafer method
dsfrnt.pcx	58,611	front end slide for demo of Dempster-Shafer combination method (used in SPANS Map)
dspls2w.pcx	132,487	map of Chisel-Anderson area showing "plausibility" calculated by Dempster-Shafer method
dsslogr.pcx	105,220	map comparing rsults of Dempster-Shafer support logistic regression method
dssup2w.pcx	134,443	map of Chisel-Anderson area showing "support" calculated by Dempster-Shafer method
dsunc2w.pcx	118,511	map of Chisel-Anderson area showing "uncertainty" calculated by Dempster-Shafer method
dykebuf.pcx	75,506	map of distance buffers around synvolcanic dykes
dykebufb.pcx	46,078	binary map showing optimum distance to synvolcanic dykes for hosting a VHMS deposit
fflowb.pcx	48,880	binary map showing felsic flows present and felsic flows absent
fivenet.pcx	9,358	inference net showing how the five intermediate factor maps were combined in fuzzy logic
fuzdsup.pcx	107,838	map comparing the results of fuzzy logic method and Dempster-Shafer support method
fuzfrnt.pcx	60,841	front end slide for demo of fuzzy logic method (used in SPANS Map)
fuzlogr.pcx	107,824	map comparing results of fuzzy logic method with logistic regression method
fuzwoe.pcx	105,659	map comparing results of fuzzy logic method with weights of evidence method
fuzzpot.pcx	116,958	map showing VMS potential using fuzzy logic method
fuzzy.pcx	48,453	diagram explaining fuzzy operators
geol2c2.pcx	74,179	distance buffers around felsic flows
geol2c2b.pcx	46,018	binary map showing optimum distance to felsic flows for hosting VHMS deposits
geol4c2.pcx	70,255	distance buffers around felsic volcaniclastic rocks
geol4c2b.pcx	46,260	binary map showing optimum distance to felsic volcaniclastic rocks for hosting VHMS deposits

Picture file Name	Size (bytes)	Description
geol5c2.pcx	68,231	map showing distance buffers to mafic volcaniclastic rocks in the Chisel-Anderson map sheet
geol5c2b.pcx	45,792	binary map showing the optimum distance to mafic volcaniclastic rocsks for hosting VHMS deposits
geolrc1.pcx	73,463	map showing simplified geology at 1:20000 for the Chisel-Anderson map sheet
geomod.pcx	79,880	map showing simplified geology at 1:20000 and a cartoon showing ideal geologic model for VHMS deposits
gphsfac.pcx	76,540	intermediate map showing the "geophysical factor" used in the fuzzy logic method
gphsnet.pcx	13,834	inference net showing how the 5 geophysical evidence maps are combined in the fuzzy logic method
gravbgr.pcx	44,899	map showing Bouger gravity for the Chisel-Anderson area
grvnc25.pcx	88,148	map showing vertical gradient gravity values reclassified into 25 classes
grvnc25b.pcx	46,135	binary map of vertical gradient gravity showing optimum pattern for hosting VHMS deposits
heatfac.pcx	81,502	intermediate map showing the "heat factor" used in the fuzzy logic method
heatnet.pcx	5,478	inference net showing how the two evidence maps related to the heat factor were combined in fuzzy logic
intrfmt.pcx	43,501	front end slide to introduce mineral potential modelling
krglncu.pcx	51,542	kriged natural log values of Cu in tills
krglncub.pcx	45,341	binary map of kriged Cu values showing pattern most favourable for hosting VHMS deposits
krglnpb.pcx	49,253	kriged natural log values of Pb in tills
krglnpbb.pcx	45,127	binary map of kriged Pb values showing pattern most favourable for hosting VHMS deposits
krglnzn.pcx	50,183	kriged natural log values of Zn in tills
krglnznb.pcx	44,606	binary map of kriged Zn values showing pattern most favourable for hosting VHMS deposits
lkpc1nc.pcx	47,295	map of Principal Component 1 Scores for lake sediment geochemistry
lkpc1ncb.pcx	44,615	binary map of PC1 Scores for lake sediment geochemistry
lkpc2nc.pcx	48,363	map of Principal Component 2 Scores for lake sediment geochemistry
lkpc2ncb.pcx	45,328	binary map of PC2 Scores for lake sediment geochemistry
lkpc3nc.pcx	48,046	map of Principal Component 3 Scores for lake sediment geochemistry
lkpc3ncb.pcx	44,384	binary map of PC3 Scores for lake sediment geochemistry
lksmpcm.pcx	56,966	lake sediment sample locations in Chisel-Anderson area
logreg.pcx	110,615	VMS potential resulting from using logistic regression method
logrfmt.pcx	62,244	front end slide for logistic regression demonstration (used in SPANS Map)
logrstdv.pcx	116,276	error map (standard deviations) for results of logistic regression method
logrunc.pcx	50,274	relative uncertainty (Post P / sd) associated with logistic regression method
matrix.pcx	48,658	slide of matrix used in comparing results of different combination methods
mgntcm.pcx	79,274	map of total field magnetics
mgntcmb.pcx	46,208	binary map of total field magnetics showing pattern having the optimum association with VHMS deposits
mgnvcm.pcx	100,931	map of vertical gradient magnetics for Chisel-Anderson area
mgnvcmb.pcx	48,672	binary map of vertical gradient magnetics for showing pattern having the optimum assoication with VHMS

Picture file Name	Size (bytes)	Description
mindeps.pcx	56,430	map showing mineral deposit locations (including VMS type) in the Chisel-Anderson area
naltapc.pcx	52,727	map of areas exhibiting apatite alteration and distance buffers around them
naltapcb.pcx	44,522	binary map showing pattern of optimum assoiation of apatite alteration with VHMS deposits
naltepc.pcx	52,433	map of areas exhibiting epidote type alteraton and distance buffer zones around them
naltepcb.pcx	44,654	binary map showing pattern of optimum association of epidote type alteration with VHMS deposits
naltfec.pcx	76,087	map of areas exhibiting iron alteration and distance buffer zones around them
naltfecb.pcx	47,614	binary map showing pattern of optimum association of iron type alteration with VHMS deposits
naltppc.pcx	53,511	map areas exhibiting pipe alteration and distance buffer zones around them
naltppcb.pcx	43,888	binary map showing pattern of optimum association of pipe alteration zones with VHMS deposits
naltpyc.pcx	69,906	map areas exhibiting pyrite alteration and distance buffer zones around them
naltsic.pcx	73,361	map areas exhibiting silica alteration and distance buffer zones around them
naltsicb.pcx	45,628	binary map showing pattern of optimum association of silica alteration and VHMS deposits
npvlf25.pcx	147,293	processed airborne VLF reclassified to 25 classes
npvlf25b.pcx	46,370	binary map showing pattern of optimum association of the processed VLF and VHMS deposits
process.pcx	4,976	slide describing the four step process in implementing a GIS mineral potential project
sillbuf.pcx	64,360	map of distance buffers surrounding subvolcanic tonalite sills
sillbufb.pcx	45,708	binary map showing optimum distance to tonalite sills for hosting VHMS deposits
slide1r1.pcx	44,712	introduction slide to mineral potential mapping in Snow Lake area
slvlf25.pcx	164,365	map of total field airborne VLF reclassified into 25 classes
slvlf25b.pcx	168,009	binary map showing the pattern having the optimum association of TF VLF with VHMS deposits
srcor.pcx	37,908	slide showing Spearman's area weighted rank correlation coefficient equations used to compare maps
strtfac.pcx	70,973	intermediate map showing the "stratigraphic factor" used in fuzzy logic modelling
strtnet.pcx	12,500	inference net showing how evidence maps related to the stratigraphic factor were combined using fuzzy logic
studara.pcx	36,773	map showing location of study area
syndykb.pcx	53,616	binary map showing the optimum distance to synvolcanic dykes for hosting VHMS deposits
target4.pcx	71,067	potential target areas based on results from all four methods
tillsmp.pcx	38,931	till sample location map for the Chisel-Anderson area
uncertai.pcx	40,079	slide showing equations for calculating uncertainty in weights of evidence method
uncm.pcx	77,467	map showing uncertainty due to missing data (weights of evidence method)
uncr.pcx	60,295	map showing relative uncertainty (Post P/ total unc) for weights of evidence method
unctot.pcx	74,529	totals uncertainty related to weights of evidence method
uncww.pcx	100,615	uncertainty due to weights (weights of evidence method)
vmsdep.pcx	63,633	location of VMS type deposits in the Chisel-Anderson area

Picture file Name	Size (bytes)	Description
vmsdepbw.pcx	112,427	VMS deposits in simplified black and white figure
woedsup.pcx	104,087	map showing differences between results from weights of evidence method and Dempster-Shafer support
woefrnt.pcx	65,851	front end slide for weights of evidence method
woelogr.pcx	87,227	map showing differences between results from weights of evidence method and logistic regression method
woevms2.pcx	124,675	VMS potential using weights of evidence method

Contents of Appendix C «Compact disk» consists of the digital geoscience data and related information compatible with SPANS GIS, required to carry out the mineral potential modeling applied in this thesis.

If you have any questions please contact the author at

Danny Wright
Geological Survey of Canada
481-601 Booth St.,
Ottawa, Ont.
K1A 0E8
Phn. 613-947-0186 Fax. 613-996-3726

Thank you,

Danny Wright